SKB

# TECHNICAL REPORT 93-25

# Radially converging tracer test in a low-angle fracture zone at the Finnsjön site, central Sweden. The Fracture Zone Project – Phase 3

Erik Gustafsson, Rune Nordqvist

Geosigma AB, Uppsala, Sweden

October 1993

**SVENSK KÄRNBRÄNSLEHANTERING AB**
*SWEDISH NUCLEAR FUEL AND WASTE MANAGEMENT CO*
BOX 5864 S-102 40 STOCKHOLM
TEL. 08-665 28 00 TELEX 13108 SKB S
TELEFAX 08-661 57 19

# RADIALLY CONVERGING TRACER TEST IN A LOW-ANGLE FRACTURE ZONE AT THE FINNSJÖN SITE, CENTRAL SWEDEN. THE FRACTURE ZONE PROJECT - PHASE 3

Erik Gustafsson, Rune Nordqvist

Geosigma AB, Uppsala, Sweden

October 1993

**GEOSIGMA**
MARK BERG VATTEN

Client: **SKB**
Grap: 92 026
1992-09-15
revised
1993-10-15

# RADIALLY CONVERGING TRACER TEST IN A LOW-ANGLE FRACTURE ZONE AT THE FINNSJÖN SITE, CENTRAL SWEDEN

## The Fracture Zone Project - Phase 3

Erik Gustafsson
Rune Nordqvist

GEOSIGMA AB
Uppsala

October 1993

## ABSTRACT (ENGLISH)

The performance and results of a radially converging tracer test in a low-angle major fracture zone in crystalline rock are described. The extensive, about 100 m thick, Zone 2 was encountered by means of borehole investigations at depths ranging from 100 to 250 metres at the Finnsjön site, central eastern Sweden. The zone studied (Zone 2) consists of highly conductive, metre thick interconnected minor shear and fracture zones (sub-zones) with low conductive rock in between.

The objective of the tracer test was primarily to determine flow and transport characteristics in a major fracture zone. Secondly new equipment, experimental design and methods of interpretation were developed, tested and improved.

The converging flow field was created by pumping in a central borehole from a packed-off interval enclosing the whole thickness of Zone 2. The pumped flow rate was 120 litres/minute and pumping lasted for about 6 months after beginning of tracer injections. Injections of 11 different tracers were made in totally 9 borehole sections straddling highly conductive sub-zones in three peripheral boreholes, located in different directions from the pumped tracer withdrawal borehole. The tracers used were rare earth metal-DTPA and EDTA complexes, ions and fluorescent dyes. Eight tracers were continuously injected for 5-7 weeks and three were injected as pulses. The distances ranged from 155 to 200 metres and the average hydraulic gradient during the test was low, about 0.005 in the tracer flow paths.

Interpretation of the tracer breakthrough curves was strongly helped by independent supporting measurements, such as tracer mass release per time unit into the fracture system. These data could be calculated due to the injection techniques developed; passive continuous injection and deacying pulse injection. Further, possible interconnections between sub-zones were checked by sampling major hydraulic conductors in the withdrawal borehole. Groundwater flow rates, hydraulic heads and delay and dispersion in the withdrawal borehole were also measured. The evaluation and interpretation of the tracer breakthrough curves was made with one-dimensional models. Several solutions were applied, depending on injection technique used. Also described is two-dimensional modelling, based on hydraulic test results, performed as prediction and subsequent evaluation/re-calibration.

Tracer breakthrough was registered from all nine injection points, with first arrivals ranging from 24 to 3200 hours. Evaluated flow and transport parameters included; flow porosity, dispersivity, flow wetted surface, fracture aperture and hydraulic conductivity in fracture flow paths.

Directional variations were found in the flow and transport parameters determined, which is concluded to be due to heterogeneity and/or anisotropy. This condition is more pronounced at depth in Zone 2. The results from the tracer test also clearly show that the upper boundary of Zone 2 is highly conductive and consistent over hundreds of metres. Within Zone 2, and between upper and lower margins, interconnected discrete minor shear and fracture zones (sub-zones) constitute flow paths of considerable variable residence times. The dispersion within the sub-zones of Zone 2, expressed as Peclet numbers ranged from 16 to 40. Flow porosity was determined to be 0.001 - 0.05 in the upper sub-zone and 0.01 - 0.1 in the intermediate and lower ones and flow wetted surface area per volume of rock was calculated to be within 1 - 92 $m^2/m^3$.

# ABSTRACT (SWEDISH)

Denna rapport beskriver ett radiellt konvergerande spårförsök i en stor flack sprickzon i kristallin berggrund, Zon 2, i Finnsjöns försöksområde. Den cirka 100 m mäktiga zonen påträffades på djup från 100 till 250 meter och karaktäriserades med borrhålsundersökningar. Zon 2 utgörs av metertjocka konnekterade mindre skjuv- och sprickzoner (sub-zoner) med lågkonduktivt berg emellan.

Syftet med spårförsöket var primärt att bestämma flödes- och transportegenskaper i en större sprickzon. I andra hand att utveckla, testa och förbättra utrustning, experimentella metoder och utvärdering.

Det konvergerande flödesfältet skapades genom pumpning i ett centralt borrhål. Pumpflödet var 120 liter/minut och pumpningen varade i ca 6 månader efter det att spårämnesinjiceringarna startade. Injicering av 11 olika spårämnen gjordes i tre borrhål i 9 begränsade borrhålssektioner vilka avgränsade högkonduktiva sub-zoner. De tre injiceringsborrhålen var placerade i olika riktningar från pumphålet. Använda spårämnen var metaller komplexbundna till DTPA och EDTA, samt anjoner och färgspårämnen. Åtta spårämnen injicerades kontinuerligt under 5-7 veckor och tre injicerades som pulser. Transportavstånden sträckte sig från 155 till 200 m och den hydrauliska gradienten var låg, cirka 0.005.

För utvärderingen av spårämnenas genombrottskurvor var oberoende stödjande mätningar till stor hjälp, så som spårämnesutflöde per tidsenhet ut till spricksystemet från injiceringsborrhålet. Detta kunde mätas tack vare de utvecklade injiceringsteknikerna; passiv kontinuerlig injicering och avklingande pulsinjicering. Vidare kunde flödesförbindelser mellan sub-zonerna bestämmas genom provtagning av större hydrauliska ledare i pumpborrhålet. Grundvattenflöden genom borrhålssektioner, grundvattennivåer samt fördröjning och dispersion av spårämne i pumpborrhålet mättes också. Utvärdering och tolkning av genombrottskurvorna gjordes med en-dimensionella modeller. Flera lösningar till transportekvationen tillämpades, beroende på antagna randvillkor och använd injiceringsteknik. En två-dimensionell modellering utfördes också med prediktion och följande utvärdering/kalibrering.

Spårämnesgenombrott erhölls från alla 9 injiceringspunkter, med första genombrott uppmätt från 24 till 3200 timmar. Transportparametrar som bestämdes för Zon 2 inkluderade; flödesporositet, dispersivitet, våt yta, sprickapertur och hydraulisk konduktivitet i flödesvägarna.

De bestämda transportparametrarna uppvisade riktningsberoende som tolkas bero på heterogenitet och/eller anisotropi. Detta förhållande är mer uttalat på djupet i Zon 2. Resultaten från spårförsöket visar också klart att sub-zonen som utgör övre begränsningen av Zon 2 är mycket konduktiv och uthållig i hundratals meter. Inom Zon 2 och mellan övre och undre begränsningarna utgörs flödesvägarna av diskreta mindre skjuv- och sprickzoner (sub-zoner) med mycket varierande transporttider. Dispersionen inom sub-zonerna, uttryckt som Peclet tal varierade från 16 till 40. Flödesporositeten bestämdes till 0.001-0.05 i övre sub-zonen och 0.01-0.1 i sub-zoner inom Zon 2 och den våta ytan per bergvolym beräknades ligga mellan 1-92 $m^2/m^3$.

# TABLE OF CONTENTS

## SUMMARY

In crystalline rock groundwater flow through the intact rock matrix is very low. The rate at which radionuclides in groundwater can migrate through the rock is chiefly dependent upon the fracture system. Hence, fractures and fracture zones represent the primary flow paths along which radionuclides may migrate from a nuclear waste repository to the biosphere. The SKB Fracture Zone Project at the Finnsjön site was focused on the geologic/tectonic and hydrogeologic charactersitics of the extensive, about 100 m thick, low-angle fracture zone, Zone 2, which was encountered at depths ranging from 100 to 250 metres. Phase 3 of the Fracture Zone Project was concentrated on the flow and transport characteristics of Zone 2 and started up with three large-scale interference tests and one preparatory tracer test. The results from these tests and phase 1 and 2 investigations constituted the basis for the Radially Converging Tracer Test presented in this report.

The objective of the Radially Converging Tracer Test was primarily to determine flow and transport characteristics in a major fracture zone. Secondly new equipment, experimental methods and interpretation methods were developed, tested and improved for future applications in the subsequent dipole tracer test and planned large scale tracer experiments, e.g. at the Äspö HRL site.

The tracer test was performed in a radially converging flow geometry in a low-angle major fracture zone in a country rock of greyish, medium-grained granodiorite. Zone 2 consists of interconnected minor shear and fracture zones with low conductive rock in between. The converging flow field was created by pumping in a central borehole from a packed-off interval enclosing the whole thickness (c. 100 m) of the highly conductive, low-angle Zone 2. The pumped flow rate was 120 litres/minute. Injections of 11 different tracers were made in totally 9 borehole sections straddling highly conductive sub-zones in three peripheral boreholes located in different directions from the pumped tracer withdrawal borehole. The distances ranged from 155 to 200 metres. The hydraulic head differences between injection points and tracer withdrawal borehole were low, giving an average hydraulic gradient of about 0.005 in the tracer flow paths during the test.

The pumping for steady state was started on April 12th, dilution measurements May 6 and the tracer injections on May 27th. After beginning of tracer injections, pumping and tracer sampling continued for 4510 hours, i.e. about 6 months. The diluton measurements were conducted to get a measure of the groundwater flow rate through the selected borehole injection sections, in order control that they belonged to the system of active flowing fractures, and to obtain input data for the detailed design of the tracer injections.

Sampling for measurement of tracer breakthrough was made at the ground surface in the water discharged from the pumped borehole. In addition a sampling of major conductors (sub-zones) was performed in the withdrawal borehole towards the end of the tracer injections. This was done in order to determine possible interconnections between highly conductive parts (sub-zones) of Zone 2.

The tracer injections were performed in two different ways, continuous (extended step inputs) and pulse injections. The techniques developed; passive continuous injection and decaying pulse injection, made it possible to inject tracers without applying excess pressure to the fracture flow system. The advantages of the techniques were that tracer mass release per time unit into the fracture system and also the groundwater flow rate through the injection borehole sections could be calculated. Also, enhanced tailing and/or dispersion in tracer breakthrough curves due to tracer forced out into stagnant parts of fractures was avoided. Dispersion within the borehole injection sections due to large volumes and/or trapping effects were also minimized.

The evaluation and interpretation of the tracer breakthrough curves was made with one-dimensional models. Primarily, fluid velocity and dispersion were determined by fitting the tracer breakthrough curves to theoretical solutions. Several solutions were applied, depending on injection technique used. At the secondary level the estimated residence times along with groundwater flow and head measurements were used to evaluate other properties describing flow and transport, e.g flow porosity.

The one-dimensional modelling allowed detailed evaluation of flow and transport properties within the individual fracture flow paths, and in different directions from the pumped tracer withdrawal borehole. Two-dimensional modelling was carried out as a complement and aimed at simultaneous understanding of the overall flow and transport conditions in Zone 2. The 2-D modelling was performed as prediction and subsequent evaluation and re-calibration. The previously performed hydraulic single hole and inteference tests gave information enough to predict flow, but results from the tracer test were neccesary to obtain parameters essential to predict the solute transport. The results of the re-calibrated 2-D model showed flow porosity and dispersivity in the upper sub-zone of Zone 2 in good agreement with the independently performed 1-D evaluation of the breakthrough curves. For the rest of Zone 2 it was not possible from the 2-D modelling to make generalisations about transport parameters.

The experimental design used made it possible to determine the following entities, describing flow and transport within the major fracture zone investigated:

- hydraulic conductivity in fracture flow paths
- flow porosity and fracture apertures
- dispersivity
- volume of fracture flow paths
- flow wetted surface

In addition, the tracer test results could be utilizied to study the heterogeneity and flow path interconnections within Zone 2.

The results from the tracer test clearly shows that the upper boundary of Zone 2 is highly conductive and consistent over hundreds of metres. Within Zone 2, and between upper and lower margins, interconnected discrete minor shear and fracture zones (sub–zones) constitute flow paths of considerable variable residence times.

Directional variations were found in the flow and transport parameters determined for Zone 2 and its sub–zones, which is concluded to be due to heterogeneity and/or anisotropy. This condition is more pronounced at depth in Zone 2.

The dispersion lengths, D/v, within the sub–zones were determined to range from 4 – 11 metres, and Peclet numbers from 16 to 40. The dispersion length over the entire thickness of Zone 2, due to superposed breakthroughs from solute transport in interconnected sub–zones, range from 20 to 90 metres and Peclet numbers from 2 to 8.

Evaluation of the flow porosities and fracture apertures determined from the tracer test shows that there are a few relatively large aperture fractures in the upper highly conductive sub–zone. In the intermediate and lower sub–zones of Zone 2 there are many small aperture fractures, which together gives larger porosity (volume) accessible to groundwater flow in these zones than in the upper one. Representative values of flow porosity are 0.001 – 0.05 in the upper sub–zone and 0.01 – 0.1 in the intermediate and lower sub–zones.

The hydraulic conductivity of the fracture flow paths were determined both with the flow rate and with the residence time of the tracers as the basic variable. The flow rate determined conductivities are all much higher than corresponding conductivities determined with the residence time as basic variable. This difference reflects large geometrical variations, i.e. of apertures and breadths, in the flow paths of the fracture system. The fracture flow paths within the upper sub–zone all have about the same hydraulic conductivity, with a mean value of $3.8 \cdot 10^{-1}$ m/s, expressed as the conductivity of an open smooth fracture. In intermediate and lower sub–zones the hydraulic conductivity of the fracture flow paths were lower and the mean value was $2.8 \cdot 10^{-2}$ m/s.

The flow wetted surface area was calculated in two ways; 1) as surface area per volume of flowing water, and 2) as surface area per volume of rock, i.e. the rock defined as fracture zone with matrix rock and apertures. In the upper sub–zone of Zone 2 the flow wetted surface per volume of rock (i.e. fracture zone) ranged from 1 to 56 $m^2/m^3$. In the lower sub–zone of Zone 2 basic data for calculations of flow wetted surface was obtained in only one direction. However, in that direction the surface area per volume of rock was calculated to be within 6 – 92 $m^2/m^3$. The flow wetted surface expressed as surface area per volume of water ranged from 1180 to 3850 $m^2/m^3$ in the upper sub–zone, depending on how fracture aperture was determined.

If the total pore volume in the upper sub–zone is represented by one single fracture the fracture surface area per volume of water was within 182 – 952 $m^2/m^3$. In the lower sub–zone basic data for calculations of flow wetted surface area per volume of water was obtained in only one direction, where the calculated value ranged from 1180 to 8700 $m^2/m^3$.

# 1. INTRODUCTION

## 1.1 BACKGROUND

In crystalline rock groundwater flow through the intact rock matrix is very low. The rate at which radionuclides in groundwater can migrate through the rock is chiefly dependent upon the fracture system. Hence, fractures and fracture zones represent the primary flow paths along which radionuclides may migrate from a nuclear waste repository to the biosphere.

In the earlier safety assessment studies in Sweden /KBS-3, 1983/ no credit was taken for any radionuclide retention in the fracture zones. They were considered to be pathways for transport of dissolved radionuclides with no retention, as the understanding of the flow and transport properties of fracture zones was limited. Only the relatively low conductive rock between the fracture zones and the nearest zone was considered as a geosphere barrier to radionuclide transport. It was assumed that the deposition holes had been arranged is such a way that at least 100 m of acceptable rock was available with good radionuclide retention properties.

In the early site selection studies for a repository of spent nuclear fuel, only a few point measurements were available from some fracture zones at each site. The data were too sparse to make a thorough 3D-characterization of a fracture zone and the surrounding rock mass. The need of an increased knowledge regarding geological, hydrogeological, and geochemical characteristics of fracture zones, and the variation of these characteristics in time and space, made it necessary to investigate a fracture zone in more detail. Therefore, in 1984, SKB initiated studies of fracture zones including occurence and characteristics of fracture zones in tunnels /Palmqvist and Stanfors, 1987/, a litterature review /Tirén, 1986/, and an in situ survey of a major fracture zone at the Finnsjön study site, central Sweden.

The Fracture Zone Project at the Finnsjön site was focused on the geologic/tectonic and hydrogeologic charactersitics of the extensive, about 100 m thick, low-angle fracture zone, Zone 2, which was encountered at depths ranging from 100 to 250 metres.

In Phase 1 and 2 of the Fracture Zone Project an extensive amount of background information regarding the hydrogeolgical and hydrochemical properties was gathered /Ahlbom et al., 1988/, /Smellie et al., 1987/. Finally, Phase 3 was concentrated on the flow and transport characteristics of Zone 2. Phase 3 started up with three large-scale interference tests and one preparatory tracer test performed in the same radial geometry as the subsequent radially converging tracer experiment /Andersson et al., 1989/. The results from these tests and phase 1 and 2 investigations constituted the basis for the Radially Converging Tracer Test presented in this report.

## 1.2 OBJECTIVES

The objective of the Radially Converging Tracer Test was primarily to determine flow and transport characteristics in a major fracture zone. Experimental results were also intended to be utilized for modelling efforts with models describing fluid flow and radionuclide transport (the international INTRAVAL project /SKI/NEA, 1990/ and the SKB 91 study /SKB, 1992/).

Secondly equipment, experimental methods and interpretation methods were developed, tested and improved for application in the subsequent dipole tracer test /Andersson et al., 1993/ and planned future large scale tracer experiments, e.g. the Äspö HRL site.

The experimental design used made it possible to determine the following entities, describing flow and transport:

- hydraulic conductivity in fracture flow paths
- fracture apertures
- flow porosity
- dispersivity
- volume of fracture flow paths
- flow wetted surface

In addition, the tracer test results could be used to study the heterogeneity and flow path interconnections within the major fracture zone (Zone 2) investigated.

# 2. SITE CHARACTERIZATION

The Finnsjön study site is located in northern Uppland, central Sweden, see Figure 2–1. The site has a flat topography with differences in altitude of less than 15 m. Although outcrops are common, the area is covered to 85 % by Quaternary sediments, mainly moraine. The site was originally investigated during 1977–1982 as a part of the site investigation programme for a repository for spent nuclear fuel /Olkiewicz et al., 1979/, /Carlsson et al., 1980/, /Carlsson & Gidlund, 1983/, among others. The investigations performed within the Fracture Zone Project were mainly located in the Brändan area (Figure 2–1 and 2–2). A summary of all investigations performed at the Finnsjön site is presented in Ahlbom et al. /1992/.

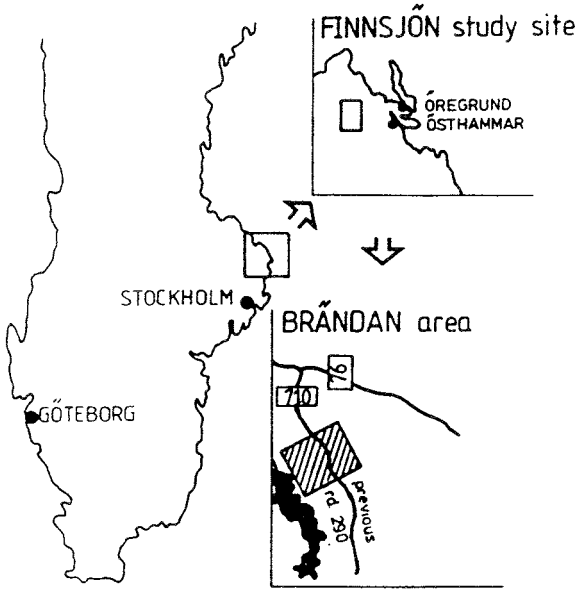


Figure 2–1 Location of the Finnsjön site

## 2.1 GEOLOGY

In the Brändan area, where the Radial Convergent Tracer Test was conducted, two major fracture zones have been identified and characterized. The Brändan fracture zone (Zone 1) has a NNE strike with a dip of about 75 degrees to the east, see Figures 2–2 and 2–3. The second fracture zone (Zone 2) trends N28W with a dip of about 16 degrees to the west. The low-angle Zone 2 is defined in nine boreholes located within an area of about 1500 x 500 m in the northern part of the Finnsjön Rock Block, see Figures 2–2 and 2–3. In the eastern part the upper boundary of Zone 2 is almost planar and located between 100 to 240 m below the ground surface.

The location of the lower boundary is less distinct. Zone 2 is about 100 m thick as an average. Zone 2 consists of sections with high fracture frequency and tectonisation. The colour of the rock is red within the tectonized sections and the fracture infillings are dominated by calcite and chlorite. Other common minerals within the low-angle zone are hematite, laumontite, asphaltite and clay minerals.

Zone 2 was formed about 1700-1800 million years ago as a some hundred meters wide ductile shear zone in a country rock of grayish, medium-grained granodiorite. The ductile shear is evident in the borehole cores by the frequent occurrence of mylonites /Ahlbom et al., 1988/. This type of structure is formed during a regional tectonic event at pressures and temperatures corresponding to depths of about 5-15 km. Intrusion of red granite 1700 million years ago caused alteration of the granodiorite and reactivation of existing zones of weakness. The most pronounced effect was the hydrothermal alteration of the bedrock adjacent to water conducting shear zones and fractures, causing a distinct red coloration of e.g. Zone 2 /Tirén, 1991/.

The next period of deformation influencing Zone 2 occurred about 1000-1100 million years ago and resulted in reactivation of shear zones, block faulting, and fracturing of the host rock. Fracture infillings of prehnite are typical for this period. Fractures overprinting the prehnite-infilled fractures are rare outside the fracture zones indicating that the transport of fluid in the rock was controlled by the fracture zones. This is also supported by infillings of pinkish red laumontite restricted to Zone 2.

Then, 600 to 900 million years ago, Zone 2 was displaced by Zone 1 and transport pathways were opened in Zone 2 adjacent to Zone 1. This is indicated by a random scatter of Fe-oxyhydroxide infilled fractures in Zone 2 close to Zone 1 while away from Zone 1 these infilled fractures become more regularly distributed along distinct levels /Tirén, 1991/. This suggests that the transport of water became more restricted, occurring within distinct levels of Zone 2. During this period a major uplift and peneplanization occurred, resulting in the sub-Cambrian peneplain which roughly coincides with the ground surface of today.

The distribution of different types of infillings indicates an overall decrease in temperature with time and that few new fractures appeared. Younger fractures seam to be restricted to minor sections within and immediately above Zone 2. However, the growth of low temperature minerals on older, high temperature minerals, indicates that reactivation of existing fractures occurred several times throughout the later stages of the geological evolution of Zone 2.

Possible late tectonic movements were briefly studied by Ahlbom & Tirén /1991/. They concluded that there have been no or only small movements along Zone 2 after the ductile deformation ceased. The conclusion was based on observations of a dike on both sides of the zone and of borehole radar reflectors interpreted to continue without displacement across the zone.

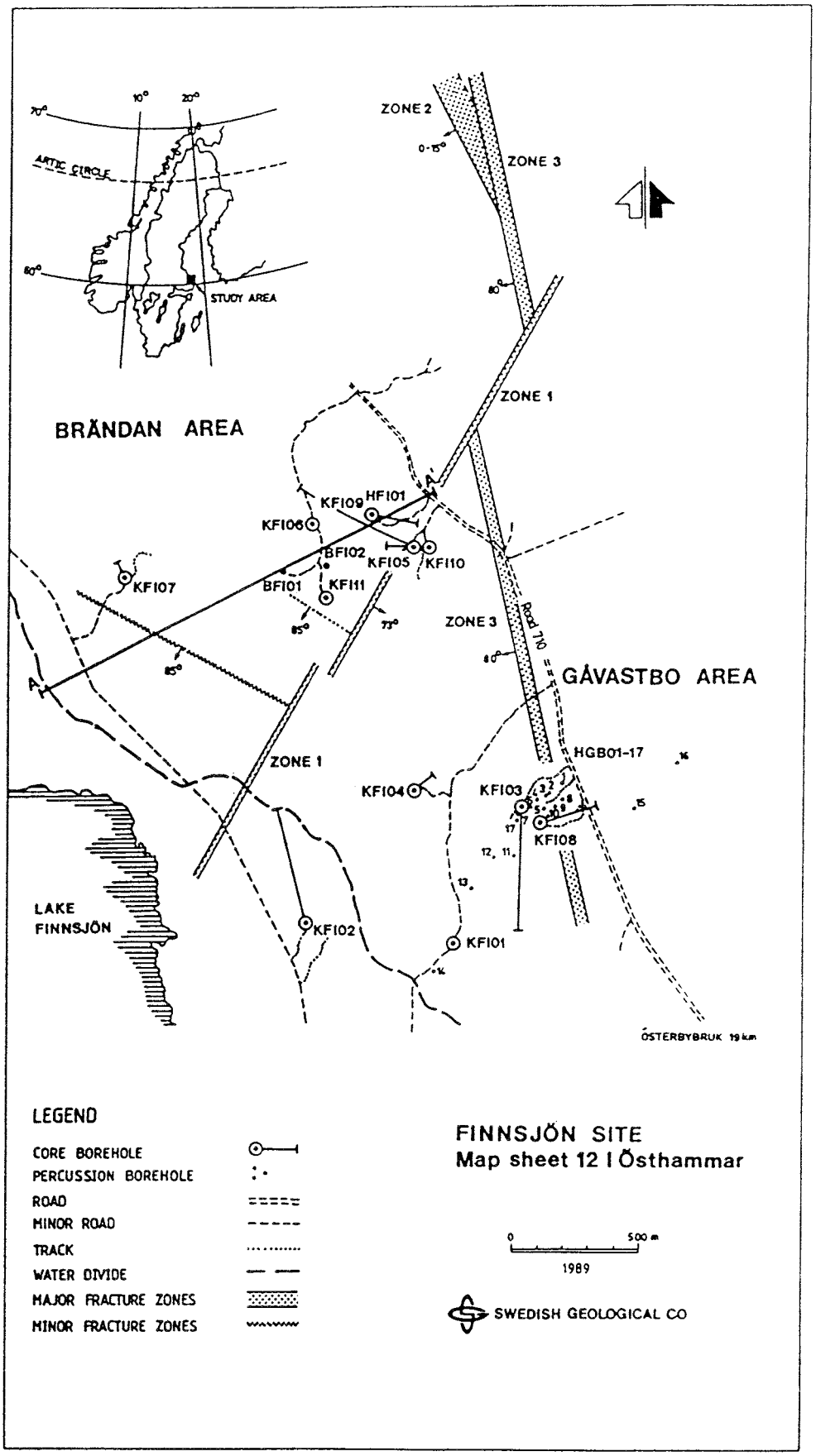


Figure 2–2 Map of the Finnsjön site showing borehole locations and fracture zones. The location of profile A – A' illustrated in Figure 2–3 is also marked.

Although Zone 2 is expressed as a 100 m wide, more or less altered zone, the fracture frequency is generally low, except for two to five sections in each borehole. These sections are narrow, 2–5 m wide (in some cases up to 30 m) and are mainly located at the upper and lower boundaries of the zone. In Figure 2–4 a tentative, early stage, fracture model of Zone 2 is presented. The zone is a planar shear zone from which minor, moderately inclined zones (splays) project upwards into the overlying rock block. Tension fractures are formed at the root zone of the splays and the splays are offset by vertical shears parallel to the direction of the displacement /Tirén, 1991/.

From a rock mechanical point of view, Zone 2 may not be considered as a distinct feature but rather as a part of the continuous rock mass. The features of major concern are the narrow highly transmissive parts of the zone, especially at and close to the upper bound of Zone 2 /Leijon & Ljunggren, 1992/. These narrow discontinuities can transfer normal compressive forces, resulting in only local disturbances in the vertical stress field. However, stress changes induced by glaciation and deglaciation may cause reactivation and shear displacements.

## 2.2 GEOHYDROLOGY

The geohydrology of the Brändan area is dominated by the two highly conductive fracture zones, The Brändan zone (Zone 1) and the low-angle zone (Zone 2).

Zone 1, the Brändan fracture zone, strikes NNE and dips 75 degrees to the east. The thickness of the zone is about 20 m and the lineament representing the fracture zone is well defined from surface geophysical measurements for more than one km of length. The hydraulic conductivity of Zone 1 ranges between 1 E–6 – 5 E–6 m/s (2 m intervals) as compared to 1 E–7 m/s in the country rock.

Zone 2, the low-angle fracture zone, is well defined in seven boreholes located within an area of approx. 500x500 m, where the Radially Convergent Tracer Test was conducted (Figure 2–2 and 2–3). In this area the fracture zone is almost planar with the upper surface located between 100 to 240 m below the ground surface. The orientation of Zone 2 is 28°W with a dip of 16 degrees to the west. The location of the lower boundary of the zone is somewhat uncertain. However, in general the zone has a thickness of about 100 m. The hydraulic character of Zone 2 has been extensively investigated by means of a large number of hydraulic tests performed within nine boreholes penetrating the zone. The zone typically consists of two to five narrow, highly transmissive ($T=1\text{–}4\cdot10^{-4}$ $m^2/s$), sections as illustrated in Appendix J by the results from the single hole injection tests for boreholes BFI01, BFI02, KFI06 and KFI11. Above the zone, a general decrease of transmissivity towards depth is observed. This decrease is interrupted by the upper bound of the zone, where transmissivity increases by one to four orders of magnitude. Thus, the hydraulic contrast between the upper part of the zone and the overlying rock is very high. Representative values of the hydraulic conductivity, measured in 2 m sections by single hole water injection tests, above and below the fracture zone are 5 E–8 and 1 E–9 m/s,

respectively. Within the fracture zone the mean value is 5 E-6 m/s, but the hydraulic conductivity is higher in the upper and lower margins of the fracture zone, where the values are 2 E-4 and 1 E-5 m/s respectively, while other parts have conductivities similar to the country rock.

Detailed hydraulic testing indicates that the highly transmissive sections have a width of only about 0.5 m. Interference tests and the preaparatory tacer test /Andersson et al., 1989/ have shown that the upper highly transmissive "subzone" is hydraulically interconnected between the boreholes over a distance of several hundred meters. Within Zone 2 there are several narrow parts (minor shear and fracture sub-zones) with high transmissivity separated by bedrock with low transmissivity. These "subzones" cannot be geometrically correlated as planar structures between the boreholes, c.f. Figure 2-2 and Appendix J.

## 2.3 HYDROCHEMICAL CHARACTER

The groundwater chemistry of Zone 2 and the surrounding bedrock is characterized by the sharp distinction between the non-saline (calcium-bicarbonate type) and saline waters via a transition zone of mixing in the upper part of Zone 2. The salinity shows an abrupt increase of more than 5000 mg/l of equivalent chlorine at the uppermost part of Zone 2, as measured in all boreholes intersecting the zone. The salinity remains high from the upper part of the fracture zone and downwards. The pH, in contrast, shows a decrease with depth from just above Zone 2, which is contrary to that normally indicated by Swedish groundwaters at increasing depth /Smellie & Wikberg, 1991/. The redox conditions, defined by the Eh and the contents of ferrous iron, uranium, and dissolved oxygen, are reducing within Zone 2.

The stable isotope data shows very little variation with depth and can be considered to be meteoric in origin. Radioisotope data clearly indicate the extent of a young, near-surface derived component characterized by high amounts of modern-derived carbon and significant tritium contents. With increasing depth and salinity the groundwater rapidly exhibits a reduction in modern-derived carbon with a minimum at the lower horizons of Zone 2. At these depths no significant tritium has been detected /Smellie & Wikberg, 1991/.

Based on the hydrochemical data available, the upper part of Zone 2 seems to act as a "sump" whereupon saline water from below the zone is mixed with non-saline water from above the zone. Interestingly, the mixed water has a similarly high carbonate content as the non-saline water. This implies the water has been subject to carbon dioxide diffusion after mixing with the saline water. Below Zone 2 the water has a constant composition with increasing depth which indicates that there is very little, if any, flow. This is also supported by the moderate to high uranium activity ratios recorded from borehole KFI09 /Smellie and Wikberg, 1991/.

The fact that Zone 2 acts as a barrier between the different types of groundwaters is not a unique occurrence, similar conditions have been found

elsewhere, e.g. in Finland. However, the Fracture Zone Project constituted the first detailed investigation of the phenomenon.

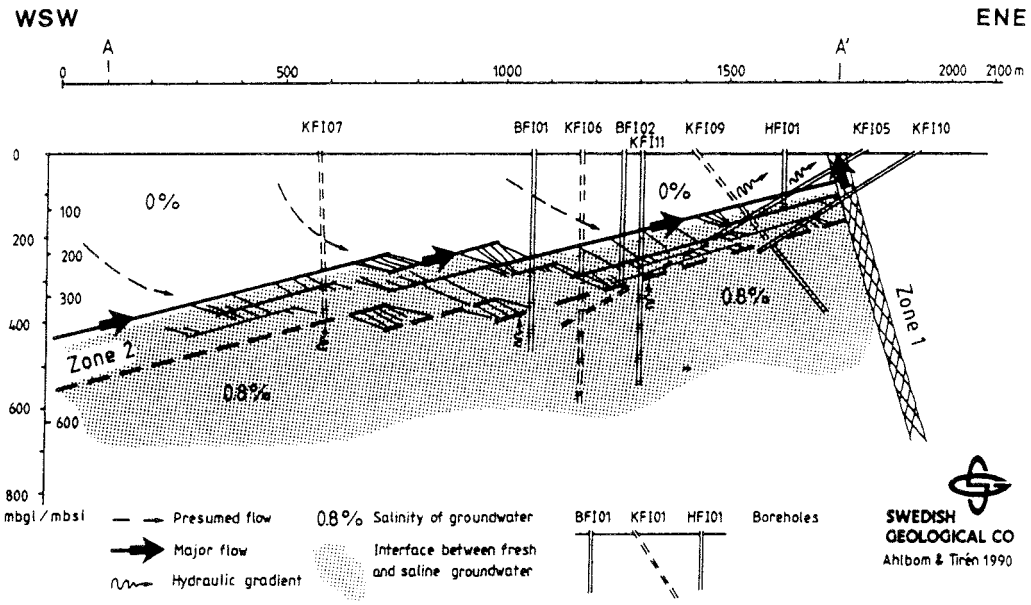


Figure 2–3 Schematic cross–section showing late fracture characteristics of Zone 2. Tentative groundwater flow conditions during natural gradient conditions is also marked. The boreholes are projected into the profile.

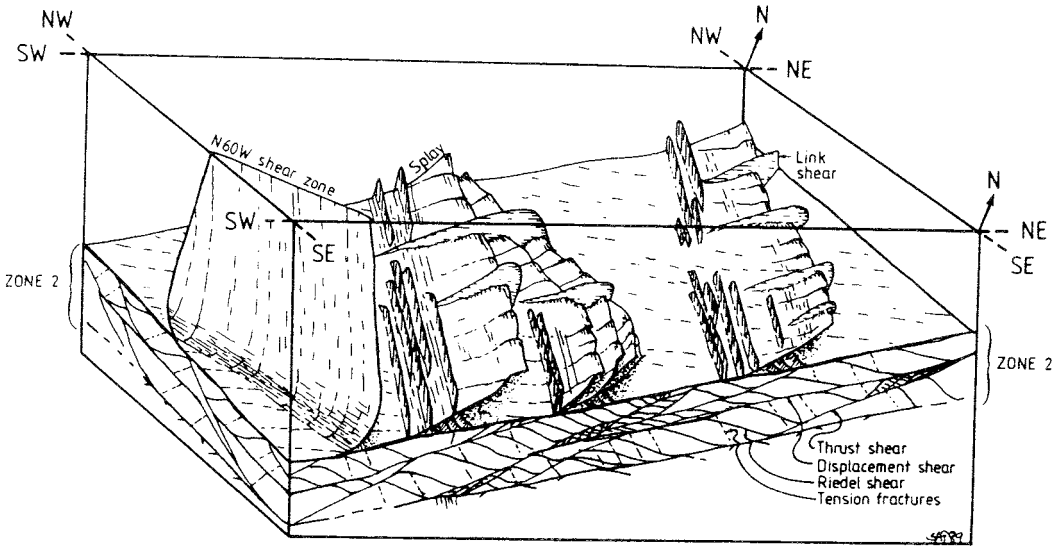


Figure 2–4 Tentative fracture model of Zone 2 at an early stage at is was formed in a thrust regime with maximum compression to the north–east /Tirén, 1991/.

## 2.4 GROUNDWATER FLOW CONDITIONS

The natural groundwater flow distribution in the Brändan area is most likely governed by Zone 1 and Zone 2. Piezometric measurements have simultaneously been made in packed-off intervals of the boreholes penetrating the low-angle zone and also in the Brändan zone. In the boreholes, up to five sections have been measured above and within the zones. The measurements of the groundwater table indicate a weak groundwater gradient varying between 1 m/350 m in the western part of the area to 1 m/150 m in the eastern part and directed towards ENE, see Figure 2-5. Within Zone 2, the direction and the gradients are roughly the same, see Figure 2-5. Zone 2 seems to act as a drain in the part of the area where it is deepest below the ground surface, while in the shallow parts, near the Brändan zone, it seems to be discharging water to the Brändan zone. A tentative model of groundwater flow in Zone 2 during natural gradient conditions is presented in Figure 2-3.

Based on natural flow rates determined with the point dilution method and estimates of possible infiltration rates from the upper bedrock, it can be concluded that regional groundwater flow to a large extent contributes to the groundwater flow in Zone 2 /Gustafsson and Andersson, 1991/.

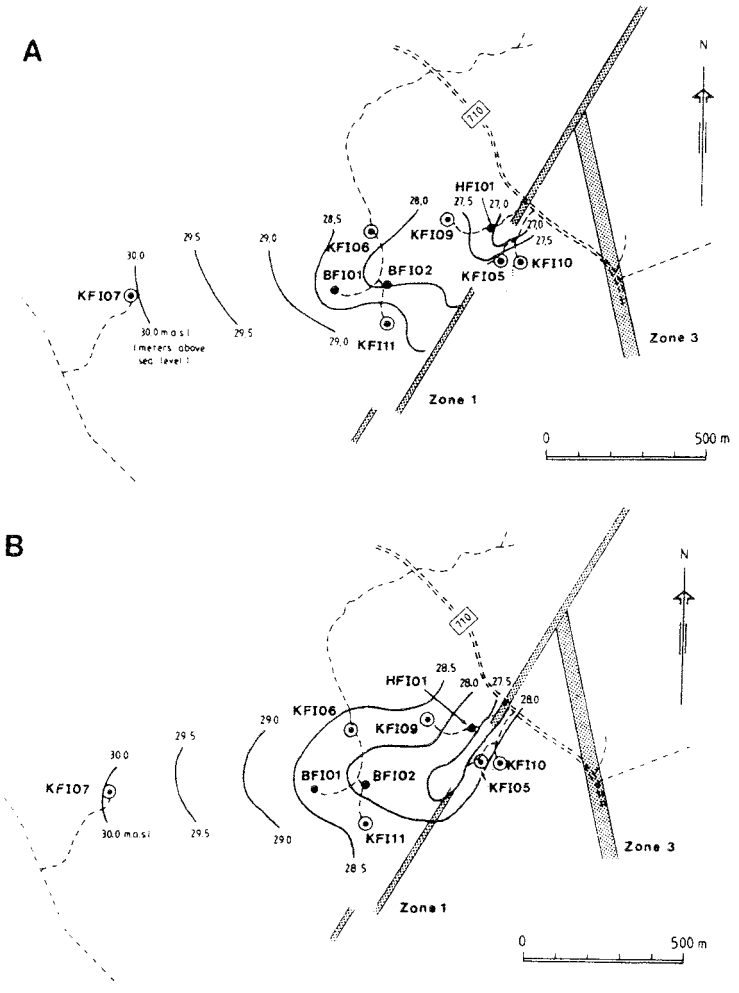


Figure 2-5 Map of the Brändan area illustrating A) the elevation of the groundwater table and B) the distribution of the hydraulic head in the upper part of Zone 2.

# 3. EXPERIMENTAL DESIGN

## 3.1 GENERAL OUTLINE

The tracer test was performed in a radially converging flow geometry in Zone 2, the low-angle major fracture zone in the Brändan area. The converging flow field was created by pumping in borehole BFI02. Tracer injections were made in three peripheral boreholes; BFI01, KFI06 and KFI11, located in different directions from the tracer withdrawal borehole BFI02. The borehole locations are presented in Figure 2-1, and a schematic of the flow field geometry in Figure 3-1.

The tracer injections in Zone 2 were made in three packed-off intervals in each borehole, enclosing sub-zones of Zone 2. The withdrawal borehole BFI02 was pumped in a packed-off interval enclosing the whole thickness of Zone 2, see Figure 3-2. Sampling for tracer content was made at the surface in the discharged water from BFI02. In addition also a sampling of major conductors (sub-zones) within Zone 2 was performed towards the end of the tracer injection, by straddle packer pumping in borehole BFI02.

The chosen pump geometry made it possible to maintain the same relative gradient within the whole thickness of Zone 2. Hence, interconnections between higly conductive intervals of Zone 2 may be determined from the sampling of major conductors in borehole BFI02.

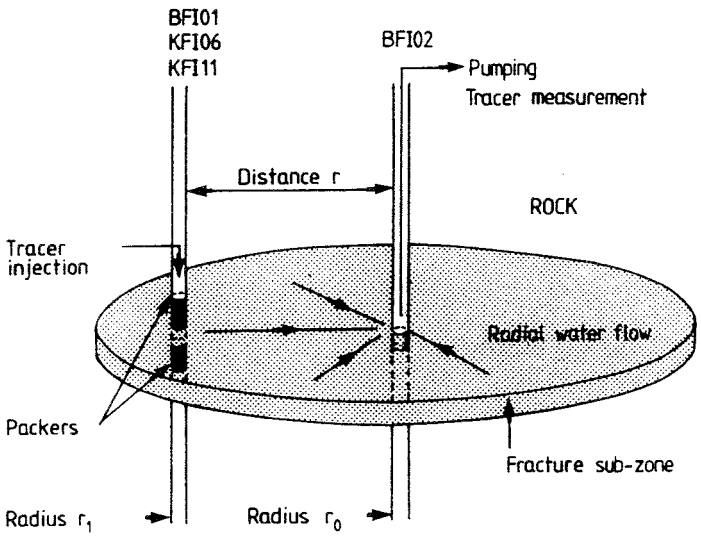


Figure 3-1 Conceptual model of the radially converging tracer test.

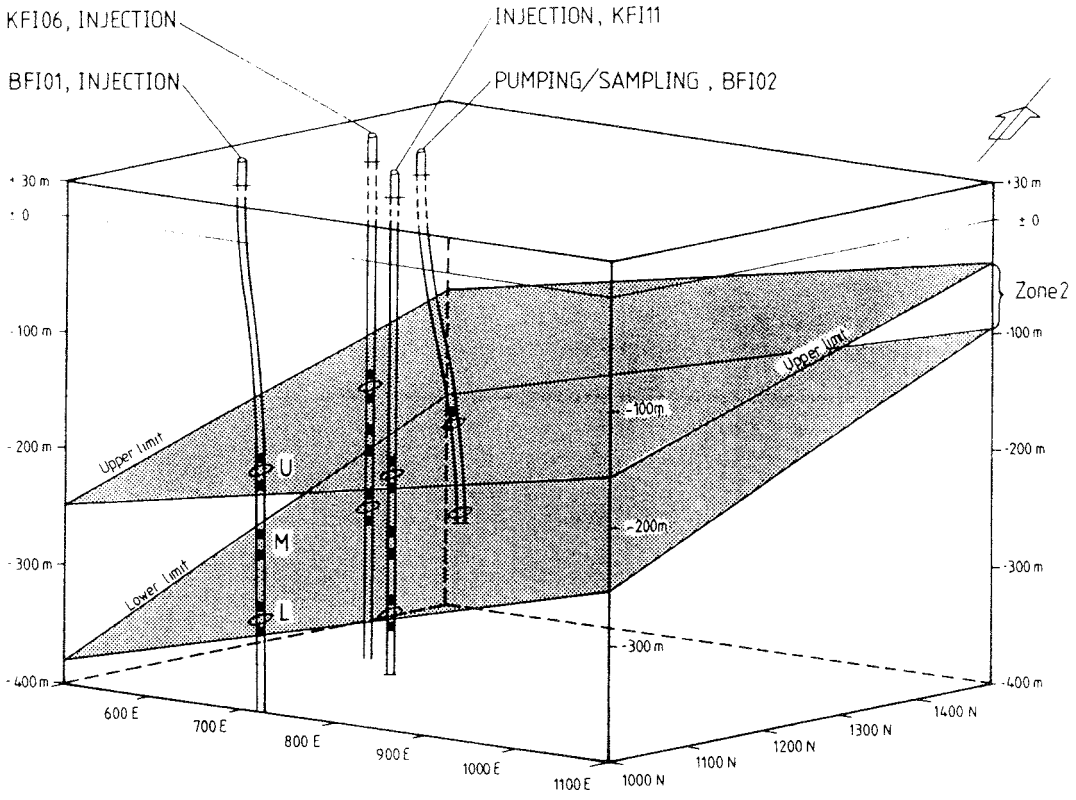


Figure 3–2 Geometry of the experimental set–up.

## 3.2 TRACER INJECTIONS

The tracer injections were performed in two different ways, continuous (extended step inputs) and as pulse injections. Totally 11 different tracers were injected in 9 borehole sections, 8 of the tracers were injected continuously for 5–7 weeks and the remaining three tracers were injected as pulses.

The continuous injections were made without applying any excess pressure in the borehole sections. The groundwater flowing through the borehole sections were continuously labelled with concentrated tracer solutions during complete mixing. This injection technique requires knowledge about the groundwater flow rates through the borehole sections intended for tracer injection. For that purpose the groundwater flow rate through the injection sections were determined by the dilution method prior to the tracer injections. The pulse injections were made according to two different techniques, forced pulse and decaying pulse, i.e. without excess pressure.

The borehole sections used for the tracer injections in BFI01, KFI06 and KFI11 were selected primarly from the results of the hydraulic injection tests in 2–m intervals described by Andersson et al. /1988a/. The transmissivities were calculated using the steady–state solution given by Moye /1967/.

In each borehole, three intervals were selected, one in the upper highly conductive part of Zone 2, one at the lower boundary of Zone 2 and the third at the most highly conductive part in between. The injection sections chosen are listed in Table 3–1 together with the transmissivities, length of the sections and the type of injection adopted (continuous and/or pulse).

Table 3–1. Borehole sections chosen for tracer injections.

| Borehole | Section (m) | Length (m) | Diameter (m) | Transmissivity T ($m^2/s$) | Hydr. Cond. K (m/s) | Type of injection |
|---|---|---|---|---|---|---|
| BFI01 | Upper; 241.5 - 246.5 | 5.0 | 0.169 | $1.3 \cdot 10^{-3}$ | $2.6 \cdot 10^{-4}$ | cont. |
| | Middle; 263.5 - 266.5 | 3.0 | 0.168 | $2.5 \cdot 10^{-6}$ | $8.3 \cdot 10^{-7}$ | cont. |
| | Lower; 351.5 - 356.5 | 5.0 | 0.166 | $1.0 \cdot 10^{-4}$ | $2.0 \cdot 10^{-5}$ | cont. |
| KFI06 | Upper; 212.0 - 217.0 | 5.0 | 0.056 | $5.6 \cdot 10^{-4}$ | $1.1 \cdot 10^{-4}$ | forced p. |
| | Middle; 236.5 - 239.5 | 3.0 | 0.056 | $4.2 \cdot 10^{-6}$ | $1.4 \cdot 10^{-6}$ | cont. |
| | Lower; 252.5 - 271.5 | 19.0 | 0.056 | $6.7 \cdot 10^{-4}$ | $3.5 \cdot 10^{-5}$ | cont. |
| KFI11 | Upper; 221.5 - 226.5 | 5.0 | 0.056 | $3.7 \cdot 10^{-4}$ | $7.4 \cdot 10^{-5}$ | cont.+ decay p. |
| | Middle; 287.5 - 294.5 | 7.0 | 0.056 | $1.6 \cdot 10^{-6}$ | $2.3 \cdot 10^{-7}$ | cont. |
| | Lower; 329.5 - 338.5 | 9.0 | 0.056 | $1.5 \cdot 10^{-5}$ | $1.7 \cdot 10^{-6}$ | cont. |

cont. = passive continuous injection, without excess pressure
forced p. = forced pulse injection
decay p. = decaying pulse injection, without excess pressure

### 3.2.1 Tracers Used

The tracers had to be very carefully selected considering the long distances involved in the tracer test and the predicted relativly long residence times from some injection points. The high transmissivity of Zone 2 also required a large dynamic range of the tracers used. The chosen pump capacity of 2 l/s for tracer withdrawal implied that the dilution of the tracers would be about 1:60 000 at steady–state concentration. The minimum allowable dilution then had to be in the order of 1:1 000 000 to achieve good enough resolution in the early breakthrough data. Thus, elements which are naturally present in the groundwater at ppm–levels could not be used.

There was a need for at least ten different tracers. One for the dilution measurements at which the groundwater flow were determined through the borehole sections selected for tracer injections. Nine tracers for injections during the test, one tracer per selected injection point. Tests of tracers were therefore started within the supporting research programme for the radially converging tracer test. Primarily DTPA and EDTA complexes with rare earth metals were tested.

The tracers finally chosen for the radially converging tracer experiment were seven rare earth metal DTPA and EDTA complexes, three fluorescent dye tracers and two ionic tracers. The tracers used are listed in Table 3–2, below.

The fluorescent dyes and one of the ions had earlier been used in tracer tests performed in Swedish crystalline basement rock. They had good records of stability, dynamic range and low tendency for sorption. The dyes Uranine (Sodium Fluorescein) and Amino G Acid were used during the tracer test and Rhodamine WT was used for the groundwater flow determinations prior to the tracer experiment. The ions selected were $I^-$ and $ReO_4^-$.

The fluorescent dyes were analyzed with a Sequoia–Turner filter fluorometer and Iodide with an ion–selective electrode. Rhenium was analyzed with ICP/MS (Inductively Coupled Plasma Mass Spectroscopy).

Metal–EDTA complexes have previously been used in groundwater tracer experiments by Knutsson et al. /1963/ and also at the Finnsjön study site by Gustafsson and Klockars /1981/. Laboratory tests of various EDTA complexes have been reported by Heemstra et al. /1961/ among others. The test programme for the candidate tracers to be used in the radially converging tracer test involved stability, solubility, sorption and interference effects. These tests are reported in Byegård & Skålberg /1992/.

The DTPA and EDTA complexes chosen are relatively stable, have low tendency for sorption and are easy to synthezise. The background concentrations of the rare earth metals were also very low, in the order of 0.01–0.1 ppb which made them suitable for this particular tracer test. The metals could be detected down to 0.01 ppb with an ICP/MS equipment.

Table 3–2. Tracers used in the radially converging tracer test.

| Element | | Atomic Number | Chemical Form |
|---|---|---|---|
| Indium | (In) | 49 | ] |
| Dysprosium | (Dy) | 66 | |
| Holmium | (Ho) | 67 | M–EDTA complexes |
| Erbium | (Er) | 68 | |
| Tulium | (Tm) | 69 | |
| Ytterbium | (Yb) | 70 | ] |
| Gadolinium | (Gd) | 64 | M–DTPA complex |
| Iodide | (I) | 53 | $I^-$ |
| Rhenium | (Re) | 75 | $ReO_4$– |
| Uranine | | | |
| Amino G Acid | | | Fluorescent dyes |
| Rhodamine WT | | | |

All the above listed tracers except Iodide were diluted to their chosen initial concentrations with distilled or deionized water. Iodide was mixed with groundwater pumped from the injection borehole section prior to the tracer test and kept under anoxic conditions. After the mixing, all the tracer storage tanks were closed and bubbled with compressed nitrogen throughout the

duration of the injection procedure to keep lowest possible oxygene content.

The selection of tracers for the different injection intervals was made according to Table 3-3 below. The natural background concentrations are also given. Dye tracers show apparent concentrations due to fluorescent species naturally occuring in the groundwater.

Table 3-3. Tracer selection and background concentrations, $C_b$, of the rare earth metals and other species used as tracers. Concentrations in ppb.

| Borehole | Injection point Upper | | Middle | | Lower | |
|---|---|---|---|---|---|---|
| BFI01 | In-EDTA | 0.10 | Uranine | 3.0 | Ho-EDTA | 0.08 |
| KFI06 | Iodide | 3.0 | Yb-EDTA | 0.25 | $ReO_4^-$ | 0.05 |
| KFI11 | Gd-DTPA | 0.23 | Er-EDTA | 0.12 | Dy-EDTA | 0.20 |
| | Tm-EDTA | 0.01 | | | | |
| | Amino G | 120 | | | | |

### 3.2.2 Dilution Measurements

The technique used for the continuous tracer injections required that the groundwater flow rate through the borehole injection sections (Table 3-1) were known. Therefore dilution measurements were performed before the tracer injections were made, but after a steady-state groundwater flow field was obtained after about three weeks of pumping in the withdrawal borehole BFI02. The dilution measurements also clearly showed if the borehole sections selected for tracer injections belonged to an active, flowing part of the fracture zone with a pattern of connected partly open fractures.

The borehole injection sections were connected to a circulation pump at the ground surface with two nylon tubes, as shown in Figure 3-5. The downward tube outlet at the bottom of the section and the inlet at the top. A small amount of RdWT tracer was constantly added to the circulating water system during one mixing cycle. The tracer concentration then decreased as the groundwater flowing through the borehole section diluted the tracer labelled water. According to the solution of the equation of continuity the dilution of the tracer, as a function of time, is proportional to the groundwater flow rate through the borehole section. At complete mixing in the borehole injection section the groundwater flow rates through the injection sections then could be determined from:

$$Q_w = -(V \cdot \ln C/C_0)/t \qquad (3.1)$$

where V is the volume of the borehole interval and C is the concentration at the time t after tracer injection. The results of the dilution measurements are presented in Table 4–8.

### 3.2.3 Injection Procedures

#### 3.2.3.1 Passive Continuous Injection

In order to minimize dispersion effects in the injection borehole caused by large borehole volumes and/or trapping effects, a new injection technique was developed. Passive continuous injecton, i.e. labelling the groundwater flowing through the borehole injection sections at instantaneous and complete mixing and without applying any excess pressure. The injection technique, which is schematically described in Figure 3–3, also has the advantage that the source term, i.e. tracer mass release per time unit from the injection section can be measured. Enhanced tailing and/or dispersion due to tracer forced out into stagnant parts of fractures is also avoided. However, a drawback is that relatively sophisticated equipment is needed to perform continuous injections according to this technique.

The passive continuous injection was made in the following way:

Groundwater was pumped from the packed-off borehole section through a nylon tube by a pump placed at the ground surface. The water was then discharged back to the packed-off interval through another nylon tube, giving a closed circulating system with a constant flow rate, $Q_c$. Concentrated tracer solution with a concentration $C_{00}$ was injected into the circulating system, with a constant flow rate, $q_{inj}$. At the same time, water was discharged from the system with a constant flow rate, $q_{out}$.

Assuming:

$$q_{inj} = q_{out} = q \tag{3.2}$$

$$Q_c \gg q \tag{3.3}$$

i.e. no pressure buildup caused by the injection and total mixing of the tracer, the equation of continuity can be written:

$$(C_0 \cdot Q_w) + (C_0 \cdot q) = (C_b \cdot Q_w) + (C_{00} \cdot q) \tag{3.4}$$

where $C_0$ is the concentration of tracer in the packed-off section, $C_b$ is the background concentration in the groundwater and $Q_w$ is the groundwater flow rate through the borehole section. Assuming $C_b = 0$, Equation (3.4) can be written:

$$C_{00} = C_0(Q_w+q) / q \tag{3.5}$$

i.e. the concentrated tracer solution, $C_{00}$, needed for a chosen injection concentration in the borehole section can be calculated if the groundwater flow rate through the borehole section is known. Hence, the groundwater flow rate, $Q_w$, has to be determined prior to the start of injection. This was done by means of dilution measurements, using the same equipment as for the tracer injections.

In order to achieve good initial mixing of the tracer in the injection section, the volume of concentrated tracer solution necessary to get the correct $C_0$ calculated from Equation (3.5), was added during one circulation cycle of the system. After this first circulation cycle, the injection pump rate, $q_{inj}$, was shifted to the constant flow rate chosen for the continuous injection.

Intermittent measurements of injection and discharge rates, $q_{inj}$ $q_{out}$, and their concentrations respectively, $C_{00}$ $C_0$, were used to determine the tracer mass release per time unit to the fracture system.

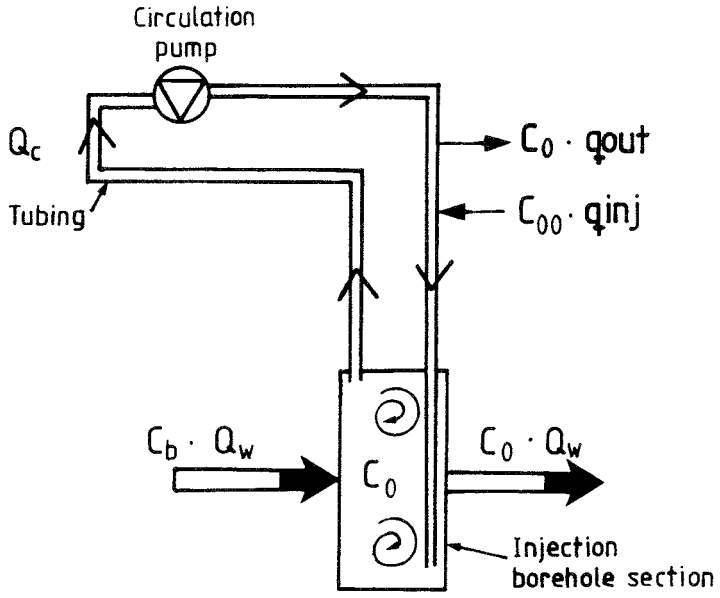


Figure 3–3 Schematic of the injection and circulation system.

### 3.2.3.2 Decaying Pulse Injection

Two tracers were injected with the decaying pulse injection technique. A tracer pulse is instantaneously introduced and completely mixed in a clearly defined borehole section. The tracer labelled water in the borehole section will be released to the connected system of flowing fractures following a logarithmic decay, analogous to the principles of dilution measurements, section 3.2.2. The injection is well defined in time and space, e.g. no dispersion of the tracer in the injection borehole section. No disturbance of the groundwater flow field and no tracer forced out to a unknown distance, and maybe also to stagnant parts, in the adjacent fracture system.

The injection technique is relatively easy to perform. A continuous follow up of the tracer concentration in the injection section also makes it possible to get a measure of the tracer mass release per time unit to the fracture system.

#### 3.2.3.3 Forced Pulse Injection

Forced pulse injection was accidently applied to one tracer. A volume of tracer solution is then forced into the fracture system by excess pressure during a short time period.

### 3.2.4 Equipment

The equipment used for the tracer injections is schematcally presented in Figures 3–4 and 3–5 and consisted of the following components:

- circulation pump
- injection pump
- precision valve
- regulation valves
- filters
- tubing
- storage tank
- inflateable packers

**The circulation pump** was used to circulate the borehole water in order to achieve complete mixing. The pump should preferably be placed as close to the injection interval as possible in order to avoid large tubing volumes. However, two of the boreholes used, KFI06 and KFI11, only have a diameter of 56 mm which made it very difficult to install pumps within the boreholes, especially when each borehole also had three packed–off injection sections. It was therefore necessary to place the pumps at the ground surface. The chosen pump type was an electric centrifugal pump, self–priming to 5 m.

**The injection pump**, used to inject tracer into the circulating system, was a plunger pump with a capacity range of 1–10 ml/min.

In order not to create any excess pressure in the injection interval, water has to be discharged from the system ($q_{out}$) at the same flow rate as the concentrated tracer solution is injected ($q_{inj}$). This was made through a **fine precision needle valve**. Thus, the water discharged through this valve should have a constant concentration of tracer if the mixing is good. In addition to the needle valve, several **regulation and shut off valves** are needed for regulation of the circulation flux and for manual sampling of the borehole fluid and the concentrated tracer solution. The valves also simplifies the replacement of defect parts during the tracer test.

**Filters** were used to prevent damage to the injection pump and the precision valve caused by particles.

The choise of **tubing** dimensions was restricted by the maximum allowed pressure drop and the available space in the boreholes. Theoretical calculations of the pressure drop in the circulation system indicated that the minimum inside diameter of the suction tubing could be 8 mm. The

maximum outside diameter that could be used in a 56 mm borehole was 10 mm. Hence, the chosen tubing (nylon PA 12) had the dimensions 10/8 mm (outside/inside diameter). In the large diameter borehole BFI01 (dia. 150 mm), the tubing dimensions were increased to 12/10 mm in order to increase the circulation flux. A third tube from each borehole interval with the dimensions 6/4 mm (increased to 10/8 mm in upper part of borehole) was used for pressure registration. In total 10 tubes from each borehole including the inflation tube to the packer system.

The **storage tanks** for concentrated tracer solutions, $C_{00}$, were made of Polyethylene and designed to maintain low-oxygene conditions by nitrogen bubbling through the tracer solution. A check valve opening at 1 psi excess pressure ensured that no air could enter the tanks except than through diffusion. Two volumes were used 500 and 1200 litres.

The **inflatable packers** were specially designed with 10 connections. The packers were water filled and inflated hydraulically with compressed nitrogen.

The equipment and the passive continuous injection technique was tested both in laboratory and in a borehole test and found to be applicable to field conditions. The tests are described by Andersson et al. /1988b/.

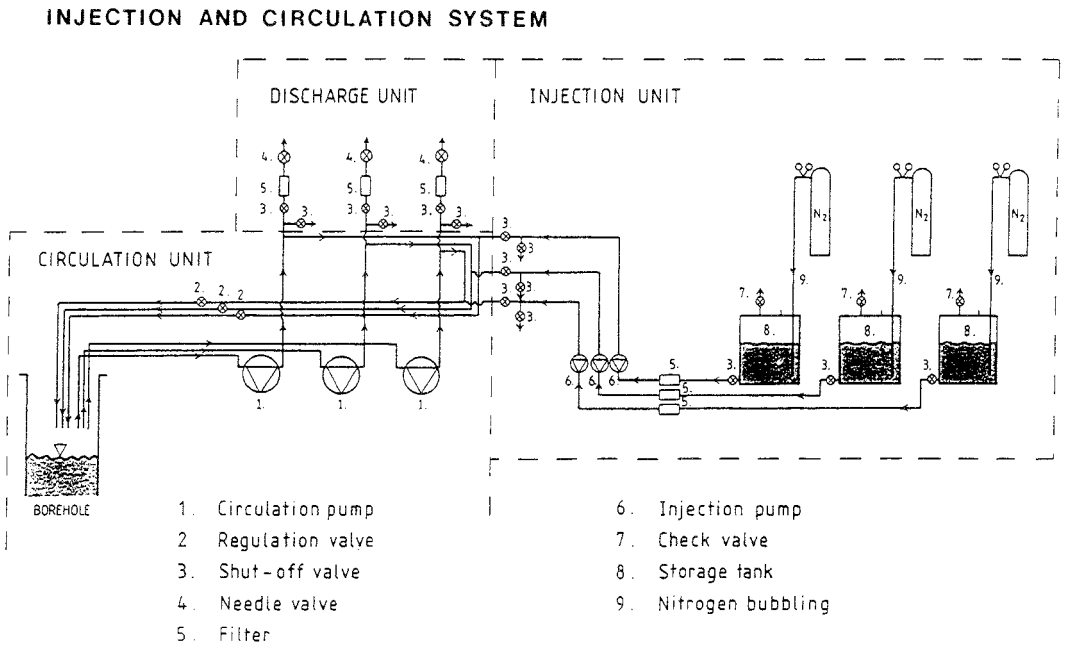


Figure 3-4 Injection and circulation system at ground surface.

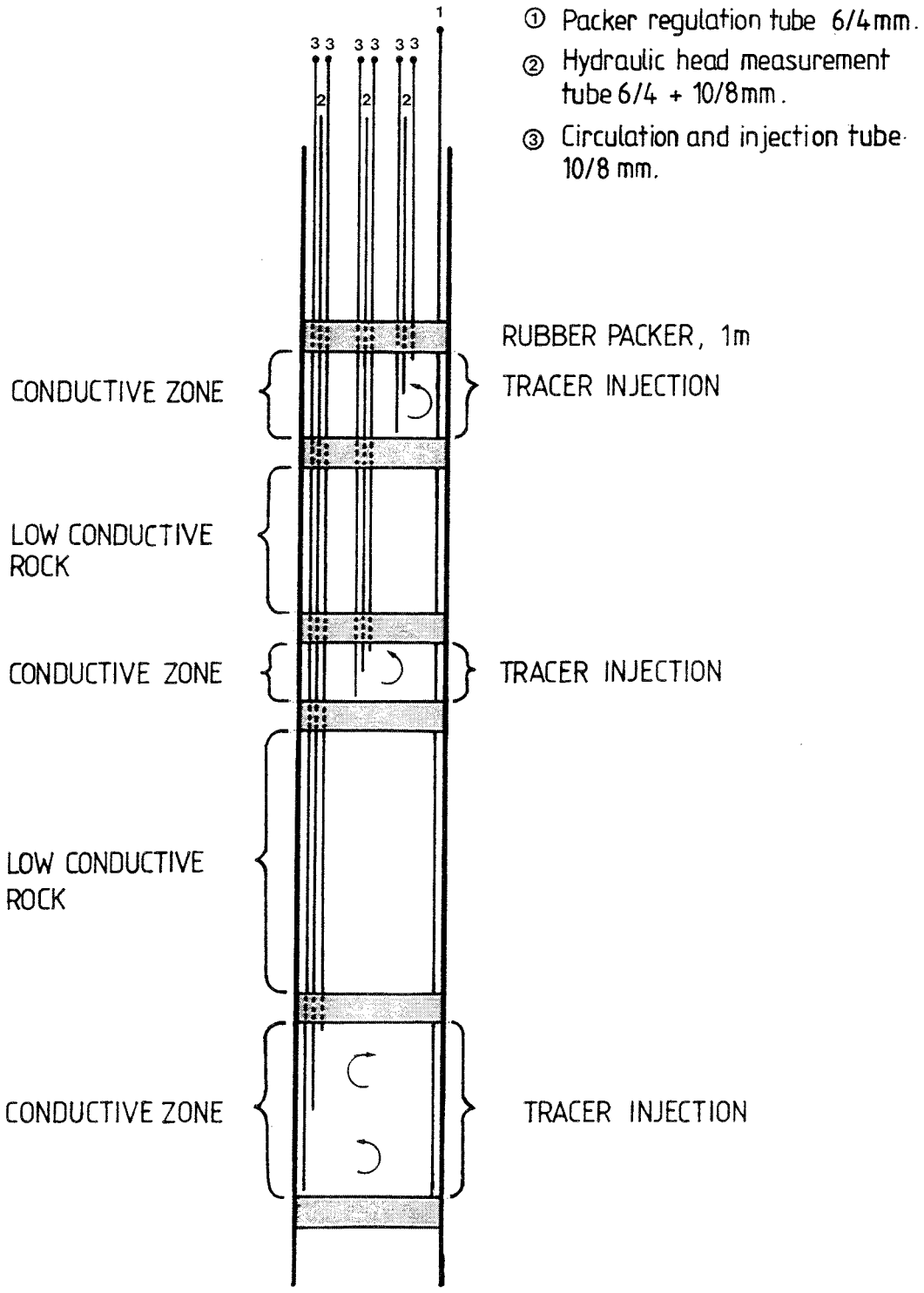


Figure 3–5 Principal outline of instrumentation in injection boreholes.

## 3.3 PUMPING FOR TRACER WITHDRAWAL

The tracer withdrawal was made by pumping in borehole BFI02 from a packed-off interval including the entire thickness of Zone 2, see Figure 3-6. However, the borehole was only drilled to 288 m depth i.e. just penetrating Zone 2 implying that only one packer at the upper limit of Zone 2 was needed.

In Table 3-4 the basic data from the tracer withdrawal are listed. The transmissivity value was derived from Ekman et al./1988/. Plots of the pumping capacity versus time are given in Appendix A. In addition, the temperature and electrical conductivity of the pumped water was measured. These plots are also presented in Appendix A.

Table 3-4 Basic data for tracer withdrawal in borehole BFI02.

| | |
|---|---|
| Pumping interval: | 193.0 m - 288.7 m |
| Section length: | 95.7 m |
| Borehole diameter: | 160 mm; 193 - 262 m, 152 mm; 262 - 288.7 m |
| Transmissivity: | 2.6 E-3 $m^2/s$ |
| Pumping rate: | 2.0 l/s |
| frictional loss: | < 0.01 m / 100 m at pumped rate 2.0 l/s |

The pumping for steady state was started on April 12th, dilution measurements May 6 and the tracer injections on May 27th. After beginning of tracer injections, pumping and tracer sampling continued for 4510 hours, i.e. about 6 months.

The groundwater head measurements indicated that the groundwater table was sinking slowly at the start of tracer injection but the head differences between the withdrawal and injection boreholes were constant. This suggests that steady state conditions were prevailing and that the sinking trend of the groundwater table was due to ordinary seasonal fluctuations. Plots of the groundwater level in the pumped interval are presented in Appendix A.

During the pumping, some pump stops occured due to power failure caused by stroke of lightning. The duration of these pump stops were registered and they are given in Appendix D. They are also plotted together with the breakthrough data.

A schematic of the withdrawal equipment for the radially converging tracer experiment is shown in Figure 3-6. During the experiment water was withdrawn from borehole BFI02 using a submersible pump placed immediately below the packer which delimits the pumped interval including Zone 2. The water was discharged through 193 m of 3" pipes and past a regulation valve where a small part of the flow was shunted through a filter to the sampling equipment. The water was finally discharged through 100 m of 6" pipes to a small wetland area north-east of BFI02.

The hydraulic head in the pumped interval and also the groundwater level was manually registered with an electrical summer device.

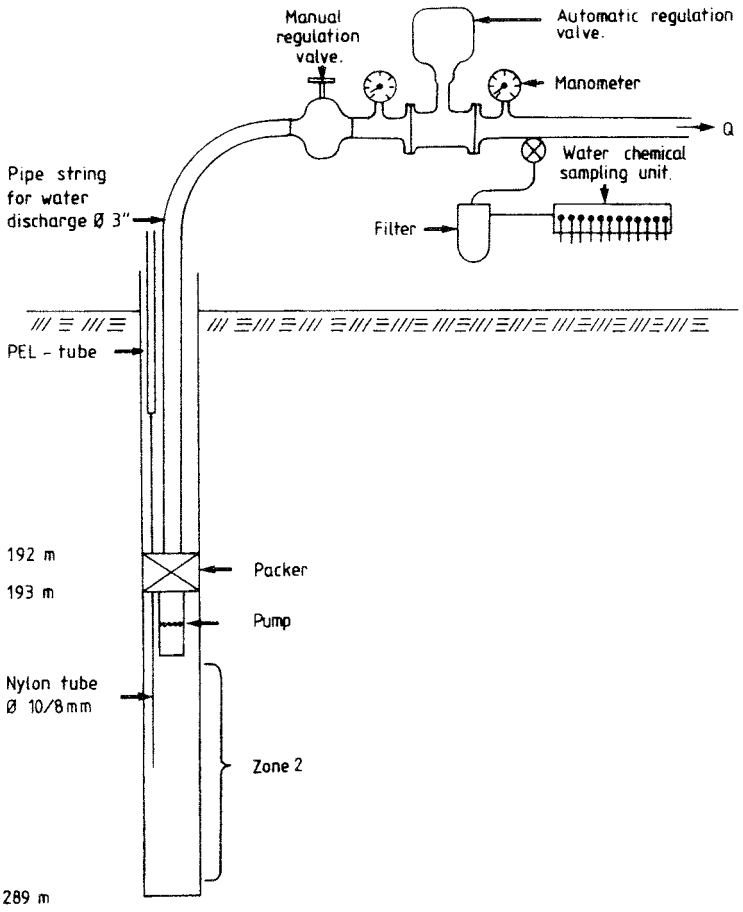


Figure 3–6 Equipment for pumping and tracer withdrawal in borehole BFI02.

## 3.4 TRACER SAMPLING IN WITHDRAWAL BOREHOLE

Sampling for tracer content was made in the discharge water at the ground surface throughout the tracer test. In addition, a sampling of major conductors (sub–zones) intersecting the withdrawal borehole BFI02 was made after the end of the tracer injections, between July 18–22nd, while the pumping was stopped for 104 hours. The pumping and sampling of the discharge water was restarted on July 22nd in the same manner and at the same pumping rate as before.

Three samples were taken at every sampling occasion. One preserved with nitric acid, for analysis of rare earth metal complexes. Two without any special treatment for ionic– and dye tracers.

### 3.4.1 Sampling of Discharge Water

The sampling was made with an automatic sampler connected to the

discharge pipe (Figure 3–6). The sampling equipment is shown in detail in Figure 3–7. It consisted of three units:

- time–step unit which controlled the time interval between the sampling occasions and the sampling duration

- distribution unit which made it possible to withdraw up to 16 samples at the same time

- sampling unit with 12 solenoid valves.

The time between each sampling occasion could be varied from 0.3 hours to 9 hours and the sampling duration from 1 to 9 minutes.

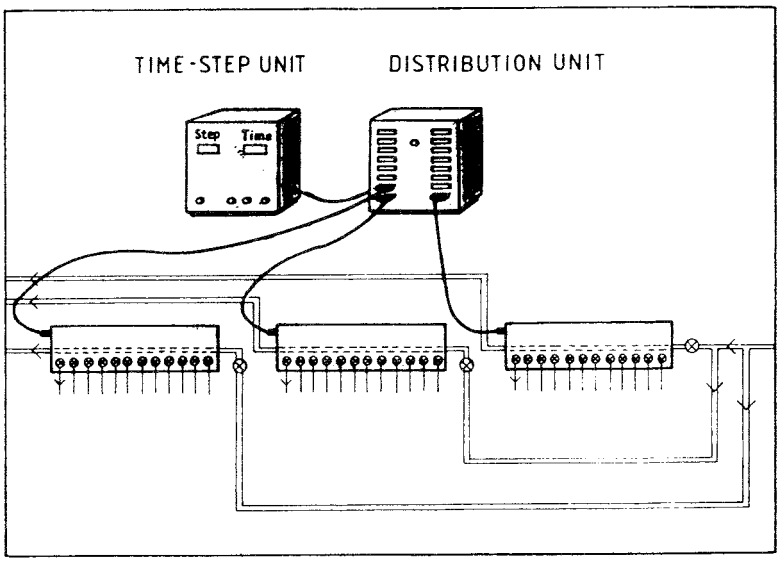


Figure 3–7 Sampling equipment.

### 3.4.2 Sampling of Major Conductors

Sampling of major conductors in the withdrawal borehole BFI02 was made in order to determine possible interconnections between highly conductive intervals (sub–zones) of Zone 2. Hence, seven highly conductive 2 m intervals of Zone 2 were chosen from the hydraulic test data reported by Ekman et al./1988/. The intervals chosen and the hydraulic transmissivities, respectively are presented in Table 3–5 below. The transmissivity of all sampling intervals summarized is $2.55 \cdot 10^{-3}$ $m^2/s$, which makes up almost 100% of the total transmissivity of the borehole and thus also of Zone 2.

The sampling of major conductors in BFI02 was made by pumping from 2–m sections inclosed by a duble–packer assembly (Figure 3–8). A suction pump placed at the ground surface and tubing down to the sampled section were used. The most important factor to be considered for the design of the equipment was the pump capacity versus the borehole interval volume. The pump capacity needed to be restricted to a maximum 2–3 l/min in order not to create too large drawdown and thereby cross–contamination of tracers

from different levels. Thereby, the borehole interval volume should be as small as possible. This was achieved by using short packer spacing, dummy infillings in the borehole interval and small tubing volumes.

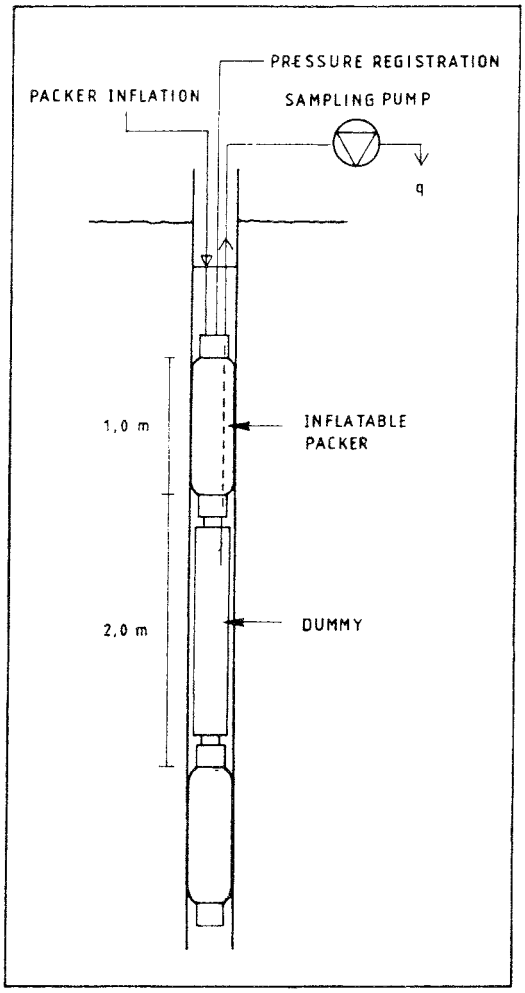


Figure 3-8 Equipment for sampling of major conductors in borehole BFI02.

The sampling was performed 1250 hours (52 days) after the beginning of tracer injection. The submersible withdrawal pump was removed from the borehole and the double-packer system described above was lowered to Interval No 1. Then pumping was started from the ground surface at a rate of 2 l/min and continued until at least 5 section volumes, including the tubing, had been withdrawn. During the pumping samples were taken at four occations for analysis of tracer content. The packers were then lowered to the next interval and the process repeated. After the sampling, the submersible pump and the packer was reinstalled in the borehole and the pumping of the entire Zone 2 was restarted with the same capacity (120 l/min) as before sampling. The results of the sampling in major conductors are presented in section 4.3 and Appendix E.

Table 3–5 Highly conductive intervals of borehole BFI02 chosen for the detailed sampling of Zone 2.

| Interval No | Depth (m) | Transmissivity, T ($m^2/s$) | Fraction of $\Sigma$ T (%) |
|---|---|---|---|
| 1 | 203.0 – 205.0 | $1.7 \cdot 10^{-3}$ | 66.7 |
| 2 | 208.0 – 210.0 | $1.9 \cdot 10^{-6}$ | 0.1 |
| 3 | 212.0 – 214.0 | $1.4 \cdot 10^{-5}$ | 0.5 |
| 4 | 238.0 – 240.0 | $1.6 \cdot 10^{-6}$ | 0.1 |
| 5 | 257.1 – 259.1 | $7.3 \cdot 10^{-6}$ | 0.3 |
| 6 | 260.0 – 262.0 | $8.2 \cdot 10^{-4}$ | 32.2 |
| 7 | 276.0 – 278.0 | $2.0 \cdot 10^{-6}$ | 0.1 |
| All | | $2.55 \cdot 10^{-3}$ | 100.0 |

## 3.5 SUPPORTING MEASUREMENTS

The supporting measurements can be divided into two groups; in situ measurements before and during the tracer injection and independent laboratory measurements. The in situ measurements made were:

- Hydraulic heads, h
- Groundwater flow rates through injection borehole sections, $Q_w$, during pumping in BFI02 with 2 l/s, but before, during and after tracer injection
- Determination of dispersivity and delay in the withdrawal hole BFI02
- Electrical conductivity and temperature in the withdrawn water from BFI02

### 3.5.1 Hydraulic Head

The hydraulic heads were monitored manually 2–5 times/week in all 9 injection sections in boreholes BFI01, KFI06 and KFI11 and in the pumped section of borehole BFI02. In addition, the groundwater levels were monitored in the above mentioned boreholes and also in boreholes KFI09 and HFI01 situated closer to Zone 1 (see Figure 2–1). From the head data, head differences were calculated which are presented in section 4.4.1 and Appendix A together with the groundwater levels.

### 3.5.2 Groundwater Flow Rates through Borehole Sections

The groundwater flow rates through borehole sections, $Q_w$, were determined in all the injection sections prior to the injection of tracers by means of the point dilution technique as described in section 3.2.2. Later, during the injection of tracers, sampling and analysis of the discharged tracer solution made it possible to calculate the groundwater flow rate from Equation (3.5). After stop of injection, the groundwater flow rate again could be determined from the dilution of tracer versus time according to Equation (3.1). The groundwater flow rates are presented in Table 4–8, section 4.4.2 and in

Appendix B.

### 3.5.3 Delay and Dispersion in Withdrawal Borehole

Prior to the start of tracer injection, a test was performed in the withdrawal borehole BFI02 in order to determine the delay and dispersion of the tracers in the borehole and sampling system. The borehole was packed off with an inflateable packer at 194 m depth. A submersible pump was attached just below the packer and connected to the surface with a pipe string (Figure 3-9). Two small tubes for tracer injection, emerging within the upper and lower highly conductive parts of Zone 2, were attached to a string of rods hanging below the pump. During pumping at the same flow rate as was intended to use in the radially converging tracer test, a concentrated Uranine tracer solution was injected. First in the upper tube, and later on in the lower tube. The injections were performed as continuous injections and the tracer breakthroughs were registered in the sampling equipment at the surface. Methods of interpretation are described below and the results are summarized in Table 4-9, section 4.4.3. The experiment is described in detail in Andersson et al./1988b/.

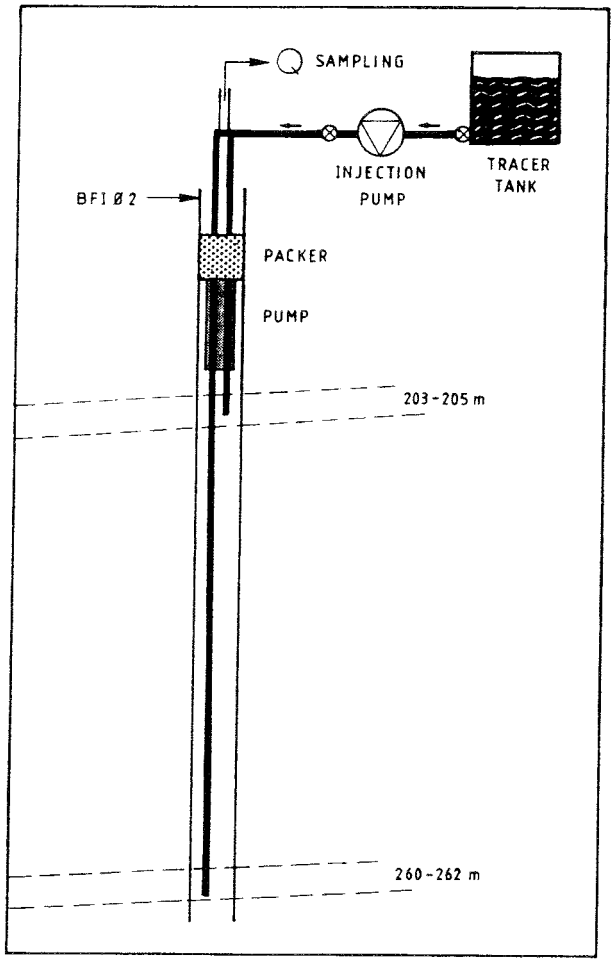


Figure 3-9 Test set-up of for determination of delay and dispersion in borehole BFI02.

The delay of a tracer from inflow to borehole at a major conductor and up to sampling tube at ground surface can be theoretically calculated if the distribution of the transmissivity, T, in the borehole and the position of the pump is known. The flow from each conductive interval, $Q_i$, can be determined from:

$$Q_i = Q \cdot T_i / T \tag{3.6}$$

where T is the total transmissivity of the pumped interval, $T_i$ is the transmissivity of the conductive interval and Q is the total pump flow rate. Knowing the volumes, $V_i$, of the borehole intervals corresponding to $T_i$ and the discharge pipe volume, the time delay for a plug flow may be calculated from:

$$t_d = \sum_i V_i/Q_i \tag{3.7}$$

The dispersion along the borehole of a tracer labelled inflow will be small if flow is turbulent. In that case dispersion may be calculated by using the equation derived by Taylor /1954/ for dispersion in straight pipes at turbulent flow.

$$D = 10.1 \cdot r_0 \cdot u_* \tag{3.8}$$

where D = dispersion coefficient
$r_0$ = radius of pipe
$u_*$ = shear flow velocity

$$u_* = v\,(f / 8)^{1/2}$$

where f is the Darcy–Weisbach friction factor which is determined from a Moody–diagram /Fischer et al., 1979/. Dispersivity along the borehole axis is then expressed by D/v.

The Reynolds number, Re, expresses the ratio between inertia and viscous forces and if Re is less than 2000 flow will be laminar. At $2000 < Re < 4000$ a transition to turbulent flow will appear and if Re is higher than 4000 inertia forces dominates and fully turbulent flow will be developed /Cederwall & Larsen, 1979/.

$$Re = v \cdot d/\nu \tag{3.9}$$

where v = mean velocity Q/A

d = diameter of tube
$\nu$ = kinematic viscosity ($1.31 \cdot 10^{-6}$ $m^2s^{-1}$ at 10 °C)

The dispersivity and delay, $t_{50}$, was also calculated from the expression given by Gelhar /1987/ for a step input case:

$$D/v = 3 \cdot r(\Delta t/t_{50})^2/(16 \cdot \pi) \qquad (3.10)$$

where $\Delta t$ and $t_{50}$ are defined as depicted in Figure 3–10 and r is the distance between injection and withdrawal. However, it should be noted that equation (3.10) is valid in a radially converging flow field and not within the pumping hole. The calculation is merely used to compare this apparent dispersivity with the dispersivities expected in the flow paths of the present radially converging tracer experiment.

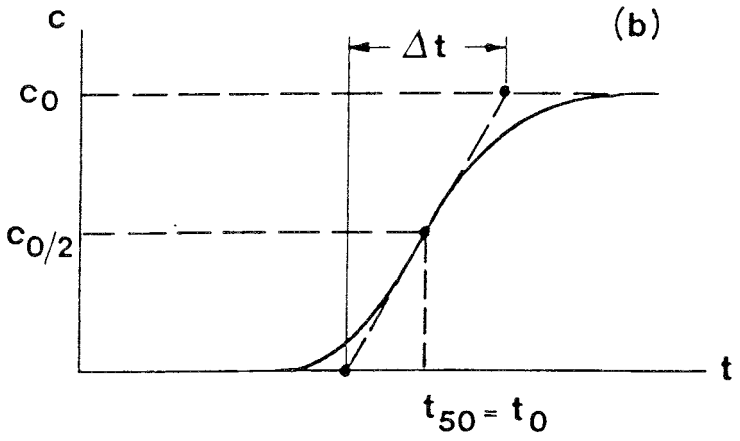


Figure 3–10 Schematic tracer breakthrough curve resulting from continous injection in a radial convergent tracer test /Gelhar, 1987/.

### 3.5.4 Electrical Conductivity and Temperature

The electrical conductivity and temperature were measured once a day in the withdrawn water from BFI02. The results are presented in Appendix A, page A:2. Electrical conductivity in waters withdrawn from the different inflow levels in BFI02 are presented in Table 4–6, section 4.3.

### 3.5.5 Laboratory Measurements

The amount of an injected tracer that can be delayed by diffusion into the rock matrix is determined by the residence time and the effective diffusivity. Therefore laboratory measurements of porosity and diffusivity were carried out on drillcore samples from boreholes KFI06 and KFI11, representing the rock adjacent to the fracture walls. The results aimed to be utilized in the intrpretation and transport modelling of the experiment. The measurements

were performed at the Dep. of Chemical Engineering at the Royal Institute of Technology, Stockholm (KTH). Results of the laboratory measurements are presented in section 4.4.4.

The rare earth metal–DTPA and EDTA complexes finally chosen for the tracer experiment were subject to comprehensive tests including stability, solubility, sorption and interference effects. The tests were performed at the Department of Nuclear Chemistry at Chalmers University of Technology, Gothenburg. The tests also included analysis of water samples from Zone 2 for determination of natural background concentrations of the tracers and for the groundwater chemistry of Zone 2 in general. Results of the laboratory measurements are presented in section 4.4.4.

# 4. EXPERIMENTAL RESULTS

## 4.1 TRACER INJECTIONS

### 4.1.1 Continuous Injections

The injection of tracers in the nine injection sections was started on May 27th with a time lag of 6 hours between the first and the last to be started. The procedure of injection is described in detail in section 3.2. The initial mixing of tracer was made during one circulation cycle of the system in order to achieve the best initial mixing possible. The circulation pump capacities varied somewhat depending on the tubing dimensions (see section 3.2.4) and also the volumes of the injection sections varied due to borehole diameter, length of the sections and tubing dimensions. The volumes of the injection sections and the circulation capacities are given in Table 4–1.

Table 4–1 Circulation pump capacities and volumes of the injection sections, including tubing and instrumentation.

| Borehole section | Circulation Pump cap. (l/min) | Volume (litres) section | tubing | total |
|---|---|---|---|---|
| BFI01:U | 2 | 106.2 | 31.8 | 138.0 |
| BFI01:M | 2 | 62.7 | 34.4 | 97.1 |
| BFI01:L | 2 | 104.8 | 45.7 | 150.5 |
| KFI06:U | 0.5 | 9.5 | 16.8 | 26.3 |
| KFI06:M | 0.5 | 5.8 | 18.7 | 24.5 |
| KFI06:L | 0.4 | 40.2 | 20.1 | 60.3 |
| KFI11:U | 0.5 | 9.5 | 17.6 | 27.1 |
| KFI11:M | 0.5 | 14.0 | 22.8 | 36.8 |
| KFI11:L | 0.4 | 18.9 | 26.1 | 45.0 |

U = Upper, M = Middle, L = Lower

The injection flow rate was set to 2 ml/min for all injections, however this flow rate being close to the lower limit for the pump was difficult to set exactly. The injection flow rates were therefore also registered as injected volume versus time by measuring the levels in the tracer storage tanks. The calculated mean injection flow rates, $q_{inj}$, and the initial concentrations, $C_{00}$, of the tracers injected are given in Table 4–2. The tracer volumes in the storage tanks versus time are presented in Appendix B and the total injected masses are given together with the recoveries in Table 4–5, section 4.2. The water volumes discharged from the circulating injection system were

collected and measured and a mean discharge rate, $q_{out}$, was calculated. Ideally the discharge rates should be equal to the injection rates in order not to create any excess pressure in the injection intervals. However, trapping of gas bubbles in the fine needle valves used to control the discharge rates, intermittently stopped the discharge completely leading to somewhat lower discharge rates. The discharged water was also sampled and analyzed in order to determine the tracer concentration in the injection interval and thereby calculate the tracer mass release per time unit into the fracture system and also the groundwater flow rate through the interval according to Equation (3.5). The discharge rates are given in Table 4-2 below and the tracer concentrations in the discharged water versus elapsed time are presented in Appendix B. Injection schemes, with calculated tracer mass release per time unit, are presented in Appendix G.

Table 4-2 Selected tracers, initial concentrations, $C_{00}$, injection mean flow rates, $q_{inj}$ and discharge rates, $q_{out}$.

| Borehole interval | Tracer | $C_{00}$ (ppm) | $q_{inj}$ (ml/min) | $q_{out}$ (ml/min) |
|---|---|---|---|---|
| BFI01:U | In-EDTA | 985 | 2.35 | 1.26 |
| BFI01:M | Uranine | 10139 | 1.84 | 0.73 |
| BFI01:L | Ho-EDTA | 3718 | 2.34 | 0.50 |
| KFI06:U | $I^-$ | 177800 | forced pulse | - |
| KFI06:M | Yb-EDTA | 4032 | 2.58 | 0.99 |
| KFI06:L | $ReO_4^-$ | 368 | 1.36 (0-262 h)<br>5.62 (262-500 h)<br>1.67 (500-988 h) | 0.39 |
| KFI11:U | Gd-DTPA | 2274 | 2.51 | 1.30 |
| | Tm-EDTA | 2034 | decaying pulse | - |
| | Amino G | 20000 | decaying pulse | - |
| KFI11:M | Er-EDTA | 2368 | 1.86 | 1.08 |
| KFI11:L | Dy-EDTA | 2310 | 3.29 | 1.19 |

U = Upper, M = Middle, L = Lower

During the first two weeks disturbances of the injection occured as a result of gas bubbles being caught in the pump heads. The gas bubbles originated from the tracer storage tanks as a result of the heat, created by the sun, in the containers covering the experimental set-up. Unfortunately, this problem did not occur during the tests of the equipment /Andersson et al., 1988b/ and the warm-up of the containers by the sun exceeded by far that calculated. Some shorter power failures also occured during thunderstorms. All disturbances occuring during the injection are presented in the log of events in Appendix D.

For most of the intervals the injection capacities were quite constant as indicated by the good correlations in the linear regression of the tracer volume versus time plots given in Appendix B. The injection in KFI06:L

was somewhat disturbed by a racing injection pump which is indicated by the three injection capacities given in Table 4–2.

### 4.1.2 Pulse Injections

The pulse injection in KFI11, upper section with Tm–EDTA and Amino G Acid was performed on August 1st i.e. after the sampling of major conductors in BFI02. The intention was to make the injection without creating excess pressure in the injection section, according to the decaying pulse technique. This was accomplished by simultaneously discharging water from the top of the packed–off section and injecting tracer solution at the bottom with the same flow rates. After the borehole section had been filled with tracer solution, the solution was circulated in the same manner as in the dilution measurements in order to maintain a homogeneously distributed tracer solution. Samples were taken in the circulating water in order to determine the decrease of tracer concentration versus time and thereby make it possible to calculate the tracer mass release per time unit into the fracture system. Which then could be utilizied in the evaluations of the obtained tracer breakthrough curves. The decay of the injected tracer pulses are presented in Appendix B, page B:10 and B:11. From these plots it can be seen that the injections did not follow the ideal decay throughout the injection. Calculated mass release per time unit for the Amino G Acid tracer is presented in Appendix G.

In borehole KFI06, upper section Iodide was accidently injected as a forced pulse injection. The injection of Iodide was started as a contionuous injection, but after 124 hours of injection the circulation pump collapsed while the tracer injection still continued. This resulted in a siphon effect whereas the entire volume of tracer unintendedly was injected during a 3.5 hour period.

## 4.2 TRACER BREAKTHROUGH IN TOTAL DISCHARGE

Tracer breakthroughs were obtained from all nine injection points and of all eleven tracers used, with first arrivals ranging between 24 – 3200 hours. The most rapid first arrivals, 24 – 106 hours, were monitored, as expected, for the tracers injected in the upper highly conductive part of Zone 2. Tracers injected in the lower part of Zone 2 shows the largest variation of first arrivals ranging from 194 – 3200 hours while tracers injected in the middle intervals shows the most homogeneous distribution of first arrivals. In Table 4–3 tracer first arrivals are presented. In the table also arrivals before and after the detailed sampling is marked. The breakthrough curves are presented in Appendix C.

The types of injections used, pulse and step input, ideally results in two classical types of breakthrough curves. In field applications however, changes in the hydraulic conditions and instrumental drift/malfunction may affect the shape of the breakthrough curves. To make it possible to compensate or account for these discrepancies and to avoid evaluating them as functions of rock properties events of importance have been noted on the breakthrough

curves and in a log of events, Appendix D.

In the case of a continuous injection (long step input) the steady-state concentration of the tracers in the water discharged from the withdrawal borehole can be calculated from:

$$C_s = C_0 \cdot Q_w / Q \qquad (4.1)$$

where $C_0$ = concentration in the borehole injection interval
$Q_w$ = groundwater flow rate through the borehole interval
$Q$ = groundwater discharge

Table 4-3 Tracer first arrivals measured in the discharge water from borehole BFI02.

| Event | I | Yb | Re | Gd | Er | Dy | In | UR | Ho |
|---|---|---|---|---|---|---|---|---|---|
| Measured before sampling of major conductors | I | - | Re | Gd | Er | - | In | UR | - |
| Measured after sampling of major conductors | Yb | - | - | - | - | Dy | - | - | Ho |
| First arrival (hours) | 106 | 1250 | 194 | 24 | 850 | 3200 | 75 | 600 | 1300 |

The groundwater discharge was kept constant throughout the tracer experiment, as can be seen in Appendix A. The injection concentrations and flow rates through the injection intervals are presented in Appendix B. The concentration increased in some injection intervals indicating a decreasing groundwater flow rate, but the product of the concentration and flow rate remained nearly constant in most cases and only a negligible mass of tracer was accumulated in the injection interval.

Steady-state concentrations in the withdrawal borehole calculated according to equation (4.1) are presented in Table 4-4 together with measured ones, where applicable. Only the Er-EDTA concentration has a variation of importance.

The recovered mass of the injected tracers presented in Table 4-5 were determined by integration of the breakthrough curves. It is obvious that the tracers in the upper part of Zone 2 all obtained a high recovery. A high recovery was also obtained from a tracer injected in the lower part of Zone 2 in borehole KFI06. The breakthrough curves of the tracers that obtained a high recovery and was continuously injected also all reached a steady-state concentration. For these tracers the recovery was calculated at several points of elapsed time, making it possible to estimate the volume of the flow paths involved.

Table 4–4 Calculated and measured steady–state concentrations, $C_s$, in the discharge water at the withdrawal borehole BFI02, in the case of continuous injections.

| Injection section | Tracer | Steady–state concentration Calculated | Measured |
|---|---|---|---|
| BFI01:U | In–EDTA | 19 | 16 |
| BFI01:M | Uranine | 127 – 154 | No S.S. |
| BFI01:L | Ho–EDTA | 68 – 70 | No S.S. |
| KFI06:U | Iodide | Not applicable, pulse injection | |
| KFI06:M | Yb–EDTA | 54 – 71 | No S.S. |
| KFI06:L | $ReO_4^-$ | 4.2 – 5.1 | 4.5 |
| KFI11:U | Gd–DTPA | 47 | 45 |
| KFI11:M | Er–EDTA | 16 – 31 | No S.S. |
| KFI11:L | Dy–EDTA | 56 – 58 | No S.S. |

U = Upper, M = Middle, L = Lower
No S.S. = could not be measured, due to steady–state concentration was not reached

Table 4–5 Recovery of tracers in the pumping hole BFI02.

| Injection section | Tracer | Elapsed time (hours) | Injected mass* (grams) | Recovered mass (grams) | (%) |
|---|---|---|---|---|---|
| BFI01:U | In–EDTA | 600 | 83.2 | 33.7 | |
| | | 1200 | 166 | 92.8 | |
| | | 4510 | 173 | 168.8 | 97.6 |
| BFI01:M | Uranine | 4510 | 1151 | 207.4 | 18.0 |
| BFI01:L | Ho–EDTA | 4510 | 609 | 37.2 | 6.1 |
| KFI06:U | Iodide | 3119 | 31400 | 21880 | 69.7 |
| KFI06:M | Yb–EDTA | 4510 | 537 | 63.1 | 11.8 |
| KFI06:L | $ReO_4^-$ | 792 | 57.1 | 10.8 | |
| | | 988 | 65.0 | 14.1 | |
| | | 4510 | 65.0 | 42.4 | 65.3 |
| KFI11:U | Gd–DTPA | 500 | 171 | 113 | |
| | | 789 | 269 | 208 | |
| | | 1194 | 398 | 314 | |
| | | 4510 | 398 | 353 | 88.6 |
| | Tm–EDTA | 860 | 50.9 | 36.7 | 72.1 |
| | Amino G | 600 | 563 | 488 | 86.7 |
| KFI11:M | Er–EDTA | 4510 | 189 | 3.5 | 1.9 |
| KFI11:L | Dy–EDTA | 4510 | 363 | 2.7 | 0.7 |

U = Upper, M = Middle, L = Lower
* Tracer mass injected into borehole section

### 4.2.1 Comments on the Breakthrough Curves

#### 4.2.1.1 BFI01, Upper; In-EDTA

The breakthrough curve is presented in Appendix C, page C:1 and the log of events in Appendix D, page D:1.

A few hours after the tracer first arrival, at 80 hours of elapsed time, the breakthrough curve levels out for about 40 hours before ascending again. This is caused by an injection stop between 22 - 62 hours. The calculated steady state concentration, 19 ppb, is reached just before the descending part of the breakthrough curve.

At injection finish, 0.5 grams of Indium had been accumulated in the injection borehole section, which makes up 0.3 % of the injected mass. The tracer remaining in the injection section after injection is finished is rather quickly washed out, as shown in Appendix B, page B:1. The injection performance is assumed not to have any greater impact on the breakthrough curve, besides the injection stop at the early beginning.

Two pump stops of about 40 hours duration respectively, between 800 and 915 hours of elapsed time and the 104 hours long pump stop during sampling of major conductors in BFI02 causes increasing concentrations when pumping was restarted.

#### 4.2.1.2 BFI01, Middle; Uranine

The breakthrough curve is presented in Appendix C, pages C:2 and C:3. Background readings of the tracer are not excluded. The log of events is presented in Appendix D, page D:2.

The background concentration of Uranine is about 3.0 ppb. Hence, the first arrival is approximately at 600 hours of elapsed time. The Uranine concentration never levels out to a steady-state or reaches the calculated concentration at 127 - 154 ppb. The obtained maximum concentration is 25 ppb. Only the longer pump stop during detailed sampling in the withdrawal borehole BFI02 causes any marked disturbance on the curve.

During the tracer injection the groundwater flow through the injection section decreased and due to that 451 grams of Uranine had been accumulated at injection finish. This is equivalent to 39.2 % of the tracer mass injected into the borehole section and it is washed out very slowly from the injection interval (Appendix B, page B:1). This may affect the descending part of the breakthrough curve.

#### 4.2.1.3 BFI01, Lower; Ho-EDTA

The breakthrough curve is presented in Appendix C, pages C:4 and C:5 and the log of events in Appendix D, page D:3.

Tracer first arrival is at about 1300 hours of elapsed time, which is nearly 200 hours after injection is finished. The curve never levels out to a steady-state, which was calculated to 68 – 70 ppb, instead it has the shape resulting of a pulse injection. The maximum concentration obtained is 3.2 ppb.

Due to decreasing groundwater flow through the injection interval 86.6 grams of Ho (as Ho-EDTA) had been accumulated at injection finish. This is 14.2 % of the injected mass. The major part of it is washed out to the aquifer within 500 hours (Appendix B, page B:1).

#### 4.2.1.4 KFI06, Upper; Iodide

The tracer breakthrough curve is presented in Appendix C, page C:6 and the log of events in Appendix D, page D:4.

The injection of Iodide was started as a continuous injection, but after 125 hours of injection, the circulation pump collapsed while the tracer injection still continued. This resulted in a siphon effect whereas the entire volume of tracer unintendendly was injected during a 3.5 hour period. The elapsed time on the breakthrough curve is related to the start of the pulse injection. Because of that, the concentration at t=0 is not at background level (0.003 ppm). The tracer first arrival determined from the continuous injection was 108 hours.

#### 4.2.1.5 KFI06, Middle; Yb-EDTA

The tracer breakthrough curve is presented in Appendix C, pages C:7 and C:8 and the log of events Appendix D, page D:5.

The first arrival of Yb-EDTA unfortunately occured during the sampling of major conductors in the withdrawal borehole BFI02, at 1250 – 1350 hours of elapsed time. The curve levels out at approximately 4.5 ppb but never reaches the calculated steady-state concentration of 54 -71 ppb. The breakthrough curve has the shape that would be the result of a lower mass per time unit release of tracer than that actually measured in the injection borehole section. There could be several processes explaining this phenomena.

Due to decreasing groundwater flow through the injection interval 54.7 grams of Yb (as Yb-EDTA) had accumulated at injection finish equivalent to 10.2 % of the injected mass. The rate at which the remaining tracer was washed out to the aquifer was not measured because dissolved gases in the groundwater made it impossible to circulate and sample the injection section. The background concentration of 0.25 ppb is very steady.

#### 4.2.1.6 KFI06, Lower; $ReO_4^-$

The breakthrough curve is presented in Appendix C, pages C:9 and C:10 and the log of events in Appendix D, page D:6.

Tracer first arrival is at approximately 200 hours of elapsed time. The calculated steady state level at 4.2 – 5.1 ppb is reached. However, the curve does not level out to a steady-state concentration. The peak in the first part of the curve is the result of a racing injection pump between 262 and 500 hours. The groundwater flow rate through the injection interval decreases rapidly in the beginning, but thereafter the flow is constant (Appendix B, page B:8) and only a minor mass of tracer accumulated in the injection interval, 0.84 grams of Re making up 1.3 % of the injected mass. Most of the remaining tracer is washed out into the aquifer within 100 hours after injection finish (Appendix B, page B:2).

#### 4.2.1.7 KFI11, Upper; Gd-DTPA

The breakthrough curve is presented in Appendix C, page C:11 and the log of events Appendix D, page D:7.

The tracer first arrival is very distinct at 24 hours of elapsed time and the breakthrough curve levels out at the calculated steady state concentration of 47 ppb. Three injection stops within the first 213 hours of injection result in some disturbances in the ascending part of the breakthrough curve. Due to the high groundwater flow rate through the injection interval (Appendix B, page B:9) there was no tracer accumulated during the injection and the tracer remaining in the interval after injection finish was washed into the aquifer within 50 hours (Appendix B, page B:3).

#### 4.2.1.8 KFI11, Upper; Tm-EDTA and Amino G Acid

A simultaneous pulse injection of one rare earth metal complex, Tm-EDTA, and a fluorescent dye tracer, Amino G Acid (optic brightener), was performed on August 1st i.e. after the sampling of major conductors in the withdrawal borehole BFI02. The injection interval was then completely free from the previous injected Gd-DTPA. The procedure adopted to make the injection without creating any excess pressure or initially forcing the tracer distances away from the injetion borehole is described in sections 3.2.3 and 4.1.2.

The breakthrough curves are presented in Appendix C, pages C:16 and C:17 and the log of events Appendix D, page D:8. The wash out (decay) of the tracers from the injection interval is shown in Appendix B, pages B:10 and B:11.

The breakthrough curves of Tm-EDTA and Amino G Acid are identical and the first arrival is at 23 hours of elapsed time for both tracers. The background concentration of Amino G Acid (0.12 ppm) is somewhat increased due to the use of this tracer in the previous performed interference and tracer test /Andersson et al.,1989/. The natural apparent concentration due to species occuring in the groundwater is about 0.07 ppm.

The second peak of the breakthrough curves is not caused by a withdrawal stop in borehole BFI02. It must hence be the result of the flow path

configuration and/or tracer injection. This is further discussed in section 5.2.1.

#### 4.2.1.9 KFI11, Middle; Er-EDTA

The breakthrough curve is presented in Appendix C, pages C:12 and C:13 and the log of events Appendix D, page D:9.

The first arrival is at 850 hours of elapsed time. The calculated steady-state level, 16 – 31 ppb, is never reached. After the first peak, with maximum concentration 0.9 ppb, the breakthrough curve levels out as would be the result of a lower mass per time unit release of tracer to the aquifer than actually measured during the injection.

As a result of a decreasing groundwater flow through the injection interval, 52.2 grams of Er (as Er-EDTA) had accumulated at injection finish (Appendix B, page B:9). The total remaining Er at injection finish (84.0 grams or 44 % of injected mass) is also washed out to the aquifer very slowly, see Appendix B, page B:3.

#### 4.2.1.10 KFI11, Lower; Dy-EDTA

The breakthrough curve is presented in Appendix C, pages C:14 and C:15 and the log of events Appendix D, page D:10.

The tracer first arrival is at about 3200 hours of elapsed time.

At injection finish 9.9 grams of Dy had accumulated in the injection section due to decreasing groundwater flow. Of the 32.8 grams Dy (9 % of injected mass) remaining in the interval at injection finish, 50 % is released to the aquifer within 500 hours and 80 % within 1400 hours, see Appendix B, pages B:9 and B:3.

## 4.3 TRACER BREAKTHROUGH IN MAJOR CONDUCTORS

In order to determine possible interconnections between highly conductive parts (sub-zones) of Zone 2 the tracers injected in the peripheral boreholes BFI01, KFI06 and KFI11 was sampled in major hydraulic conductors in the withdrawal borehole BFI02. The procedure and equipment used is described in section 3.4.2.

As the hydraulic conductivity of the tracer flow paths involved ranged within three orders of magnitude, resulting in a wide range of tracer first arrivals, the sampling was performed at the optimum elapsed time when most of the injected tracers were detected in BFI02 and steady state conditions prevailed, i.e. the breakthrough curves had leveled out. The tracers Ho-EDTA, Yb-EDTA and Dy-EDTA injected in the most low conductive intervals had not reached steady state concentration at the time of sampling major cunductors. Iodide, which was injected as a pulse, was on the tail part when the sampling

was performed (Appendix C). However, at the procedure adopted for the sampling in short intervals, dilution with groundwater from other conductive intervals not containing the tracer of interest was avoided. Hence, the tracers main flow paths were considered to be determined even though the concentration in the water discharged from the withdrawal borehole BFI02 was low at the time of sampling.

At each interval four samples were taken for tracer analysis, as described in section 3.4.2. The results are given in Appendix E as concentration versus time after start of pumping. The criterions used to determine whether a tracer measured at a specific sampling interval was present due to transport in a main flow path or not, was primarily the concentration of the tracer in the sample compared to that of the background. Secondly, the trend of the concentration in the samples versus time (Appendix E) was used. Decreasing concentration versus time indicates contamination from the previous sampled interval. Increasing or a high, constant concentration indicates the sampled interval being a main flow path.

The results of sampling in major hydraulic conductors are summarized in Table 4–6 and illustrated in Figures 4–1, 4–2 and 4–3.

At distances of 155 – 200 metres there is an extensive mixing between high conductive sub–zones of Zone 2, separated by 15 – 110 metres of low conductive rock at the injection points.

Table 4–6 Tracer breakthrough in major hydraulic conductors in withdrawal borehole BFI02. Tracers recovered at straddle packer pumping.

| No | Section | I | Yb | Re | Gd | Er | Dy | In | UR | Ho | mS/m* |
|---|---|---|---|---|---|---|---|---|---|---|---|
| 1 | 203 – 205 | (I) | Yb | – | Gd | Er | (Dy) | In | – | Ho | 420 |
| 2 | 208 – 210 | I | Yb | (Re) | Gd | Er | (Dy) | In | – | Ho | – |
| 3 | 212 – 214 | I | – | – | – | – | – | – | UR | – | 780 |
| 4 | 238 – 240 | – | – | – | – | – | – | – | UR | – | 1040 |
| 5 | 257 – 259 | – | Yb | Re | Gd | Er | – | (In) | (UR) | – | 1030 |
| 6 | 260 – 262 | – | Yb | Re | – | – | – | – | – | – | 990 |
| 7 | 276 – 278 | – | – | – | – | – | – | – | – | – | 1290 |

* electrical conductivity of water in sampled section

Regardless of the position of the injection interval the tracer is recovered in one or more of the three uppermost conductive intervals of Zone 2, in borehole BFI02. Tracers injected in the upper part of Zone 2 are recovered both in the upper part of Zone 2 and in high conductive intervals at depth. These results imply a solute transport both upwards and downwards within

Zone 2. This flow condition is further pointed out by the fact that tracers injected in intermediate parts of Zone 2 also are recovered at the upper and lower conductive parts of Zone 2. The mixing between sub-zones is possible due to the geologic structure of Zone 2, were groundwater flow is concentrated to a few interconnected minor shear and fracture zones about one metre thick, c.f. Figure 2-2.

The electrical conductivity of the water sampled at each interval was also measured, given in Table 4-6. The results show that despite the mixing of tracer labelled groundwater between sub-zones, the general picture with more saline waters in the lower parts of Zone 2 still holds after 1250 hours of pumping.

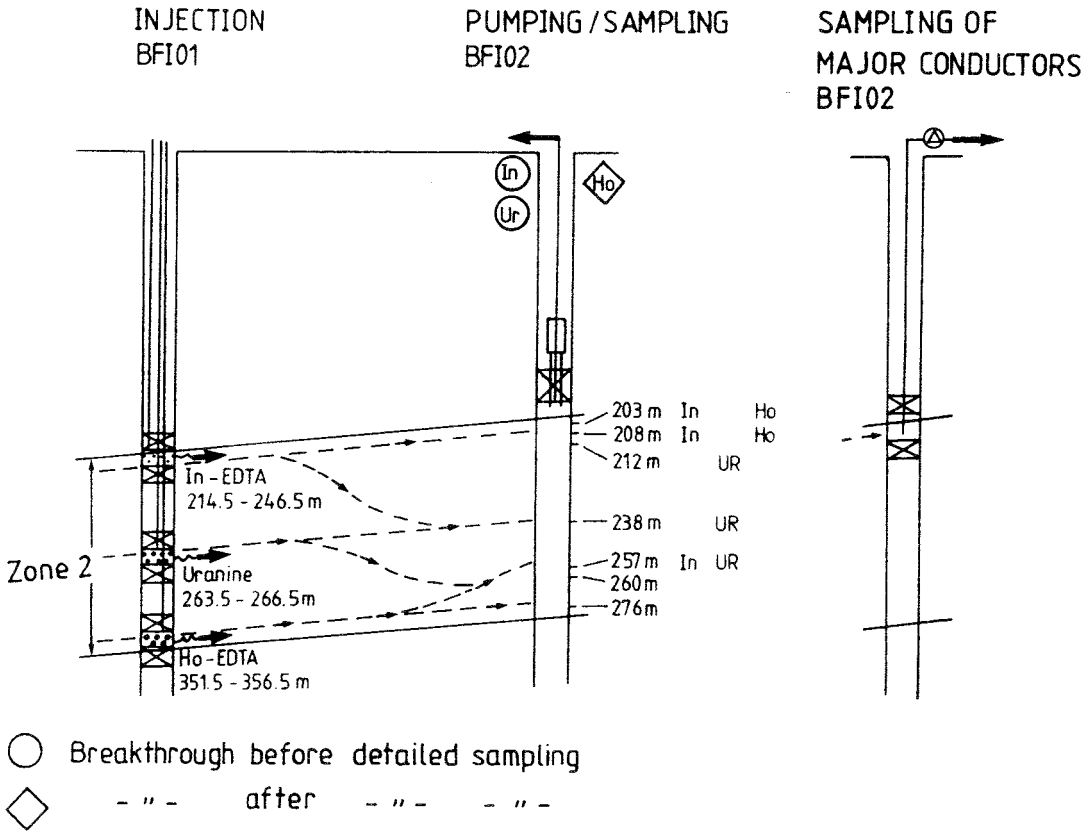


Figure 4-1 Illustration of results from tracer injections in BFI01 and pumping for tracer withdrawal in BFI02.

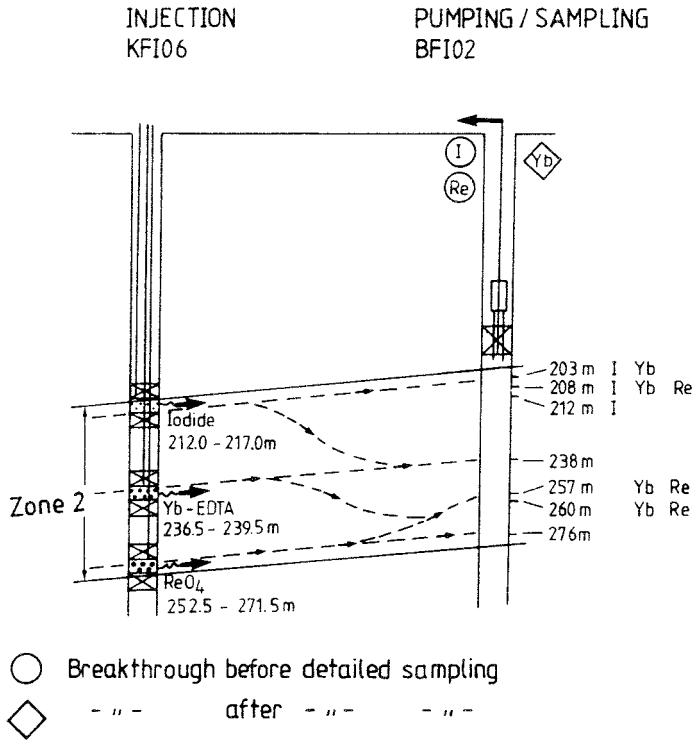


Figure 4–2 Illustration of results from tracer injections in KFI06 and pumping for tracer withdrawal in BFI02.

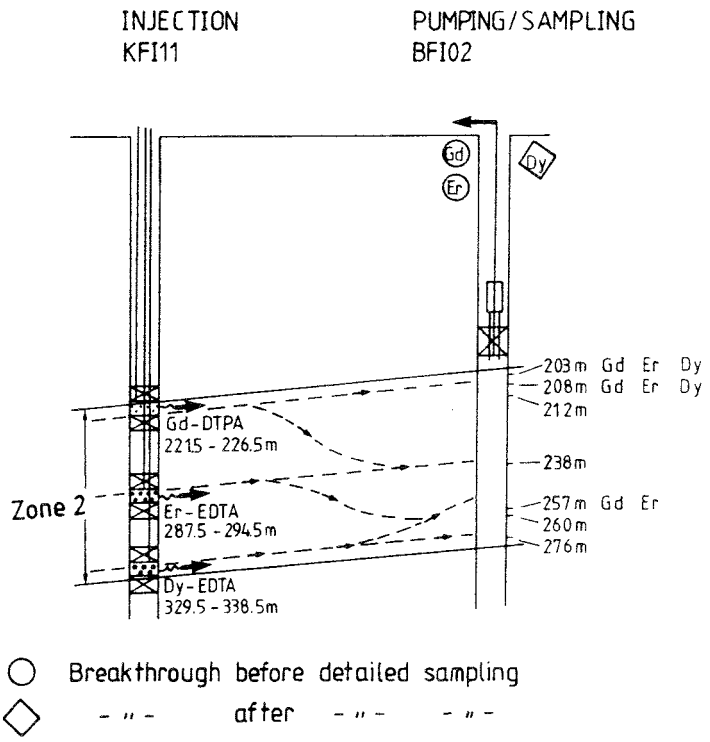


Figure 4–3 Illustration of results from tracer injections in KFI11 and pumping for tracer withdrawal in BFI02.

## 4.4 SUPPORTING MEASUREMENTS

### 4.4.1 Hydraulic Head

The hydraulic heads were monitored manually with an electrical summer device as described in section 3.5.1. The data were transformed into meters above sea level and head differences between the pumped interval in BFI02 and the injection intervals in BFI01, KFI06 and KFI11 were calculated. The head differences versus elapsed time are presented in Appendix A together with the groundwater levels in the above mentioned boreholes and in borehole HFI01. The mean head differences are given in Table 4-7 below.

The pumping and withdrawal of tracer was, as earlier mentioned, stopped for 104 hours during the sampling of major conductors in BFI02 and then restarted with the same pumping rate. However, the measured head differences were quite differerent after the restart. This can be clearly seen in Table 4-7 comparing the values before and after the sampling of major conductors.

The reason for the changed head differences, which also can be seen in the graphs in Appendix A, has not been fully understood. Checks of the hydraulic head monitoring device, pumping rate, packer positioning, data errors etc. have been made but none of these potential sources of error can explain the occurence of the difference in hydraulic head. One explanation might be that a positive skin was developed in borehole BFI02 during the interference test 3, preceeding the tracer test. When the pump was stopped 104 hours for the sampling of major conductors, the skin caused by drilling debris or precipitates was partly removed due to the changed head and flow situation (L. Carlsson, 1989). Another possible explanation is found in the site notebook. In the standpipe (10/8 mm tube) for measurement of hydraulic head, gas bubbles was noted in section KFI06:U after the pump stop in BFI02, made for the sampling of major conductors. The gas bubbles will result in incorrect measured head values. Even if not observed, gas bubbles may have occured in other sections also. That hydraulic head values are incorrect measured after the pump stop is also indicated by the fact that tracers $ReO_4^-$ and Dy-EDTA, with measured $\Delta h$ having negative values (i.e. hydraulic gradient directed from the pumped borehole BFI02), were withdrawn to BFI02 without decreasing concentrations for hundreds of hours after the pump stop. Also, the Amino G tracer injected as a pulse in KFI11 after the 104 hours of pump stop in BFI02 for sampling of major conductors, obtained about the same residence time to BFI02 as Gd-DTPA injected in the same borehole section before pump stop.

Table 4–7 Mean values of head differences, Δh, between the pumped section in BFI02 and the tracer injection sections in the surrounding boreholes.

| Injection section | Tracer | $\Delta h_1$ (m) | $\Delta h_2$ (m) |
|---|---|---|---|
| BFI01:U | In-EDTA | 1.14 | 0.80 |
| BFI01:M | Uranine | 1.25 | 0.84 |
| BFI01:L | Ho-EDTA | 1.41 | 0.55 |
| KFI06:U | Iodide | 0.62 | - 0.15 |
| KFI06:M | Yb-EDTA | 0.64 | 0.28 |
| KFI06:L | $ReO_4^-$ | 0.59 | - 0.34 |
| KFI11:U | Gd-DTPA | 0.81 | 0.42 |
| KFI11:M | Er-EDTA | 0.74 | 0.33 |
| KFI11:L | Dy-EDTA | 0.77 | - 0.74 |

U = Upper, M = Middle, L = Lower
$\Delta h_1$ = before pumpstop in BFI02 for sampling of major conductors
$\Delta h_2$ = after pumpstop in BFI02

### 4.4.2 Groundwater Flow Rates

Groundwater flow rate measurements were performed in the tracer injection boreholes at three occations during the pumping of BFI02; prior to, during and after the injection of tracers. Flow rate measurements after the injection of tracers were measured after the 104 hours long pump stop in BFI02 for sampling of major conductors. All 9 injection intervals were measured as described in sections 3.2.2 and 3.5.2. The results of the measurements are presented in Table 4–8. Here, the groundwater flow rates during the injection are given as mean values. The fluctuations can be seen in Appendix B.

In two of the intervals in KFI06 circulation pump failure occured and due to the gradually sinking seasonal trend of the hydraulic heads, the replacement pumps were not able to withdraw the water from a depth exceeding 5 metres. Thus, the circulation had to be stopped and consequently the groundwater flow rates could not be determined.

The general trend of the data in Table 4–8 is that the groundwater flow rates decrease. There is also a trend towards decreasing groundwater flow rates during injection which can be seen in Appendix B. The decrease during the tracer injection period is largest in the already low flowing and relatively low conductive intervals. As there are no decreases in the relative head differences during the injection, one possible explanation might be chemical clogging of the injection intervals.

Table 4-8 Groundwater flow rate, $Q_w$, through borehole tracer injection sections during pumping in BFI02; before, during and after injection of tracer.

| Injection section | Distance to BFI02 (m) | $Q_w$ before (ml/min) | $Q_w$ during* (ml/min) | $Q_w$ after (ml/min) |
|---|---|---|---|---|
| BFI01:U | 168 | 268 | 532 | 55 |
| BFI01:M | | 26 | 8 | 3 |
| BFI01:L | | 11 | 9 | 15 |
| KFI06:U | 189 | 23 | NM | NM |
| KFI06:M | | 7 | 2 | NM |
| KFI06:L | | 114 | 55 | 8 |
| KFI11:U | 155 | 376 | 352 | 3 |
| KFI11:M | | 8 | 1.5 | 0.5 |
| KFI11:L | | 24 | 10 | 1 |

U = Upper, M = Middle, L = Lower NM = Not Measured
* = mean value during injection period

### 4.4.3 Delay and Dispersivity in the Withdrawal Borehole

The delay and dispersivity in the pumping hole BFI02 calculated from the tracer experiment described in section 3.5.3 are given in Table 4-9 below. The values of dispersivity, D/v, from the analytical solution given by Gelhar/1987/ (Eqn (3.10)) are calculated as the apparent dispersivity of a tracer injected at a distance of 150 m from the withdrawal borehole and the values from Taylor/1954/ represents the dispersion in a straight pipe for turbulent flow.

Even though turbulence may not have been fully developed (Re = 3660) the Taylor theory, valid for turbulent flow, and tracer test result was in the same order of magnitude, 0.06 and 0.24 m respectively from the lower inflow level. Mean velocity within the borehole was calculated to 0.032 m/s (Q/A) and from the tracer breakthrough ($t_{50}$) 0.030 m/s was determined.

Table 4-9 Delay and dispersivity in the withdrawal borehole BFI02.

| Part of Zone 2 | Delay (minutes) | | Dispersivity, D/v (m) | |
|---|---|---|---|---|
| | $t_{50}$ Gelhar | $t_d$ Eqn.(3.7) | Gelhar | Taylor |
| Upper (204 m) | 10 | 10 | 0.07 | 0.02 |
| Lower (261 m) | 42 | 42 | 0.24 | 0.06 |

The results presented above shows that the delay and dispersivity in the withdrawal borehole BFI02 is neglible compared to the values obtained in the fracture flow paths during the radially converging tracer experiment. Consequently, no corrections for the delay and dispersivity in the withdrawal borehole and sampling equipment has been made in the present evaluation of the breakthrough curves.

### 4.4.4 Laboratory Measurements

The **porosity and diffusivity** measurements of drillcore samples representing the rock adjacent to the fracture wall showed porosity mean values slightly higher near the fracture wall (0 – 5 mm) than further into the rock. Mean porosities was about 2.9 and 2.2 % respectively. Porosity was dependent on rock type. Mean value for Tectonite samples 5.4 % and Aplite and Red Granodiorite samples approximately 1.6 % porosity. The effective diffusivity correlated to the sample porosity. For Iodide a representative value is $1 \cdot 10^{-13} m^2/s$ at 1 % porosity and $1 \cdot 10^{-12}$ $m^2/s$ at 5 %, and for Uranine it is about one order of magnitude lower. The laboratory measurements are presented in detail in Gidlund et al./1990/.

The tests of the **tracer metal–complexes** indicated that long term stability may be a problem for some of the 11 tracers used. Gd–DTPA considered to be a very stable tracer, whereas the EDTA complexes with In, Dy, Ho, Er, Tm, and Yb may be sorbed at long residence times due to instability of the complexes. Amorphous iron and a high fracture surface/volume ratio will enhance possibility for sorption. These studies are reported in detail by Byegård & Skålberg /1992/.

## 4.5 SOURCES OF ERROR

### 4.5.1 General

A large scale field experiment with an extensive amount of equipment is very difficult to perform without having any kind of problems with either the equipment or the field conditions. Equipment failures may be sources of error that have to be accounted for in the interpretation and evaluation of an experiment. This section describes the experimental sources of error and their effects on the breakthrough curve form.

### 4.5.2 Equipment Errors

A continuous injection of tracer requires a constant injection flow rate in order to get smooth breakthrough curves. In the radially converging experiment, some of the injection pumps stopped several times during the injection due to the earlier mentioned trapping of gas bubbles in the pump head. This problem only occured during very hot days when the containers covering the experimental set–up were heated by the sun. The problem was finally solved after about 300 hours of injection by installing gas bubble traps. The effect on the breakthrough curves will be larger for shorter residence times as illu–

strated by the breakthrough of Gd-DTPA from KFI11:U (Appendix C). The pumps were checked once every day in the beginning of the injection so fairly good estimates of the duration of the pump stops can be made.

Power failures during thunder storms also resulted in some pump stops and pump breakdowns. The pumps were usually replaced within 24 hours but some of the stops may have effects on the breakthrough curves, especially withdrawal pump stops. All pump stops are listed in the log of events in Appendix D.

The injection technique also involved a discharge of water from the injection borehole section at the same rate as tracer labelled water was injected in order to avoid pressure buildup in the injection interval. In the experiment, the discharge rates were lower than the injection rates but considering the high transmissivities and the low injection flow rates, this effect should be neglible.

### 4.5.3 Tracer Related Errors

The tracers used should ideally be non-sorbing and non-reactive with the rock and the groundwater. Some of the tracers used in the radially converging experiment had not been used in groundwater studies before and therefore extensive laboratory studies regarding sorption and stability were carried out. They indicated that long term stability may be a problem for some of the 11 tracers used, resulting in sorption of the tracer metal.

The effects of sorption on the breakthrough curve would be a delay and a lower equilibrium concentration resulting in a low recovery of tracer.

# 5. INTERPRETATION OF EXPERIMENTAL RESULTS

There are a number of theoretical concepts developed describing fluid flow and solute transport in fractured crystalline rock, for example porous medium within deterministic determined entities in the rock volume to describe e.g. fracture zones and matrix rock. Other concepts are stochastic continuum and discrete fractures with plane parallel or varying aperture.

In this report, some of those concepts are used to evaluate tracer breakthrough from the radially converging tracer test, together with supporting measurements such as hydraulic gradients, withdrawal rate and tracer inflow distribution.

The purpose is to determine some properties essential to fluid flow and solute transport, and to highlight the differences in the determined parameters depending on the approach used. The values of these parameters will in turn be of importance for the transport modelling associated with the safety analysis.

The interpretation of tracer breakthrough curves using non-sorbing tracers can be considered to be divided into two parts. The primary interpretation involves estimation of tracer residence time and the magnitude of dispersion, assuming some quantitative model for solute transport. These are the only properties that can be evaluated directly from the tracer breakthrough data. A secondary level of interpretation uses the estimated residence time, along with groundwater flow and head measurements, to evaluate properties such as hydraulic conductivity of fracture flow paths, fracture aperture, flow porosity and flow wetted surface area. Thus, the variables of direct use for interpretation that are actually measured during the tracer experiment are tracer concentration, and groundwater flow and heads in samling and injection sections.

The interpretation of residence times and dispersion effects from breakthrough curves depends entirely on the assumed transport model, including transport processes, boundary conditions, etc. Different model assumptions can give widely different estimates of parameter values, especially when transport occurs along more that one transport path. In addition, tracer injection conditions may have a significant effect on estimated values.

Further, the interpretation of conductivity, aperture and porosity can be made using two basically different approaches. One approach uses measured flowrates and heads only, which requires that a relationship can be defined between the conductivity and the aperture (cubic law). The other approach uses residence time and measured heads, and is not dependent on the cubic law for estimation of the fracture conductivity.

Ideally, the two approaches should give identical results, if the transport path is homogeneous. Usually this is not the case, and the differences in results from the two approaches may be used to assess the heterogeneity along the transport path. In either approach, greatly simplifying assumptions about fracture geometry and transport properties are made. With such assumptions in mind, use of the obtained values for transport predictions should be made with considerable caution.

The geological and hydraulical interpretation of the fracture zone is that Zone 2 not really consist of separate sub-layers as was thought in erlier stages of the fracture zone project. Only the upper highly conductive part is considered with certainty to be a well-defined, widespread and plane sub-zone, with the possibility of a similiar plane at the bottom delimitation of the zone as well /Ahlbom & Tirén, 1991/. In between, there is a network of connected sub-zones, which in turn consists of interconnected single fractures. The conceptual approach used for the evaluation of the tracer breakthrough curves from the radially convergent tracer test in Zone 2 has been to treat the individual sub-zones as porous media flow paths, valid due to an frequent interconnection between fractures, and aperture variations within the single fractures.

Details of the methods of interpretation will be described below, along with the evaluation of the data. A division is made so that one section (5.1) describes the method of inverse modelling, i.e. curve fitting to determine residence times and dispersion. Another section (5.2) describes the direct interpretation of the breakthrough curves and a following section (5.3) describes the interpretation of fracture transport properties.

## 5.1 INVERSE MODELLING METHOD

### 5.1.1 Models Used

The evaluation and interpretation of the tracer breakthrough curves was made with one-dimensional porous media models. The dispersion and fluid velocity are determined by fitting the tracer breakthrough curve to one of the theoretical solutions given below. They can be determined for each identified main flow path as well as the total breakthrough curve (macro dispersion).

The dispersion is defined as the spreading in time and space of a solute transported with the groundwater. The dispersion originates from /Bear, 1979/:

- local variations of the velocity in the flow field
- molecular diffusion in the groundwater

The first process is called mechanical dispersion. The second one, molecular diffusion, takes place also in the absence of advection but is a time depending process. Its effect on the overall dispersion will thus be more significant at low flow velocities. These two processes can not be separated

from each other in an experimentally obtained breakthrough curve.

In the models fluid velocity is assumed to be constant, and transverse dispersion is ignored. The governing equation is /Van Genuchten and Alves, 1982/:

$$R \cdot \partial C/\partial t = D(\partial^2 C/\partial x^2) - v \cdot \partial C/\partial x \qquad (5.1)$$

where: D = dispersion coefficient
v = fluid velocity (m/s)
C = concentration of solute ($kg/m^3$)
x = distance from injection point (m)
R = retardation factor
t = time (s)

According to Ogata and Banks, /1961/ and Zuber, /1974/, the dispersion in a radial convergent flow field can be calculated with good approximation by equations valid for one-dimensional flow. Although a linear flow model (constant velocity) is used for a convergent flow field, it can be demonstrated that breakthrough curves and parameter estimates are similar for Peclet numbers of about 10 and higher. For Peclet numbers on the order of 1 the linear flow model may underestimate the mean travel time and dispersivity with 35 - 40 % compared to a radial flow model /Nordqvist, 1991/ The Peclet number (Pe) is defined by:

$$Pe = x \cdot v / D \qquad (5.2)$$

Mixing in the sampled borehole of tracers travelling through several different major flowpaths is considered. The concentration in the sampled section is assumed to be a weighted contribution from all the main transport paths.

$$C = \sum_i f_i C_i \qquad (5.3)$$

where: C = tracer concentration in borehole
$f_i$ = fractional volume parameter
$C_i$ = tracer concentration from flowpath i

The fitting was generally made for three parameters, dispersion coefficient, D, mean velocity, v, and proportionality factor, f. The f parameter is the product of injection concentration, dilution in the sampling section, and a weight representing the contribution from each main flow path. It may be noted here that no assumption need to be made regarding mixing mechanics in the sampled section, in order to determine f. The fitted parameters were transformed into the form of more conventional transport parameters; residence time, $t_0$ (hours), dispersivity, D/v (m), and Peclet number. The solutions used, to Equation (5.1), are listed below.

### 5.1.1.1 Model 1C Continuous Injection

In the case of a continous injection, and with the assumtion of no dispersion over the boundary of the injection point, the one-dimensional solution for semi-infinite flow is /Ogata and Banks, 1961/:

$$C/C_0 = 1/2\ \mathrm{erfc}[(1-t/t_0) / Y] + 1/2\ \exp(vx/D)\ \mathrm{erfc}[(1+t/t_0) / Y] \quad (5.4)$$

where: $Y = 2[(t \cdot D) / (t_0 \cdot v \cdot x)]^{1/2}$

### 5.1.1.2 Model 3E Step Input

Van Genuchten /1982/ gives a solution for a step input (continous injection) with dispersion over the injection boundary, which states that the mass flux of the solute at the injection boundary at any time is equivalent to the total flux of the solute carried by dispersion and advection:

$$v \cdot f(t) = - D \cdot \partial C/\partial x + v \cdot C \quad , \ x = 0 \quad (5.5)$$

The solution of the dispersion equation is then:

$$C/C_0 = 1/2\ \mathrm{erfc}[(x-v \cdot t) / Z] + (V/\pi)^{1/2} \exp[(x-v \cdot t)^2/(4 \cdot D \cdot t)] - \quad (5.6)$$

$$1/2\ [1+v \cdot x/D+V]\ \exp[v \cdot x/D]\ \mathrm{erfc}[(x+v \cdot t) / Z]$$

where: $Z = 2(D \cdot t)^{1/2}$
$V = v^2 t/D$

Variable injection schemes (e.g. Figure 5-8) were simulated by superposition of the solution given in Equation (5.6).

### 5.1.1.3 Model 4C Pulse Injection

In the case of an instantaneous pulse injection, Equation (5.1) has the following solution /Lenda and Zuber, 1970/, /Kreft et al., 1974/:

$$C/C_0 = 1 / [(4 \cdot \pi \cdot n(t/t_0)^3)^{1/2}]\ \exp[-(1-t/t_0)^2/(4 \cdot n \cdot t/t_0)] \quad (5.7)$$

where: $n = D/v \cdot x$

### 5.1.1.4 Model 5C Decying Pulse Injection

Van Genuchten /1982/ gives a solution of the one-dimensional problem in the case the concentration at the injection point f(t) varies as an exponential function of time:

$$f(t) = C_0 \exp(-a \cdot t) \qquad , t > 0 \tag{5.8}$$

where a is a constant

This is the injection condition prevailing in a packed off borehole interval where the groundwater is instantaneously labelled with a tracer, without applying any excess pressure to the system. The constant, a, in Equation (5.8) is then equal to $Q_w/V$, where $Q_w$ is the flow rate through the borehole interval and V is its volume.

The solution at the point of detection is then given by:

$$C/C_0 = B \exp(-a \cdot t) \tag{5.9}$$

where:
$$B = v/(v+U) \exp[x(v-U)/(2 \cdot D)] \operatorname{erfc}[(x-U \cdot t)/Z] +$$
$$v/(v-U) \exp[x(v+U)/(2 \cdot D)] \operatorname{erfc}[(x+U \cdot t)/Z] +$$
$$v^2/(2 \cdot D(-a)) \exp[v \cdot x/D + a \cdot t] \operatorname{erfc}[(x+vt)/Z]$$

with:
$$U = (v^2 - 4 \cdot D \cdot a)^{1/2}$$
$$Z = 2(Dt)^{1/2}$$

## 5.1.2 Parameter Estimation Method

For the one-dimensional analysis, non-linear least squares regression was used. The technique that was used for regression is sometimes referred to as the Marquardt method /Marquardt, 1963/ and is in this report formulated as, in an iterative form, see also /Cooley, 1985/:

$$\mathbf{B}_{r+1} = \mathbf{B}_r + p_{r+1}(\mathbf{X}_r^T \mathbf{W} \mathbf{X}_r + u_{r+1})^{-1} \mathbf{X}_r^T \mathbf{W} (\mathbf{C}_r^o - \mathbf{C}_r^m) \tag{5.10}$$

where
$\mathbf{B}_r$ = vector of parameter estimates
$\mathbf{X}$ = vector of parameter sensitivities
$\mathbf{W}$ = reliability weight matrix
$\mathbf{C}_r^o$ = vector of observed concentrations
$\mathbf{C}_r^m$ = vector of model concentrations
p = damping parameter ($\leq 1$)
u = Marquardt parameter

Equation (5.10) gives the updated parameter estimate at the (r+1)th iteration. The parameter sensitivity vector is obtained by taking partial derivatives of the dependent variable with respect to each parameter. Thus, for an element in the **X** matrix:

$$X_{ij} = \partial C_j^m / \partial B_i \qquad (5.11)$$

The parameter sensitivities are obtained by taking analytical derivatives.

The reliability weight matrix, **W**, usually reflects the error structure of the observed data. However, it may also be used by the modeller to emphasize/de-emphasize certain components of the data. If the observations are assumed to be random (no correlation between observations) and have a common variance **W** reduces to an identity matrix, and that is what is assumed in this work.

Standard errors of the parameters and linear correlation between parameters were obtained from the variance-covariance matrix, $s^2(\mathbf{X}^T\mathbf{W}\mathbf{X})^{-1}$, where $s^2$ is the error variance. Further details of the parameter estimation method and the statistical analysis procedures of regression results are given in Appendix F.

## 5.2 MODELLING PERFORMANCE AND RESULTS

As a first step, the delay and dispersivity in the withdrawal borehole BFI02 and in the tubing system up to the sampling equipment at ground surface was examined. The tracer test performed to determine these parameters is described in section 3.5.3, and the results in section 4.4.3. The flow was turbulent from the inflow level at 261 m, corresponding to the lowest sub-zone of Zone 2, and upwards in the borehole. The delay in the borehole and tubing system was very small, 10 minutes from upper sub-zone and about 40 minutes from the lowest, and considered negligible compared to the residense time in Zone 2 from location of tracer injection to the withdrawal borehole. The dispersivity within the withdrawal borehole was low, about 0.04 m from inflow at upper sub-zone (204 m) and 0.15 m from the lowest sub-zone.

Model fits to breakthrough curves originating from continuous, or step inputs of tracer was made with two models. Model 1C, Equation (5.4), applying the solution of Ogata & Banks /1961/ and model 3E, Equation (5.6), the solution by Van Genuchten and Alves /1982/. In model 1C there is no dispersion over the boundary of the injection point, whereas in 3E there is both advection and dispersion over this boundary. Model 3E also considers variable injection scheme, e.g. accidental injection stops.

Tracer breakthrough curves originating from pulse injections were interpreted by choosing one from three models; Model 3E, as a short step input, Model 4C, Equation (5.7), the injection boundary condition of an instantaneous pulse /Kreft et al.,1974/, or Model 5C, the boundary conditions of a decying pulse injection as given by Van Genuchten /1982/, Equation (5.9).

The 1-D modelling was performed for all breakthrough curves obtained, with the exception of Tm-EDTA. This tracer was simultaneously injected with Amino G tracer in a pulse, and the breakthrough curves obtained was nearly identical.

Independent field measurements, i.e. sampling for tracer content in inflow from sub-zones of Zone 2, were used to identify and verify the existence of more than one main flow path in Zone 2, from point of injection to detection in the withdrawal borehole BFI02. When possible these main flow paths were separated in the inverse modelling of the breakthrough curves.

The uniqueness of the parameter estimates was made by studying the regression statistics of each model run; the correlation coefficients, standard errors of the parameters and the correlation between the parameters. If the correlation coefficient is high, the standard errors are low and the correlation between parameters are low, the model is good. If there is a high degree of correlation between parameters, there are too many parameters and the model should be rejected. The classification was made on a scale from 1 to 3, where 1 represents a poor model, 2 represents an acceptable model and 3 a good model. Details of regression statistics are presented in Appendix I.

Results of the model estimates are presented in tables below showing; mean residence time, $t_0$, dispersivity, D/v, Peclet number, Pe, proportionality factor, f, representing the contribution of tracer transport from each main flow path, correlation between model estimate and experimentally obtained breakthrough curve, R, and finally classification of model fit.

### 5.2.1 Tracers Injected in Upper Part of Zone 2

#### 5.2.1.1 In-EDTA, BFI01 Upper Section

In-EDTA was injected as a continuous injection (step input) that lasted for 1246 hours. After 22 hours the injection pump was accidently stopped for 40 hours. In Figure 5-1 the injection scheme is presented as tracer mass release into the fracture zone per time unit. The injection technique used is described in section 3.2.1. Without applying excess pressure, the groundwater flowing through the borehole is labelled with tracer. From the sampling of the major hydraulic conductors in the tracer withdrawal borehole BFI02 during the radially converging test, it was evident that at least two major flow paths (sub-zones) within Zone 2 was contributing to tracer arrival in the water sampled from the pumped borehole BFI02, see Figure 4-1. Similiar indications were also found from the interference tests, by analysis of primary and secondary pressure responses /Andersson et al, 1989/.

As can be seen from the breakthrough curve of In-EDTA in Appendix C, page C:1 there was a 104 hours long pump stop for detailed sampling of inflow levels in the withdrawal borehole BFI02. Unfortunately the start of this pumpstop coincided with the termination of the In-EDTA tracer injection. The models applied in this study does not take changes in the flow field into account, e.g. pumpstops. Therefore, model fits were primarily made

to the ascending part of the breakthrough curve. However, some model fits were made to the complete breakthrough curve. The results are discussed below.

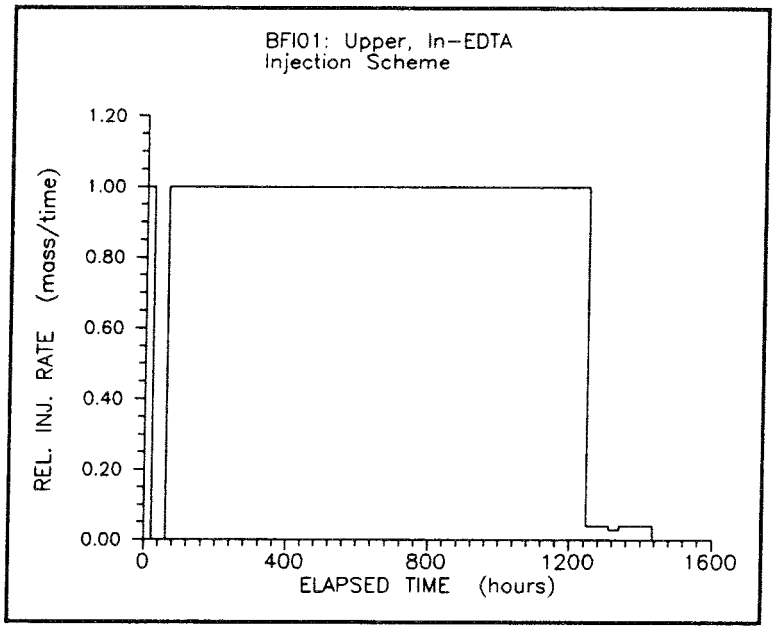


Figure 5-1 Injection scheme for In-EDTA in BFI01 upper section

**Model fits to ascending part**

Model fits were made to the ascending part of the breakthrough curve using two solutions. Model 1C applying the solution of Ogata & Banks /1961/ and Model 3E the solution presented by Van Genuchten and Alves /1982/. In model 1C there is no dispersion over the boundary of the injection point, whereas in 3E there is both advection and dispersion over this boundary. Model 3E also considers a variable injection scheme, i.e. also injection stops. Even though there was independent field measurements showing the existence of at least two main flowpaths (Figure 4-1) model fits were made also with one flow path in order to get an idea of the macro dispersion of the fracture Zone 2. Model estimates are presented in Appendix H.

Figure 5-2 demonstrates the breakthrough curve for In-EDTA and a model estimate assuming two main flowpaths. Model 3E is applied to the ascending part of the breakthrough curve.

The results of the inverse modelling with models 1C and 3E are summarized in Table 5-1 and the regression statistics for the model fits are presented in Appendix I. Model fits obtained were good (class 3) both if one and if two main flow paths (fracture sub-zones) were given to contribute to the tracer transportation from the injection borehole to the pumped tracer withdrawal borehole. In this case an independent measure of the number of contributing main flow paths by means of sampling in major conductors in the withdrawal borehole was crucial for the descision of two main flow paths contributing to tracer transportation and being the right approach for the inverse modelling.

Model 3E considering both injection stop and dispersion over the injection point boundary shows somewhat larger dispersivities and shorter tracer mean travel times than the continuous solution by Ogata & Banks /1961/ utilized in model 1C. Model 3E was judged the most appropriate for the experimental conditons during the radially converging tracer experiment and in the subsequent modelling of other tracer breakthroughs model 3E was prefered compared to 1C.

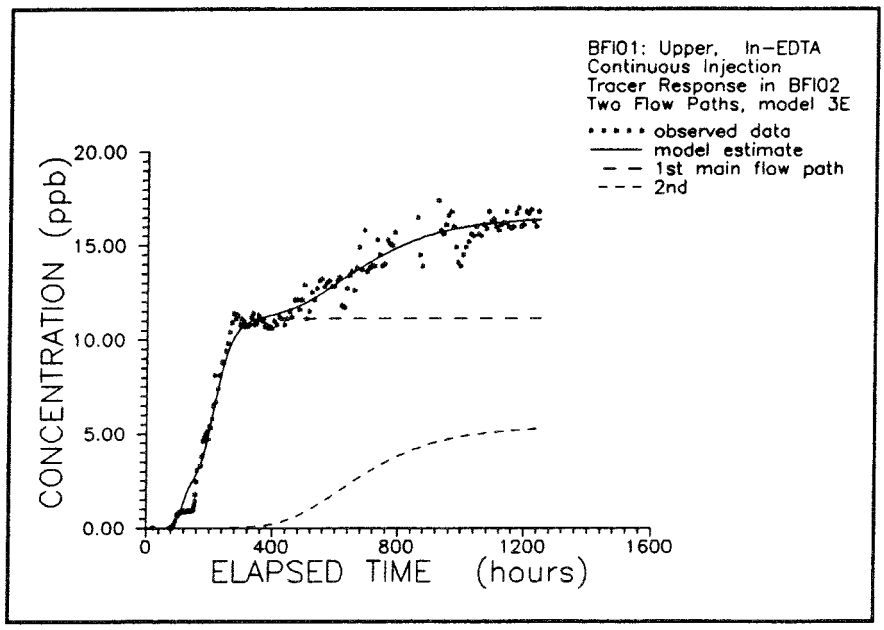


Figure 5-2 Model estimate assuming two main flow paths. Model 3E. Ascending part of In-EDTA breakthrough curve.

Table 5-1 Results of inverse modeling of In-EDTA tracer breakthrough in borehole BFI02. 1-D model fit to the ascending part of the breakthrough curve. The tracer originates from injection in borehole BFI01, upper section. Distance is 168 metres.

| Applied model | Number of flow paths | | $t_0$ (h) | D/v (m) | Pe | f | R | Class* |
|---|---|---|---|---|---|---|---|---|
| 1C | one | 1st | 333 | 45.7 | 3.7 | - | 0.983 | 2 |
| | two | 1st | 202 | 4.9 | 34.0 | 0.68 | 0.995 | 3 |
| | | 2nd | 696 | 7.3 | 22.9 | 0.32 | | |
| 3E | one | 1st | 201 | 82.5 | 2.0 | - | 0.984 | 3 |
| | two | 1st | 154 | 6.3 | 26.8 | 0.69 | 0.994 | 3 |
| | | 2nd | 630 | 7.6 | 22.2 | 0.31 | | |

* Classification; 1-poor, 2-acceptable, 3-good

**Model fits to the complete breakthrough curve**

An attempt was made with model fits to the complete breakthrough curve, both with actual injection stop time and adjusted injection stop time, compensating for the pumpstop that coincided with termination of tracer injection. A summary of the model fits to the complete breakthrough curve is presented in Table 5–2. Correlation, R, between model estimate and experimentally obtained breakthrough curve was high, but no good model fit was obtained. Correlations were very high between parameters and the standard deviations very high for the determined parameters.

Table 5–2 Results of inverse 1–D modeling of the complete In–EDTA breakthrough curve in borehole BFI02. The tracer originates from injection in borehole BFI01, upper section. Distance is 168 metres.

| Applied model | Number of flow paths | | $t_0$ (h) | D/v (m) | Pe | f | R | Class* |
|---|---|---|---|---|---|---|---|---|
| 3E, act.inj stop | two | 1st | 188 | 44.2 | 3.8 | 0.73 | 0.971 | 1 |
| | | 2nd | 661 | 12.3 | 13.7 | 0.27 | | |
| 3E, adj.inj stop | two | 1st | 182 | 25.0 | 6.7 | 0.76 | 0.983 | 1 |
| | | 2nd | 606 | 15.8 | 10.6 | 0.24 | | |

* Classification; 1–poor, 2–acceptable, 3–good
act. = injection scheme with actual stop time used for model fit
adj. = injection scheme with adjusted stop time used for model fit, see text for explanation

### 5.2.1.2 Iodide, KFI06 Upper Section

Iodide was injected as a step injection in borehole KFI06 in the upper part of the fracture zone. However, after 125 hours of injection the entire volume of tracer labelled water accidentally was released during a 3.5 hour period. Hence, the main part of the Iodide tracer solution was injected as a pulse, forced into the straddled upper sub–zone of Zone 2. Results from the sampling of major conductors with straddle packers in the withdrawal borehole BFI02 showed at least two inflow levels for Iodide in the upper part of Zone 2, 208 and 212 m (Fig 4–2 and Table 4–6). Regression was carried out for one, two and three flow paths and the results are presented in Table 5–3 and Appendices H and I.

Within the Fracture Zone Project, phase 3 a preparatory tracer run was carried out in the upper highly conductive part of Zone 2 during interference test no. 2 /Andersson et al, 1989/. Pumping in BFI02 was then done in only the upper part of Zone 2, isolated by packers. An iodide tracer pulse was injected in KFI06 and a comparison can be made with the present tracer test. The hydraulic head difference between point of injection and tracer withdrawal (BFI02) was much higher during the preparatory test, 4.5 m, compared to 0.6 m in the present test. Accordingly the tracer residence time

were much larger in the present low gradient test. Notably is the dispersivity, which for the high gradient case in the preparatory tracer run was about half the value obtained in the present test. Both in the case of one and two main flow paths interpreted to transport tracer from point of injection to tracer withdrawal. Similar results are also reported by Raven et al. /1988/. They found forced gradient tests to underestimate dispersion in natural fracture flow.

Table 5-3. Results of inverse 1-D modeling of the complete Iodide breakthrough curve in borehole BFI02. The tracer originates from injection in borehole KFI06, upper section. Distance is 189 metres.

| Applied model | Number of flow paths | $t_0$ (h) | D/v (m) | Pe | f | R | Class* |
|---|---|---|---|---|---|---|---|
| 3E | one 1st | 288 | 24.0 | 7.9 | - | 0.977 | 3 |
| | two 1st | 236 | 11.0 | 17.2 | 0.42 | 0.997 | 2 |
| | 2nd | 623 | 56.8 | 3.3 | 0.58 | | |
| | three 1st | 240 | 12.0 | 15.8 | 0.47 | 0.997 | 1 |
| | 2nd | 594 | 23.8 | 8.0 | 0.26 | | |
| | 3rd | 1236 | 79.4 | 2.4 | 0.27 | | |

* Classification; 1-poor, 2-acceptable, 3-good

### 5.2.1.3 Gd-DTPA, Amino G and Tm-EDTA, KFI11 Upper Section

In borehole KFI11 tracer injections were made at two occations in the upper part of Zone 2. At the first occation Gd-DTPA was continuously injected during 1194 hours. The second injection was made after the sampling of major conductors in the tracer withdrawal borehole BFI02 was finished. Amino G and Tm-EDTA were then simultaneously injected in a short tracer pulse.

**Gd-DTPA** was injected as a long step input, but without excess pressure according to the procedure described in section 3.2.3. Detailed sampling with straddle packers showed two inflow levels in the upper highly conductive part of Zone 2 (203 and 208 m) and one inflow level in the lower part of the zone, at 257 m depth in BFI02. Model fits were made with both one and two main flow paths. An attempt with three main flow paths did not reach the convergence limits set for the regression algorithm. The results of the model fits are presented in Table 5-4.

**Amino G** and **Tm-EDTA** were injected with a decying pulse technique, as described in section 3.2.3. The tracer is then released into the flowing water in the fractures without any overpressure while the tracer mass release per time unit can be measured. Amino G has been widely used in earlier tracer experiments while Tm-EDTA had not been used in swedish crystalline rock

earlier, it was then descided to perform a simultaneous injection of these tracers. The breakthrough curves obtained was nearly identical, except that the tracer recovery was somewhat higher for Amino G. Only the Amino G breakthrough curve was utilized for regression estimates with the models. The results of model fits are presented in Table 5-5 below.

Table 5-4 Results of inverse 1-D modeling of the complete Gd-DTPA breakthrough curve in borehole BFI02. The tracer originates from injection in borehole KFI11, upper section. Distance is 155 metres.

| Applied model | Number of flow paths | | $t_0$ (h) | D/v (m) | Pe | f | R | Class* |
|---|---|---|---|---|---|---|---|---|
| 3E, act.inj stop | one | 1st | 72 | 52.6 | 3.0 | - | 0.970 | 3 |
| 3E, adj.inj stop | one | 1st | 68 | 40.4 | 3.8 | - | 0.976 | 3 |
| 3E, adj.inj stop | two | 1st | 38 | 3.6 | 42.7 | 0.35 | 0.978 | 2 |
| | | 2nd | 100 | 10.7 | 14.5 | 0.65 | | |

* Classification; 1-poor, 2-acceptable, 3-good
act. = injection scheme with actual stop time used for model fit
adj. = injection scheme with adjusted stop time used for model fit, see text for explanation

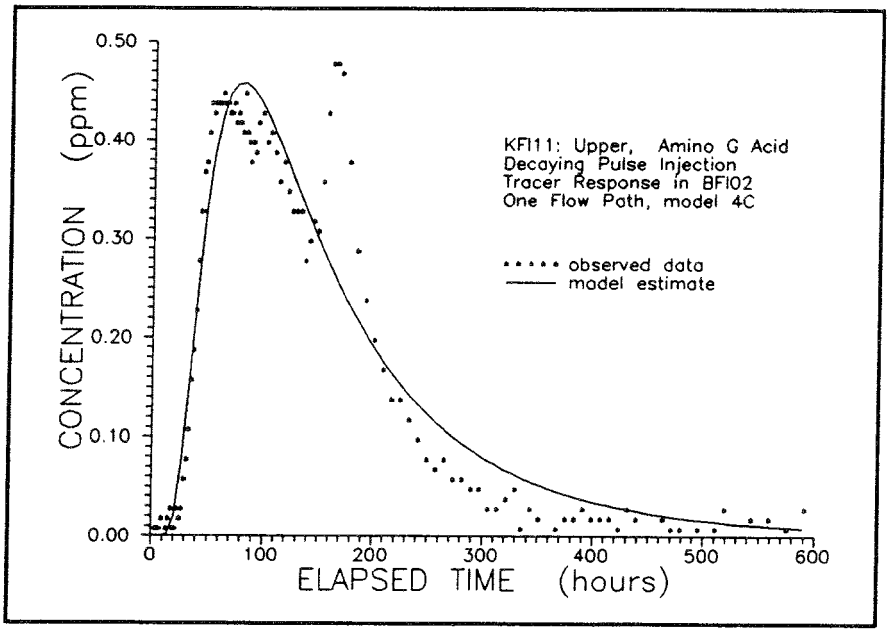


Figure 5-3 Regression result Amino G. Instantaneous pulse (4C) one flow path.

Figure 5-3 shows the regression results, assuming one flow path and using model 4C. In this case the injection boundary condition was an instantaneous pulse according to the solution by Kreft et al./1974/ (Equation 5.7). However, as this was an undisturbed pulse injection one might expect that the

appropriate upper boundary condition would be that of a decaying pulse injection as given by Van Genuchten /1982/, i.e. model 5C with the solution given by Eqn. (5.9). As a comparison, a regression estimate using model 5C with the latter boundary condition is shown in Figure 5–4. As can be seen, there is almost no difference between the two. Thus, in this case, explanation of observed data is not improved by accounting for a decaying inlet concentration.

Table 5–5 Results of inverse 1–D modeling of the complete Amino G Acid breakthrough curve in borehole BFI02. The tracer originates from injection in borehole KFI11, upper section. Distance is 155 metres.

| Applied model | Number of flow paths | | $t_0$ (h) | D/v (m) | Pe | f | R | Class* |
|---|---|---|---|---|---|---|---|---|
| 4C, inst. pulse | one | 1st | 169 | 43.6 | 3.6 | – | 0.967 | 2 |
| | two | 1st | 142 | 36.3 | 4.3 | 0.90 | 0.992 | 3 |
| | | 2nd | 170 | 0.5 | 306.1 | 0.10 | | |
| 5C, decay. pulse | one | 1st | 49 | 29.6 | 5.2 | – | 0.967 | 2 |
| | two | 1st | 39 | 3.3 | 47.3 | 0.58 | 0.976 | 2 |
| | | 2nd | 103 | 9.6 | 16.2 | 0.42 | | |
| 3E, short step | one | 1st | 52 | 18.7 | 5.2 | – | 0.964 | 3 |
| | two | 1st | 46 | 9.1 | 17.0 | 0.57 | 0.971 | 2 |
| | | 2nd | 103 | 65.2 | 2.4 | 0.43 | | |

* Classification; 1–poor, 2–acceptable, 3–good

For Gd–DTPA, previously injected in the same borehole section as Amino G there was observational evidence from the sampling of hydraulic conductors in BFI02 for the occurence of more than one major flow path in the fracture zone between the injection point and the pumped tracer withdrawal borehole BFI02. Thus, a model assuming two major flow paths was also applied to Amino G breakthrough data even though this tracer was injected after that the detailed sampling of inflow levels in the withdrawal borehole was terminated. An instantaneous pulse (model 4C) was fitted to the breakthrough curve, which is shown in Figure 5–5. At a first glance, one can see that observed data is explained extremely well by this model. The bulk of the transport appears to take place in the upper plane with relatively large dispersion (D/v = 36.3 m in this case), while there is a second preferential flow path with very little dispersion. However, although the statistical analysis of the regression results showed that the fitted parameters were unique, this model was rejected. The reason was that the second flow path in this case had a dispersivity of 0.5 m, which was regarded as unreasonably low. A regression estimate assuming a decaying pulse injection, model 5C, and two main flow paths could not fit the second peak, see Figure 5–6.

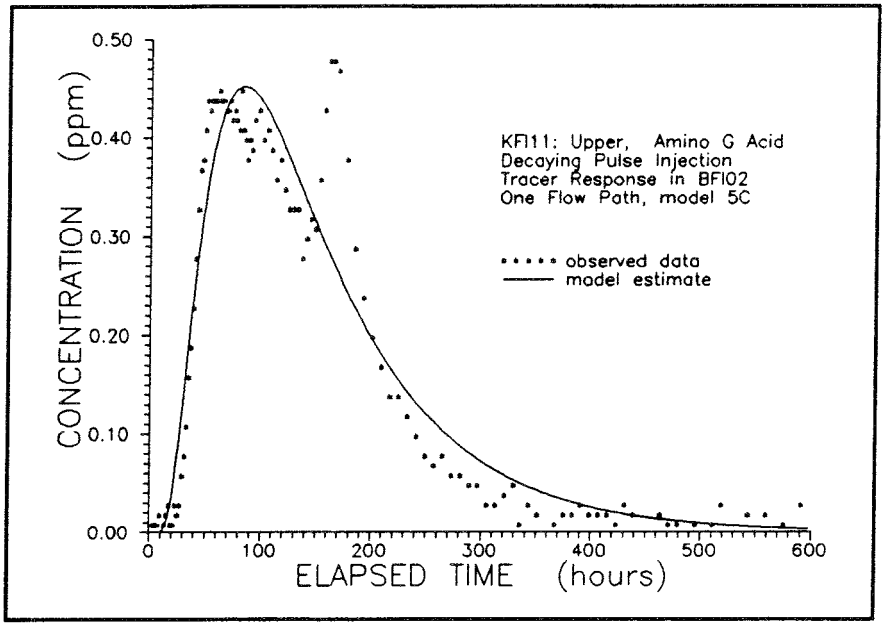


Figure 5–4 Regression estimate.Decaying pulse (5C) one flow path.

Instead, a more careful analysis of the injection data was undertaken, showing that tracer mass was not leaving the injection section as an exponential function (Figure 5–7). Accordingly, a variable injection scheme was considered, estimated from the tracer injection data (Figure 5–8). Model 3E, which can account for a variable injection rate, was tried for one and two flow paths, of which the latter is shown in Figure 5–9. Considering that the injection tracer data only allowed for an approximate estimate of the injection scheme, it can be seen that the second peak in the breakthrough curve is explained very well by using the injection data in more detail. In addition, the assumption of two flow paths (which previously had been observed between injection point and withdrawal borehole) explains the complete breakthrough curve very well. The correlations between parameters were reasonable low, so it was judged that none of the fitted parameters were redundant in this case. This should be seen as a demonstration of the importance of accounting for the tracer injection. In this case, an erroneous interpretation of the breakthrough curve was avoided due to the monitoring of tracer injection flow rate and concentration.

A similar conceptual idea, but another approach to account for variable injection flow rates was used by the LBL/USDOE project team /Long and Coworkers ,1990/ in their evaluation of the Stripa 3–D tracer experiment. Normalized breakthrough curves, where the number of peaks corresponds to the number of flow paths, was derived from Toepliz analysis and subsequent a 1–D advection–diffusion solution was fitted to the calulated breakthrough curves. However, in the present radially convergent tracer test part of the analysis of the breakthrough curves is sudden measured changes at a few occations in the tracer mass release per time unit into the fracture system. With that knowledge it was judged more straightforward to use the method described above to account for variable injection flow rates, adopted in the present test.

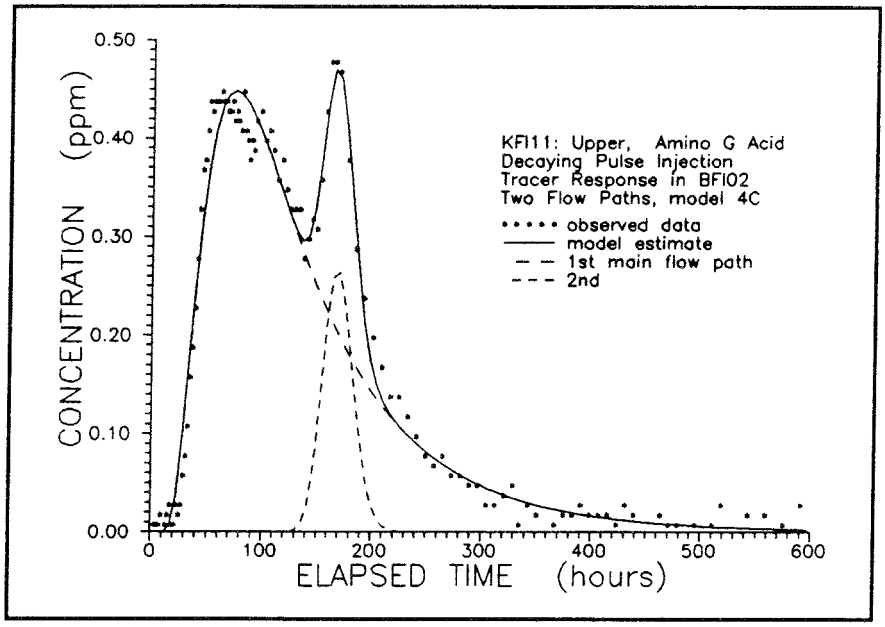


Figure 5-5 Model estimate (4C) two flow paths. Amino G.

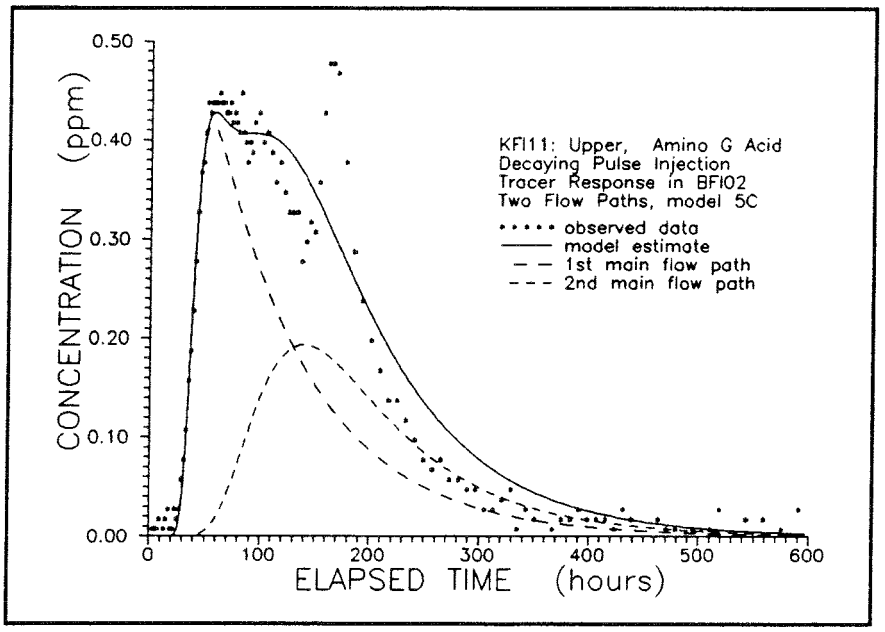


Figure 5-6 Model estimate (5C) two flow paths. Amino G.

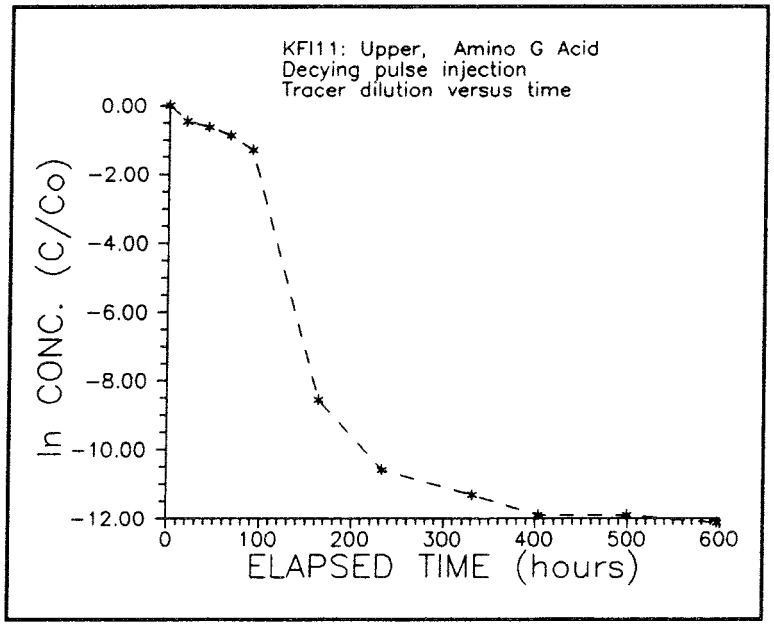


Figure 5–7 Measured concentrations of Amino G in borehole section used for the tracer injection.

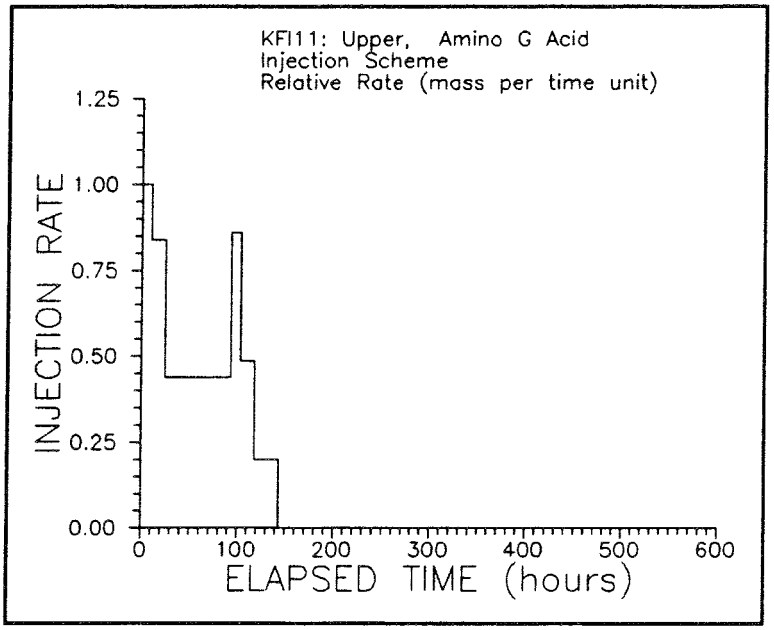


Figure 5–8 Tracer Amino G injection scheme, expressed as tracer mass release per time unit into the fracture zone.

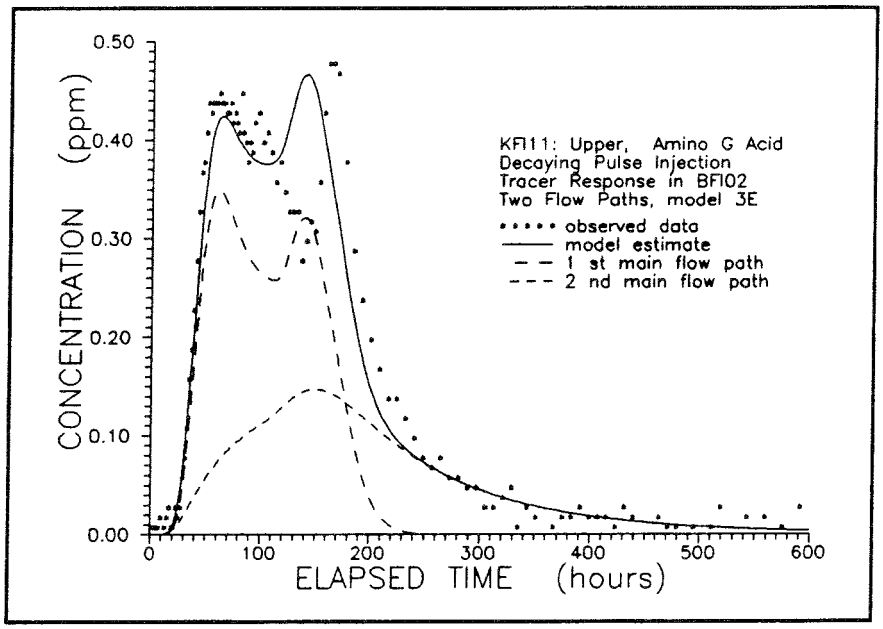


Figure 5-9 Model estimate (3E) accounting for the variable injection scheme. Amino G.

## 5.2.2 Tracers Injected in Intermediate Parts of Zone 2

### 5.2.2.1 Uranine, BFI01 Middle Section

Uranine was injected as a 1133 hours long step input. During this period the injection was interrupted five times due to accidental injection pump stops lasting for 2 to 25 hours. The sampling of major conductors in tracer withdrawal borehole BFI02 showed tracer arrivals of Uranine both in the upper, middle and lower parts of Zone 2. Inverse modeling was made assuming one flow path. The result is presented in Table 5-6.

Table 5-6 Results of inverse 1-D modeling of the complete Uranine breakthrough curve in borehole BFI02. The tracer originates from injection in borehole BFI01, middle section. Distance is 168 metres.

| Applied model | Number of flow paths | $t_0$ (h) | D/v (m) | Pe | f | R | Class* |
|---|---|---|---|---|---|---|---|
| 3E | one 1st | 1309 | 21.6 | 7.8 | - | 0.972 | 3 |

* Classification; 1-poor, 2-acceptable, 3-good

### 5.2.2.2 Yb-EDTA, KFI06 Middle Section

At the sampling of hydraulic conductors in the withdrawal borehole BFI02 the tracer Yb-EDTA was found in both upper and lower part of Zone 2. The regression estimate was made considering the variable injection rate of the step input. One and two main flow paths were assumed and the results of the inverse modelling are presented in Table 5-7.

Table 5-7 Results of inverse 1-D modeling of the complete Yb-EDTA breakthrough curve in borehole BFI02. The tracer originates from injection in borehole KFI06, middle section. Distance is 191 metres.

| Applied model | Number of flow paths | $t_0$ (h) | D/v (m) | Pe | f | R | Class* |
|---|---|---|---|---|---|---|---|
| 3E | one 1st | 2056 | 28.4 | 6.7 | - | 0.798 | 2 |
| | two 1st | 1544 | 7.0 | 27.5 | 0.37 | 0.960 | 1.5 |
| | 2nd | 4116 | 11.4 | 16.8 | 0.63 | | |

* Classification; 1-poor, 2-acceptable, 3-good

### 5.2.2.3 Er-EDTA, KFI11 Middle Section

Er-EDTA was found in both upper and lower parts of Zone 2 in the withdrawal borehole BFI02. Both one and two main flow paths were assumed in the model fits to the breakthrough curve. The variable injection scheme of the step input (Appendix G) was accounted for. The results are presented in Table 5-8.

Table 5-8. Results of inverse 1-D modeling of the complete Er-EDTA breakthrough curve in borehole BFI02. The tracer originates from injection in borehole KFI11, middle section. Distance is 169 metres.

| Applied model | Number of flow paths | $t_0$ (h) | D/v (m) | Pe | f | R | Class* |
|---|---|---|---|---|---|---|---|
| 3E | one 1st | 1040 | 1.3 | 132.4 | - | 0.838 | 2 |
| | two 1st | 1039 | 1.2 | 136.0 | 0.61 | 0.864 | 2.5 |
| | 2nd | 3220 | 2.1 | 81.8 | 0.39 | | |

* Classification; 1-poor, 2-acceptable, 3-good

## 5.2.3 Tracers Injected in Lower Part of Zone 2

### 5.2.3.1 Ho-EDTA, BFI01 Lower Section

Ho-EDTA was found in two narrow spaced inflow levels, 203 and 208 m, in the upper part of Zone 2. Model fits were made with one and two main flow paths. In the case of two main flow paths the regression statistics showed so strong correlation between parameters that there was no significance for two main flow paths, and this model was rejected. The results are presented in Table 5-9. It can be seen that the rejected regression estimate with two flow paths have practically the same values on the determined parameters.

Table 5-9. Results of inverse 1-D modeling of the complete Ho-EDTA breakthrough curve in borehole BFI02. The tracer originates from injection in borehole BFI01, lower section. Distance is 201 metres.

| Applied model | Number of flow paths | $t_0$ (h) | D/v (m) | Pe | f | R | Class* |
|---|---|---|---|---|---|---|---|
| 3E | one 1st | 2322 | 7.2 | 27.8 | - | 0.981 | 2.5 |
| | two 1st | 2310 | 6.9 | 29.2 | 0.68 | 0.981 | 1 |
| | 2nd | 2343 | 7.8 | 25.9 | 0.32 | | |

* Classification; 1-poor, 2-acceptable, 3-good

### 5.2.3.2 $ReO_4$, KFI06 Lower Section

$ReO_4$ was injected as a step input in borehole KFI06 in the lower part of the fracture zone. In this case the tracer mass injection varied significantly with time, Figure 5-10. The $ReO_4$ tracer was found in two nearby hydraulic conductors in the withdrawal borehole BFI02 (257 and 260 m) in the lower part of Zone 2 and in one conductor in the upper part of the zone. From the sampling of the hydraulic conductors in the withdrawal borehole (Appendix E:3) it was also concluded that the bulk of the tracer arrived in the lower part of the fracture zone, while a smaller part arrived in the upper part. Regression with a two path model, accounting for the variable mass injection, is presented in Figure 5-11. Data is explained by the model very well up to around 2000 hours. The remaining tailing beyond this point is not explained. Regression runs using three main flow paths did improve the correlation to experimental data to some extent (Figure 5-12), but the third main flow path did not fit the tail part of the breakthrough curve as nice as desired if advection/dispersion was the only process governing tracer transport, and if applied injection scheme is correct. Other processes, such as matrix diffusion and/or transient solute storage may explain the difference between model fit and experimentally obtained data. The results of the model fits are presented in Table 5-10.

Table 5–10 Results of inverse 1–D modeling of the complete $ReO_4$ breakthrough curve in borehole BFI02. The tracer originates from injection in borehole BFI01, lower section. Distance is 189 metres.

| Applied model | Number of flow paths | | $t_0$ (h) | D/v (m) | Pe | f | R | Class* |
|---|---|---|---|---|---|---|---|---|
| 3E | one | 1st | 691 | 106.6 | 1.8 | - | 0.896 | 2 |
| | two | 1st | 404 | 11.5 | 16.4 | 0.62 | 0.971 | 3 |
| | | 2nd | 1167 | 0.8 | 243.0 | 0.38 | | |
| | three | 1st | 375 | 10.7 | 17.6 | 0.52 | 0.978 | 3 |
| | | 2nd | 1167 | 0.7 | 266 | 0.31 | | |
| | | 3rd | 2500 | 4.0 | 47.2 | 0.17 | | |

* Classification; 1–poor, 2–acceptable, 3–good

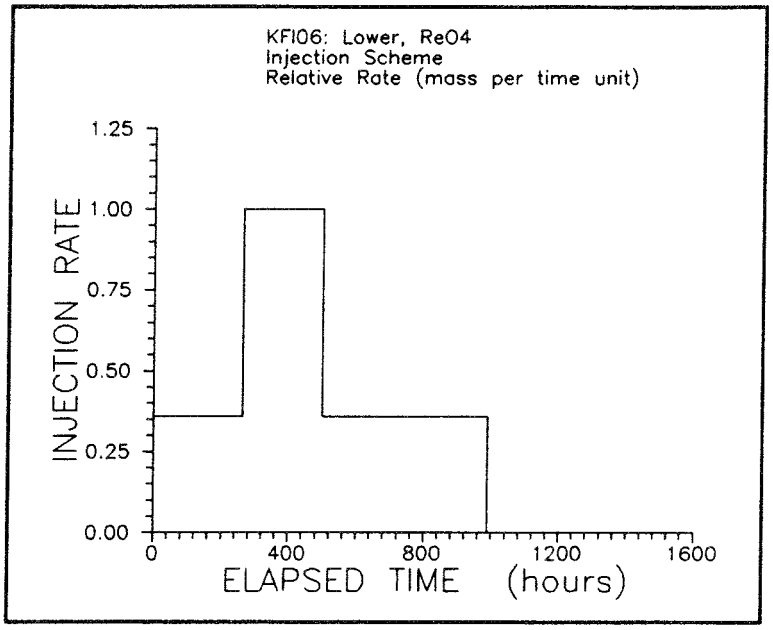


Figure 5–10 Injection scheme for $ReO_4$ tracer, KFI06 lower section.

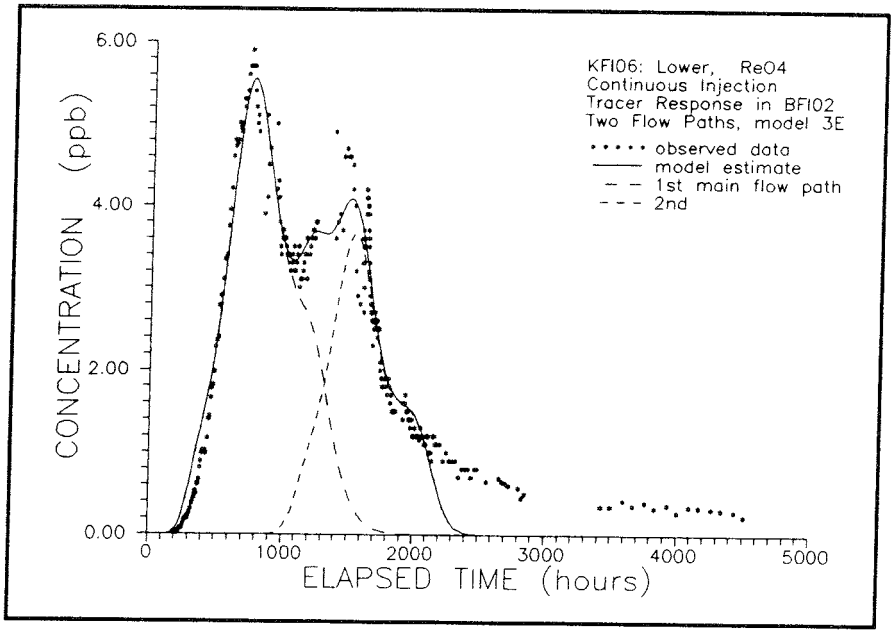


Figure 5–11 Model fit two flow paths $ReO_4$.

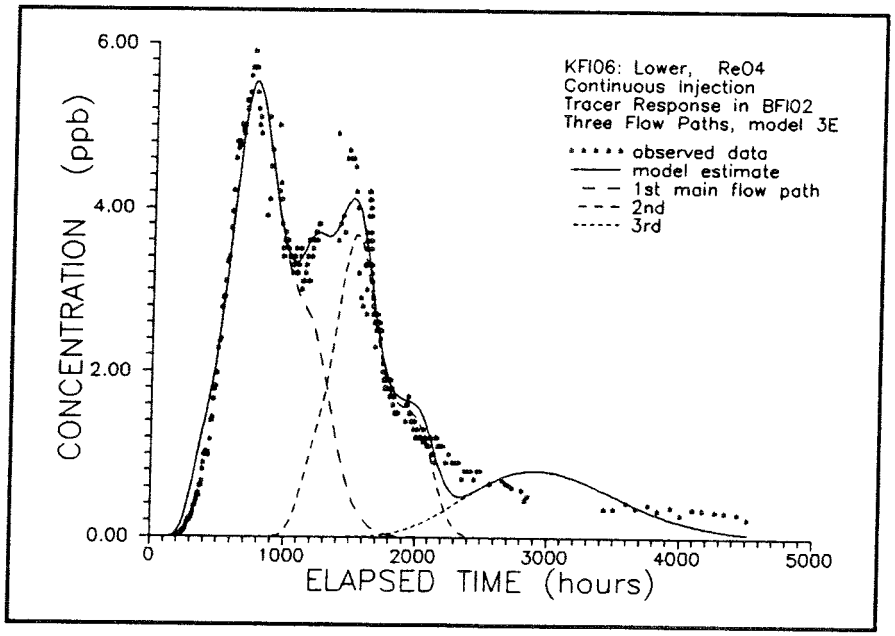


Figure 5–12 Model fit three flow paths $ReO_4$.

### 5.2.3.3 Dy–EDTA, KFI11 Lower Section

Dy–EDTA was injected as a 836 hours long step input, which was unintendly inerrupted for 24 hours after 718 hours of injection. The Dy–EDTA tracer breakthrough was delayed compared to the other tracers.

Table 5-11 Results of inverse 1-D modeling of the complete Dy-EDTA breakthrough curve in borehole BFI02. The tracer originates from injection in borehole KFI11, lower section. Distance is 190 metres.

| Applied model | Number of flow paths | $t_0$ (h) | D/v (m) | Pe | f | R | Class* |
|---|---|---|---|---|---|---|---|
| 3E | one 1st | 4319 | 6.7 | 28.5 | - | 0.734 | 1.5 |

* Classification; 1-poor, 2-acceptable, 3-good

### 5.2.4 Residence Times

The residence time, $t_0$, also called the mean transport time, of the tracer labelled groundwater, were determined from fitting procedures with theoretical solutions /Ogata and Banks, 1961/, /Lenda and Zuber, 1970/, /Kreft et al, 1974/, /Van Genuchtenand Alves, 1982/, /Van Genuchten, 1982/. Residence times are summarized in Table 5-12 together with tracer first arrivals and mean velocities. The time of first arrival and the early part of the breakthrough curve of the solute are important in nuclear safety, "whereas later flow fractions represent lower levels of radiotoxicity due to radioactive decay. This marks a distinct difference from common approaches in chemical engineering and heat extraction" /Brotzen, 1986/. At long recidence times and a high dispersion the difference between the first arrival and the residence time may be considerable.

The absolute values of residence times and first arrivals are functions of distance, hydraulic gradient and hydraulic conductivity. Thus, they are specific to the prevailed experimental conditions. However, some conclusions about the fracture flow paths within Zone 2 can anyway be drawn. In general the tracer first arrival occurs at about half the time of the mean residence time. The most rapid flow paths are found in the upper margin of Zone 2. Within Zone 2 and between upper and lower margins sub-zones constitute flow paths of considerable variable residence times. From a hundred to some thousand hours at the test conditions prevailed, where the hydraulic gradient ranged from 0.003 to 0.007 depending on direction from the pumped withdrawal borehole. In the lower margin of Zone 2 a fast flow path was measured in the direction of the strike of the zone, from KFI06 to BFI02. Velocities of tracer labelled water measured from $1.2 \cdot 10^{-5}$ to $1.1 \cdot 10^{-3}$ m/s.

### 5.2.5 Dispersivities

From the results of the inverse modelling, summarized in Table 5-12, the dispersion lengths, D/v, within main flow paths (sub-zones) in Zone 2 is estimated to range from 4 - 11 metres and Peclet numbers from 16 to 40.

The macro-dispersion is here defined as the phenomena obtained due to superposed breakthroughs from solute transport in more than one main flow

path and in Zone 2 it is estimated to give dispersivities in the range from 20 to 90 metres and the Peclet numbers from 2 to 8. Hence, in Zone 2 the macro-dispersion gives about 3 to 10 times larger dispersion length over the entire thickness of Zone 2 than in the individual main flow paths (sub-zones)

Table 5-12 Tracer first arrivals, mean residence times, velocities and dispersivities in fracture flow paths within Zone 2, Brändan area Finnsjön site.

| Injection point | | Detection* in BFI02 | Distance (m) | Flow path | $t_0$ (h) | t** (h) | D/v (m) | Pe | v (m/s) |
|---|---|---|---|---|---|---|---|---|---|
| BFI01: Upper | → | Upper part | 168 | first | 154 | 75 | 6.3 | 26.8 | $3.0 \cdot 10^{-4}$ |
| | → | Lower part | | second | 630 | 360 | 7.6 | 22.2 | $7.4 \cdot 10^{-5}$ |
| | → | Upper and Lower | | total | 201 | | 82.5 | 2.0 | $2.3 \cdot 10^{-4}$ |
| KFI06: Upper | → | Upper part | 189 | first | 236 | 106 | 11.0 | 17.2 | $2.2 \cdot 10^{-4}$ |
| | → | Upper part | | second | 623 | 165 | 56.8 | 3.3 | $8.4 \cdot 10^{-5}$ |
| | → | Upper part | | total | 288 | | 24.0 | 7.9 | $1.8 \cdot 10^{-4}$ |
| KFI11: Upper | → | Upper part | 155 | first | 38 | 24 | 3.6 | 42.7 | $1.1 \cdot 10^{-3}$ |
| | → | Lower part | | second | 100 | 50 | 10.7 | 14.5 | $4.3 \cdot 10^{-4}$ |
| | → | Upper and Lower | | total | 68 | | 40.4 | 3.8 | $6.3 \cdot 10^{-4}$ |
| BFI01: Middle | → | Entire zone | 168 | total | 1309 | 600 | 21.6 | 7.8 | $3.6 \cdot 10^{-5}$ |
| KFI06: Middle | → | Upper or Lower | 191 | first | 1544 | 1250 | 7.0 | 27.5 | $3.4 \cdot 10^{-5}$ |
| | → | Upper or Lower | | second | 4116 | 1700 | 11.4 | 16.8 | $1.3 \cdot 10^{-5}$ |
| | → | Upper and Lower | | total | 2056 | | 28.4 | 6.7 | $2.6 \cdot 10^{-5}$ |
| KFI11: Middle | → | Upper or Lower | 169 | first | 1039 | 850 | 1.2 | 136.0 | $4.5 \cdot 10^{-5}$ |
| | → | Upper or Lower | | second | 3220 | 2300 | 2.1 | 81.8 | $2.0 \cdot 10^{-5}$ |
| | → | Upper and Lower | | total | 1040 | | 1.3 | 132.4 | $4.5 \cdot 10^{-5}$ |
| BFI01: Lower | → | Upper part | 201 | total | 2322 | 1300 | 7.2 | 27.8 | $2.4 \cdot 10^{-5}$ |
| KFI06: Lower | → | Lower part | 189 | first | 404 | 194 | 11.5 | 16.4 | $1.3 \cdot 10^{-4}$ |
| | → | Upper part | | second | 1167 | 900 | 0.8 | 243.0 | $4.5 \cdot 10^{-5}$ |
| | → | Upper and Lower | | total | 691 | | 106.6 | 1.8 | $7.6 \cdot 10^{-5}$ |
| KFI11: Lower | → | Upper part | 190 | total | 4319 | 3200 | 6.7 | 28.5 | $1.2 \cdot 10^{-5}$ |

* Illustration of flow paths, see Figures 4-1, 4-2 and 4-3

** Tracer first arrival measured in withdrawn water is coupled to the first main flow path
Tracer first arrival in second flow path is determined from the model fit, Appendix H

## 5.3 DETERMINATION OF FRACTURE FLOW AND TRANSPORT PARAMETERS

The parameters determined below are to a great extent calculated with the residence time of a tracer ($t_0$) as one of the basic variables. It is here assumed that the tracers used in this experiment were not retarded compared to groundwater flow. Laboratory measurements (Sections 4.4.4 and 4.5.3) have indicated that long term stability may be a problem for some of the 11 tracers used. Long residence times were obtained from some injection points, these residence times may have been increased to some degree due to insufficient stability of the tracer metal–complex used.

### 5.3.1 Hydraulic Fracture Conductivity

The hydraulic properties of a fractured crystalline rock aquifer can be expressed as an average hydraulic conductivity for the whole thickness of the aquifer or parts thereof, e.g. fracture zones. The hydraulic average conductivity is then determined from single hole hydraulic tests or multiple borehole pumping tests (interference tests).

The hydraulic fracture conductivity can be determined by two approaches. Firstly, in a radially converging flow field the hydraulic conductivity of actual flow paths can at steady state be evaluated as a function of geometry and withdrawal rate, by assuming laminar flow in one or more smooth parallel fractures. Secondly, if a tracer is injected at some radial distance in this flow field, the hydraulic conductivity of actual flow paths can be calculated with the residence time as the basic variable.

The hydraulic conductivity calculated by the two methods mentioned above will coincide only in the case of a smooth parallel fracture. Both methods were adopted by e.g. Gustafsson and Klockars, /1981/, Andersson and Klockars, /1985/. They both found discrepancies in the hydraulic conductivity determined with fluid flux (flow rate) or residence time (velocity) as the basic variable.

Assumming that Darcy`s law is valid the hydraulic conductivity for an aquifer or a part thereof can be determined by the equation:

$$K = Q \cdot \ln(r/r_w) / (2 \cdot \pi \cdot \Delta h \cdot L) \qquad (5.12)$$

where:
- $\Delta h$ = hydraulic head difference
- $r$ = radial distance
- $r_w$ = well radius
- $L$ = length of test section

The hydraulic conductivity for laminar flow between two smooth parallel plates is governed by the square of the aperture and the kinematic viscosity

of the fluid /Snow, 1968/.

$$K_e = e^2 \cdot g/(12 \cdot \nu) \qquad (5.13)$$

where: $\nu$ = kinematic viscosity

If the the flow in the aquifer is concentrated to one single fracture then:

$$T = K_e \cdot e = K \cdot L \qquad (5.14)$$

Substitution with Equations (5.12) and (5.13) gives the hydraulic conductivity for one equivalent single fracture, with the withdrawal rate as the basic variable.

$$K_e^q = [(Q \cdot \ln(r/r_w) \cdot g^{1/2}) \,/\, (2 \cdot \pi \cdot \Delta h \cdot (12\nu)^{1/2})]^{2/3} \qquad (5.15)$$

If a tracer is injected at some distance from a pumped well the hydraulic conductivity of the actual flow paths can be calculated with the residence time as the basic variable, assuming radial flow field /Gustafsson & Andersson, 1991/.

$$K_e^t = [(r^2 - r_w^2) \cdot \ln(r/r_w)] \,/\, (2 \cdot t_0 \cdot \Delta h) \qquad (5.16)$$

where: $t_0$ = residence time
$r$ = distance to point of tracer injection

With tracers injected in many directions a comparison of the $K_e^t$ will give a measure on the degree of heterogeneity of the fracture governed by directional variations in the mean value of the square of the aperture, along the actual flow paths.

**The results of the parameter calculations** are presented in Table 5–13. The hydraulic fracture conductivities determined with the flow rate as basic variable are all higher than corresponding conductivities determined with the residence time as the basic variable. This difference reflects large geometrical variations (i.e. of apertures and breadths) in the flow paths of the fracture system. In the upper sub–zone of Zone 2 the ratio $K_e^q/K_e^t$ is about 10, whereas in middle and lower parts of Zone 2 it is much higher, in the range of 30 – 100.

A distinction between the sub–zones within Zone 2 and their corresponding main flow paths can be made by studying the $K_e^t$ values, which have been possible to calculate for all main flow paths.

Three tracers were injected in the upper sub-zone of Zone 2 and they were all found in the upper sub-zone at the withdrawal borehole, but two tracers were also retrieved in lower parts of Zone 2. The fracture flow paths within the upper sub-zone have all about the same hydraulic conductivity, $K_e^t$, and have a mean value of $3.8 \cdot 10^{-1}$ m/s. The two flow paths measured from upper to lower part of Zone 2 have conductivity values of $3.6 \cdot 10^{-1}$ and $4.1 \cdot 10^{-2}$ m/s.

Tracer injected in intermediate sub-zones are found in both upper, middle and lower part of Zone 2. The mean value of the hydraulic conductivity in these fracture flow paths is $2.8 \cdot 10^{-2}$ m/s.

Table 5-13 Hydraulic conductivity of fracture flow paths in Zone 2. Determined both with the residence time of the tracer and with the discharge flow rate as the basic variable.

| Injection point | | Detection in BFI02 | Distance (m) | Flow path | $t_0$ (h) | $K_e^t$ (m/s) | $K_e^q$ (m/s) |
|---|---|---|---|---|---|---|---|
| BFI01: Upper | → | Upper part | 168 | first | 154 | $1.7 \cdot 10^{-1}$ | $9.8 \cdot 10^{-1}$ |
| | → | Lower part | | second | 630 | $4.1 \cdot 10^{-2}$ | $7.9 \cdot 10^{-1}$ |
| | → | Upper and Lower | | total | 201 | $1.3 \cdot 10^{-1}$ | 1.4 |
| KFI06: Upper | → | Upper part | 189 | first | 236 | $3.0 \cdot 10^{-1}$ | |
| | → | Upper part | | second | 623 | $1.1 \cdot 10^{-1}$ | |
| | → | Upper part | | total | 288 | $2.4 \cdot 10^{-1}$ | 1.6 |
| KFI11: Upper | → | Upper part | 155 | first | 38 | $9.3 \cdot 10^{-1}$ | 1.3 |
| | → | Lower part | | second | 100 | $3.6 \cdot 10^{-1}$ | 1.1 |
| | → | Upper and Lower | | total | 68 | $5.2 \cdot 10^{-1}$ | 1.9 |
| BFI01: Middle | → | Entire zone | 168 | total | 1309 | $1.8 \cdot 10^{-2}$ | 1.3 |
| KFI06: Middle | → | Upper or Lower | 191 | first | 1544 | $4.5 \cdot 10^{-2}$ | |
| | → | Upper or Lower | | second | 4116 | $1.7 \cdot 10^{-2}$ | |
| | → | Upper and Lower | | total | 2056 | $3.4 \cdot 10^{-2}$ | 2.3 |
| KFI11: Middle | → | Upper or Lower | 169 | first | 1039 | $4.5 \cdot 10^{-2}$ | |
| | → | Upper or Lower | | second | 3220 | $1.4 \cdot 10^{-2}$ | |
| | → | Upper and Lower | | total | 1040 | $4.5 \cdot 10^{-2}$ | 2.0 |
| BFI01: Lower | → | Upper part | 201 | total | 2322 | $1.3 \cdot 10^{-2}$ | $8.7 \cdot 10^{-1}$ |
| KFI06: Lower | → | Lower part | 189 | first | 404 | $1.8 \cdot 10^{-1}$ | 1.4 |
| | → | Upper part | | second | 1167 | $6.4 \cdot 10^{-2}$ | 2.2 |
| | → | Upper and Lower | | total | 691 | $1.1 \cdot 10^{-1}$ | 2.4 |
| KFI11: Lower | → | Upper part | 190 | total | 4319 | $1.3 \cdot 10^{-2}$ | 1.4 |

Tracers injected in lowermost sub–zone of Zone 2 were retrieved in both lower and upper sub–zone. Mean value of conductivity in fracture flow paths from lower to upper part of Zone 2 is $3.0 \cdot 10^{-2}$ m/s. Only one tracer was transported within the lower sub–zone, from point of injection to detection. It was along the strike of Zone 2 (KFI06 → BFI02) and the conductivity, $K_e^t$, of the fracture flow path was determined to $1.8 \cdot 10^{-1}$ m/s.

## 5.3.2 Fracture Aperture

### 5.3.2.1 Frictional Loss Aperture

The fracture aperture can be calculated from the tracer residence time, $t_0$, and hydraulic head loss, $\Delta h$, as basic variables by substitution of $K_e$ in Equation (5.13) with $K_e^t$ determined according to Eqn. (5.16), giving the relation between aperture and hydraulic conductivity for laminar flow between parallel plates. This aperture is denoted frictional loss aperture /Tsang, 1992/ and is here symbolised by $e^t$.

$$e^t = (K_e^t \cdot 12 \cdot \nu / g)^{1/2} \tag{5.17}$$

### 5.3.2.2 Cubic Law Aperture

Alternatively the fracture aperture can be related to the transmissivity of the fracture and calculated from flow rate, Q, and hydraulic head loss, $\Delta h$. Then $K_e$ in Equation (5.13) is substituted with $K_e^q$ determined according to Eqn. (5.15). This aperture is symbolised by $e^q$ and is by Tsang /1992/ denoted cubic law aperture.

$$e^q = (K_e^q \cdot 12 \cdot \nu / g)^{1/2} \tag{5.18}$$

The aperture calculated will thus be governed by the flux (cubic law) or the velocity (square dependence). The aperture calculated with the flow rate as the basic variable will thus coincide with that calculated from the velocity of a tracer solute only in the case of parallel planar plates representing the fracture surfaces /Brown, 1984/. Hence, in a natural fracture where the flow paths participating in the solute transport are mainly concentrated to inter–connected patches of elevated aperture the ratio $e^q/e^t$ will increase from unity the more pronounced the fracture flow path differ from parallel planar plates. Silliman /1989/ concluded from his theoretical study that in a fracture with isotropic aperture variation in two dimensions $e^q$ is larger than $e^t$.

### 5.3.2.3 Mass Balance Aperture

The mass balance aperture relates to the arithmetic mean of apertures in the flow path, i.e. the pore volume of the fracture. It is derived from tracer

residence time, $t_0$, flow rate, Q, and the assumtion that the areal extent of the water bearing fracture is known. In a radial flow geometry it is given by.

$$e^m = Q \cdot t_0 / [\pi(r^2 - r_w^2)] \quad (5.19)$$

By definition the cubic law aperture, $e^q$, in a single fracture can be expressed as a product of the square of the frictional loss aperture and the mass balance aperture of the same fracture.

$$(e^q)^3 = (e^t)^2 \cdot e^m \quad (5.20)$$

However, it can be demonstrated /Andersson et al., 1989/ that when a tracer is injected in a fracture zone or main flow path, made up of a few parallel plate fractures, the mass balance aperture, $e^m$, will on the one hand give a measure on the sum of the apertures of all hydraulically active fractures in the zone, i.e. pore volume of the zone. The frictional loss derived aperture, $e^t$, gives on the other hand the aperture of the single fractures and hence, the ratio $e^m/e^t$ gives the number of fractures constituting the main flow path or fracture zone. In accordance with the result of Silliman /1989/ the ratio $e^m/e^q$ may give a better estimate of the number of fractures contributing to water flow in a zone with a couple of rough-walled fractures of varying aperture. These relationships can be utilized for estimates of the flow wetted surface of a main flow path or fracture zone, as shown below.

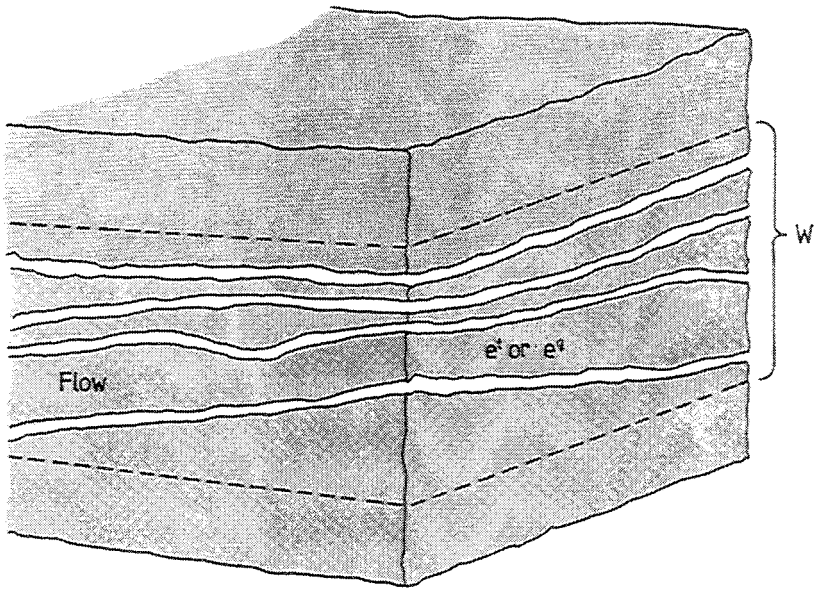


Figure 5-34 Principle of fracture zone made up of a few narrow spaced fractures in an otherwise low conductive rock mass.

### 5.3.2.4 Calculated Apertures

The fracture apertures within Zone 2 have been calculated according to the three different concepts presented above and the results are presented in Table 5–14. The relative magnitudes of the experimentally obtained apertures follows the theoretical relationship, that $e^q$ is larger than $e^t$ in the fracture flow paths /Silliman, 1989/ and /Tsang, 1992/.

On an average the residence time determined apertures, $e^t$, of the fracture flow path are a bit larger in the upper sub–zone than in flow paths in intermediate and lower parts of the Zone 2. The mass balance determined aperture, $e^m$, representing the total pore volume accessible to advective flow, i.e. the sum of apertures of all fractures contributing to flow within the studied sub–zone, is smaller in the upper and lower sub–zones than in the intermediate ones.

The ratios $e^m/e^t$, giving the number of fractures in the smooth fracture cases, indicates that 2 – 20 fractures contributes to groundwater flow in the upper sub–zone of Zone 2. The ratio $e^m/e^q$, which may be more appropriate for rough walled fractures, indicate 1 – 7 fractures in the upper highly conductive sub–zone. In lower sub–zones of Zone 2 the number of fractures contributing to groundwater flow is markedly higher, based on $e^m/e^t$ and $e^m/e^q$ ratios.

From the results presented in Table 5–14 representative values of apertures within the sub–zones of Zone 2 can be estimated. The fracture flow path aperture, $e^t$, has a mean value of $7.1 \cdot 10^{-4}$ m in the upper sub–zone, and $1.2 \cdot 10^{-4}$ m in intermediate parts of Zone 2. There is only one value obtained from tracer transport completely within the lower sub–zone, $2.3 \cdot 10^{-4}$ m. Representative values of the mass balance aperture, $e^m$, i.e. the sum of the apertures of all hydraulically active fractures in the sub–zones, are $1.0 \cdot 10^{-2}$ m in the upper sub–zone and $5.8 \cdot 10^{-2}$ and $1.1 \cdot 10^{-2}$ m in intermediate and lower sub–zones respectively.

The apertures calculated for Zone 2 can be compared with some fracture zones at Äspö HRL, where apertures have been estimated from a large scale tracer test /Gustafsson et al., 1991/. The mass balance aperture, $e^m$, of the 100 m thick zone EW–5 was estimated to $2.0 \cdot 10^{-2}$ m and in the 1 – 3 m thick zones NNW–1 and NNW–2 it was $3.2 \cdot 10^{-3}$ and $8.0 \cdot 10^{-3}$ m respectively.

In the Stripa mine /Andersson et al.,1989b/ ,a minor fracture zone in massive, fine to medium grained granite was investigated with radar and saline tracer. In the 14.5 m thick zone, having an hydraulic conductivity of about $1.3 \cdot 10^{-8}$ m/s, the aperture of the flow paths, $e^t$, was in the order of $1.2 \cdot 10^{-5}$ m and the sum of the apertures of all fractures contributing to flow within the zone, $e^m$, was $2.7 \cdot 10^{-3}$ m.

The comparison shows that the mass balance determined aperture, $e^m$, representing the total pore volume accessible to advective flow, i.e. the sum of apertures of all fractures contributing to flow, is in the same order of magnitude in Zone 2 at the Finnsjön site and in zone EW–5 at Äspö HRL,

both being about 100 m thick. Comparison of apertures in individual flow paths shows that apertures is about one order of magnitude larger in individual flow paths within Zone 2 than in a minor fracture zone in Stripa.

Table 5–14 Apertures of fracture flow paths within Zone 2.

| Injection point | | Detection in BFI02 | Distance (m) | Flow path | $t_0$ (h) | $e^t$ (m) | $e^q$ (m) | $e^m$ (m) |
|---|---|---|---|---|---|---|---|---|
| BFI01: Upper | → | Upper part | 168 | first | 154 | $5.2 \cdot 10^{-4}$ | $1.2 \cdot 10^{-3}$ | $7.2 \cdot 10^{-3}$ |
| | → | Lower part | | second | 630 | $2.6 \cdot 10^{-4}$ | $1.1 \cdot 10^{-3}$ | $2.1 \cdot 10^{-2}$ |
| | → | Upper and Lower | | total | 201 | $4.6 \cdot 10^{-4}$ | $1.5 \cdot 10^{-3}$ | $1.6 \cdot 10^{-2}$ |
| KFI06: Upper | → | Upper part | 189 | first | 236 | $6.9 \cdot 10^{-4}$ | - | $8.8 \cdot 10^{-3}$ |
| | → | Upper part | | second | 623 | $4.3 \cdot 10^{-4}$ | - | $2.3 \cdot 10^{-2}$ |
| | → | Upper part | | total | 288 | $6.3 \cdot 10^{-4}$ | $1.6 \cdot 10^{-3}$ | $1.1 \cdot 10^{-2}$ |
| KFI11: Upper | → | Upper part | 155 | first | 38 | $1.2 \cdot 10^{-3}$ | $1.7 \cdot 10^{-3}$ | $2.1 \cdot 10^{-3}$ |
| | → | Lower part | | second | 100 | $4.5 \cdot 10^{-4}$ | $1.3 \cdot 10^{-3}$ | $4.0 \cdot 10^{-3}$ |
| | → | Upper and Lower | | total | 68 | $6.6 \cdot 10^{-4}$ | $2.4 \cdot 10^{-3}$ | $6.5 \cdot 10^{-3}$ |
| BFI01: Middle | → | Entire zone | 168 | total | 1309 | $1.7 \cdot 10^{-4}$ | $1.5 \cdot 10^{-3}$ | $1.1 \cdot 10^{-1}$ |
| KFI06: Middle | → | Upper or Lower | 191 | first | 1544 | $5.7 \cdot 10^{-5}$ | | |
| | → | Upper or Lower | | second | 4116 | $2.1 \cdot 10^{-5}$ | | |
| | → | Upper and Lower | | total | 2056 | $4.3 \cdot 10^{-5}$ | $1.9 \cdot 10^{-3}$ | $1.3 \cdot 10^{-1}$ |
| KFI11: Middle | → | Upper or Lower | 169 | first | 1039 | $5.7 \cdot 10^{-5}$ | | |
| | → | Upper or Lower | | second | 3220 | $1.8 \cdot 10^{-5}$ | | |
| | → | Upper and Lower | | total | 1040 | $5.7 \cdot 10^{-5}$ | $2.6 \cdot 10^{-3}$ | $8.3 \cdot 10^{-2}$ |
| BFI01: Lower | → | Upper part | 201 | total | 2322 | $1.5 \cdot 10^{-4}$ | $1.2 \cdot 10^{-3}$ | $7.6 \cdot 10^{-2}$ |
| KFI06: Lower | → | Lower part | 189 | first | 404 | $2.3 \cdot 10^{-4}$ | $1.7 \cdot 10^{-3}$ | $1.1 \cdot 10^{-2}$ |
| | → | Upper part | | second | 1167 | $4.5 \cdot 10^{-6}$ | $1.9 \cdot 10^{-3}$ | $4.3 \cdot 10^{-2}$ |
| | → | Upper and Lower | | total | 691 | $1.4 \cdot 10^{-4}$ | $3.0 \cdot 10^{-3}$ | $4.4 \cdot 10^{-2}$ |
| KFI11: Lower | → | Upper part | 190 | total | 4319 | $1.7 \cdot 10^{-5}$ | $1.8 \cdot 10^{-3}$ | $1.6 \cdot 10^{-1}$ |

### 5.3.3 Volume of Fracture Flow Paths

The volume of the flow paths between the point of injection and tracer withdrawal can be estimated in the case of a continuous tracer injection with negligible transverse dispersion and matrix diffusion. It is equal to the difference between injected and recovered volume of tracer labbelled water at any time when the breakthrough curve has reached steady state.

During the present tracer test the tracers In-EDTA and Gd-DTPA reached steady state (Appendix C, pages C:1 and C:11 respectively) and showed a

high recovery (Table 4-5). The measured steady state concentration of the tracers also agreed with the theoretical ones, calculated according to Equation (4.1), see Table 4-4. In a radial convergent flow geometry the steady state tracer concentration in the withdrawal borehole, $C_s$, is lower than the concentration in the labelled water injected, $C_0$, due to dilution in the withdrawal borehole with water from the surrounding radial inflow.

The volume of the fracture flow paths was calculated at steady state breakthrough from Equation (5.21).

$$V = C_0 \cdot M \tag{5.21}$$

Where M is the amount of tracer in the fracture flow paths between point of injection and withdrawal at any time moment. It is determined as the difference between injected and recovered mass of tracer. Data were taken from Table 4-5. The $C_0$ values used were derived from Appendices B:1 and B:3. Results are presented in Table 5-15.

With knowledge about the flow paths volume and the two entities length and aperture the breadth and surface to volume ratio (flow wetted surface) in the fracture flow paths can be estimated. Estimates was made based on the mass balance apertures $e^m$ given in Table 5-14, which gives a lower limit of the surface to volume ratio. Results are presented in Table 5-15 together with calculated fracture flow path volumes.

Table 5-15 Volume and breadth of fracture flow paths within Zone 2.

| Injection point | Detection in BFI02 | Fraction of flow | Distance (m) | Volume ($m^3$) | Breadth (m) | Flow wetted* surface ($m^2/m^3$) |
|---|---|---|---|---|---|---|
| BFI01: Upper In-EDTA | Upper part | 0.69 | 168 | 9.158 | 7.57 | 278 |
| | Lower part | 0.31 | 175 | 4.114 | 1.12 | 95 |
| KFI11: Upper Gd-DTPA | Upper part | 0.35 | 155 | 1.128 | 3.46 | 951 |
| | Lower part | 0.65 | 162 | 2.094 | 3.23 | 500 |

* wet area per volume of water

### 5.3.4 Flow Porosity

The flow porosity of a rock is defined as the volume of pore space involved in fluid transportation and is a part of the total porosity of the rock, as given by Norton and Knapp /1977/.

$$\theta_T = \theta_k + \theta_d + \theta_r \qquad (5.22)$$

where: $\theta_T$ = total porosity
$\theta_k$ = flow porosity
$\theta_d$ = diffusion porosity
$\theta_r$ = residual porosity

Besides the flow porosity the total porosity also includes the diffusion porosity representing discontinuous (dead end) fractures and fractures and parts of fractures of such small aperture that water cannot move under the prevailing hydraulic conditions. The residual porosity includes all remaining pore volumes and makes up more than 90 % of the total porosity. Residual porosity, including micro fissures between mineral grains, is essential for the matrix diffusion capacity of the rock adjacent to the walls of the water conducting fractures.

Flow paths participating in the transport are mainly concentrated to interconnected patches of elevated aperture in the single fracture, which in turn is a part of a system of interconnected fractures and zones. The configuration of the participating flow paths, and thus the ratio between flow porosity and diffusion porosity will depend on the flow boundary conditions, i.e. change with the direction of the hydraulic gradient. Consequently, in fractured rock flow porosity is a directional property.

The flow porosity can be expressed as the ratio between the average hydraulic conductivity of the fracture zone, K, and the hydraulic fracture conductivity of the flow paths, $K_e$, providing that Darcy's law applies.

$$\theta_k = K / K_e \qquad (5.23)$$

In Equation (5.23) the $K_e$ value can be the one determined with the residence time of a tracer as the basic variable, $K_e^t$, or with flow rate as basic variable, $K_e^q$.

The flow porosity can also be expressed as the ratio between the volume of flowing water in the fracture zone and the total volume of the fracture zone. In a radial flow field the ratio is:

$$\theta_k^m = e^m / W \qquad (5.24)$$

where: W = thickness fracture zone

Note that by definition $e^m$ and $\theta_k^m$ will be equal if determined for a one metre thick aquifer.

Contrary to the porous media case, values of porosity determined in a heterogeneous rock aquifer from Equations (5.23) or (5.24) are dependent on the length of the interval where the hydraulic conductivity, K, was determined, or on W being the assumed thickness of the aquifer contributing to the flow. For example, this is the case for one single fracture (or a few closely spaced fractures) in an otherwise low conductive rock mass.

Directional values of K were derived from hydraulic crosshole testing and geologic mapping/core logging in order to make it possible to calculate flow porosity according to Eqn. (5.23). Basic data from Tiren /1991/, Ahlbom & Tiren /1991/ and Andersson et al./1989/ were utilized.

Table 5–16 Directional values of hydraulic conductivity in sub–zones within Zone 2.

| Direction and sub–zone | Width* (m) | T** ($m^2/s$) | K (m/s) |
|---|---|---|---|
| BFI01: Upper → BFI02: Upper | 0.5 - 2.0 | $1.4 \cdot 10^{-3}$ | $0.7 \cdot 10^{-3}$ - $2.8 \cdot 10^{-3}$ |
| KFI06: Upper → BFI02: Upper | 0.5 - 2.0 | $1.4 \cdot 10^{-3}$ | $0.7 \cdot 10^{-3}$ - $2.8 \cdot 10^{-3}$ |
| KFI11: Upper → BFI02: Upper | 0.5 - 2.0 | $1.4 \cdot 10^{-3}$ | $0.7 \cdot 10^{-3}$ - $2.8 \cdot 10^{-3}$ |
| KFI06: Lower → BFI02: Lower | 0.5 - 2.0 | $1.6 \cdot 10^{-3}$ | $0.8 \cdot 10^{-3}$ - $3.2 \cdot 10^{-3}$ |
| KFI11: Lower → BFI02: Lower | 0.5 - 2.0 | $1.3 \cdot 10^{-3}$ | $0.6 \cdot 10^{-3}$ - $2.6 \cdot 10^{-3}$ |
| BFI01: Upper → BFI02: Lower | 0.5 - 2.0 | $2.4 \cdot 10^{-3}$ | $1.2 \cdot 10^{-3}$ - $4.8 \cdot 10^{-3}$ |

* assumtion from core logging, geological mapping and single hole hydraulic testing
** values from hydraulic crosshole testing /Andersson et al.,1989/

### 5.3.4.1 Calculated Porosities

The flow porosities have been calculated for the sub–zones of Zone 2, and the results are presented in Table 5–17. Calculation of $\theta_k^t$ and $\theta_k^q$ porosities requires knowledge about the K–values of the sub–zones. Hence, these porosities could only be calculated for a few sub–zones (flow paths), c.f. Table 5–16. According to theory $\theta_k^t$ is a bit higher than $\theta_k^q$. The mass balance derived flow porosity $\theta_k^m$ is generally higher than $\theta_k^t$ and $\theta_k^q$ values.

Comparison between sub–zones can be made utilizing $\theta_k^m$ values, which have been possible to calculate for all sub–zones and flow paths. Flow porosities shows no large difference between the 0.5 - 2.0 m thick sub–zones, but intermediate sub–zones have somewhat higher flow porosity than the upper and lower ones. In the upper sub–zone the calculated flow porosity $\theta_k^m$ ranged from $1.0 \cdot 10^{-3}$ to $4.6 \cdot 10^{-2}$. In the lower sub–zone it ranged from $5.5 \cdot 10^{-3}$ to $2.2 \cdot 10^{-2}$, and in the intermediate sub–zones from $2.1 \cdot 10^{-2}$ to $1.3 \cdot 10^{-1}$.

Assuming the Zone 2 as build up of three sub-zones (upper,middle and lower) with very low conductive, no-flow, rock inbetween, the flow porosity of the entire 100 m thick Zone 2 will then be in the range from $5.4 \cdot 10^{-4}$ to $7.0 \cdot 10^{-4}$.

Table 5-17 Flow porosity. Directional values in sub-zones within Zone 2.

| Direction | Sub-zone and flow path to pumped hole BFI02 | $\theta_k^t$ | $\theta_k^q$ | $\theta_k^m$ |
|---|---|---|---|---|
| BFI01: Upper | → Upper part, 1st | $4.1 \cdot 10^{-3}$ - $1.6 \cdot 10^{-2}$ | $7.1 \cdot 10^{-4}$ - $2.8 \cdot 10^{-3}$ | $3.6 \cdot 10^{-3}$ - $1.4 \cdot 10^{-2}$ |
| | → Lower part, 2nd | $2.9 \cdot 10^{-3}$ - $1.2 \cdot 10^{-2}$ | $1.5 \cdot 10^{-3}$ - $6.1 \cdot 10^{-3}$ | $1.0 \cdot 10^{-2}$ - $4.2 \cdot 10^{-2}$ |
| | → Upper and Lower | - - - - - - - - | - - - - - - - - | $4.0 \cdot 10^{-3}$ - $1.6 \cdot 10^{-2}$ |
| KFI06: Upper | → Upper part, 1st | - - - - - - - - | - - - - - - - - | $4.4 \cdot 10^{-3}$ - $1.8 \cdot 10^{-2}$ |
| | → Upper part, 2nd | - - - - - - - - | - - - - - - - - | $1.1 \cdot 10^{-2}$ - $4.6 \cdot 10^{-2}$ |
| | → Upper part, both | $2.9 \cdot 10^{-3}$ - $1.2 \cdot 10^{-2}$ | $4.4 \cdot 10^{-4}$ - $1.8 \cdot 10^{-3}$ | $5.5 \cdot 10^{-3}$ - $2.2 \cdot 10^{-2}$ |
| KFI11: Upper | → Upper part, 1st | $7.5 \cdot 10^{-4}$ - $3.0 \cdot 10^{-3}$ | $5.4 \cdot 10^{-4}$ - $2.2 \cdot 10^{-3}$ | $1.0 \cdot 10^{-3}$ - $4.2 \cdot 10^{-3}$ |
| | → Lower part, 2nd | - - - - - - - - | - - - - - - - - | $2.0 \cdot 10^{-3}$ - $8.0 \cdot 10^{-3}$ |
| | → Upper and Lower | - - - - - - - - | - - - - - - - - | $1.6 \cdot 10^{-3}$ - $6.5 \cdot 10^{-3}$ |
| BFI01: Middle | → Entire zone | - - - - - - - - | - - - - - - - - | $2.8 \cdot 10^{-2}$ - $1.1 \cdot 10^{-1}$ |
| KFI06: Middle | → Upper and Lower | - - - - - - - - | - - - - - - - - | $3.3 \cdot 10^{-2}$ - $1.3 \cdot 10^{-1}$ |
| KFI11: Middle | → Upper and Lower | - - - - - - - - | - - - - - - - - | $2.1 \cdot 10^{-2}$ - $8.3 \cdot 10^{-2}$ |
| BFI01: Lower | → Upper part | - - - - - - - - | - - - - - - - - | $3.8 \cdot 10^{-2}$ - $1.5 \cdot 10^{-1}$ |
| KFI06: Lower | → Lower part, 1st | $4.4 \cdot 10^{-3}$ - $1.8 \cdot 10^{-2}$ | $5.7 \cdot 10^{-4}$ - $2.3 \cdot 10^{-3}$ | $5.5 \cdot 10^{-3}$ - $2.2 \cdot 10^{-2}$ |
| | → Upper part, 2nd | - - - - - - - - | - - - - - - - - | $2.2 \cdot 10^{-2}$ - $8.6 \cdot 10^{-2}$ |
| | → Upper and Lower | - - - - - - - - | - - - - - - - - | $1.1 \cdot 10^{-2}$ - $4.4 \cdot 10^{-2}$ |
| KFI11: Lower | → Upper part | - - - - - - - - | - - - - - - - - | $0.8 \cdot 10^{-1}$ - $3.2 \cdot 10^{-1}$ |

The flow porosities calculated for Zone 2 can be compared with some zones at the Äspö HRL and Stripa. The mass balance derived flow porosities $\theta_k^m$ in the sub-zones of Zone 2 are compareable to zone NE-1 at Äspö HRL, but somewhat higher than porosity in the zones NNW-1 and NNW-2 (Table 5-18). Flow porosity in the entire Zone 2, if assumed as one 100 m thick uniform zone, is in the same order of magnitude as the about 100 m thick zone EW-5 at Äspö HRL. Also the minor fracture zones in Stripa have corresponding flow porosities as Zone 2, if it is treated as being uniform and 100 m thick. However, it must be noted that more than 95 % of the transmissivity, and hence also the groundwater flow in Zone 2 is concentrated to a few interconnected shear and fracture zones (sub-zones) not more than 0.5 - 2.0 m thick, with low conductive rock inbetween. For solute transport calculations a network of interconnected sub-zones with

flow porosity somewhere in the range of 0.001 – 0.1 should be considered.

Table 5–18 Mass balance derived flow porosity, $\theta_k^m$, in Zone 2 and sub–zones, compared to other fracture zones.

| Site | Zone | Flow porosity $\theta_k^m$ | Thickness (m) | Hydraulic conductivity (m/s) | Remarks | Reference |
|---|---|---|---|---|---|---|
| Finnsjön | Entire Zone 2 | 0.0005 – 0.0007 | 100 | $3 \cdot 10^{-5}$ | dip c. 16° | This report |
| | Sub–zones of Zone 2 | | | | | |
| | Upper | 0.001 – 0.05 | 0.5 – 2.0 | $0.7 \cdot 10^{-3}$ – $2.8 \cdot 10^{-3}$ | | – " – |
| | Intermediate | 0.02 – 0.1 | 0.5 – 2.0 | $1.2 \cdot 10^{-3}$ – $4.8 \cdot 10^{-3}$ | | – " – |
| | Lower | 0.006 – 0.02 | 0.5 – 2.0 | $0.6 \cdot 10^{-3}$ – $3.2 \cdot 10^{-3}$ | | – " – |
| Äspö HRL | EW–5 | 0.0001 – 0.0003 | 100 | c. $4 \cdot 10^{-7}$ | dip c. 35° | 1) |
| | NNW–1 | 0.0006 – 0.005 | 1 – 3 | c. $2 \cdot 10^{-5}$ | approx. vertical | 1) |
| | NNW–2 | 0.002 – 0.01 | 1 – 3 | c. $2 \cdot 10^{-5}$ | – " – | 1) |
| | NE–1 | 0.003 – 0.02 | 10 – 30 | $8 \cdot 10^{-7}$ – $8 \cdot 10^{-6}$ | dip c. 60° | 2) |
| Stripa Crosshole site | Zone C | 0.0002 | 14.5 | $1.3 \cdot 10^{-8}$ | dip c. 75° | 3) |
| Stripa SCV site | Zone H | 0.0001 | 5 | $1.4 \cdot 10^{-8}$ | approx. vertical | 4) |

1) /Gustafsson et al., 1991/ 2) /Gustafsson, 1992/ 3) /Andersson et al., 1989b/ 4) /Olsson et al., 1991/

### 5.3.5 Flow Wetted Surface

Flow wetted surface is an important parameter regarding radionuclide migration since it constraints the capability for sorption and matrix diffusion. It can be expressed in basically two ways. Surface area wetted by advective flow of water per volume of rock, or surface area per volume of water.

Determination of **wetted surface per volume of rock**, $a_r$, requires, if smooth planar fractures is assumed, knowledge about fracture density and the areal extent of the preferential flow paths within the fractures. In a fracture zone with thickness W and n number of fractures the flow wetted surface is then given by:

$$a_r = n\ 2\ f\ /\ W \qquad (5.25)$$

where: n = number of fractures
f = fraction of preferential flow paths

In Table 5–19 the flow wetted surface per volume of rock, determined from

Equation (5.25) is presented. Number of fractures, n, is given by quotients $e^m/e^t$ and $e^m/e^q$ and the f factor is set to 1.0, which gives the upper limit. Several investigations indicate that the fraction of preferential flow paths is lower than 1.0 in a natural fracture.

Preferential flow paths within a minor fracture zone was determined in the Stripa Project /Andersson et al.,1989/ with saline tracer injection and radar difference tomography technique. The measurement indicated a fraction of preferential flow paths of about 20 - 37 % in the investigated zone, in which about 80 % of the injected tracer labelled water was flowing. Hence, there is about 20% of mass flow in other parts of the zone where interactions between rock surface and solute transported by water may take place. In the low velocity case, i.e. repository conditions with a more linear gradient picture, this flow fraction may increase. And also molecular diffusion into stagnant parts of the fracture becomes more pronounced resulting in larger surface area accessible for sorption of solutes transported by the groundwater.

In the calculations of flow wetted surface, presented in Table 5-19, estimates of the number of fractures, n, within the sub-zones or main flow paths of Zone 2 are based on results from the tracer test. They are to be compared with independent estimates from geological data. From geological mapping within the test site and core logging /Tiren 1991/ it is concluded that the sub-zones parallel to the upper margin of Zone 2 constitutes of only a few fractures. This is in good agreement with the results from the tracer test. The ratio $e^m/e^t$, giving the number of fractures in the smoth fracture case, indicates that 2 - 20 fractures contribute to the groundwater flow in the upper sub-zone of Zone 2 (Table 5-14). The ratio $e^m/e^q$, which may be more appropriate for rough-walled fractures, indicates 1 - 7 fractures in the upper highly conductive sub-zone.

In the upper sub-zone of Zone 2 the flow wetted surface per volume of rock (i.e. fracture zone) ranged from 1 to 56 $m^2/m^3$, if the f factor was set to 1.0. In the lower sub-zone of Zone 2 basic data for calculations of flow wetted surface was obtained in only one direction. However, in that direction the surface area per volume of rock is calculated to be within 6 - 92 $m^2/m^3$ (f = 1.0). If the preferential flow paths are restricted to 20 - 37 % of the fractures, as the Stripa case shows, the flow wetted surface should decrease accordingly.

In Stripa the flow wetted surface was calculated to 1.8 $m^2/m^3$, with consideration to preferential flow paths occupying 20 - 37 % of the fractures /Andersson et al.,1989b/. Comparing the major fracture Zone 2 at Finnsjön site with the minor Stripa Zone C, it is indicated that in Zone 2 there exists sub-zones both with larger and with smaller wetted surface area than Zone C. In the reference case in SKB91 /SKB, 1992/ a flow wetted surface of 0.1 $m^2/m^3$ was used for the migration calculations at the Finnsjön site.

The **flow wetted surface per volume of water**, $a_w$, is analogous to the inverse of the hydraulic radius R used for decades in fluid engineering

/Rouse, 1961/. R = A/P, in which P represents the perimeter of the wetted boundary ,whereas A refers to the cross sectional area of the flow channel. In a tube the wetted surface is 2/r $m^2/m^3$. Applied to fracture flow it requires knowledge about the single fracture aperture, e. If e << w, being the breadth of flow path, it can be expressed by:

$$a_w = 2 / e \qquad (5.26)$$

In Table 5-19 the wetted surface per volume of water in Zone 2 is presented, where the fracture aperture, e, determined according to definitions $e^t$ and $e^q$ have been used for the calculations following Equation (5.26).

Calculations have also been made assuming that the total pore volume in the fracture sub-zones constitute only one single fracture, i.e. fracture aperture is given by $e^m$.

Table 5-19 Directional values of flow wetted surface ($m^2/m^3$) in sub-zones within Zone 2.

| Direction and sub-zone | surface per volume of water | | | surface per volume of rock | |
|---|---|---|---|---|---|
| | $2/e^t$ | $2/e^q$ | $2/e^m$ | $(e^m/e^t)2/W$ | $(e^m/e^q)2/W$ |
| BFI01: Upper → BFI02: Upper | $3.85 \cdot 10^3$ | $1.67 \cdot 10^3$ | $2.78 \cdot 10^2$ | 14 - 56 | 6 - 24 |
| KFI06: Upper → BFI02: Upper | $3.17 \cdot 10^3$ | $1.25 \cdot 10^3$ | $1.82 \cdot 10^2$ | 18 - 7 | 27 - 28 |
| KFI11: Upper → BFI02: Upper | $1.67 \cdot 10^3$ | $1.18 \cdot 10^3$ | $9.52 \cdot 10^2$ | 2 - 8 | 1 - 4 |
| KFI06: Lower → BFI02: Lower | $8.70 \cdot 10^3$ | $1.18 \cdot 10^3$ | $1.82 \cdot 10^2$ | 24 - 92 | 6 - 24 |

In the upper sub-zone of Zone 2 the flow wetted surface expressed as surface area per volume of water ranged from 1180 to 3850 $m^2/m^3$ depending on how fracture aperture was determined. If the total pore volume in the zone is represented by one single fracture the fracture surface area per volume of water is within 182 - 952 $m^2/m^3$. In the lower sub-zone of Zone 2, basic data for calculations of flow wetted surface area was obtained in only one direction. However, in that direction the fracture surface per volume of water ranged from 1180 to 8700 $m^2/m^3$, and if all pores in the zone is represented by one fracture the wetted surface is 182 $m^2/m^3$.

Estimates of wetted surface per volume of water in Zone 2 at Finnsjön, presented above, can be compared with values calculated for Stripa Zone C, 1266 $m^2/m^3$ /Andersson et al.,1989/. Stripa Zone C is in the lower region of the estimates for the sub-zones of Zone 2. In the reference case in SKB91 /SKB,1992/ a value of 1000 $m^2/m^3$ was used.

## 5.4 HETEROGENEITY AND FLOW PATH INTERCONNECTIONS

### 5.4.1 Heterogeneity

In a radial convergent flow geometry with tracers injected in several directions from the withdrawal borehole, differences in tracer residence time and groundwater flow rate through the borehole sections used for tracer injections gives a measure of the degree of heterogeneity. The heterogenity can also be expressed as directional variations of parameters governed by the solute transport, as:

- hydraulic fracture conductivity
- fracture aperture and volume
- porosity
- dispersion

The heterogeneity within each highly conductive part may be indicated by the ratio $t_0/r^2$ or $t/r^2$ which, in a homogeneous isotropic medium, should be constant. The comparison presented in Table 5-20 assumes that the upper, middle and lower intervals packed-off in the boreholes corresponds to the same part of Zone 2. This seems clearly to be the case for the upper intervals, which all penetrates the upper highly conductive structure (sub-zone) of Zone 2. The middle and lower packed-off intervals are more difficult to connect between the boreholes, since the interconnected sub-zones within Zone 2 are interpreted not so pervasive.

Table 5-20 Indications of the heterogeneity of Zone 2 as given by the ratios $t/r^2$ and $t_0/r^2$ and by groundwater flow rate through borehole injection sections $Q_w$.

| Injection interval | $t/r^2$ ($s/m^2$) | $t_0/r^2$ ($s/m^2$) | $Q_w$ (ml/min) |
|---|---|---|---|
| BFI01:U | 9.6 | 25.6 | 268 |
| KFI06:U | 10.7 | 29.0 | 26 |
| KFI11:U | 3.6 | 10.2 | 11 |
| BFI01:M | 89 | 167.0 | 23 |
| KFI06:M | 126 | 202.9 | 7 |
| KFI11:M | 127 | 131.1 | 114 |
| BFI01:L | 159 | 206.9 | 376 |
| KFI06:L | 20 | 69.6 | 8 |
| KFI11:L | 539 | 430.7 | 24 |

In the upper part of Zone 2, the transport is very fast from the direction of KFI11 thus giving a low value of $t/r^2$. The transport seems to take place within a few different flow paths/fractures. This is also supported by the core

log /Ahlbom et al., 1988/ which shows a very narrow open fracture at 224.7–224.8 m depth. From the other directions, the transport is slower and the flow porosities are higher (Table 5–17) indicating that more flow paths/fractures are involved in the transport. According to quotients and flow rates presented in Table 5–20 heterogeneity seems more pronounced at depth in Zone 2. Although there are directional variations also in the upper highly conductive sub–zone.

The measured flow rates through the injection intervals are larger than what would be expected in a homogeneous and isotropic medium.

During pumping of a homogeneous and isotropic aquifer, the flow rate, $Q_w$, through a borehole penetrating the aquifer at distance r from the pumping borehole is given by:

$$Q_w = (Q \cdot \alpha \cdot d_w)/(2 \cdot \pi \cdot r) \qquad (5.27)$$

where:
- r = distance to injection borehole
- $d_w$ = diameter of injection borehole
- $\alpha$ = correction factor
- Q = pumped flow rate in aquifer

Correction factor $\alpha$ considers the convergence and divergence of the flow lines in the vicinity of the borehole. In a homogeneous and isotropic aquifer the value is 2.0.

With pumped flow rate, distances and borehole diameters used in the present converging tracer test the flow rates through the injection boreholes BFI01, KFI06 and KFI11 should be 38, 11 and 14 ml/min respectively in the homogeneous and isotropic aquifer case.

### 5.4.2 Flow Path Interconnections

It is obvious from the hydraulic testing that the flow within Zone 2 is concentrated to a few highly conductive parts. The results of the radially converging tracer experiment show that these highly conductive parts are hydraulically interconnected and within distances of 155 – 200 metres there was an extensive mixing of tracer labelled groundwater between the highly conductive interconnected sub–zones of Zone 2, separated by 15 – 110 metres of low conductive rock at the injection points. Regardless of the position of the injection interval the tracer was recovered in one or more of the three uppermost conductive intervals of Zone 2, in borehole BFI02. Tracers injected in the upper part of Zone 2 were recovered both in the upper part of Zone 2 and in high conductive intervals at depth. These results imply a solute transport both upwards and downwards within Zone 2. This flow condition is further pointed out by the fact that tracers injected in intermediate parts of Zone 2 also were recovered at the upper and lower

conductive parts of Zone 2. The mixing between sub-zones is possible due to the geologic structure of Zone 2, were groundwater flow is concentrated to a few interconnected minor shear and fracture zones about one metre thick, c.f. Figure 2-2. The possibility of groundwater mixing in Zone 2 at certain hydraulic gradient conditions is also indicated by the relatively homogeneous hydraulic response registered during the interference tests, i.e. irrespective of pumped sub-zone in BFI02 pressure responses were obtained in all sub-zones (upper, intermediate, lower) in the peripheral boreholes BFI01, KFI06 and KFI11 used for tracer injections in the present tracer test /Andersson et al., 1988b/. Heterogeneity and possibilities to mixing between interconnected thin sub-zones, which contribute to the major part of groundwater flow, seems most important for solute transport within Zone 2.

## 5.5 SORPTION AND MATRIX DIFFUSION

The diffusion into the rock matrix is governed by the pore diffusivity of the tracer solute and the porosity of the rock matrix. This is a time dependent process which, on the analogy of molecular diffusion for the overall dispersion, will be more important at low velocities and long distances.

The breakthrough curves obtained from the radially converging tracer test were fairly well explained by solute transport governed by advection-dispersion. Matrix diffusion was therefore considered to be of minor importance during the time scales involved in the test. At least for the fastest flow paths. According to Hautojärvi et al./1992/ matrix diffusion cannot be identified in these short term tests and therefore may be neglected. In the slowest flow paths (residence times some thousand hours) matrix diffusion is possibly more important. Moreno & Neretnieks /1992/ suggests that both advection-dispersion and matrix diffusion have influenced the tracer transport. However, the discrepancy from the advection-dispersion solution may also be due to transient solute storage in immobile fluid zones /Raven et al.,1988/ or insufficient long term stability of the tracer metal-complexes used. Which causes sorption of the tracer metal and a delayed breakthrough with a lower peak concentration than anticipated. The laboratory test of the tracers used (section 3.4.5 and 4.4.4) also indicated that long term stability may be a problem for some of the tracers.

# 6.0 TWO-DIMENSIONAL MODELLING

This chapter describes the two-dimensional simulations of the tracer experiments. The chapter is divided into a brief desription of the mathematical model in section 6.1, a detailed description of the predictive simulations in section 6.2, and an evaluation of the predictions in section 6.3.

The modelling exercise described in this chapter emphasizes the simultaneous understanding of flow and transport in the fracture zone. The prediction of the radially converging tracer test was part of a series model predictions and experiments: hydraulic interference tests, the radially converging test, and a dipole tracer test. As each experiment was completed, prediction models were evaluated, and new information could be added to the model in order to improve the predictive ability prior to the following experiment.

It should be kept in mind that the conceptual hydrogeological model of the geologic structure of the zone has evolved as new results from each experiments have become available. Prior to the interference tests, the zone was considered to consist of three relatively well defined conductive subzones, separated with low permeability rock. As the interference tests and the radially tests have been completed, it is apparent that the hydraulic connectivity structure is considerably more complex throughout the zone, c.f. chapter 2 and section 5.4.

The 2-D model evaluation complements the 1-D modelling described in chapter 5. The latter need only a few transport parameters for each transport path to reproduce breakthrough curves, and requires limited understanding of the overall flow conditions in the zone. The 1-D models allow a detailed evaluation of the tracer breakthrough curves, and may provide clues about multiple tracer path ways, etc. The 2-D flow and transport modelling, on the other hand, is more complex and can only be expected to describe the breakthrough curves very approximately.

## 6.1 MATHEMATICAL MODEL

### 6.1.1 Governing Equations

The groundwater flow is assumed to be two-dimensional and to take place in a porous medium, governed by the equation /Freeze and Cherry, 1979/:

$$\frac{\partial}{\partial x}\left(T\frac{\partial h}{\partial x}\right) + \frac{\partial}{\partial y}\left(T\frac{\partial h}{\partial y}\right) - Q = S\frac{\partial h}{\partial t} \qquad (1)$$

where T = transmissivity ($m^2/s$)

h = piezometric head (m)
S = storage coefficient
Q = fluid mass sources or sinks

Equation (6.1) is based on Darcy's law and a continuity equation. Steady state flow, constant density of fluid, saturated flow and an isotropic medium is assumed.

The transport simulations were all performed for a single non-sorbing, non-reacting solute. The transport mechanisms considered in these simulations are:

- advection, governed by the general flow field

- hydrodynamic dispersion, originating from local variations in the average velocity field

The governing equation for the solute transport model in two dimensions applied here can be written as:

$$\nabla(D\nabla C) - \nabla(vC) = \frac{\partial C}{\partial t} \qquad (6.2)$$

where C = concentration of solute ($kg/m^{3)}$
v = average linear velocity (m/s)
D = dispersion tensor

The average linear velocity is given by Darcys' law :

$$v = K/\theta \cdot \nabla h \qquad (6.3)$$

where $\theta$ is the flow porosity, K is the hydraulic conductivity (m/s), and h is obtained from solving equation (6.1). The value of the hydraulic conductivity used here is determined by dividing the transmissivity in eq. (6.1) by the estimated thickness of the modelled layer.

The dispersion tensor, D, is defined as:

$$D = \begin{bmatrix} D_{xx} & D_{xy} \\ D_{yx} & D_{yy} \end{bmatrix} \qquad (6.4)$$

and $$D_{xx} = (1/v^2)(d_L v^2_x + d_T v^2_y) \qquad (6.5)$$

$$D_{yy} = (1/v^2)(d_T v^2_x + d_L v^2_y) \quad (6.6)$$

$$D_{ij} = (1/v^2)(d_L - d_T)(v_i v_j) \quad (6.7)$$

$i \neq j$, $i = x,y$
$j = x,y$

where
$v$ = magnitude of the average linear velocity vector (m/s)
$v_x$ = magnitude of x–component of v (m/s)
$v_y$ = magnitude of y–component of v (m/s)
$d_L$ = longitudinal dispersion coefficient ($m^2/s$)
$d_T$ = transverse dispersion coefficient ($m^2/s$)

The terms $d_L$ and $d_T$ are analogous to diffusion coefficients, but are directional in nature. The longitudinal dispersion coefficient causes dispersion forward and backwards along the local direction of fluid flow, and the transverse dispersion coefficient acts normal to the direction of flow. The size of the dispersion coefficients are dependent upon the local magnitude of average velocity in a flowing system:

$$d_L = a_L v \quad (6.8)$$

$$d_T = a_T v \quad (6.9)$$

where
$a_L$ = longitudinal dispersivity of solid matrix (m)
$a_T$ = transverse dispersivity of solid matrix (m)

The dispersivities $a_L$ and $a_T$ may be considered as properties related to variations in the velocity field, applied to a particular field situation and dependent on the scale of transport.

The flow and transport equations are solved numerically by a two–dimensional finite element code, SUTRA, version 1284–2D, /Voss, 1984/.

### 6.1.2 Data Requirements for the Finite Element Code

In order to solve the flow and transport equations described above, the following input data to SUTRA is required :

- a finite element mesh with nodes and quadrilateral elements

- hydraulic conductivities for each element

- thickness and porosity for each node

- longitudinal and transverse dispersivities for each element

- fluid sources and sinks

- solute concentration of injected fluid or nodes with constant concentration

### 6.1.3 Initial and Boundary Conditions

When solving the flow equations with SUTRA, the required boundary conditions are either specified hydraulic head or constant flow. In cases where flow crosses a boundary, solute concentration of fluid entering the flow domain has to be specified.

Initial conditions are given as hydraulic head and solute concentration over the region. When solving the equations for steady-state flow, initial head distribution is rather arbitrary. Calculations involving transient solute transport require specification of initial concentrations across the computational domain.

## 6.2 PREDICTIONS OF THE RADIALLY CONVERGING TEST

The purpose of the work described in this section was to predict the results from the Radially Converging Tracer Test, simulating the tracer arrival in the pumped hole as concentration as a function of time.

The general approach was to calculate the flow field (hydraulic head distribution) in the fracture zone during the tracer experiment, which would in turn serve as input to the solute transport model. The simulations were to a large extent based on the results from previous hydraulic interference tests. These results were used to calibrate the model geometry and hydraulic parameters, aiming at acheiving a plausible description of the groundwater flow conditions. Solute transport was then predicted using the calibrated flow model. The flow calibrations are summarized below and described in detail by Andersson et al. /1989/.

### 6.2.1 Calibration of the Groundwater Flow Model

The groundwater flow was calibrated, primarily in a horizontal plane, using results from transient hydraulic interference tests performed in the subhorizontal fracture zone. In addition, detailed studies of the geology of the fracture zone made it possible to better define the geologic environment outside the fracture zone including location and nature of hydraulic boundaries /Andersson et al, 1989/. Valuable information about hydraulic parameters was also provided by detailed single hole injection tests, performed in 0.1 m sections. This resulted in a considerably larger flow domain to be modelled, compared to previous areal modelling of the fracture zone /Andersson and Andersson, 1987/. The area used for flow calibrations in the horizontal plane is shown in Figure 6-1.

Prior to the tracer experiments, the subhorizontal fracture zone, Zone 2, was considered to consist of three subzones with low permeability layers between. It should be pointed out that this distinction was not well defined and could not be correlated in all the boreholes. The interference tests and single hole injection tests indicated that the uppermost and lowermost subzones were highly transmissive, while the middle subzone had considerably lower transmissivity. It should be pointed out again, that as the fracture zone project developed, it became evident that only the upper conductive layer appeares to be consistently connected, while the remainder of the zone is considerably more heterogeneous, see chapter 2 and section 5.4.

The flow calibrations were primarily oriented towards calibrating the entire Zone 2 in a horizontal plane, thus obtaining vertically integrated hydraulic properties. The interference tests indicated that all the three sub-zones interacted significantly and at larger distances worked like a single hydraulic unit /Andersson et al, 1989/. The implication of this was that it was not possible to calibrate any of the subzones individually in a two-dimensional horizontal plane, since three-dimensional effects would have to be included in the simulations. Further, the Radially Converging Tracer Test was to be performed by pumping the entire thickness of Zone 2.

Although the flow was calibrated for Zone 2 as a single unit, the simulated gradients are considered representative for each subzone as well as the entire Zone 2. This implies that the hydraulic head was assumed to be constant in the vertical direction within Zone 2, when pumping from the entire thickness of the zone.

The boundary conditions imposed on the flow domain are shown in Figure 6-1. No natural gradient was considered, since it is inadequately defined, and is judged not to influence the drawdown distribution significantly when pumping the fracture zone. A constant head was assigned to one end of Zone 2 in order to account for regional inflow of groundwater. Flow was also allowed to originate from the Gåvastbo Zone, entering Zone 2 relatively close to the boreholes HFI01, KFI05, KFI09, and KFI10 (c.f. Figure 2-2).

The general calibration procedure was to simulate transient flow in such a way that agreement between simulated and measured drawdowns of the primary responses would be obtained. The "tuning parameters" were transmissivity and storage values, and to some extent the boundary conditions. An important point is that although data of high quality from the interference tests were available, there is no way to verify that any calibrated model is unique. In order to verify a calibrated model, data from a different hydraulic event, for example pumping of a different borehole, would be needed.

The results of the flow calibrations for the transient hydraulic interference test are shown in Figures 6-2 - 6-5. It can generally be said that simulated responses match observed ones relatively well. However, for the boreholes of interest for the transport predictions, some discrepancies are identified. The main discrepancy is noted for borehole BFI01, where drawdown behaviour approaching steady state is not entirely satisfactory modelled. It should be

pointed out that in Figure 6–2, observed responses in BFI02 (pumped hole) are considered not to be valid until after approximately 100 minutes due to friction losses in the equipment.

More details about the interference test modelling are given by Nordqvist and Andersson /1987/, Andersson et al. /1989/, and Andersson et al. /1991/).

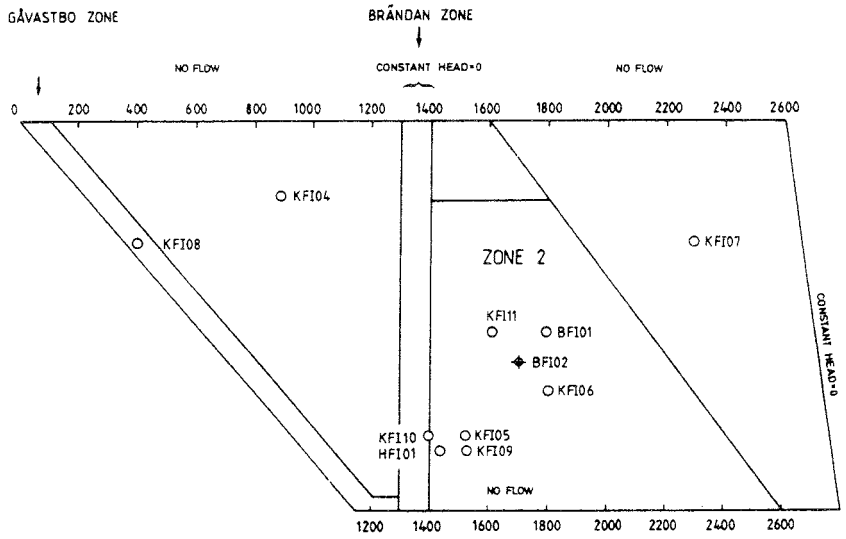


Figure 6–1a Area used and boundary conditions for flow calibrations in the horizontal plane along the dip of Zone 2.

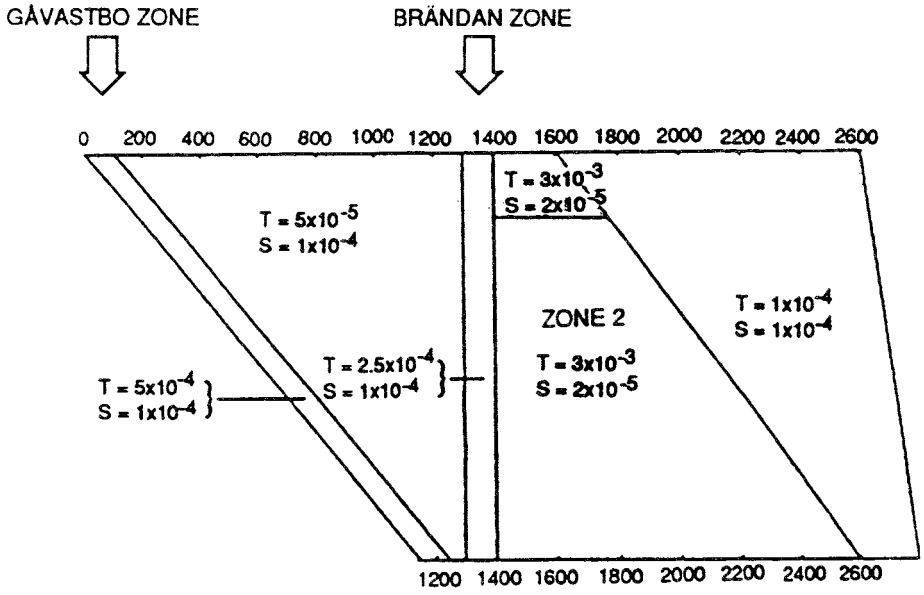


Figure 6–1b Parameter distribution for the calibrated model.

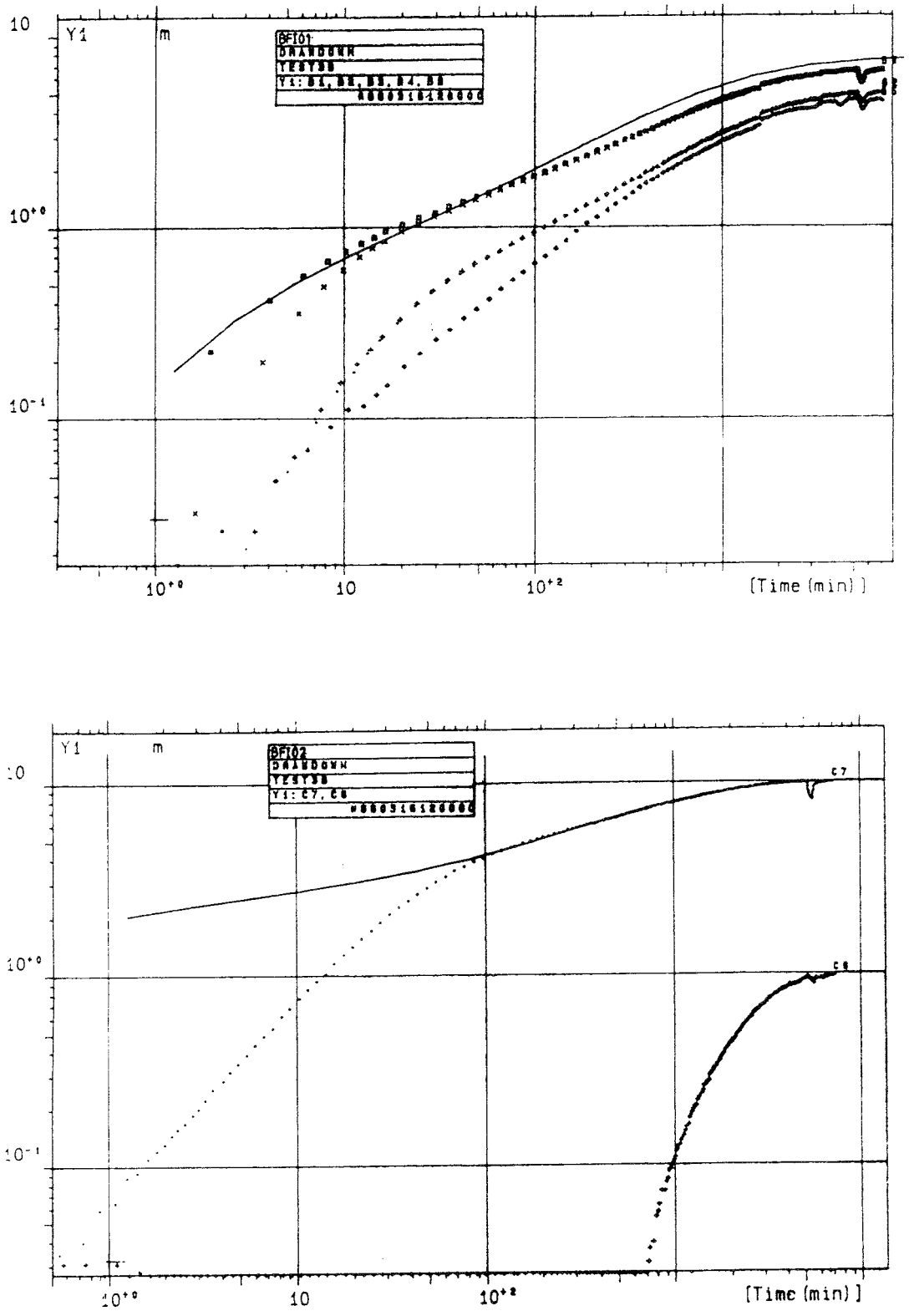


Figure 6–2 Comparison of observed versus simulated drawdowns for boreholes BFI02 (pumped hole) and BFI01, during the interference tests. Simulated responses are represented with a solid line.

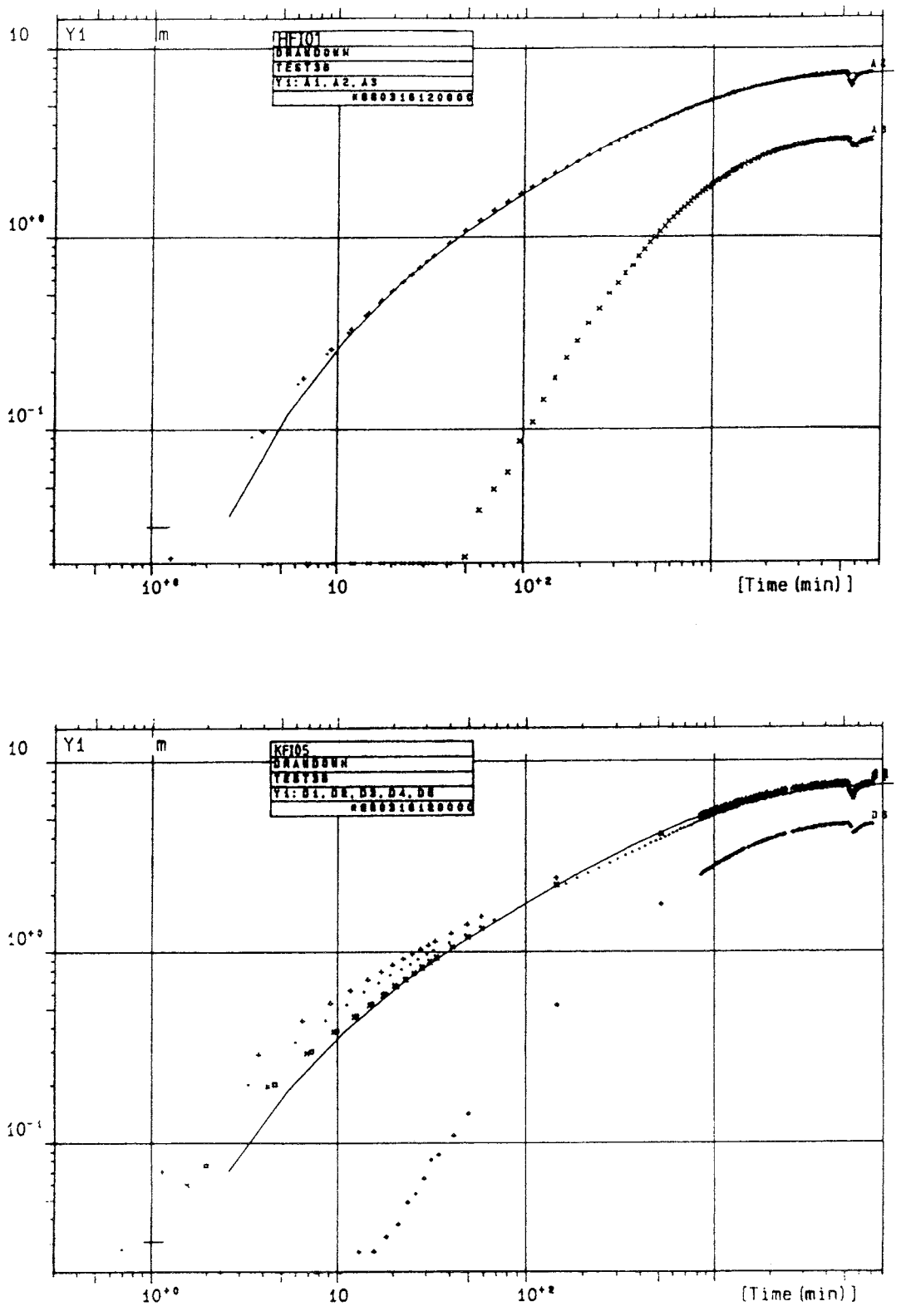


Figure 6–3 Comparison of observed versus simulated drawdowns for boreholes HFI01 and KFI05, during interference tests. Simulated responses are represented with a solid line.

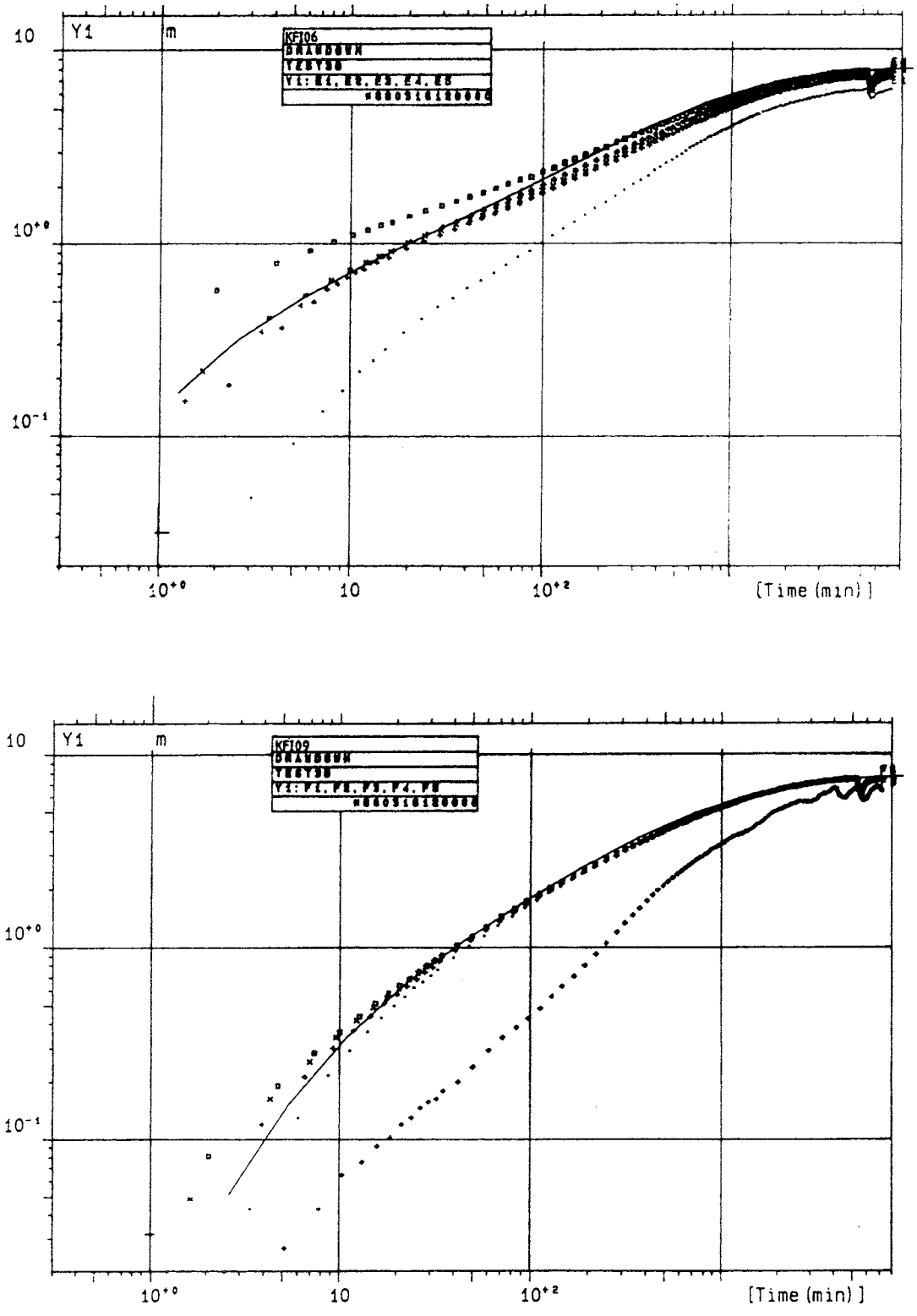


Figure 6–4 Comparison of observed versus simulated drawdowns for boreholes KFI06 and KFI09, during interference tests. Simulated responses are represented with a solid line.

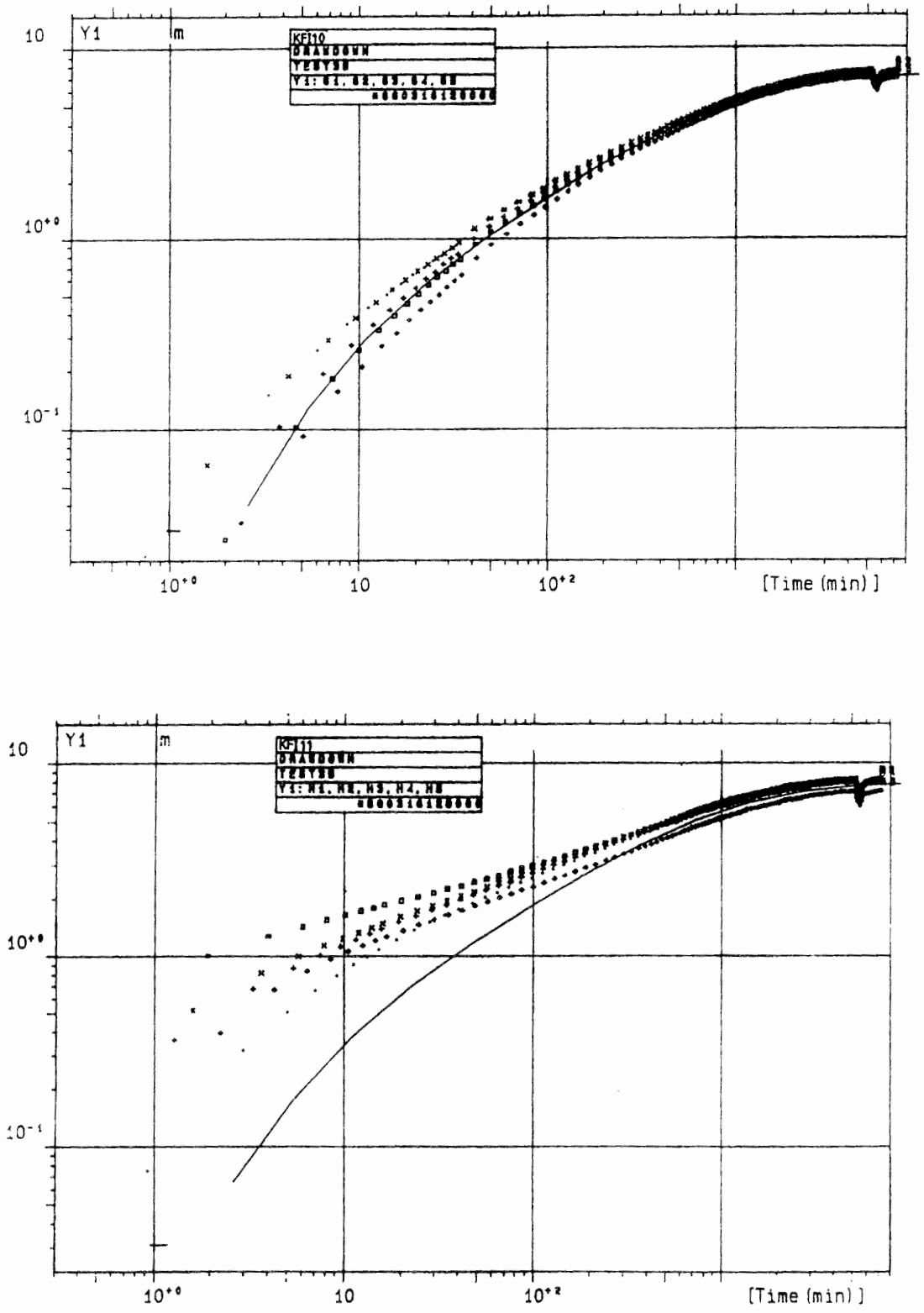


Figure 6–5 Comparison of observed versus simulated drawdowns for boreholes KFI10 and KFI11, during interference tests. Simulated responses are represented with a solid line.

### 6.2.2 Tracer Test Predictions

Based on the calibrated flow model described in the previous section, the steady state hydraulic head distribution during the Radially Converging Tracer Test was predicted. The predictions were made by simulating discharge from the entire thickness of Zone 2. The simulated steady state hydraulic head distribution at a pumping rate of 2 l/s in BFI02 is shown in Figure 6-6.

The steady state flow field was in turn used to calculate transient solute transport by adding transport parameters. The predictive simulations were oriented towards predicting tracer behaviour in horizontal planes representing the different subzones. All the subzones were assigned the same thickness. Variations between them consisted of different hydraulic conductivities. The results were obtained in the form of concentration versus time in the pumped borehole. In addition, areal plots of tracer distribution were produced.

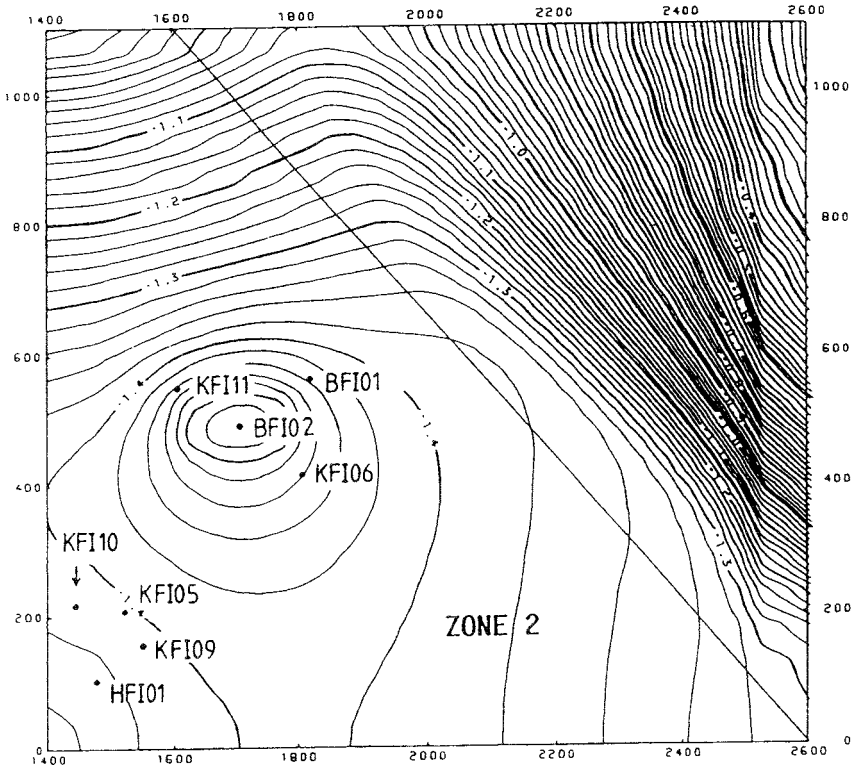


Figure 6-6 Simulated steady state hydraulic head distribution for the region of interest for the radially converging tracer.

The flow domain for the solute transport simulations was chosen as small as possible, enclosing only the boreholes included in the radially converging tracer test, BFI02, BFI01, KFI06 and KFI11. A small model domain reduces

numerical difficulties, by enabling the construction of finer finite element meshes. Separate meshes for the three injection boreholes were used, as shown in figure 6–7.

The boundary conditions for the transport domains were constant hydraulic head along all boundaries. Boundary conditions for the flow domains in Figure 6–7 were obtained by running the calibrated flow model at steady state and appropriate groundwater withdrawal schemes. The resulting hydraulic head distribution was interpolated from the flow model onto the boundaries for the transport domain.

A constant value of solute concentration, C = 1.0, was defined at the node representing the injection borehole. At all other nodes, solute concentration is initially set to zero.

Hydraulic parameters were estimated from previous hydraulic interference tests. The results from the interference test did not clearly indicate any differences between the uppermost and lowermost subzones in responses to pumping. Thus, these subzones were represented using high hydraulic conductivities, while the middle subzone was assigned significantly lower values. The values used for hydraulic conductivities were estimated from the evaluation of the interference test in combination with results from detailed water injection tests in 0.1 m sections in borehole BFI02. The latter tests provided information about thicknesses for the different subzones. The value of K is estimated using transmissivities from the interference tests, but thicknesses from borehole information. The use of a single K–value for the entire transport domain may not be realistic. In fact, the ratio K/porosity may be regarded merely as an effective scaling parameter inversely proportional to the average solute travel time.

The following parameters were used for simulations in the horizontal plane (each subzone is assumed to have a thickness of 0.5 m) :

– high conductivity zones:

| | |
|---|---|
| K = 3.5 E–03 m/s | (hydraulic conductivity) |
| n = 3 E–04 | (porosity) |
| $a_L$= 10.0 m | (longitudinal dispersivity) |
| $a_T$= 3.0 m | (transverse dispersivity) |

– low conductivity zones:

K = 7.0 E–05
n = 3 E–04
$a_L$= 10.0 m
$a_T$= 3.0 m

The used value of porosity was taken from previous tracer tests in the Brändan area /Ahlbom et al, 1988/. Dispersivity values were chosen somewhat arbitrarily. Earlier investigations /Gustafsson and Klockars, 1981/, indicated values of the order of 1 m on a scale of approximately 30 m.

However, due to scale effects, dispersivity values may be expected to be larger for the radially converging tracer test. It is commonly noted from tracer experimetns that dispersivity values typically are of the order of a tenth of the scale of the experiment.

The actual breakthrough curves were obtained by scaling the simulated responses at the point of observation (BFI02) by making some assumptions about the dilution effects in the sampling section. A flux-averaging of sample concentrations were assumed, with the fluxes assigned according to measured transmissivities for each layer (sub-zone).

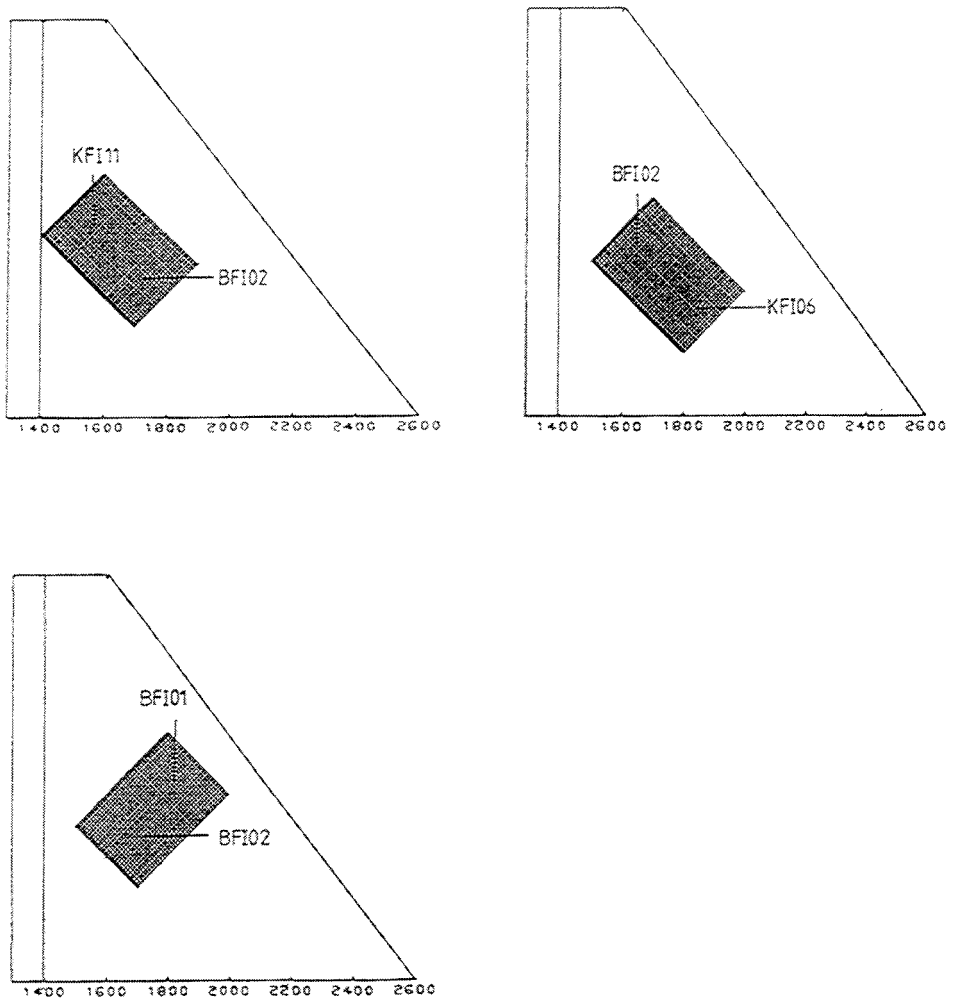


Figure 6-7 Finite element meshes used for transport simulations, representing injection boreholes BFI01, KFI06 and KFI11.

## 6.3 EVALUATION OF PREDICTIONS AND MODEL RE-CALIBRATION

The modelling work described in this report is part of a sequence of modelling efforts performed in order to increase the understanding of the hydraulic and transport properties of Zone 2 and the Brändan area. It can also partly be seen as a test of the predictability of solute transport in two dimensions based on available geological and hydrogeological information. In this case, no or very little information about transport properties was available.

In the following sections the predictions will be compared with the actual outcome of the tracer experiment. The discussion will only include processes and parameters associated with the model as described above. It is emphasized that both hydraulic gradients and breakthrough curves should be predicted satisfactorily. Obtaining an accurate breakthrough curve but failing to predict hydraulic head gradients is a rather dubious result. In other words, neglecting the importance of predicting hydraulic heads would reduce a considerable part of the assumed model to a "black box" type model.

### 6.3.1 Results and Comparison with Observed Data

The exercise described here should be seen as a test of the applicability of extrapolating a calibrated flow model to predict solute transport behaviour at other flow conditions (gradients) than the model was calibrated for. The parameters that could be considered to be known were flow parameters (hydraulic conductivities), while transport parameters were essentially unknown. In this case, the calibrated flow model reproduced aquifer responses relatively well on a large scale (500 m or more). However, it did not reproduce the flow conditions in detail at the scale of the tracer test (approximately 200 m).

Simulated tracer plumes for the injection holes, approaching steady state concentration distribution, are shown in Figure 6–8. The difference between the three plots in Figure 6–8 consists only of different hydraulic head distributions (see Figure 6–6), as obtained from running the calibrated flow model. As expected, the tracer distribution between injection hole and pumped hole is very similiar in all three cases.

The results of the transient transport predictions indicate a relatively fast transport, using the simulated gradient and the assumed hydraulic and transport parameters. Steady state concentrations in the pumped borehole were obtained after approximately 5 to 10 hours in the highly conductive zones. Results do not differ significantly when comparing different injection holes, since the hydraulic head gradient is similiar for all three cases.

Table 6–1 summarizes the hydraulic head differences for all the nine injection intervals as well as the predicted head differences. The measured values were extracted from plotted time series of head differences calculated from manually leveled (generally once a day) hydraulic heads and represents mean values.

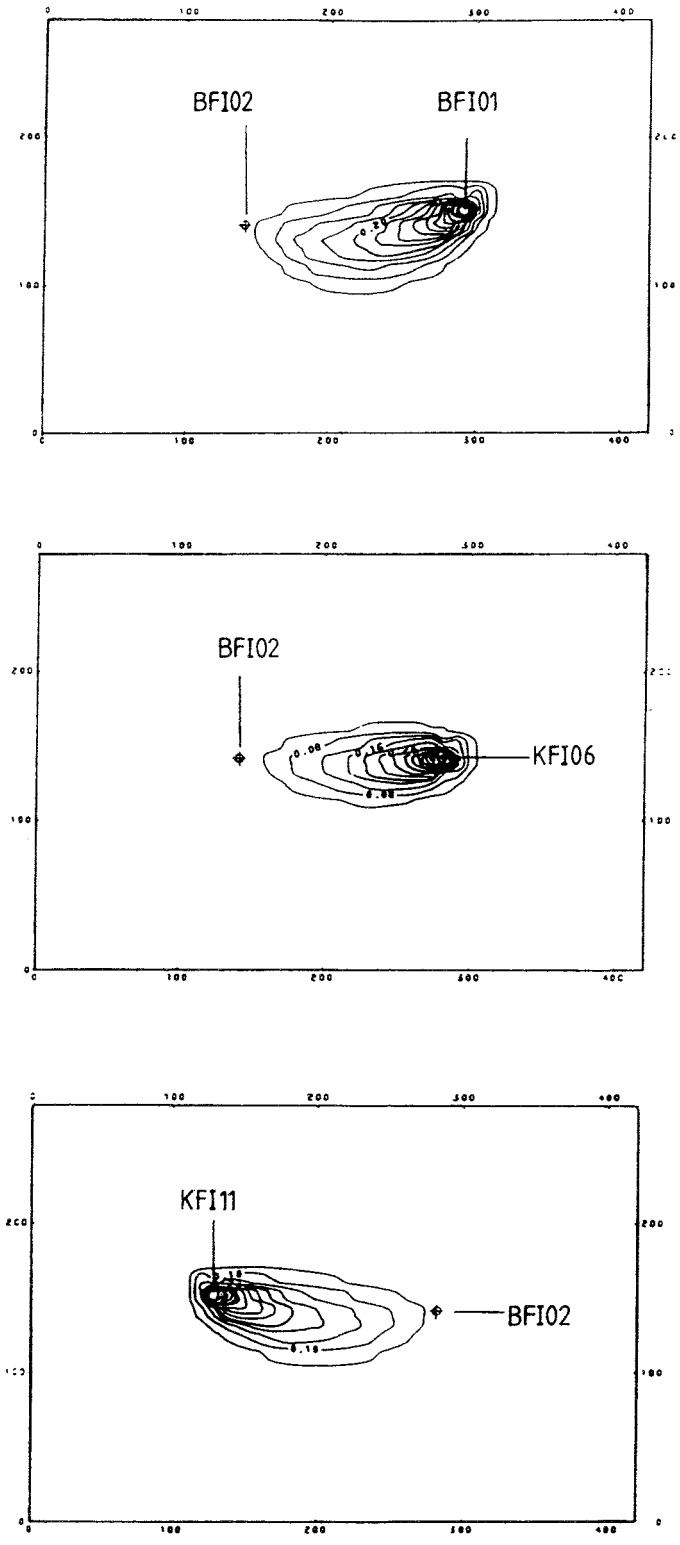


Figure 6–8 Tracer plumes for the three injection holes BFI01, KFI06 and KFI11.

Table 6–1 Comparison of measured and predicted head differences (units in metres). Measured values in parantheses denote leveling after the detailed sampling.

| Borehole | Section | Measured | Average | Predicted |
|---|---|---|---|---|
| KFI06 | Upper | 0.59 (–0.34) | | |
| | Middle | 0.64 (0.28) | 0.62 (–0.07) | 0.42 |
| | Lower | 0.62 (–0.15) | | |
| KFI11 | Upper | 0.77 (–0.74) | | |
| | Middle | 0.74 (0.33) | 0.77 (0.0) | 0.47 |
| | Lower | 0.81 (0.42) | | |
| BFI01 | Upper | 1.41 (0.55) | | |
| | Middle | 1.25 (0.84) | 1.27 (0.73) | 0.46 |
| | Lower | 1.14 (0.80) | | |

It can be seen from Table 6–1 that head differences measured prior to the sampling of major conductors in pumped borehole BFI02 differ significantly from the ones measured after the sampling of major conductors, c.f. section 4.4.1. This is clearly seen also in Appendix A. However, in order to compare predicted and measured hydraulic head differences between pumping and injection intervals, the leveled values prior to the sampling of major conductors were chosen. The reason for this was that those values are somewhat more consistent between intervals.

Table 6–1 again confirms that the present groundwater flow model does not explain hydraulic heads in borehole BFI01. For boreholes KFI06 and KFI11 the agreement is significantly better, although also here a significant discrepancy can be noted. Considering the large differences in manually leveled gradients between before and after the sampling of major conductors, it is difficult to say what is model error and what is experimental error. However, it should be kept in mind when analyzing the predicted tracer breakthrough curves.

Table 6–2 presents a comparison between measured and predicted first arrival times, as obtained for the measured and predicted breakthrough curves. It would have been more desirable to compare average travel times as the time of 50 % of the steady–state concentration, but those were not well defined in all breakthrough curves. In general, the middle section is considered to be part of a low conductivity zone, while the upper and lower are consider to be located in high conductivity zones. Regarding the predicted first arrival times, the high conductivity zones are considered more accurate with respect to the actual hydraulic conductivities given as input.

The comparison between measured and predicted travel times reveal several interesting features. Firstly, predicted arrival times are significantly underestimated for all sections. Secondly, the assumption that all the upper, middle and lower borehole sections essentially represent three high conductivity sub–zones is not correct. Thirdly, the differences between

boreholes in measured first arrival times do not correspond to the prevailing hydraulic gradients, if homogeneous hydraulic conditions are assumed.

Table 6-2 Comparison of measured and predicted first arrival times (units in hours).

| Borehole | Section | Measured t | Predicted t |
|---|---|---|---|
| KFI06 | Upper | 106 | 1 |
| | Middle | 1250 | 50 |
| | Lower | 194 | 1 |
| KFI11 | Upper | 24 | 1 |
| | Middle | 850 | 50 |
| | Lower | 3200 | 1 |
| BFI01 | Upper | 75 | 1 |
| | Middle | 600 | 50 |
| | Lower | 1300 | 1 |

### 6.3.2 Assessment of Model Performance and Re-calibration

In order to analyze the discrepancies between measured and predicted tracer transport, it is important to recognize which aspects of the flow and transport processes are influenced by the various parameters used in the model.

#### 6.3.2.1 Hydraulic Gradient

The hydraulic gradient was predicted using a calibrated model from hydraulic interference tests. The head distribution is governed by the transmissivities as well as the physical geometry of the modelled region. The fracture zone appears to be a bounded system surrounded by more or less impermeable boundaries /Andersson et al, 1989/, and the hydraulic heads in such a system can only be computed with a two-dimensional model. In this case, it may be argued that sufficient data is not available for the fracture zone for such a description. However, the principle should be clear that an accurate prediction of hydraulic heads should form a foundation on which solute transport can be simulated.

The observed hydraulic heads from the radially converging tracer experiment indicate that the predictive model is entirely plausible with regard to transmissivities and boundary configuration. As expected, borehole BFI01 was not predicted satisfactorily, which confirms that there are heterogeneities or anisotropic conditions within Zone 2 not accounted for in the model. Another possibility is the presence of a natural gradient having considerably larger influence than assumed. Some experiments incorporating anisotropy into the model are described in Andersson et al, /1989/, which may partly explain the deviant behaviour of BFI01. However, these experiments were somewhat inconclusive. In addition, complete verification of the calibrated

flow model could not be made, as observations during the tracer test were not obtained from all the boreholes within Zone 2.

Any natural hydraulic gradients have been neglected during the predictive modelling, since the gradient are not well defined over the entire area. However, the measurements that are available indicate a gradient directed from BFI01 to BFI02. If this gradient is large, it may (at least partly) account for some of the unexplained behaviour in BFI01.

A conclusion of the discussion of hydraulic gradients is that based on the observations made during the tracer test, large prediction errors of groundwater velocities and solute transport would not arise from ill-defined geometry, incorrectly estimated transmissivities or neglected gradients. At the most, predicted velocities would differ with a factor 2-3 for BFI01.

#### 6.3.2.2 Groundwater Velocity

Given the hydraulic gradient (the spatial distribution of head), the average groundwater velocity is given by the spatial distribution of hydraulic conductivity and flow porosity. In turn, the groundwater velocity determines the residence times for the injected tracers. Above, it could be seen that the predicted residence times were significantly shorter than the observed. Given that the hydraulic gradients apparently were predicted relatively accurately (except for BFI01), the reason for the discrepancy is to be found in either the hydraulic conductivities or the flow porosities.

Hydraulic conductivities have been measured extensively by single hole injection tests. The conductivities from these agrees well with values estimated from the results from the interference test, and subsequently used in the predictive modelling. Thus, only relatively small errors in predicted travel times can be attributed to erronously assumed hydraulic conductivities.

The flow porosity for the fracture zone was essentially unknown prior to the tracer experiment, and it appears that the prediction error regarding travel times can be explained by this lack of information. The value used for the predictions, $3.0 \cdot 10^{-4}$, was obtained from measurements over a 75 m large section /Ahlbom et al, 1986/ straddling both conductive sub-zones and low conductive rock. However, it is reasonable to expect that the flow porosity would be greater in the fracture sub-zone than for the surrounding rockmass. Thus, the value obtained from the 75 m section may significantly underestimate the porosity in the fracture sub-zones, where the main part of flow and solute transport occure. By scaling the porosity value used in the predictions to a fracture zone with a width of 1.0 m, one would obtain a flow porosity of $2.25 \cdot 10^{-2}$.

Using a flow porosity of $2.25 \cdot 10^{-2}$ and with other parameters as before, new breakthrough curves were simulated for some tracers with a high tracer mass recovery. An example of this re-calibration is given in Figure 6-9, showing the observed breakthrough for In-EDTA, injected in BFI01, upper section. As porosity merely works as a scaling factor for the tracer residence time, it

is not surprising that the observed data is simulated fairly well.

### 6.3.2.3 Tracer Distribution

Given the average groundwater velocity distribution, the actual tracer distribution is then governed by dispersive and/or diffusive effects. Steady state concentrations, as measured in samples obtained from the pumping hole, is influenced by the injection concentration, the general flow pattern (transverse dispesion) as well as dilution effects in the sampling section. Longitudinal and transversal dispersivities determine the general shape of the breakthrough curve.

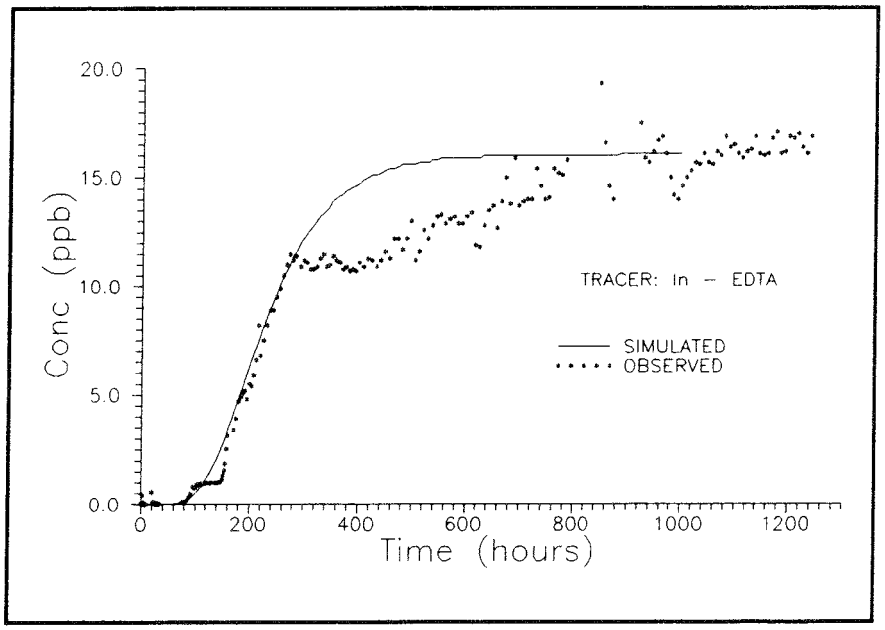


Figure 6–9 Simulated versus observed data in pumped borehole BFI02 using an adjusted porosity value of $2.25 \cdot 10^{-2}$. Tracer injection in borehole BFI01, upper section.

The simulated breakthrough curve in Figure 6–9 also contains a revised injection boundary condition. The predictions were made using fixed concentrations in the injections node, a boundary condition that is unlikely to simulate the correct injection mass, due to discretization effects of the finite element technique used. Instaed, the boundary condition was changed to constant mass injection. The effect is essentially a scaling of the breakthrough curve, based on the measured tracer mass injected. As expected for a tracer with a high mass recovery, the simulated steady state concentration level agrees relatively well to the observed. By comparison of the general shape of the scaled predicted curves and observed breakthrough curves, one can conclude that the predictions of the dispersive effects are plausible. It is not possible to assess the individual dispersion parameters (longitudinal and transversal dispersivities) with only one observation location. It can also be noted that part of the observed data is not explained by the model in Figure 6–9. As is discussed in chapter 5, this is most likely due to the heterogeneous nature of the fracture zone, resulting in preferential

tracer pathways with varying flow and velocity distributions. However, this would be likely to happen in any geologic medium at this scale of transport.

In summary, the calibration of the model after the radially converging experiment mainly concerned adjustment of the flow porosity, in addition to some minor adjustment of the hydraulic conductivity. The updated model was then used for subsequent prediction of the dipole tracer experiment /Nordqvist 1989/, /Andersson et al, 1990/.

## 6.4 CONCLUDING REMARKS

The groundwater flow and transport modelling presented here should be seen as an integral part of a series of modelling efforts in order to obtain a deeper understanding of the hydrogeology of Zone 2. It is also a test of the predictability, using this type of model, of transport processes based on available data on basic rock properties in the area.

The model employed in this case assumes that flow and transport processes can be described as phenomena occurring in a continous porous medium. The separate highly conductive zones within Zone 2 are treated as thin layers, with a thickness of 0.5 metres, consisting of many interconnected flow paths that will approach a porous medium at the scale of the tracer test. The transport distances during the Radially Converging Tracer Test (155–189 m) may, or may not, be sufficient for a porous media description.

Although the model has proven to relatively well simulate flow (hydraulic heads) on a large scale, it lacks sufficient detail to predict detailed hydraulic head distributions for the radially converging tracer experiment. In addition, the tracer experiment has also shown that only solute transport in the upper highly conductive part show somewhat consistent behaviour. Thus, the only well extensive and hydraulically well connected part of the zone, is the contact between the upper part of the zone and the rock mass above. The rest of Zone 2, also contain connected paths available for solute transport, but in a much more complex and unpredictable manner.

The solute travel times between injection and withdrawal holes depend entirely on the hydraulic properties along the particular transport transport paths activated during the experiment. In the particular model employed here that would mean the variability of hydraulic conductivity and flow porosity along the transport path. All the required properties for describing transport can not be determined from large–scale pumping tests only, and thus travel times can not be predicted with confidence. For the uppermost subzone, it is reasonable to regard the determined effective hydraulic conductivity from the interference tests as a representative value. Given that, the evaluation of the tracer test with the 2–D model has shown that the effective flow porosity is of the order of 0.01 for this subzone. Typical values of the longitudinal dispersivity may be on the order of 10 m, or about a tenth of the scale of the experiment. For the rest of Zone 2, it is difficult to make generalisations about the values of the transport parameters.

It is likely that the observed breakthrough curves for the different injection

intervals can be simulated very accurately by adjusting flow and transport parameters until a good fit between curves are obtained. However, given the a priori information on flow and transport parameters in this case, solute transport can at best be predicted within the correct order of magnitude (travel times). Considerably more knowledge about the spatial distribution of parameters in the fracture zone would be needed in order to make more detailed predictions. Nontheless, it may be argued that the fracture zone, at least the upper conductive layer, behaves as much as a porous medium as could be expected from any unconsolidated aquifer formation.

# 7. DISCUSSION AND CONCLUSIONS

## 7.1 EXPERIMENTAL

The tracer test was performed in a radially converging flow geometry in a low-angle major fracture zone. The converging flow field was created by pumping in a central borehole. Injections of 11 tracers were made in totally 9 borehole sections straddling highly conductive sub-zones in three peripheral boreholes located in different directions from the pumped tracer withdrawal borehole.

Sampling for measurement of tracer breakthrough was made at the ground surface in the water discharged from the pumped borehole. In order to determine possible interconnections between highly conductive parts (sub-zones) of the investigated zone also a sampling of major conductors (sub-zones) was performed in the withdrawal borehole towards the end of the tracer injections.

The tracer injections were performed in two different ways, continuous (extended step inputs) and as pulse injections.

There were three reasons for the choice of continuous injection; 1) the tracer test aimed at investigate interconnections between sub-zones within the studied fracture zone and with the technique employed for tracer sampling in the pumped borehole this was an injection technique that made that possible, 2) steady-state breakthrough resulting from a continuous injection gives the data nessesary for calculation of the volume of the fracture flow paths involved in the tracer transportation, 3) it simplifies the descision of tracer injection concentrations, as dilution is easily calculated with knowledge about withdrawal pump rate and injection flow rate.

The continuous injections worked quite well and were made without applying any excess pressure in the borehole sections. The groundwater flowing through the borehole sections were continuously labelled with concentrated tracer solutions during complete mixing. The advantages were that the tracer mass release per time unit into the fracture system and also the groundwater flow rate through the injection borehole sections could be calculated. Dispersion effects in the injection borehole caused by large borehole volumes and/or trapping effects were also minimized. Enhanced tailing and/or dispersion in tracer breakthrough curves due to tracer forced out into stagnant parts of fractures was also avoided.

However, a drawback is that relatively sophisticated equipment is needed to perform coninuous injections according to this technique. Gas bubbles trapped in the injection system caused some problems in the beginning, but improvements of the equipment were made later on during the tracer test. The tracer concentration increased in some injection intervals indicating a

decreasing groundwater flow rate, but the product of the concentration and flow rate remained nearly constant in most cases and only a negligible mass of tracer was accumulated in the injection interval. For future applications measurements of flow rates and concentrations within the injection system are recommended to be done more often in order to get a better control of the injection procedure.

The groundwater flow rate through the injection sections were determined by the dilution method prior to the tracer injections. The dilution measurements clearly showed if the borehole sections selected for tracer injections belonged to an active, flowing part of the fracture zone.

The pulse injections were made according to two different techniques, forced pulse and decaying pulse, i.e. without excess pressure. The decaying pulse injection was successfully used in one borehole section were two tracers were simultaneously injected. Although it was much easier to perform than the continuous injection technique used they had some advantages in common. No excess pressure applied to the fracture flow system and possibilities to calculate the tracer mass release per time unit into the fracture system and also the groundwater flow rate through the injection borehole section.

The technique used for sampling of major conductors in the pumped tracer withdrawal borehole required a pumpstop and removal of pump, packer, discharge pipe and equipment for hydraulic head measurements. Thereafter the double-packer assembly with 2 m spacing was lowered and 7 major conductors were pumped and sampled, one at a time. The procedure took about 100 hours to complete, and to get dependable results the tracer intended to be sampled had to be present in the conductors and in the vicinity to the pumped borehole at the time of sampling. The tracers were injected in different directions from the pumped borehole and in flow paths with different hydraulic conductivity ranging within three orders of magnitude. These conditions required continuously injected tracers, in one way or another.

To make it possible to choose another injection technique than continuous and keep the possibility to measure tracer breakthrough in major conductors without interrupting the pumping, and disturb the flow field during the tracer test, another instrumentation in the pumped tracer withdrawal borehole is necessary. One feasible design is sampling tubes down to selected major conductors. Another, precise but complicated idea, is installation of packers in hydraulically low conductive parts between the major cunductors in the borehole. Pumping is then performed between the packers with a controlled and uniform drawdown for all the borehole sections. Sampling is made in the pipes discharging water from the packed-off sections.

## 7.2 SUPPORTING MEASUREMENTS

A litterature review showed that in some previously performed tracer tests a large portion of the residence time and dispersion obtained in the tracer breakthrough curves was the result of delay and dispersion in the equipment,

and not of the medium intended to study. Therefore the delay and dispersivity of tracers in the withdrawal borehole BFI02 and in the tubing system up to the sampling equipment at ground surface was examined by theoretical calculations and a tracer test prior to injection of tracers in the peripheral injection boreholes. The results showed that the delay and dispersivity in the withdrawal borehole BFI02 were neglible compared to the values obtained in the fracture flow paths during the radially converging tracer experiment. Consequently, no corrections for the delay and dispersivity in the withdrawal borehole and sampling equipment has been made in the present evaluation of the breakthrough curves.

The tracers that should be used in the radially converging test had to be very carefully selected considering the long distances involved in the tracer test and the predicted relativly long residence times from some injection points. The high transmissivity of Zone 2 also required a large dynamic range of the tracers used. The chosen pump capacity of 2 l/s for tracer withdrawal implied that the dilution of the tracers would be about 1:60 000 at steady-state concentration. The minimum allowable dilution then had to be in the order of 1:1 000 000 to achieve good enough resolution in the early breakthrough data. Thus, elements which were naturally present in the groundwater at ppm-levels could not be used.

There were also a need for many different tracers. The minimum was one for the dilution measurements and nine tracers for injections during the test, one tracer per selected injection point. Tests of tracers were therefore started within the supporting research programme for the radially converging tracer test. The tracers should ideally be non-sorbing and non-reactive with the rock and the groundwater. Some of the tracers had not been used in groundwater studies before. Seven rare earth metal DTPA and EDTA complexes, three fluorescent dye tracers and two ionic tracers were finally chosen. The laboratory studies indicated that long term stability may be a problem for some of the EDTA complexes, resulting in sorption of the tracer metal.

The fluorescent dyes and one of the ions had earlier been used in tracer tests performed in Swedish crystalline basement rock. They had good records of stability, dynamic range and low tendency for sorption. The dyes Uranine (Sodium Fluorescein) and Amino G Acid were used during the tracer test and Rhodamine WT was used for the groundwater flow determinations prior to the tracer experiment. The ions selected were $I^-$ and $ReO_4^-$.

The recovery of the tracers used during the radially converging test ranged from 1 to 98 %. Tracers injected in upper sub-zone all reached a high recovery (70-98%). Middle ranged 2 - 18% and lower 1 - 65%. As there was a time limit set for the tracer test, some of the breakthrough curves were never measured completely before the test was teminated. Hence tracers with long residence time may have showed higher recovery rates if there had been possibilities to prolong the test period.

## 7.3 FLOW AND TRANSPORT CHARACTERISTICS OF ZONE 2

### 7.3.1 General

Tracer breakthroughs were obtained from all nine injection points and of all eleven tracers used. The most rapid first arrivals, 24 - 106 hours, were monitored, as expected, for the tracers injected in the upper highly conductive part of Zone 2. Within Zone 2, and between upper and lower margins, sub-zones constitute flow paths of considerable variable residence times. From a hundred to some thousand hours at the test conditions prevailed. Where the hydraulic gradient ranged from 0.003 to 0.007, and distance from 155 to 200 m depending on direction from the pumped withdrawal borehole.

The evaluation and interpretation of the tracer breakthrough curves was made with one-dimensional models. Primarily dispersion and fluid velocity were determined by fitting the tracer breakthrough curves to the theoretical solutions. The secondary level of interpretation used the estimated residence times, along with groundwater flow and head measurements, to evaluate properties such as hydraulic conductivity of fracture flow paths, fracture aperture, flow porosity and flow wetted surface area. The results shows that there are directional variations in most of the calculated transport parameters determined for Zone 2 and sub-zones, which is concluded to be due to heterogeneity and/or anisotropy. This condition is more pronounced at depth in Zone 2.

It is obvious from the hydraulic testing that the flow within Zone 2 is concentrated to a few highly conductive parts. The results of the radially converging tracer experiment show that these highly conductive parts are hydraulically interconnected and within distances of 155 - 200 metres there was an extensive mixing of tracer labelled groundwater between the highly conductive sub-zones of Zone 2, separated by 15 - 110 metres of low conductive rock at the injection points. The possibility of groundwater mixing within Zone 2 at certain hydraulic gradient conditions is in agreement with the gelogical structure of the zone, made up of minor shear and fracture zones. For calculations of solute transport the heterogeneity and mixing due to interconnected sub-zones should be taken into account.

The breakthrough curves obtained from the radially converging tracer test were fairly well explained by solute transport governed by advection-dispersion, when models considering variation in the source term were used, i.e. injection capacity and tracer mass release per time unit into the aquifer were accounted for in the breakthrough analysis. Matrix diffusion was therefore considered to be of minor importance during the time scales involved in the test. At least for the fastest flow paths. In the slowest flow paths (residence times some thousand hours) matrix diffusion is possibly more important. The discrepancy from the advection-dispersion solution in some breakthrough curves may also be due to transient solute storage in immobile fluid zones or insufficient long term stability of the tracer metal-complexes used.

### 7.3.2 Dispersion

The dispersion lengths, D/v, within main flow paths (sub–zones) in Zone 2 is estimated to range from 4 – 11 metres and Peclet numbers from 16 to 40. The macro–dispersion, here defined as the phenomena obtained due to superposed breakthroughs from solute transport in more than one main flow path (sub–zone) in Zone 2, is estimated to give dispersivities in the range from 20 to 90 metres and the Peclet numbers from 2 to 8. Hence, in Zone 2 the macro–dispersion gives about 3 to 10 times larger dispersion length over the entire thickness of Zone 2 than in the individual main flow paths (sub–zones). Litterature values are often referred to with dispersion length about 1/10 of transport path length. Here about 1/20 was obtained in the sub–zones of Zone 2. In the entire Zone 2, transport length was about 1.5 – 2 times the thickness of transport layer (aquifer) and D/v obtained was 1/7 – 1/2 of transport path length.

### 7.3.3 Flow Porosity and Fracture Apertures

Within Zone 2 flow porosities shows no large difference between the 0.5 – 2.0 m thick sub–zones, but intermediate sub–zones have somehwat higher flow porosity than the upper and lower ones. In the upper sub–zone the calculated flow porosity $\theta_k^m$ ranged from $1.0 \cdot 10^{-3}$ to $4.6 \cdot 10^{-2}$. In the lower sub–zone it ranged from $5.5 \cdot 10^{-3}$ to $2.2 \cdot 10^{-2}$, and in the intermediate sub–zones from $2.1 \cdot 10^{-2}$ to $1.3 \cdot 10^{-1}$. The flow porosities in the sub–zones of Zone 2 are compareable to zone NE–1 at the Äspö HRL, but somehwat higher than porosity in zones NNW–1 and NNW–2. Assuming the structure of Zone 2 as three sub–zones (upper,middle and lower) with very low conductive, no–flow, rock inbetween, the flow porosity of the entire 100 m thick Zone 2 will then be in the range from $5.4 \cdot 10^{-4}$ to $7.0 \cdot 10^{-4}$. However, it must be noted that more than 95 % of the transmissivity, and hence also the groundwater flow in Zone 2 is concentrated to a few interconnected shear and fracture zones (sub–zones). For solute transport a network of interconnected sub–zones with flow porosity somewhere in the range of 0.001 – 0.1 should be considered.

Fracture apertures were calculated following three concepts; 1) Frictional loss, i.e. residence time $e^t$, 2) Cubic law, i.e. flow rate $e^q$, 3) Mass balance $e^m$. The relative magnitudes of the experimentally obtained apertures follows the theoretical relationship, that $e^q$ is larger than $e^t$ in the fracture flow paths.

On an average the residence time determined apertures, $e^t$, of the fracture flow path are a bit larger in the upper sub–zone than in flow paths in intermediate and lower parts of the Zone 2. Representative values are $7 \cdot 10^{-4}$ m in the upper sub–zone, and $1 \cdot 10^{-4}$ m in intermediate parts of Zone 2.

The mass balance determined aperture, $e^m$, representing the total pore volume accessible to advective flow, i.e. the sum of apertures of all fractures contributing to flow within the studied sub–zone, is smaller in the upper and lower sub–zones than in the intermediate ones. Representative values are $1.0 \cdot 10^{-2}$ m in the upper sub–zone and $5.8 \cdot 10^{-2}$ and $1.1 \cdot 10^{-2}$ m in intermediate and lower sub–zones respectively.

The ratios $e^m/e^t$, giving the number of fractures in the smooth fracture case, where tracer is injected in a fracture zone made up of a package of equal fractures, indicates that 2 – 20 fractures contributes to groundwater flow in the upper sub–zone of Zone 2. The ratio $e^m/e^q$, which according to the results of Silliman /1989/ and Tsang /1992/ may be more appropriate for rough walled fractures, indicate 1 – 7 fractures in the upper highly conductive sub–zone. In lower sub–zones of Zone 2 the number of fractures contributing to groundwater flow is markedly higher, based on $e^m/e^t$ and $e^m/e^q$ ratios. This is in good agreement with independent results from geological mapping within the test site and core logging /Tiren 1991/. It was concluded that the sub–zones parallel to the upper margin of Zone 2 constitutes of only a few fractures.

The conclusion is that there are a few relatively large aperture fractures in the upper highly conductive sub–zone. Whereas in intermediate and lower sub–zones there are many small aperture fractures, which together gives larger porosity (volume) accessible to groundwater flow in these zones than in the upper one.

### 7.3.4 Hydraulic Conductivity

The hydraulic conductivity of the fracture flow paths were determined both with the flow rate and with the residence time as the basic variable. The flow rate determined conductivities are all much higher than corresponding conductivities determined with the residence time as basic variable. This difference reflects large geometrical variations (i.e. of apertures and breadths) in the flow paths of the fracture system. In the upper sub–zone of Zone 2 the ratio $K_e^q/K_e^t$ is about 10, whereas in middle and lower parts of Zone 2 it is much higher, in the range of 30 – 100. The fracture flow paths within the upper sub–zone have all about the same hydraulic conductivity, and have a mean value of $3.8 \cdot 10^{-1}$ m/s. Tracer injected in intermediate sub–zones are found in both upper, middle and lower part of Zone 2. The mean value of the hydraulic conductivity in these fracture flow paths is $2.8 \cdot 10^{-2}$ m/s.

### 7.3.5 Flow Wetted Surface

The flow wetted surface area was calculated in two ways; 1) as surface area per volume of flowing water and 2) as surface area per volume of rock, i.e. the rock defined as fracture zone with matrix rock and apertures.

In the upper sub–zone of Zone 2 the flow wetted surface per volume of rock (i.e. fracture zone) ranged from 1 to 56 $m^2/m^3$. In the lower sub–zone of Zone 2 basic data for calculations of flow wetted surface was obtained in only one direction. However, in that direction the surface area per volume of rock is calculated to be within 6 – 92 $m^2/m^3$. If the preferential flow paths are restricted to 20 – 37 % of the fractures in Zone 2, as the results from the Stripa radar and saline experiments indicates, then the flow wetted surface should decrease accordingly.

In Stripa the flow wetted surface was calculated to 1.8 $m^2/m^3$ in zone C, with

consideration to preferential flow paths occupying 20 – 37 % of the fractures /Andersson et al.,1989b/. In the reference case in SKB91 /SKB, 1992/ a flow wetted surface of 0.1 $m^2/m^3$ was used for the migration calculations at the Finnsjön site.

The flow wetted surface expressed as surface area per volume of water ranged from 1180 to 3850 $m^2/m^3$ in the upper sub–zone of Zone 2, depending on how fracture aperture was determined. If the total pore volume in the upper sub–zone is represented by one single fracture the fracture surface area per volume of water is within 182 – 952 $m^2/m^3$. In the lower sub–zone of Zone 2, basic data for calculations of flow wetted surface area per volume of water was obtained in only one direction and there the calculated value ranged from 1180 to 8700 $m^2/m^3$. In Stripa Zone C the corresponding value was 1266 $m^2/m^3$. In the reference case in SKB91 /SKB,1992/ a value of 1000 $m^2/m^3$ was used.

## 7.4 TWO–DIMENSIONAL MODELLING

The 2–D modelling aimed at simultaneous understanding of flow and transport. The general approach was to calculate the flow field (hydraulic head distribution) in the fracture zone during the tracer experiment, which in turn served as input to the solute transport model.

The steady state hydraulic head was predicted based on the calibrated flow model from the previously performed interference test.

The transport of tracer labelled groundwater was predicted as concentration versus time in the pumped borehole. In addition, areal plots of tracer distribution were produced.

The hydraulic gradients were predicted relatively accurately, but the predicted residence times were significantly shorter than the observed. Given the hydraulic gradient (the spatial distribution of head), the average groundwater velocity is given by the spatial distribution of hydraulic conductivity and flow porosity. The reason for the discrepancy in the predicted residence times is then to be found in either the hydraulic conductivities or the flow porosities.

Hydraulic conductivities have been measured extensively by single hole injection tests. The conductivities from these agreed well with values estimated from the results from the interference test, and subsequently used in the predictive modelling. Thus, only relatively small errors in predicted travel times can be attributed to erronously assumed hydraulic conductivities. The flow porosity, on the other hand, was essentially unknown prior to the tracer experiment, and it appears that the prediction error regarding travel times can be explained by this lack of information. The value used for the predictions, 3.0 E–04, was obtained from measurements over a 75 m large section straddling both conductive sub–zones and low conductive rock. It is reasonable to expect that the flow porosity would be greater in the fracture zones than for the surrounding rockmass. Thus, the value obtained from the 75 m section may significantly underestimate the

porosity in the fracture sub-zones, where the main part of flow and transport occure. By scaling the porosity value used in the predictions to a fracture zone with a width of 1.0 m, a flow porosity of 2.25 E-02 was obtained. Using this flow porosity and other parameters as before, new breakthrough curves were simulated for some tracers with a high tracer mass recovery. simulated and observed tracer breakthrough then compared fairly well.

It can be concluded that hydraulic tests, single hole and interference tests, gives information enough to predict flow. But tracer test are neccessary to obtain parameters essential to predict solute transport, e.g. flow porosity.

The evaluation of the tracer test with the 2-D model has shown that the flow porosity is in the order of 0.01 in the upper sub-zone. Typical values of the longitudal dispersivity may be on the order of 10 m, or about a tenth of the scale of the experiment. These values are in good agreement with the independently performed 1-D evaluation of the breakthrough curves in the upper sub-zone of Zone 2. For the rest of Zone 2, it is difficult out of the performed 2-D modelling to make generalisations about the values of the transport parameters.

The results of 2-D modelling shows that the upper conductive layer behaves as much as a porous medium as could be expected from an unconsolidated aquifer formation, due to spatial aperture variations and extensive fracture interconnections.

# 8. REFERENCES


Ahlbom K., Andersson P., Ekman L., Gustafsson E., Smellie J., Tullborg E-L.,1986. Preliminary investigations of fracture zones in the Brändan area, Finnsjön study site. SKB Technical Report TR 86-05. Swedish Nuclear Fuel and Waste Management Co, Stockholm.

Ahlbom K, Andersson P, Ekman L, and Tirén S 1988. Characterization of fracture zones in the Brändan area, Finnsjön study site, Central Sweden. SKB Progress Report AR 88-09.

Ahlbom K, and Tirén S 1991. Overview of geologic and geohydrologic conditions at the Finnsjön site and its surroundings. SKB Technical Report TR 91-08.

Ahlbom K, Andersson J-E, Andersson P, Ittner T, Ljunggren C, and Tirén S 1992. Finnsjön study site. scope of activities and main results. SKB Technical Report TR 92-33.

Andersson J-E, Ekman L, and Winberg A 1988a. Detailed investigations of fracture zones in the Brändan area, Finnsjön study site. Single hole water injection tests in detailed sections. Analysis of conductive fracture frequency. SKB Progress Report AR 88-08.

Andersson J-E., Ekman L., Gustafsson E., Nordqvist R., Tirén S., 1989. Hydraulic interference tests and tracer tests within the Brändan area, Finnsjön study site. The Fracture Zone Project - Phase 3. SKB Technical Report TR 89-12. Swedish Nuclear Fuel and Waste Management Co, Stockholm.

Andersson J-E., Ekman L., Nordqvist R., Winberg A., 1991. Hydraulic testing and modelling of a low-angle fracture zone at Finnsjön, Sweden. Journal of Hydrology, Vol 126, pp 45-77. Elsevier, Amsterdam.

Andersson J. & Andersson P., 1987. Flow Simulations in a Fracture Zone in the Brändan Area, Finnsjön. SKB Progress Report AR 87-26. Swedish Nuclear Fuel and Waste Management Co, Stockholm.

Andersson P., Klockars C-E. 1985. Hydrogeological investigations and tracer tests in a well-defined rock mass in the Stripa mine. SKB Technical Report TR 85-12, 47p.

Andersson P, Eriksson C-O, and Gustafsson E 1988b. Radially converging tracer experiment, Finnsjön Sweden. Supporting research; Test of equipment and determination of transport parameters in the pumping hole BFI02. SKB Progress Report AR 88-39

Andersson P., Eriksson C-O., Gustafsson E., Ittner T., 1990. Dipole Tracer Experiment in a Low-angle Fracture Zone at Finnsjön. Experimental design and preliminary results. The Fracture Zone Project - Phase 3. SKB Progress Report AR 90-24. Swedish Nuclear Fuel and Waste Management Co, Stockholm.

Andersson P., Nordqvist R., Persson T., Eriksson C-O., Gustafsson E., Ittner T. 1993. Dipole Tracer Experiment in a Low-angle Fracture Zone at Finnsjön - Results and Interpretation. The Fracture Zone Project - Phase 3. SKB Technical Report, in prep.

Andersson P M, Andersson P, Gustafsson E, and Olsson O 1989b. Investigation of flow distribution in a fracture zone at the Stripa mine, using the radar method, results and interpretation. SKB Technical Report TR 89-33.

Bear J. 1979. Hydraulics of groundwater. Mac Graw-Hill, New York.

Brown D.M. 1984. Stochastic analysis of flow and solute transport in a variable-aperture rock fracture. Msc. Thesis, Massachusetts Inst. of Technology, 69 p.

Brotzen O. 1986. On groundwater travel times in granite and gneiss. Paper presented at the 2nd Int. Conf. on Nuclear Waste Management of the Canadian Nuclear Society. Winnipeg.

Byegård J., Skålberg M. 1992. Tracer Handbook. SKB Progress Report PR 25-92-11.

Carlsson L. 1989. Personal Communication, Swedish Geological Co., Gothenburg.

Carlsson L, Gentzschein B, Gidlund G, Hansson K, Svensson T, and Thoregren U 1980. Kompletterande permeabilitetsmätningar i finnsjöområdet. SKBF/KBS Technical Report TR 80-10.

Carlsson L, and Gidlund G 1983. Evaluation of the hydrogeological conditions at Finnsjön. SKBF/KBS Technical Report TR 83-56.

Cederwall K., Larsen P. 1979. Hydraulik för väg- och vattenbyggare. Liber läromedel. ISBN 91-40-54300-5. Lund. (In Swedish).

Cooley R.L. 1985. A comparison of several methods of solving nonlinear regression groundwater flow problems. Water Resources Research, Vol. 21, No. 10.

Ekman L, Andersson J-E, Andersson P, Carlsten S, Eriksson C-O, Gustafsson E, Hansson K, and Stenberg L 1988. Documentation of Borehole BFI02 within the Brändan Area, Finnsjön Study Site. The Fracture Zone Project- Phase 3. SKB Progress Report AR 89-21.

Fisher H.B., List E.J., Koh R.C.Y., Imberger J., Brooks N.H. 1979. Mixing in inland and costal waters. Academic press. 483 p.

Freeze R.A. & Cherry J.A., 1979. Groundwater. Prentice-Hall Inc., Englewood Cliffs, New Jersey 07632.

Gelhar L 1987. Applications of stochastic models to solute transport in fractured rocks. SKB Technical Report 87-05.

Gidlund J., Moreno L., Neretnieks I. 1990. Porosity and diffusivity measurements of samples from Finnsjön. SKB Progress Report AR 90-34.

Gustafsson E, and Klockars C-E 1981. Studies on groundwater transport in fractured crystalline rock under controlled conditions using non-radioactive tracers. SKB Tecnical Report 81-07. 32p.

Gustafsson E, Andersson P, and Larsson N-Å 1987. The Fracture Zone Project in Finnsjön, Phase 3. Proposal for tracer experiments. SKB Progress Report 87-34. 45 p.

Gustafsson E, and Andersson P 1991. Groundwater flow conditions in a low-angle fracture zone at Finnsjön, Sweden. Journal of Hydrology, Vol 126, pp 79-111.

Gustafsson E., Andersson P., Ittner T., Nordqvist R. 1991. Large Scale Three-Dimensional Tracer Test at Äspö, in Rhén (Ed.) Äspö Hard Rock Laboratory: Evaluation of the combined longterm pumping and tracer test (LPT2) in borehole KAS06. SKB Technical Report TR 92-32.

Gustafsson E. 1992. Calculations of flow porosity based on results from a tracer test. Passage of fracture zones. Passage of NE-1. SKB - Äspö Hard Rock Laboratory. Technical Note, PR 25-92-18c. Swedish Nuclear Fuel and Waste Management Co. Stockholm.

Hautojärvi A, and Coworkers 1992. VTT Analysis of Tracer Data. In Tsang and Neuman (editors). The International INTRAVAL Project. NEA/SKI 1992.

Heemstra R.J, Watkins J.E, and Armstrong F.E. 1961. Laboratory Evaluations of Nine Water Tracers. NUCLEONICS Vol 19, No 1 January 1961. pp 92-96.

KBS 1983. Final Storage of Spent Nuclear Fuel KBS-3. Svensk Kärnbränsleförsörjning AB. Stockholm I-IV.

Knutsson G, Ljunggren K, and Forsberg H.G 1963. Field and laboratory tests of Chromium-51-EDTA and tritium water as double tracer for groundwater flow. Radioisotopes in hydrology IAEA. Vienna. pp 347-367.

Kreft A., Lenda A., Turek B., Zuber A., Czauderna K. 1974. Determination of effective porosities by the two-well pulse method. Isotope Techniques in Groundwater Hydrology. Proc. Symp. IAEA Vienna.

Leijon B, and Ljunggren C 1992. A rock mechanics study of fracture zone 2 at the Finnsjön site. SKB Technical Report TR 92-28.

Lenda A., Zuber A. 1970. Tracer dispersion in groundwater experiments. Isotope Hydrology, Proceedings of a symposium. IAEA Vienna.

Long J., and Coworkers. 1992. Flow and tracer experiment in crystalline rock based on the Stripa 3-D experiment. The LBL/USDOE Project Team analysis. In Hodgkinson D., Grindrod P. (Ed.) The International INTRAVAL Project, Phase 1 Test Case 4, SKI/NEA. OECD Paris.

Marquardht D.W. 1963. An algorithm for least squares estimation of nonlinear parameters. J. Soc. Ind. Appl. Math., 11(2).

Moreno L, and Neretnieks I 1992. KTH/SKB Analysis of Radially Convergent Experiment. In Tsang and Neuman (editors). The International INTRAVAL Project. NEA/SKI 1992.

Moye D.G., 1967. Diamond drilling for foundation exploration. Civil Eng Trans, Inst Eng Australia, pp 95 - 100.

Nordqvist R. & Andersson J-E., 1987. Transient Flow Simulations in a Fracture Zone in the Brändan Area, Finnsjön. SKB Progress Report AR 88-11. Swedish Nuclear Fuel and Waste Management Co, Stockholm.

Nordqvist R., 1989. Numerical Predictions of a Dipole Tracer Test in a Fracture Zone in the Brändan Area, Finnsjön. SKB Progress Report AR 89-34. Swedish Nuclear Fuel and Waste Management Co, Stockholm.

Nordqvist R. 1991. Personal communication, Swedish Geological Co, Uppsala.

Norton D., Knapp R. 1977. Transport phenomena in hydrothermal systems: The nature of porosity. Amer. Journal of Science, Vol. 277, pp 913 - 936.

Ogata A., Banks R. 1961. A solution of the differential equation of longitudinal dispersion in porous media. U.S. Geol. Surv. Prof. Paper 411-A, Washington D.C.

Olkiewicz A, Scherman S, and Kornfält K-A 1979. Kompletterande berggrundsundersökningar inom Finnsjö- och Karlshamnsområdena. SKBF/KBS Technical Report TR 79-05.

Olsson O., Andersson P., Gustafsson E. 1991. Site Characterization and Validation - Monitoring of Saline Tracer Transport by Borehole Radar Measurements, Final Report. OECD / NEA International Stripa Project. Technical Report 91-18. Swedish Nuclear Fuel and Waste Management Co, Stockholm.

Palmqvist K, and Stanfors R 1987. The Kymmen power station. TBM tunnel. Hydrogeological mapping and analysis. SKB Technical Report TR 87-26.

Rouse H. 1961. Fluid Mechanics for Hydraulic Engineers. Dover Publications Inc. New York.

Raven K.G., Novakowski K.S., Lapcevic P.A. 1988. Interpretation of field tracer tests of a single fracture using a transient solute storage model. Water Resources Research, Vol. 24, No. 12, pp 2019-2032.

Smellie J, Gustafsson E, and Wikberg P 1987. Groundwater sampling during and subsequent to air-flush rotary drilling: Hydrochemical investigations at depth in fractured crystalline rock. SKB Progress Report 87-31. 94p.

Smellie J., Wikberg P. 1991. Hydrochemical investigations at Finnsjön, Sweden. Journal of Hydrology, Vol 126, pp 129-158.

Snow D.T. 1968. Rock fracture spacings, openings and porosities. J. Soil. Mech. Found. Div. Proc. ASCE, Vol. 14, No. SM1.

Silliman S E 1989. Interpretation of the difference between aperture estimates derived from hydraulic and tracer tests in a single fracture. Water Resources Research, Vol. 25, No 10, pp 2275-2283.

SKI/NEA 1990. The International INTRAVAL Project. Background and Results. OECD Paris 1990.

SKB 1992. SKB 91. Final disposal of spent nuclear fuel. Importance of bedrock for safety. SKB Technical Report TR 92-20.

Taylor G.I 1954. The dispersion of matter in turbulent flow through a pipe. Proc. R. Soc. London Ser. A 223, p 446-468.

Tirén S A 1986. Fractures and fracture zones. Structural elements, their character and tectonic environment. A literature review. SKB Progress Report AR 86-16.

Tirén S 1991. Geological setting and deformation history of a low-angle fracture zone at Finnsjön, Sweden. Journal of Hydrology, Vol 126, pp 17-43.

Tsang Y.W. 1992. Usage of "Equivalent Apertures" for Rock Fractures as Derived From Hydraulic and Tracer Tests. Water Resources Research, Vol. 28, No. 5, pp 1451-1455.

Van Genuchten M.Th. 1982. One-dimensional analytical transport modeling, in Proceedings: Symposium on Unsaturated Flow and Transport Modeling, Rep. PNL-SA-10325, Pacific Northwest Lab., Richland, Wash.

Van Genuchten M.Th., Alves W.J. 1982. Analytical solutions of the one-dimensional convective-dispersive solute transport equation. U.S. Dep. of Agric. Tech. Bull. 1661, 149 pp.

Voss C., 1984. A finite-element simulation model for saturated-unsaturated fluid-density-dependent groundwater flow with energy transport or chemically reactive single species solute transport. U.S. Geological Survey, Water Resourses Investigations Report 84-4369, 1984.

Zuber A., 1974. Theoretical possibilities of the two-well pulse method. Isotope Techniques in Groundwater Hydrology. Proc. Symp. IAEA Vienna.

# APPENDIX A

## WITHDRAWAL AND HYDRAULIC HEAD DATA

CONTENTS

Pump capacity borehole BFI02.

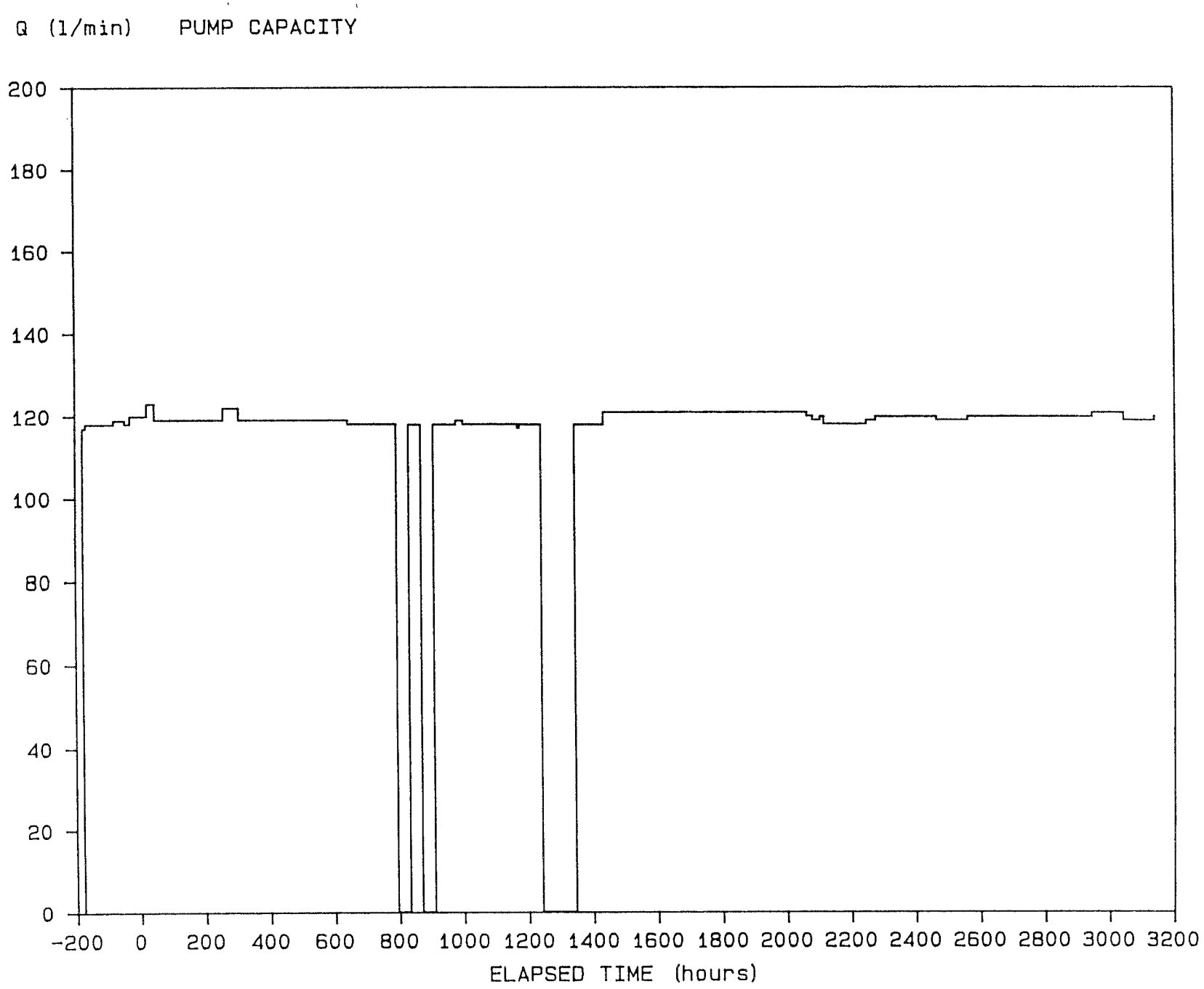


A: 1

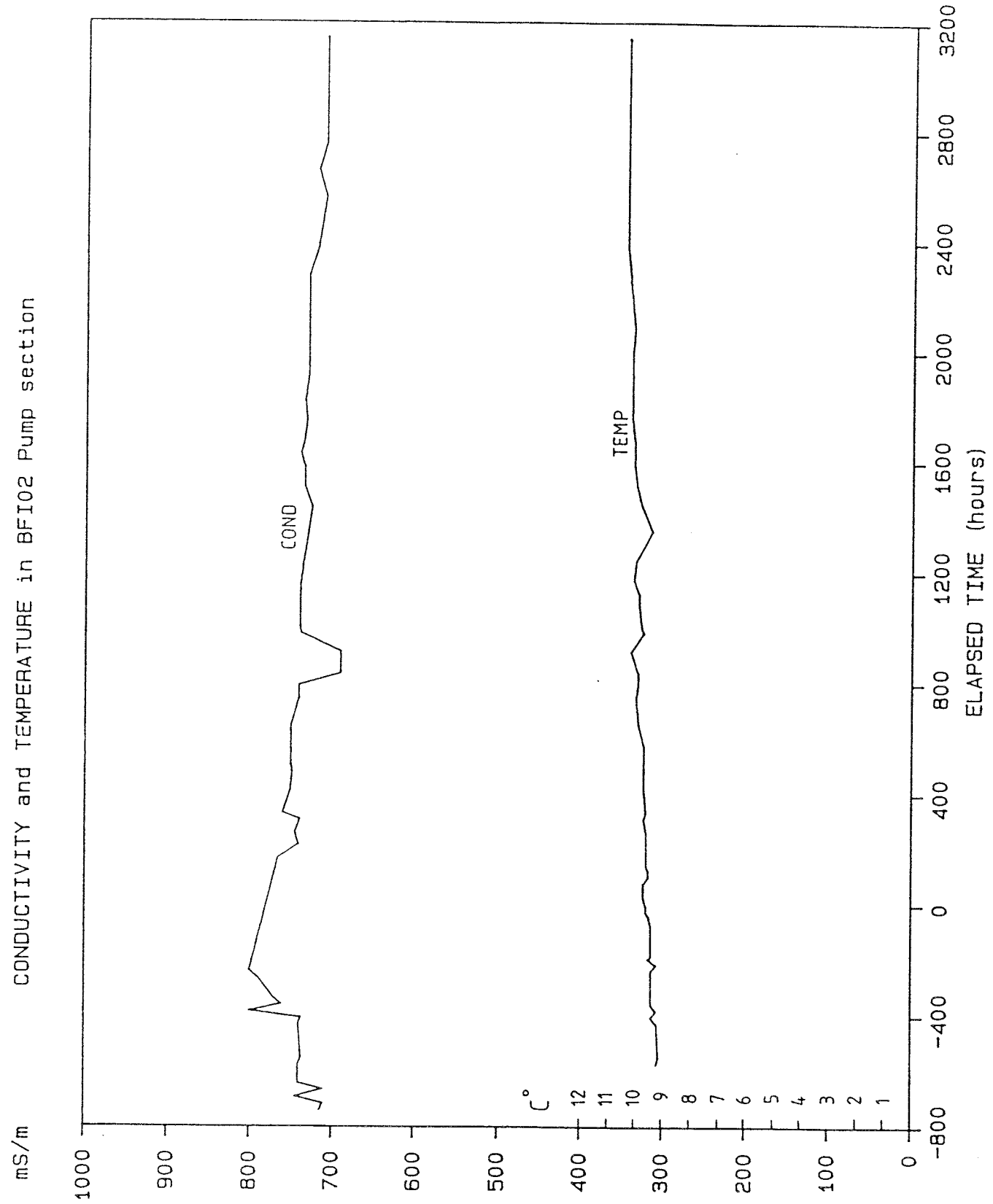


Temperature and electrical conductivity of the pumped water from borehole BFI02.

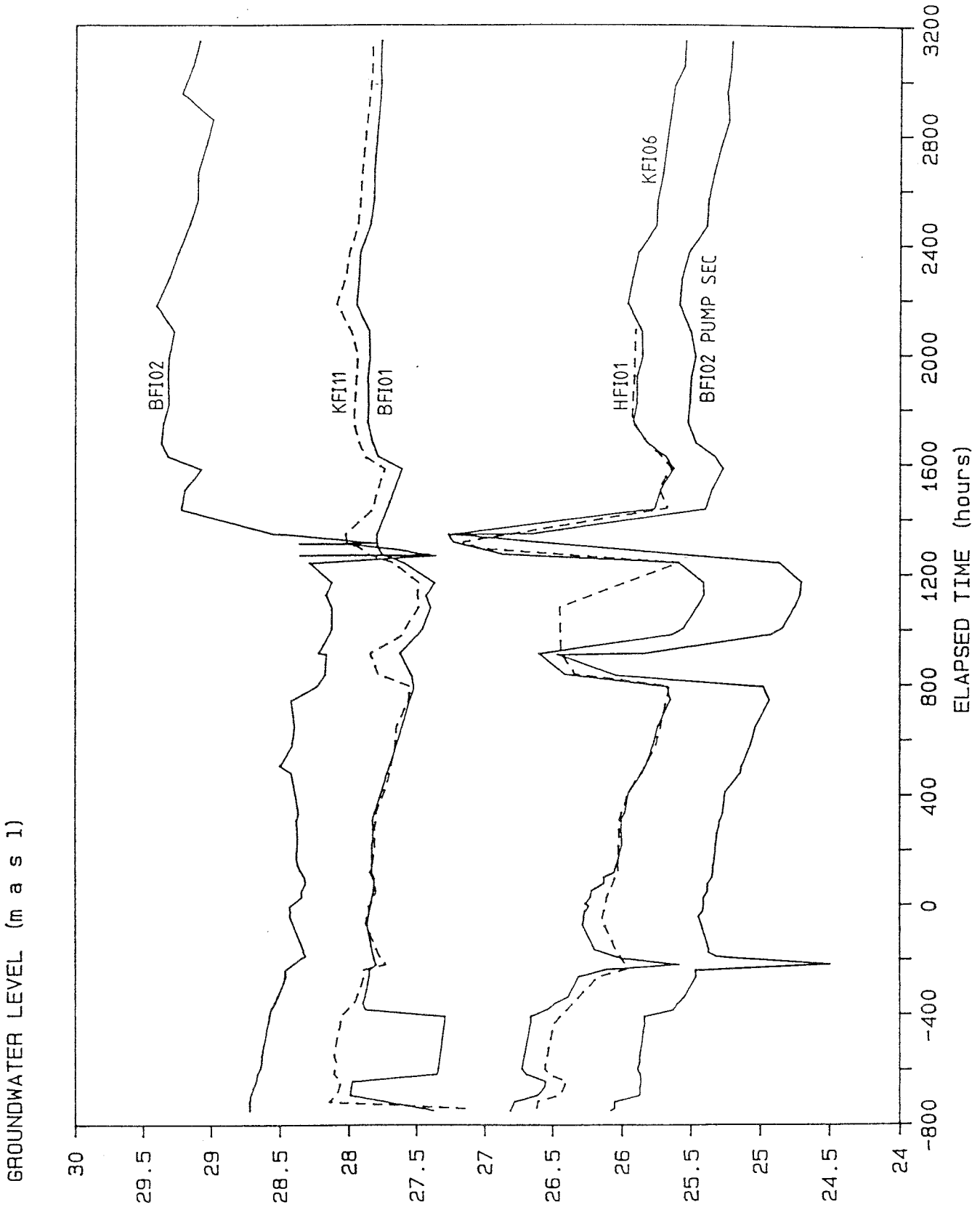


Groundwater levels in boreholes BFI01, BFI02, KFI06, KFI11, HFI01 and hydraulic head in the pumped section in BFI02.

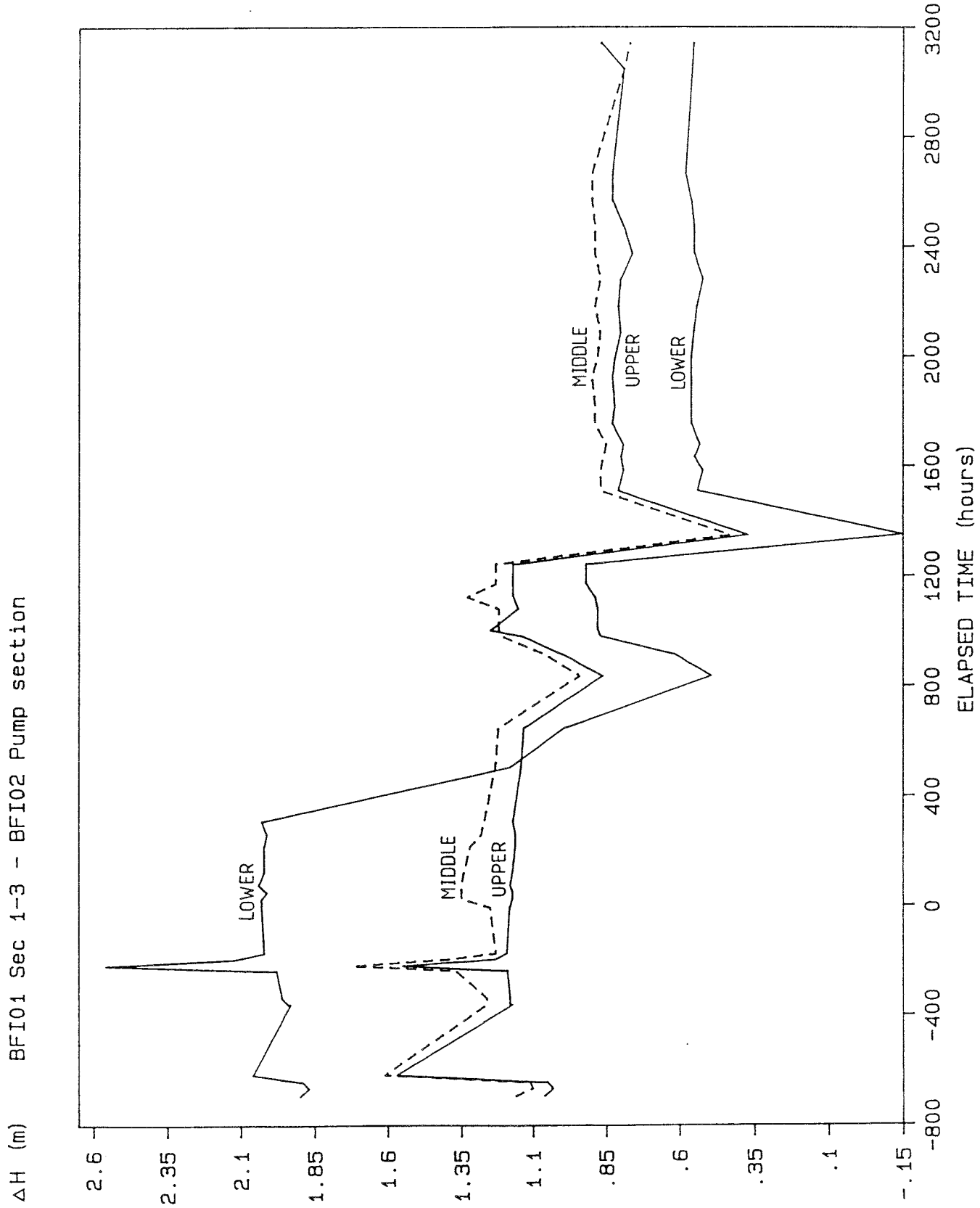


Relative head differences between the pumped interval in BFI02 and the injection intervals in BFI01.

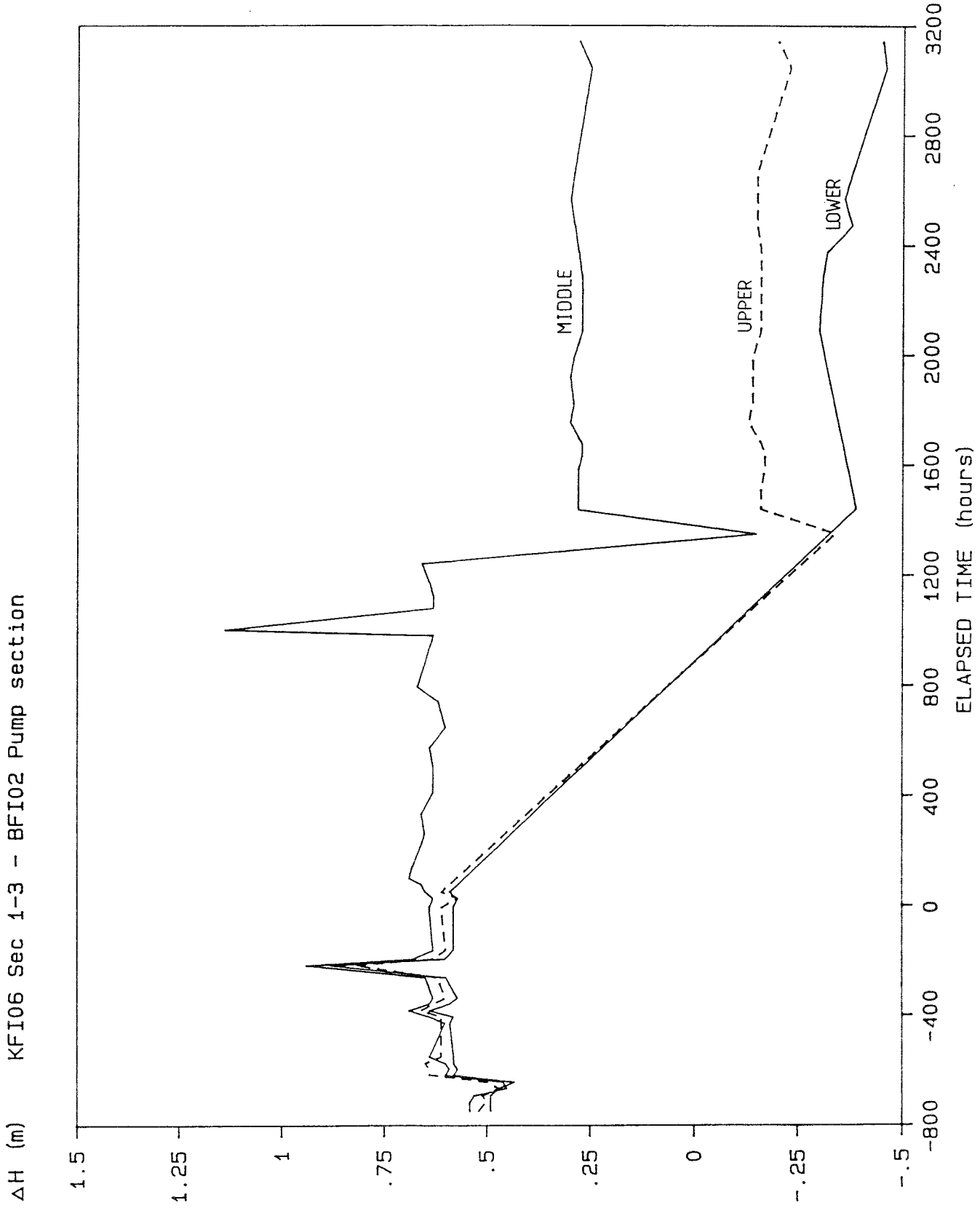


Relative head differences between the pumped interval in BFI02 and the injection intervals in KFI06.

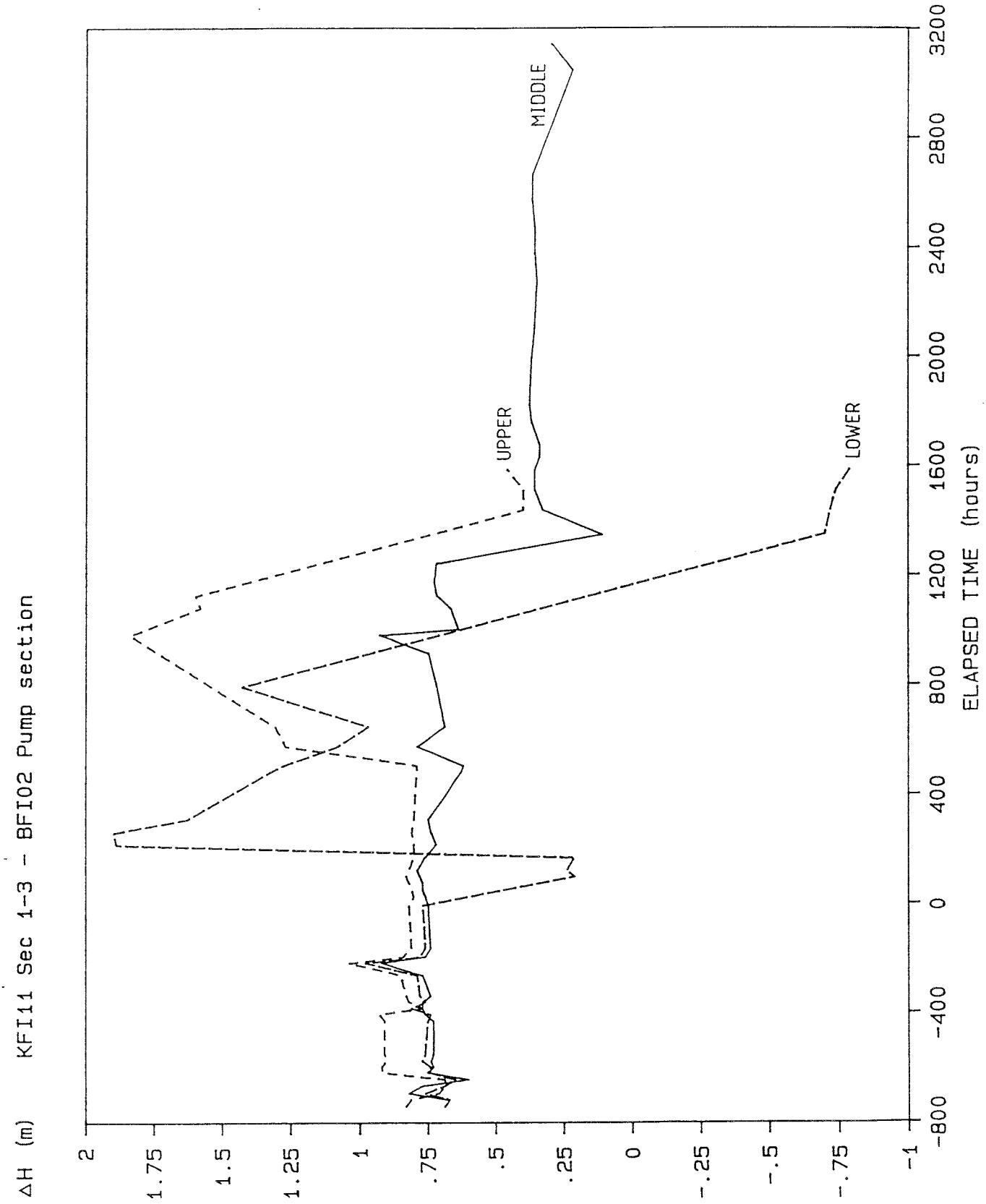


Relative head differences between the pumped interval in BFI02 and the injection intervals in KFI11.

# APPENDIX B

## TRACER INJECTION DATA

CONTENTS Page

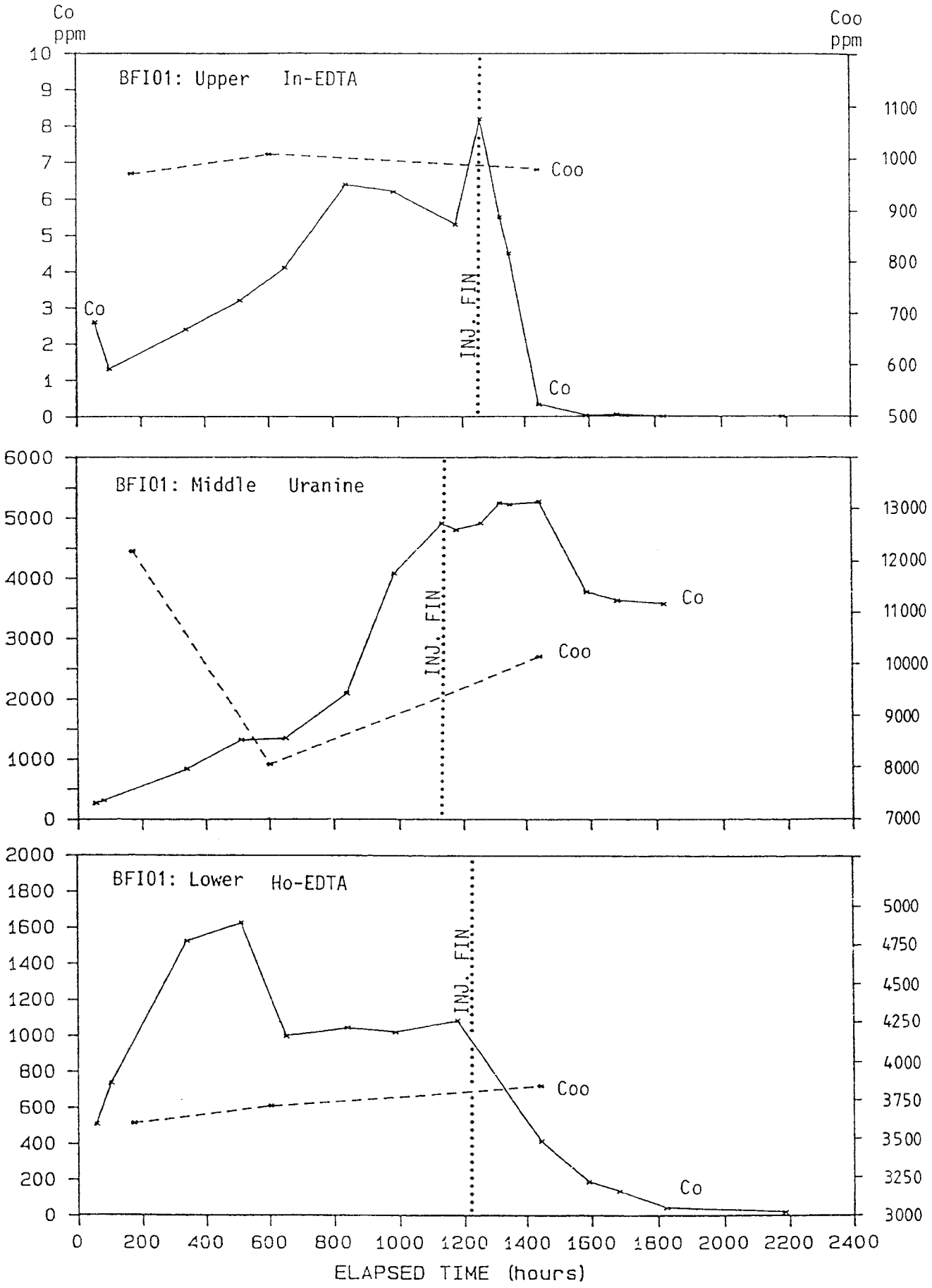


Tracer concentrations in injection intervals, $C_o$, and initial concentrations, $C_{oo}$, versus time in borehole BFI01.

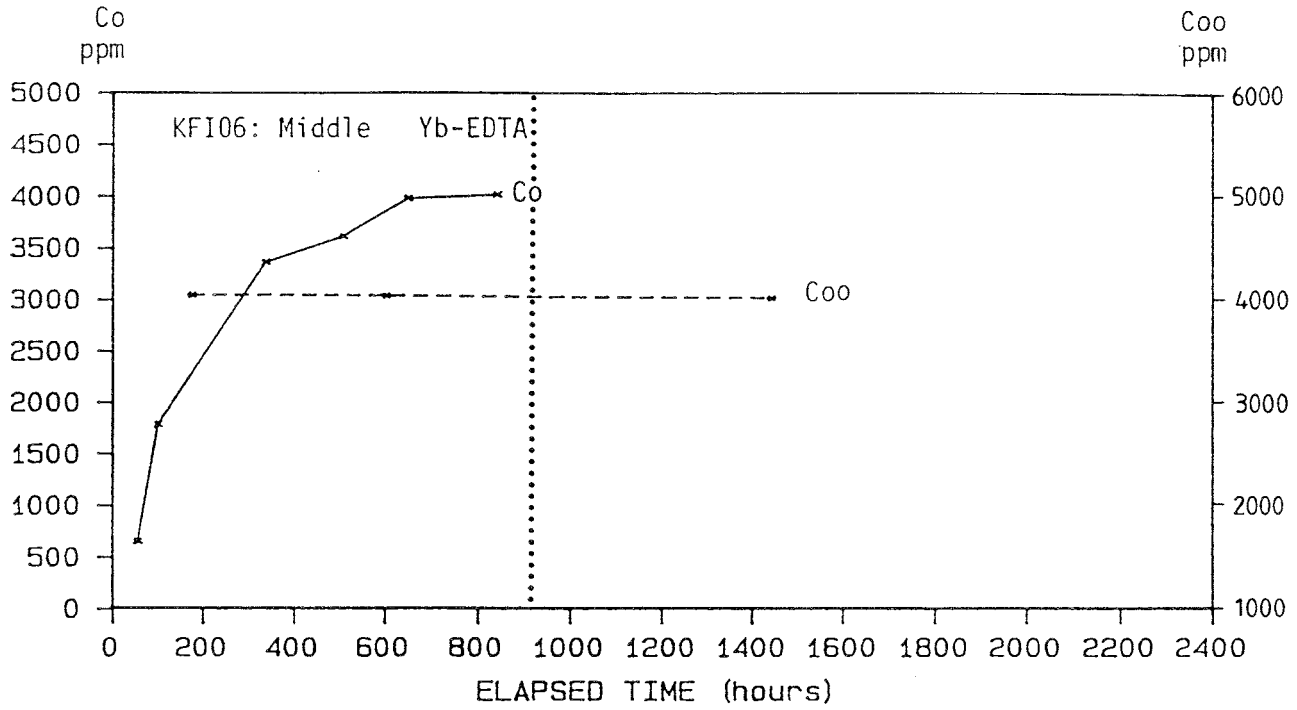


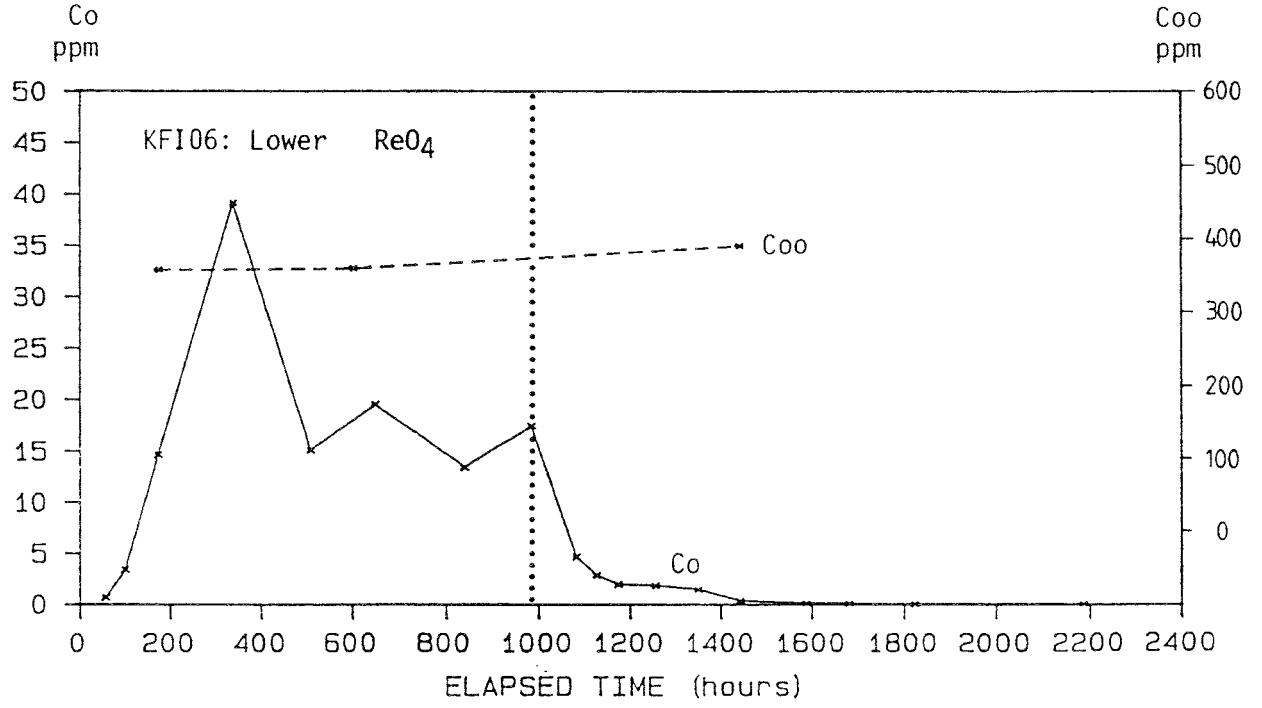


Tracer concentrations in injection intervals, $C_o$, and initial concentrations, $C_{oo}$, versus time in borehole KFI06.

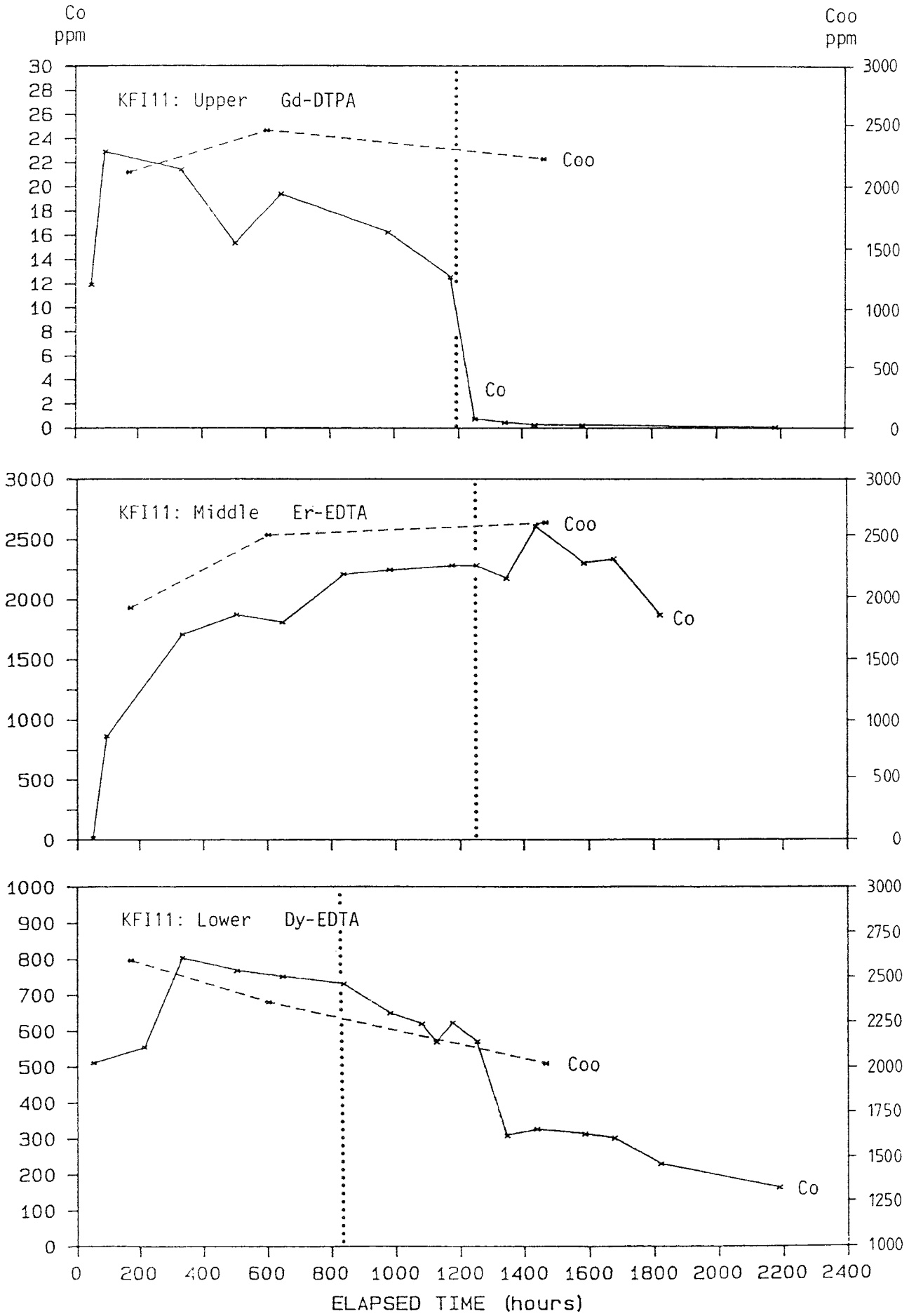


Tracer concentrations in injection intervals, $C_o$, and initial concentrations, $C_{oo}$, versus time in borehole KFI11.

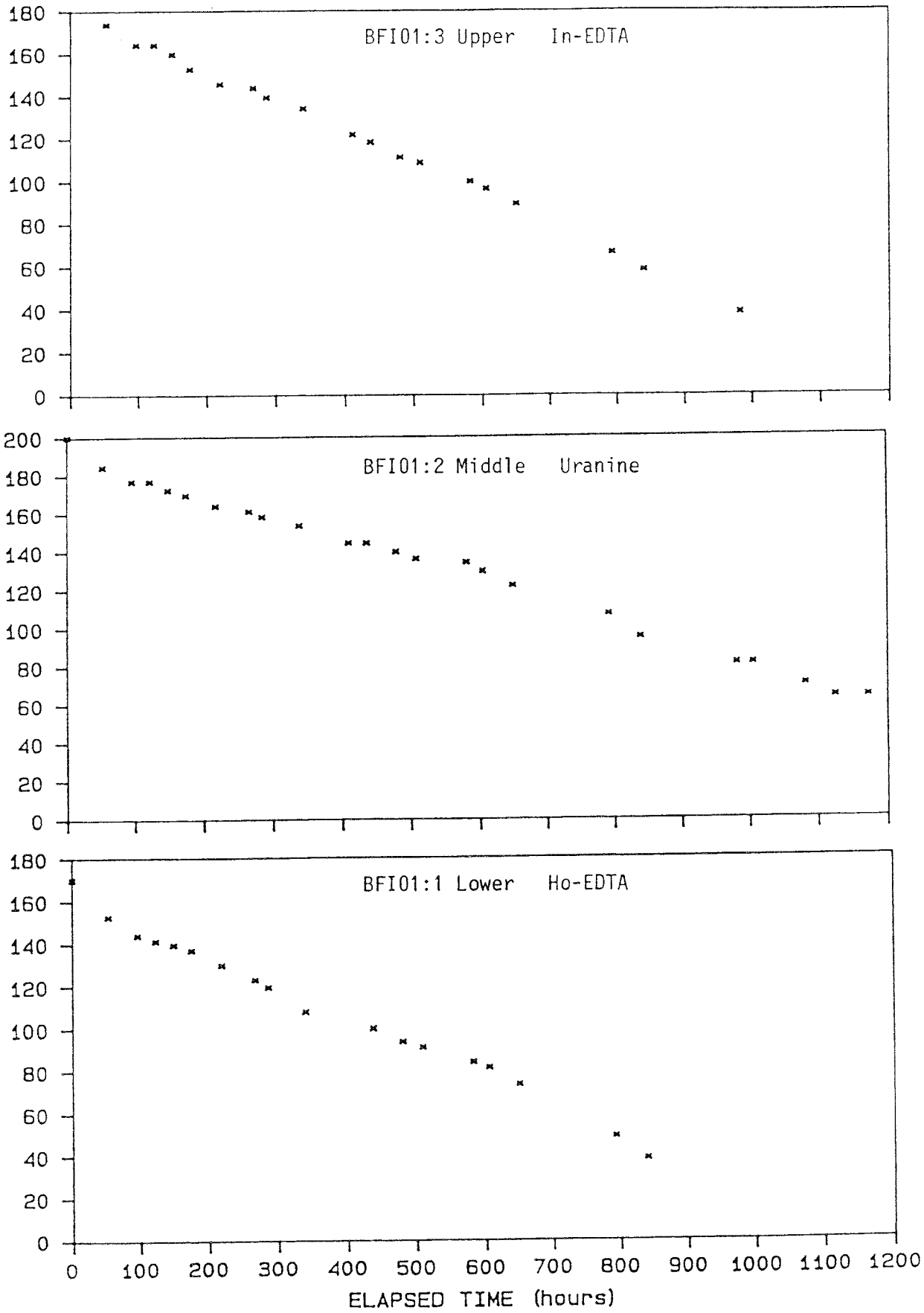


Volume in tracer storage tanks, V, versus time during continuos tracer injections in borehole BFI01.

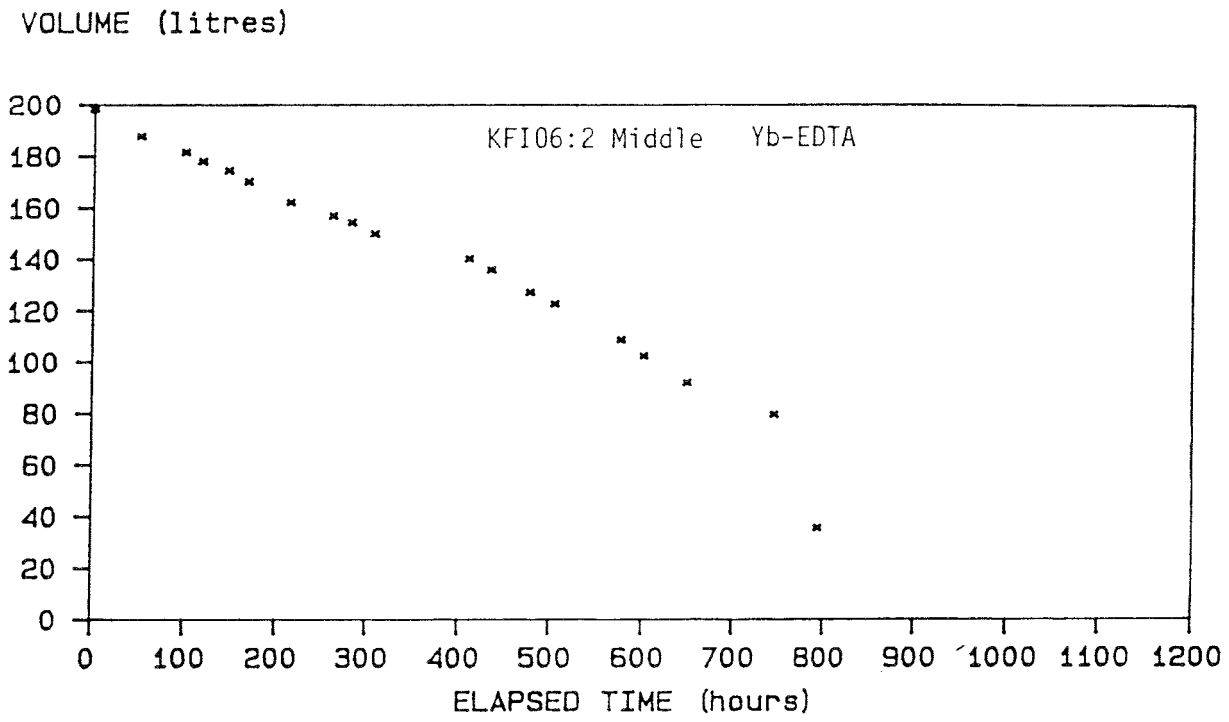


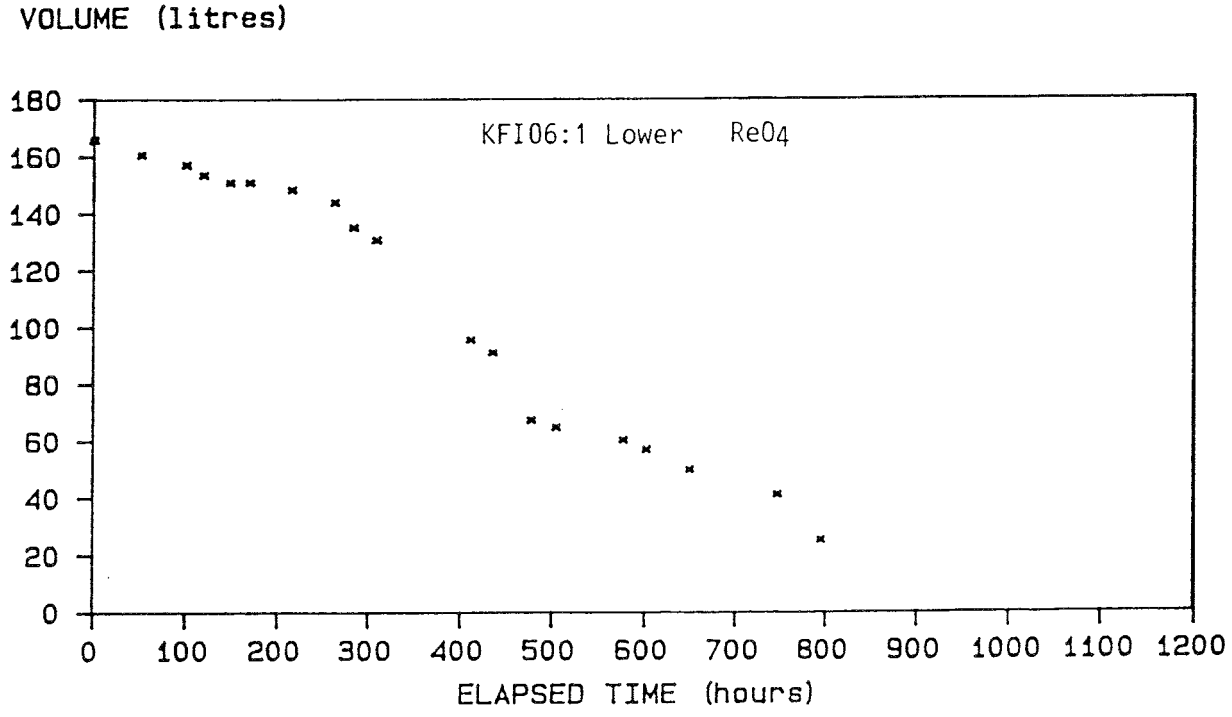


Volume in tracer storage tanks, V, versus time
during continuos tracer injections in borehole KFI06.

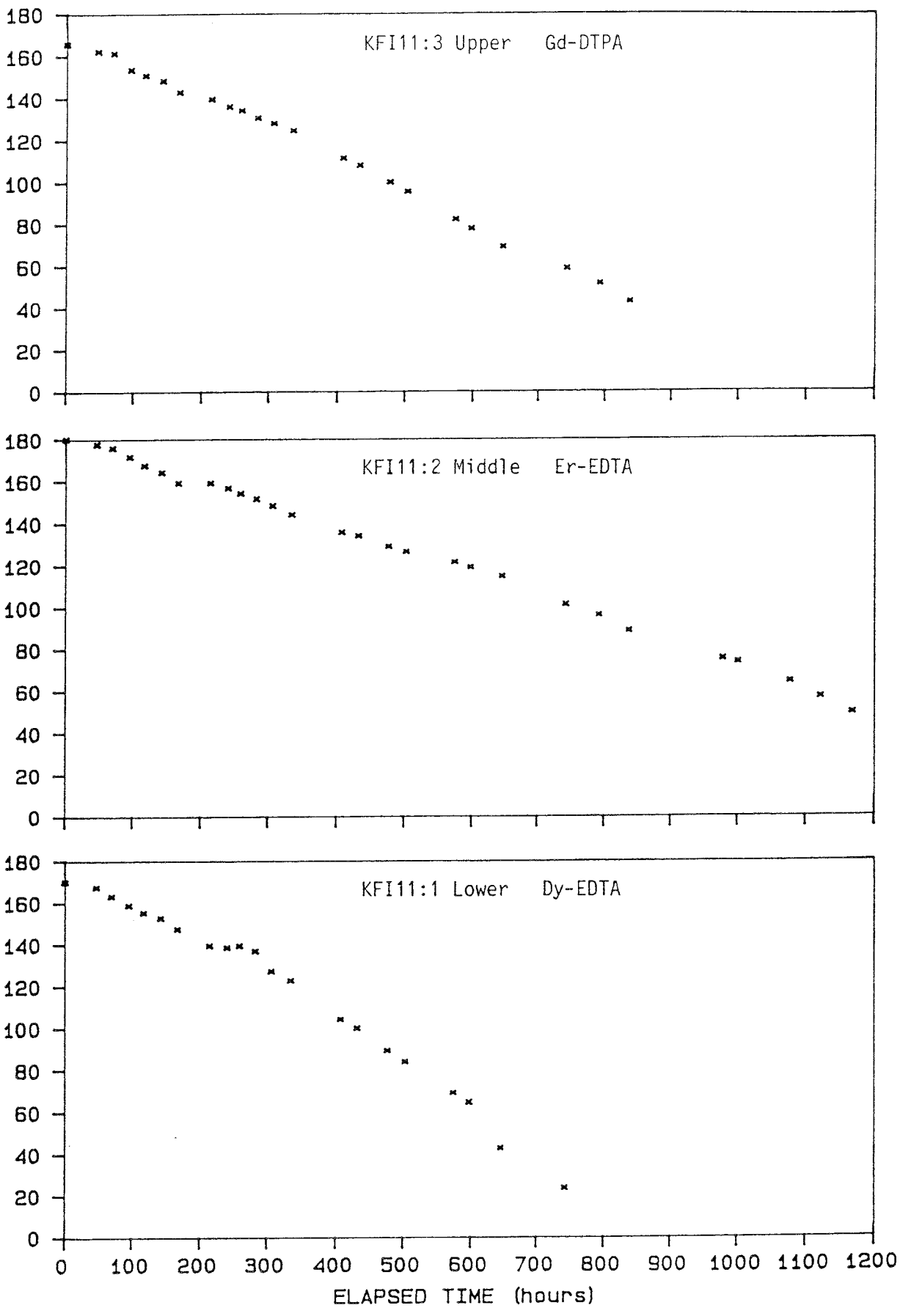


Volume in tracer storage tanks, V, versus time during continuos tracer injections in borehole KFI11.

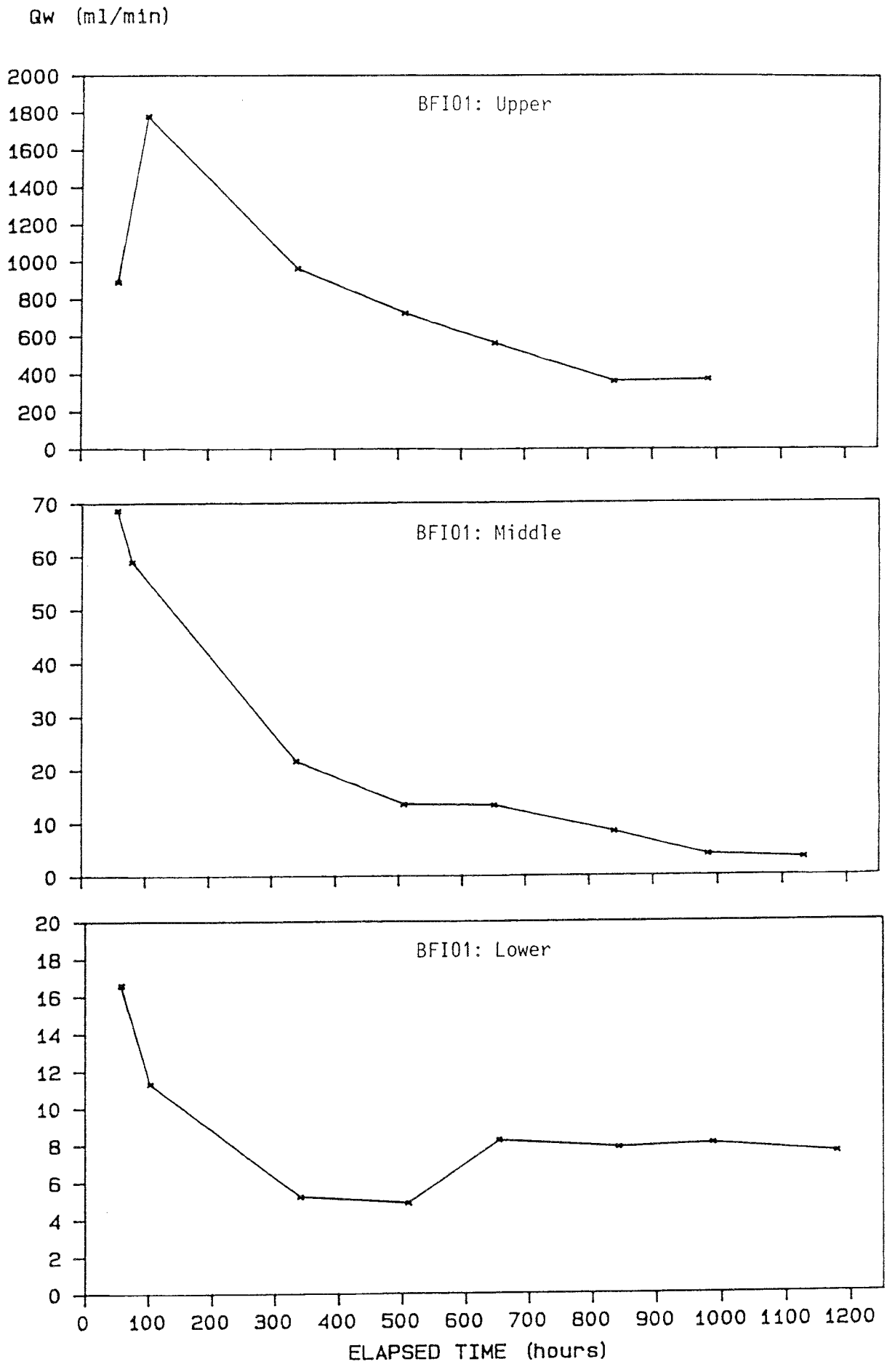


Groundwater flow rates versus time during tracer injections in borehole BFI01.

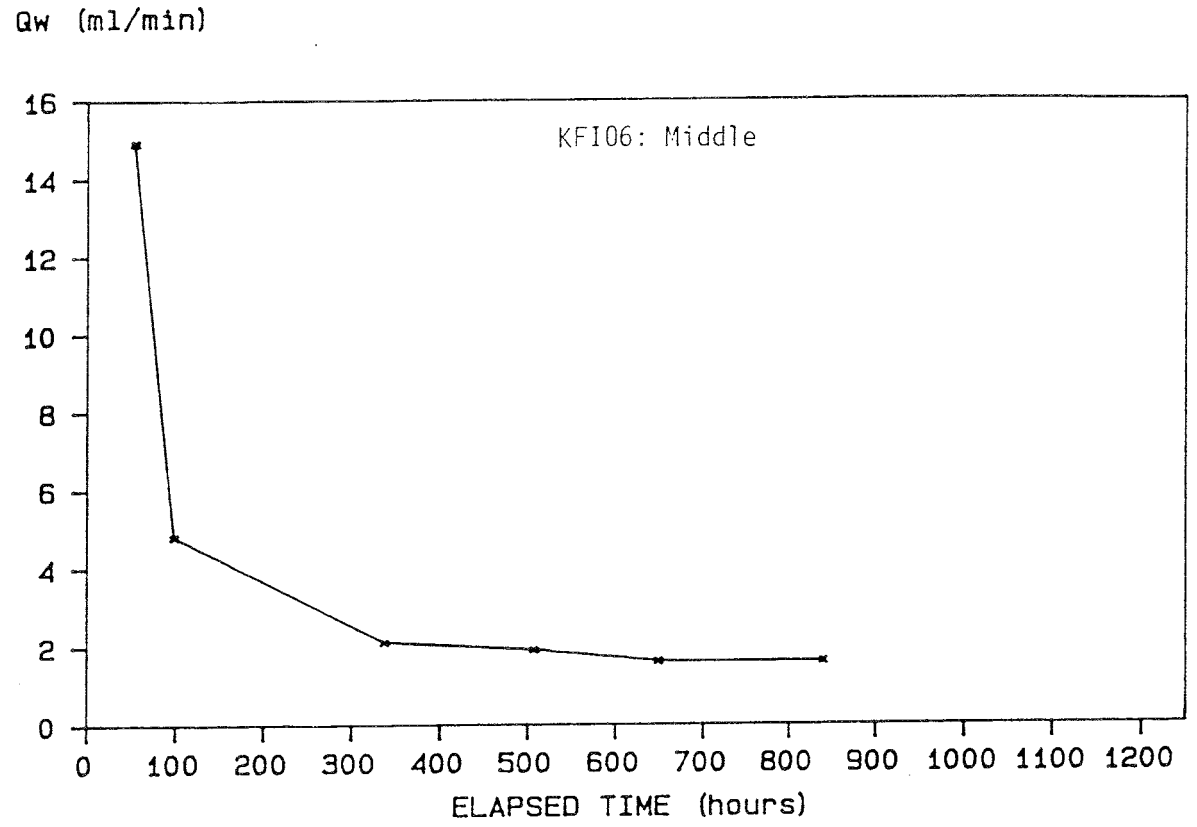


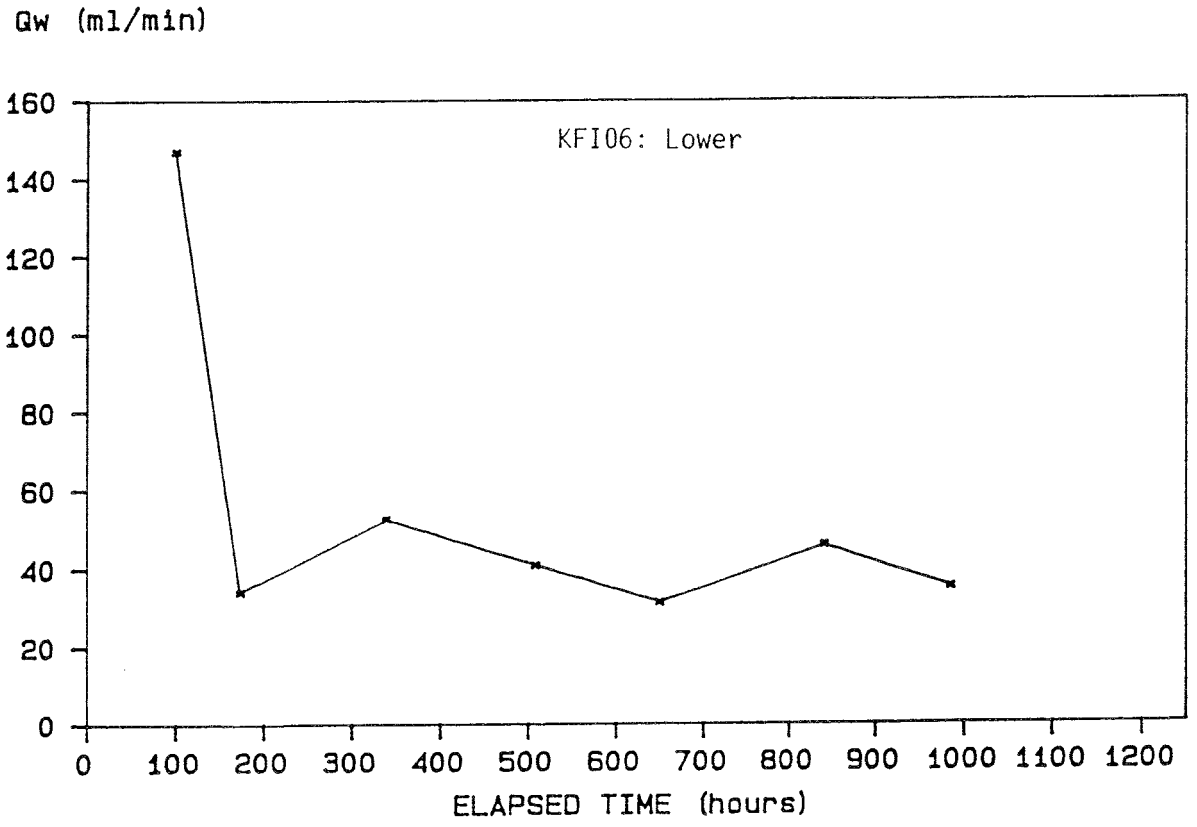


Groundwater flow rates versus time during tracer injections in borehole KFI06.

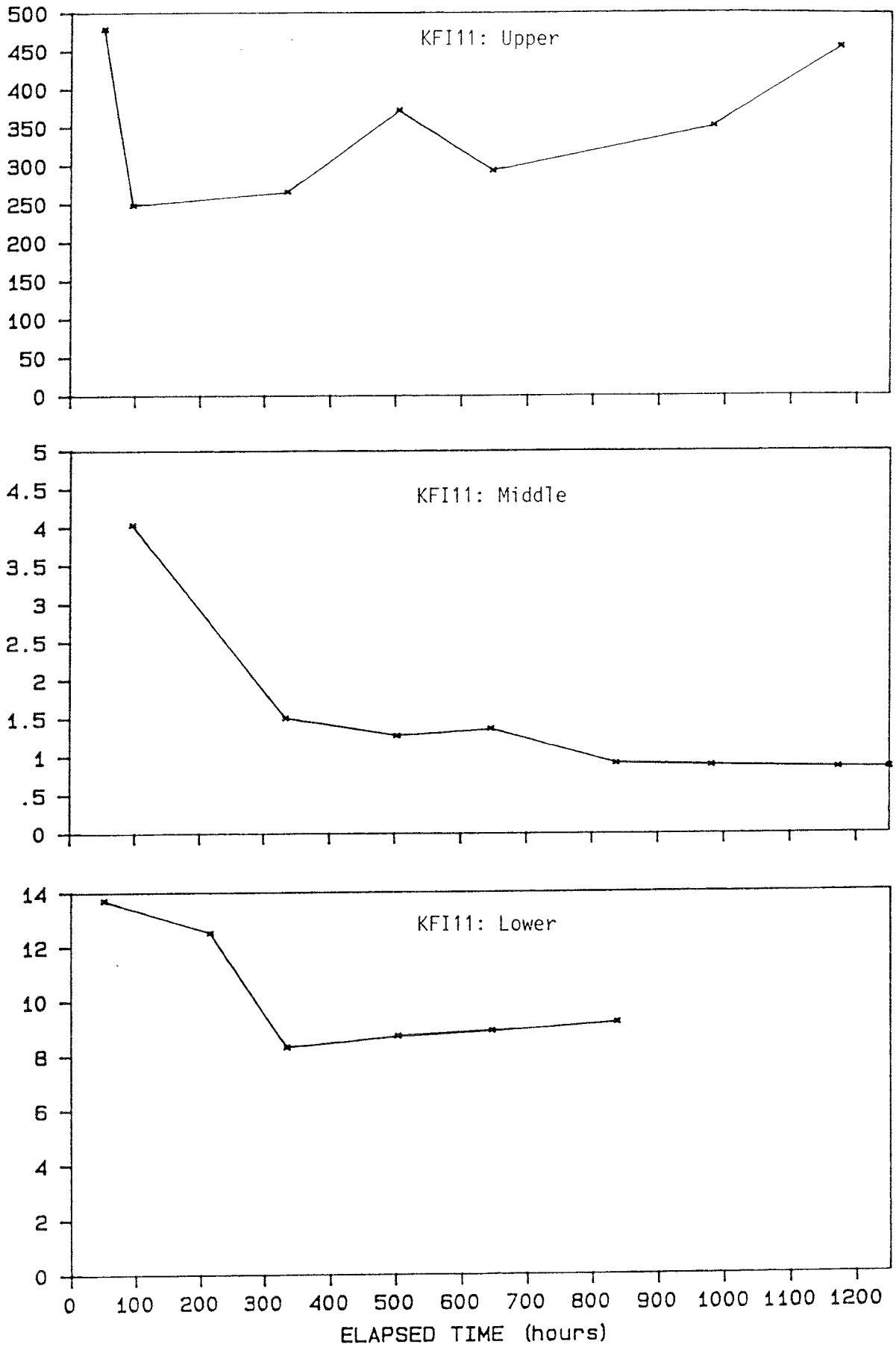


Groundwater flow rates versus time during tracer injections in borehole KFI11.

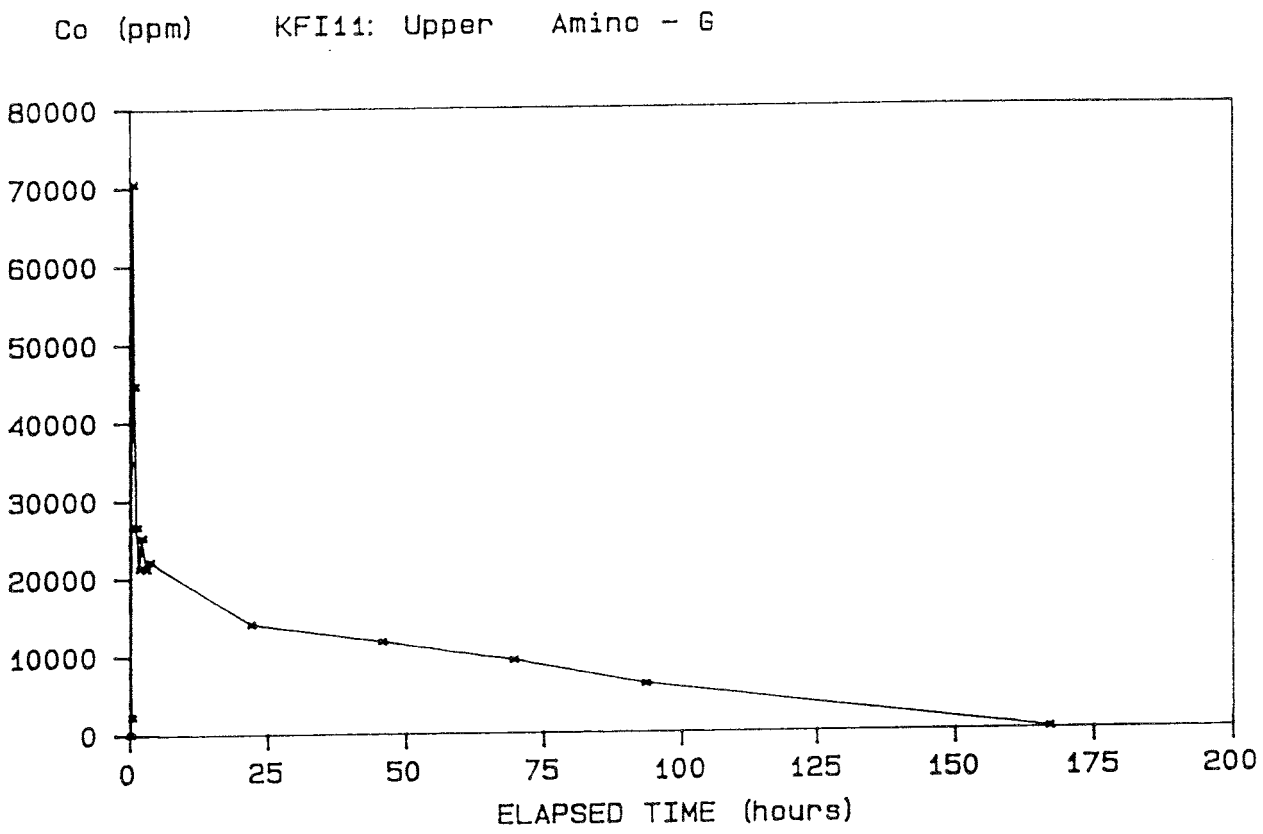


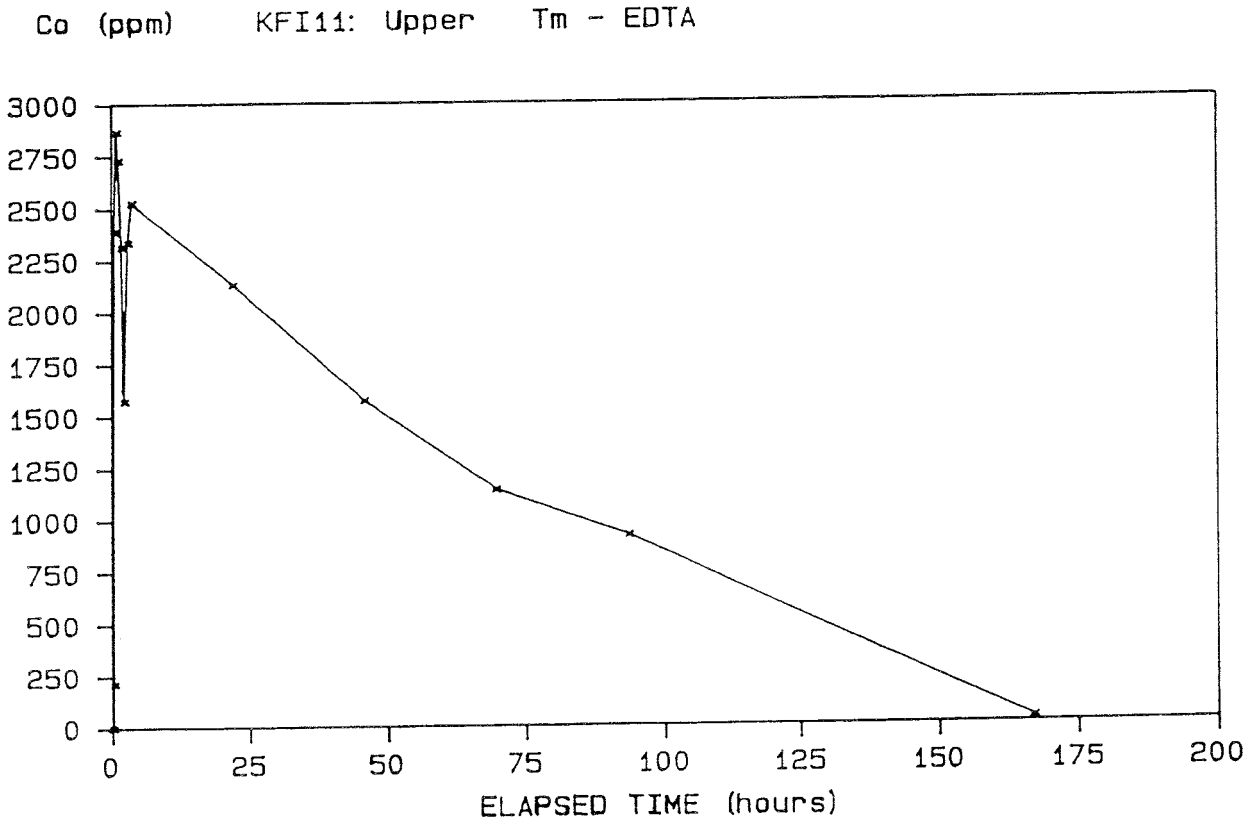


Tracer concentrations in injection intervals, $C_o$, versus time during pulse injection in KFI11:Upper.

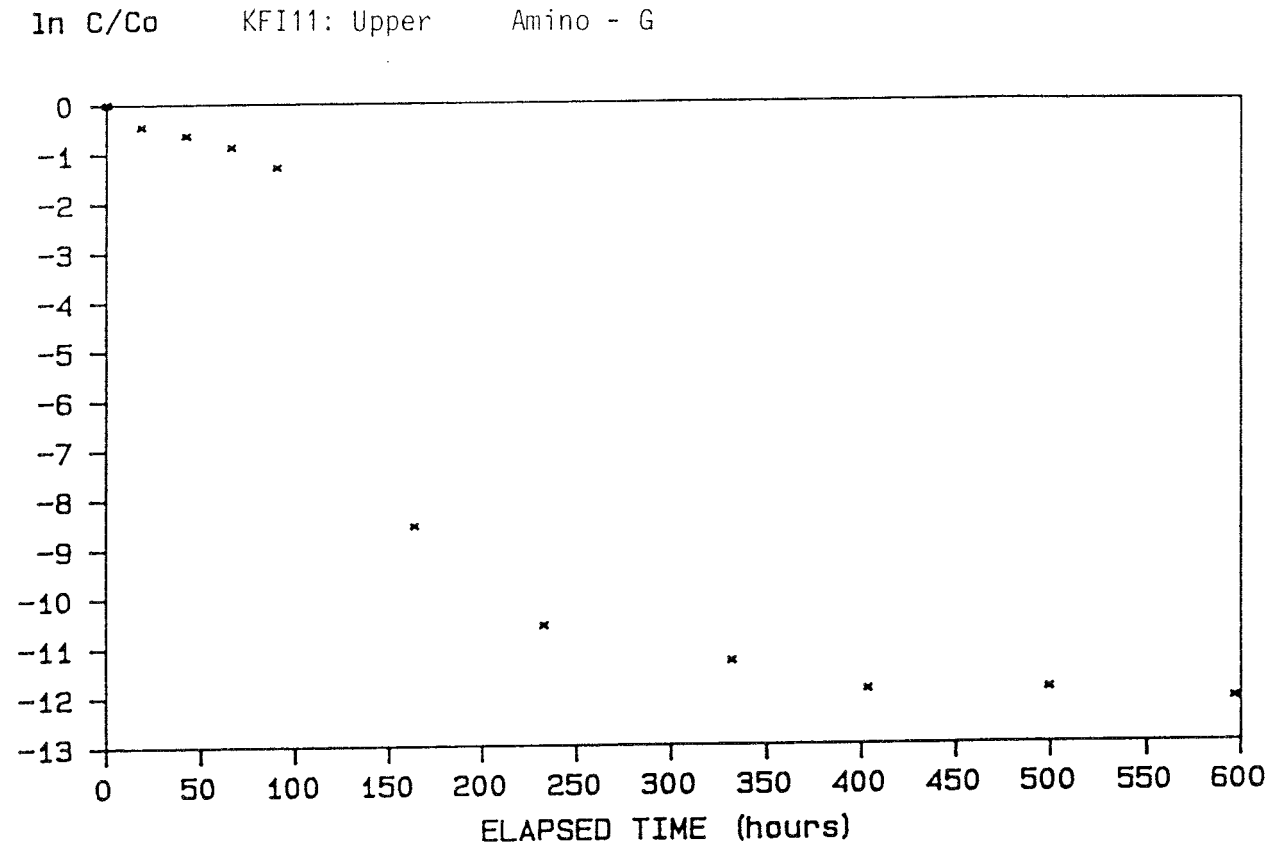


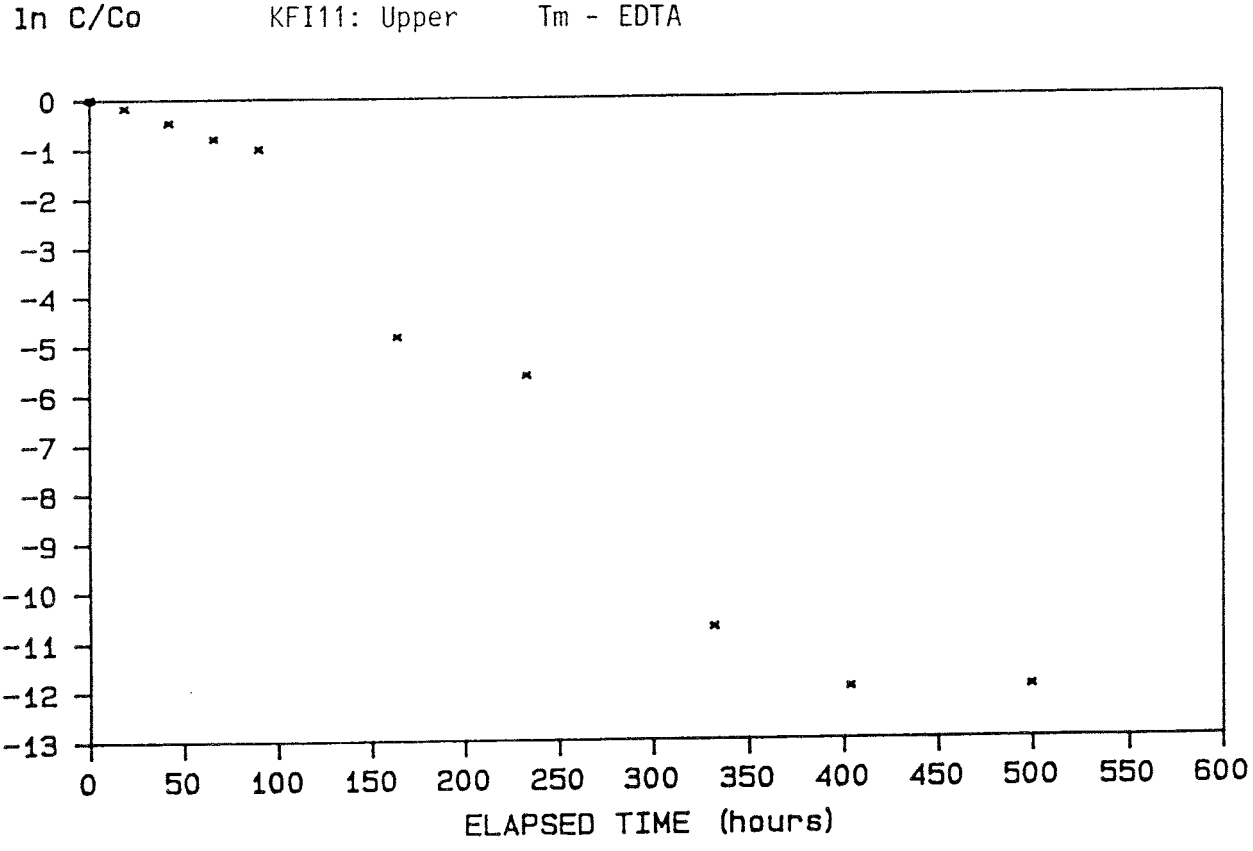


Ln $C/C_o$ versus time during pulse injection in KFI11:Upper.

# APPENDIX C

## TRACER BREAKTHROUGH CURVES

CONTENTS

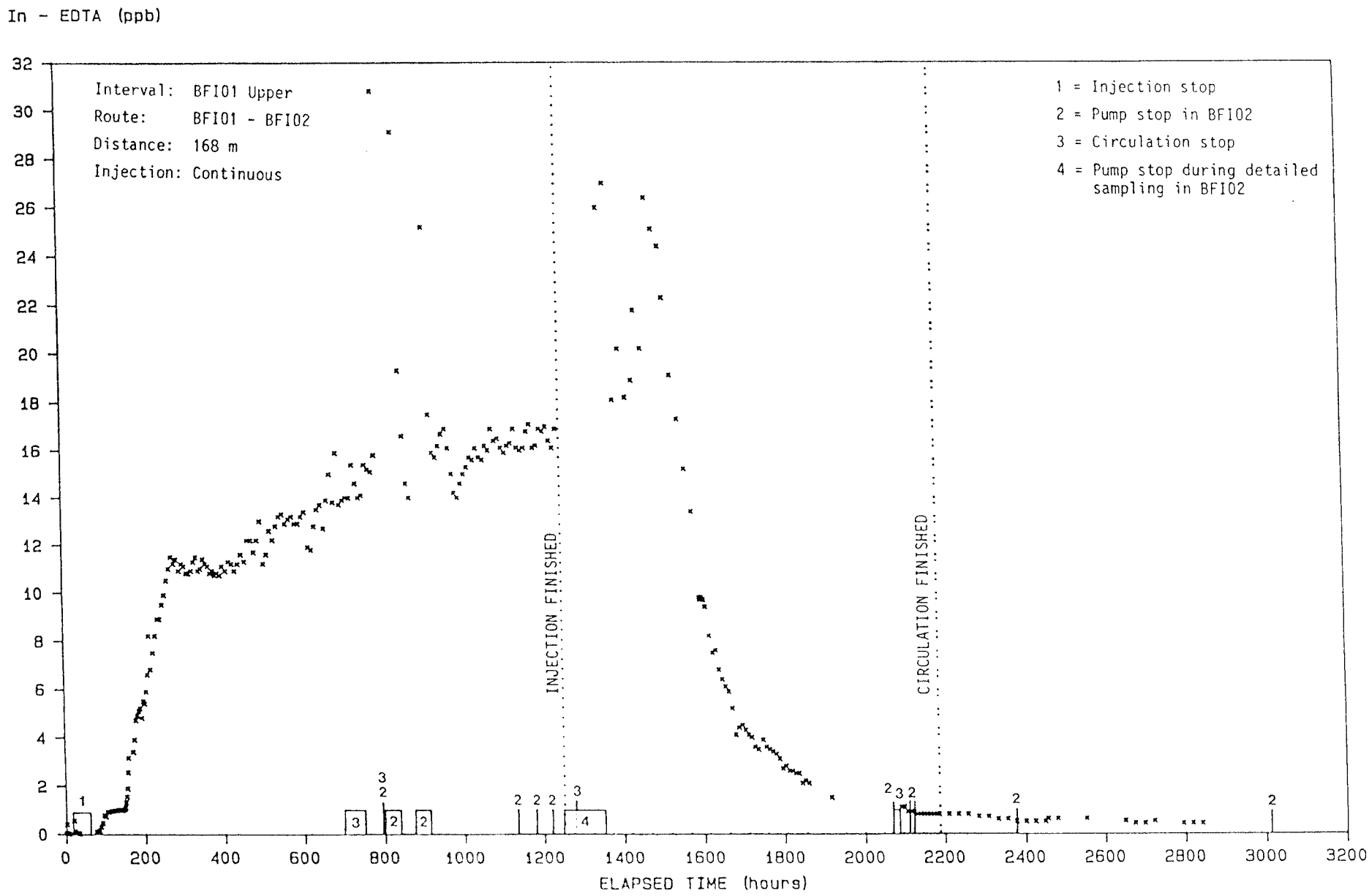


Breakthrough curve for In-EDTA injected in BFI01:U, 0-3200 h.

C: 1

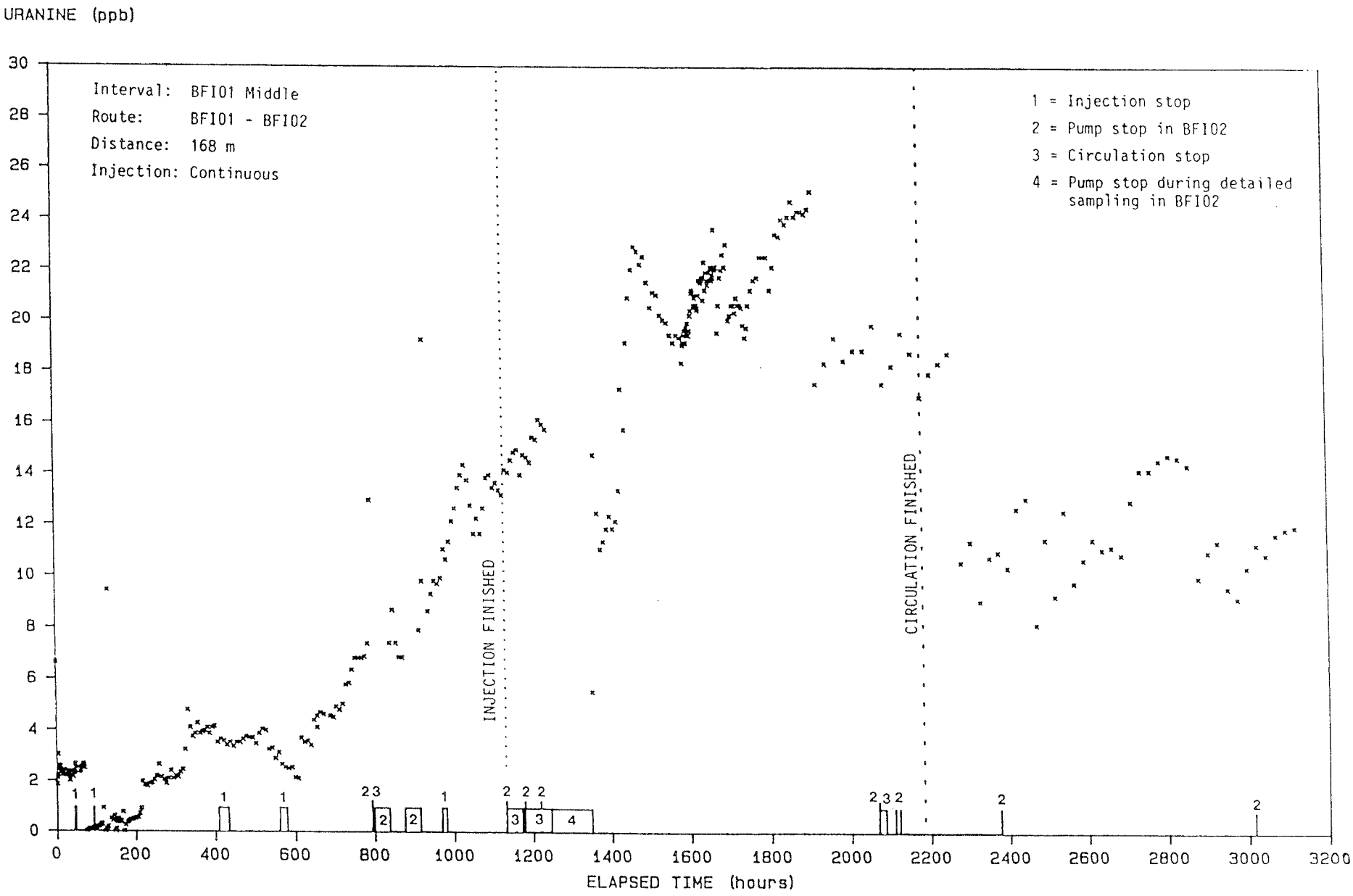


Breakthrough curve for Uranine injected in BFI01:M, 0-3200 h.

C: 2

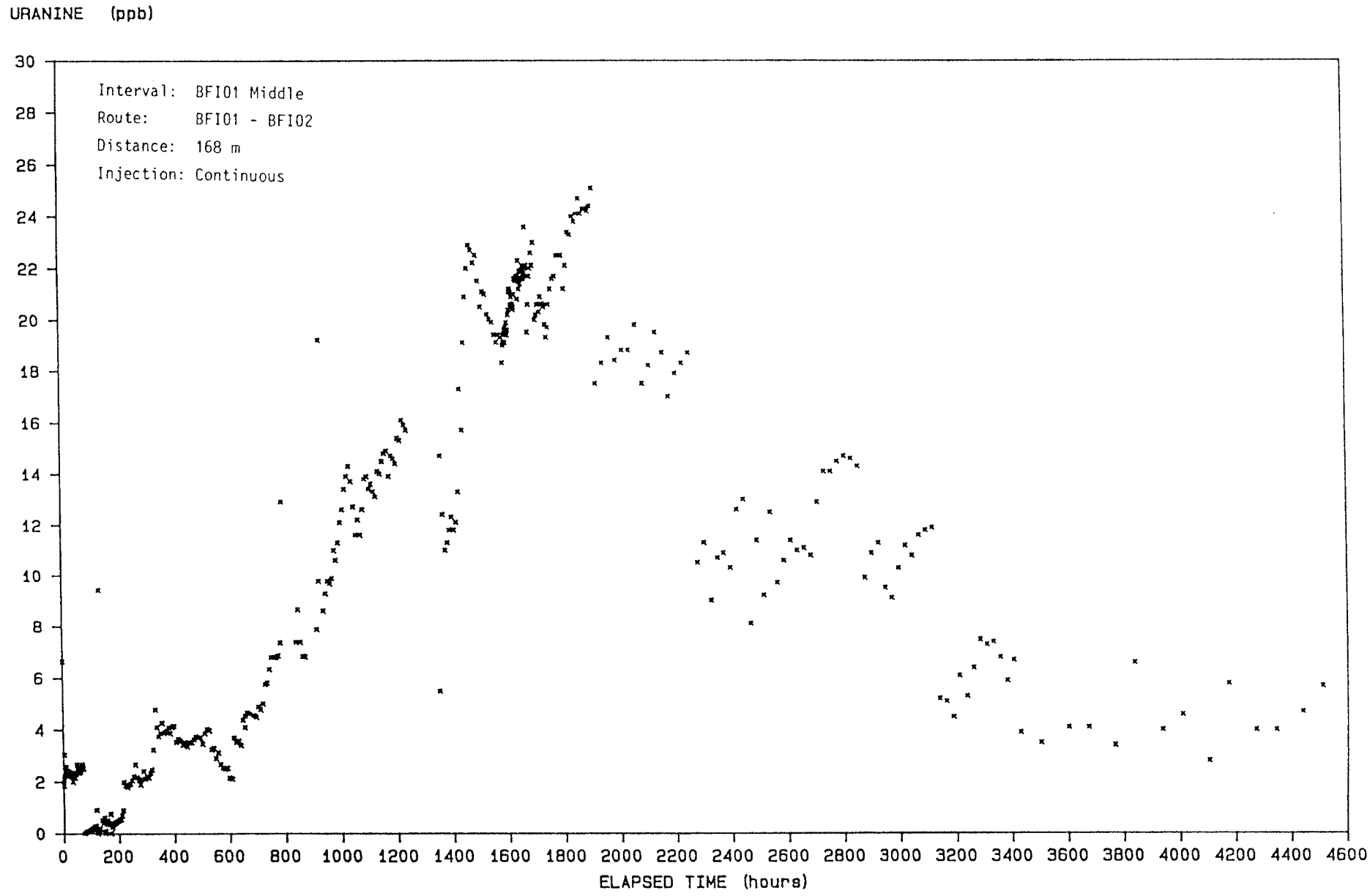


Breakthrough curve for Uranine injected in BFI01:M, 0-4600 h.

Ho - EDTA

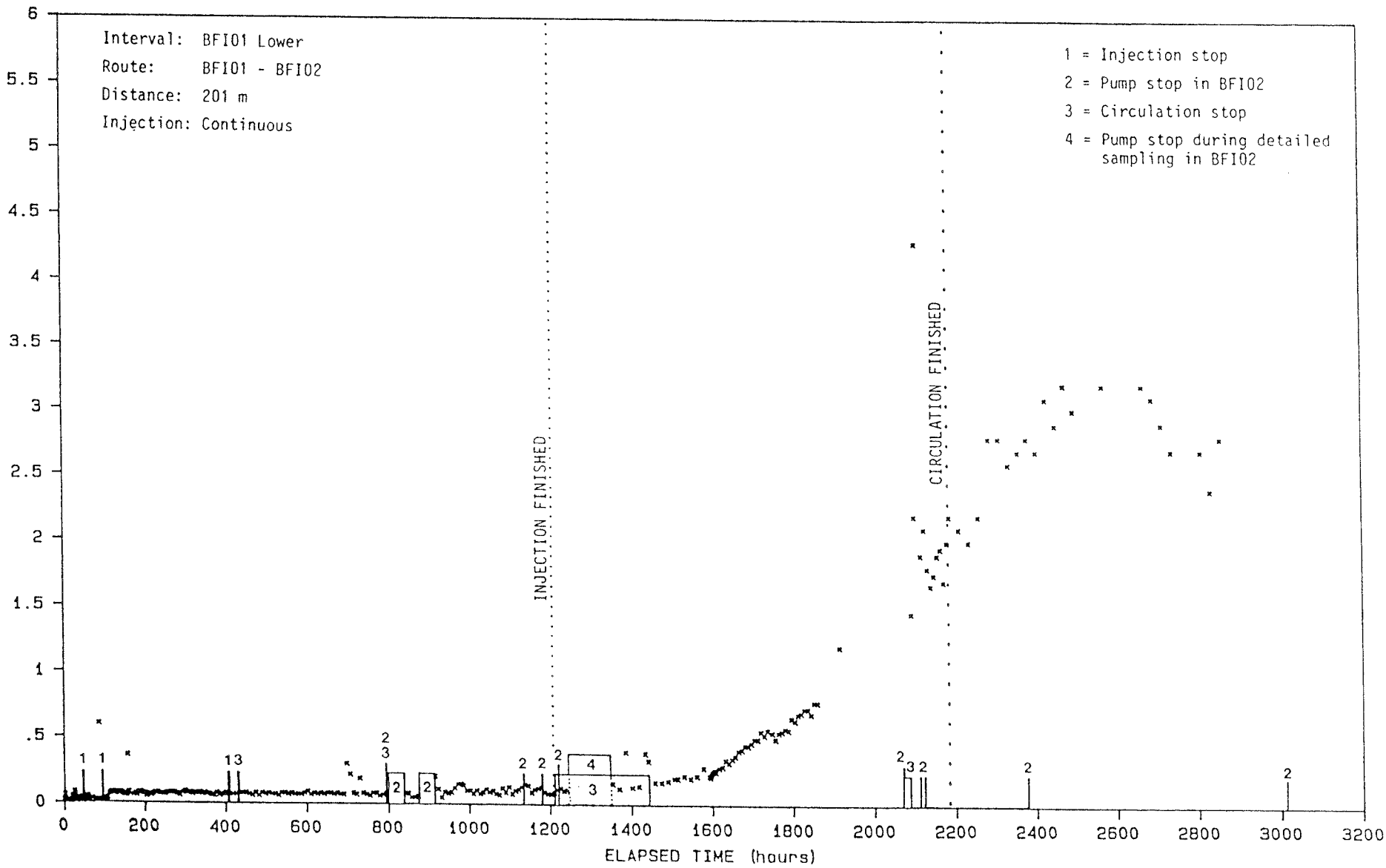


Breakthrough curve for Ho-EDTA injected in BFI01:L, 0-3200 h.

C: 4

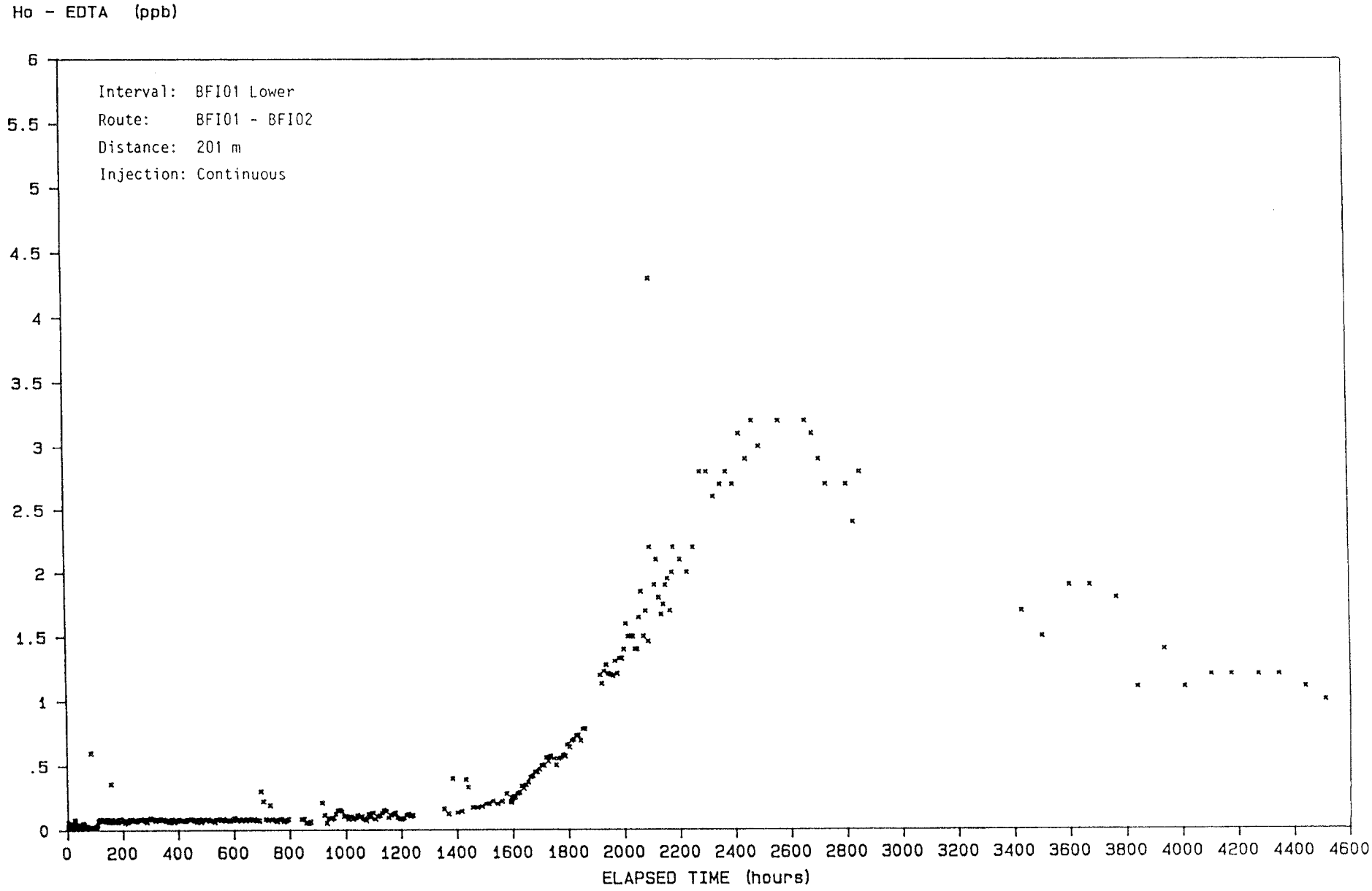


Breakthrough curve for Ho-EDTA injected in BFI01:L, 0-4600 h.

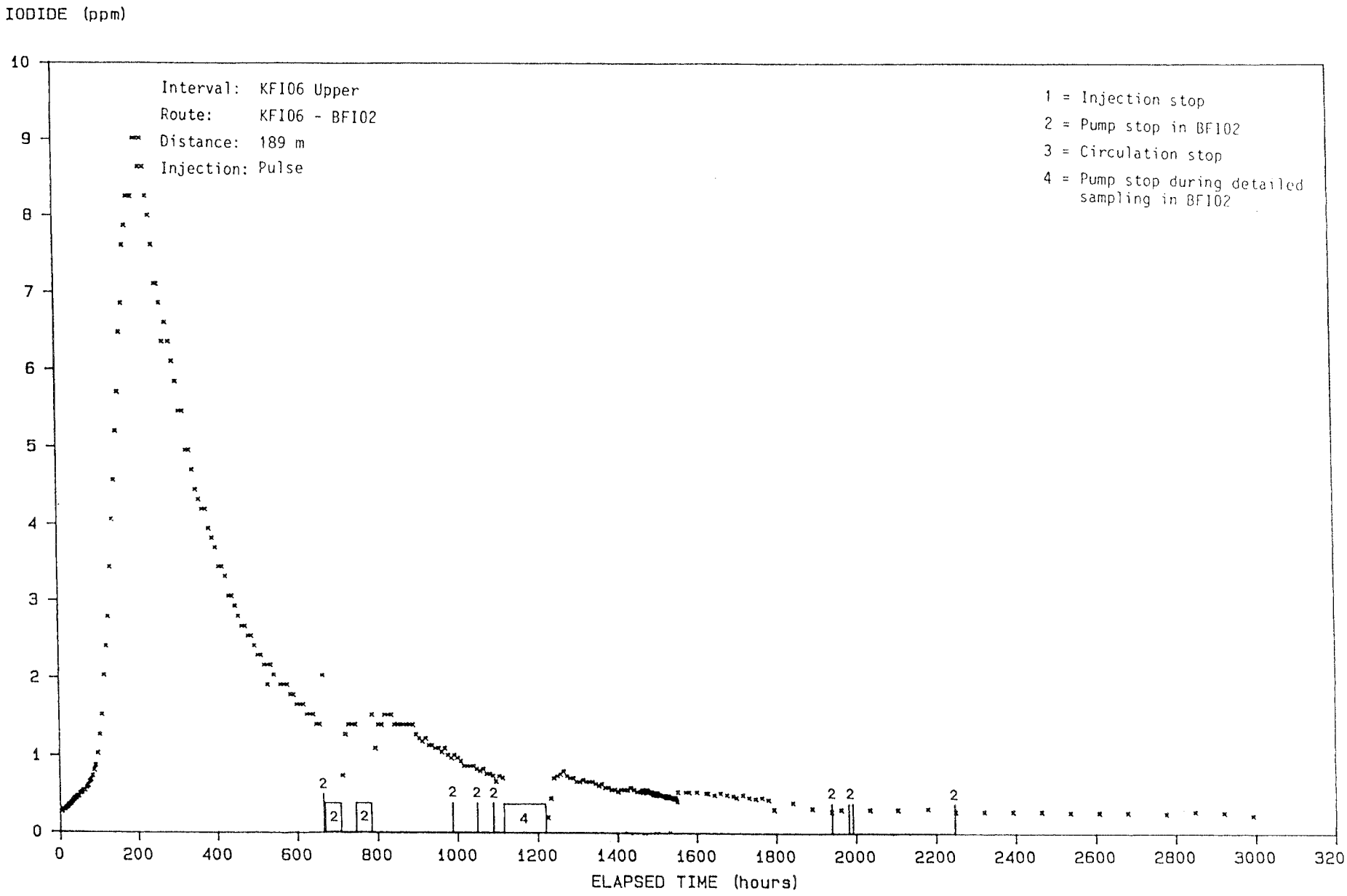


Breakthrough curve for $I_{odide}$ injected in KFI06:U, 0-3200 h.

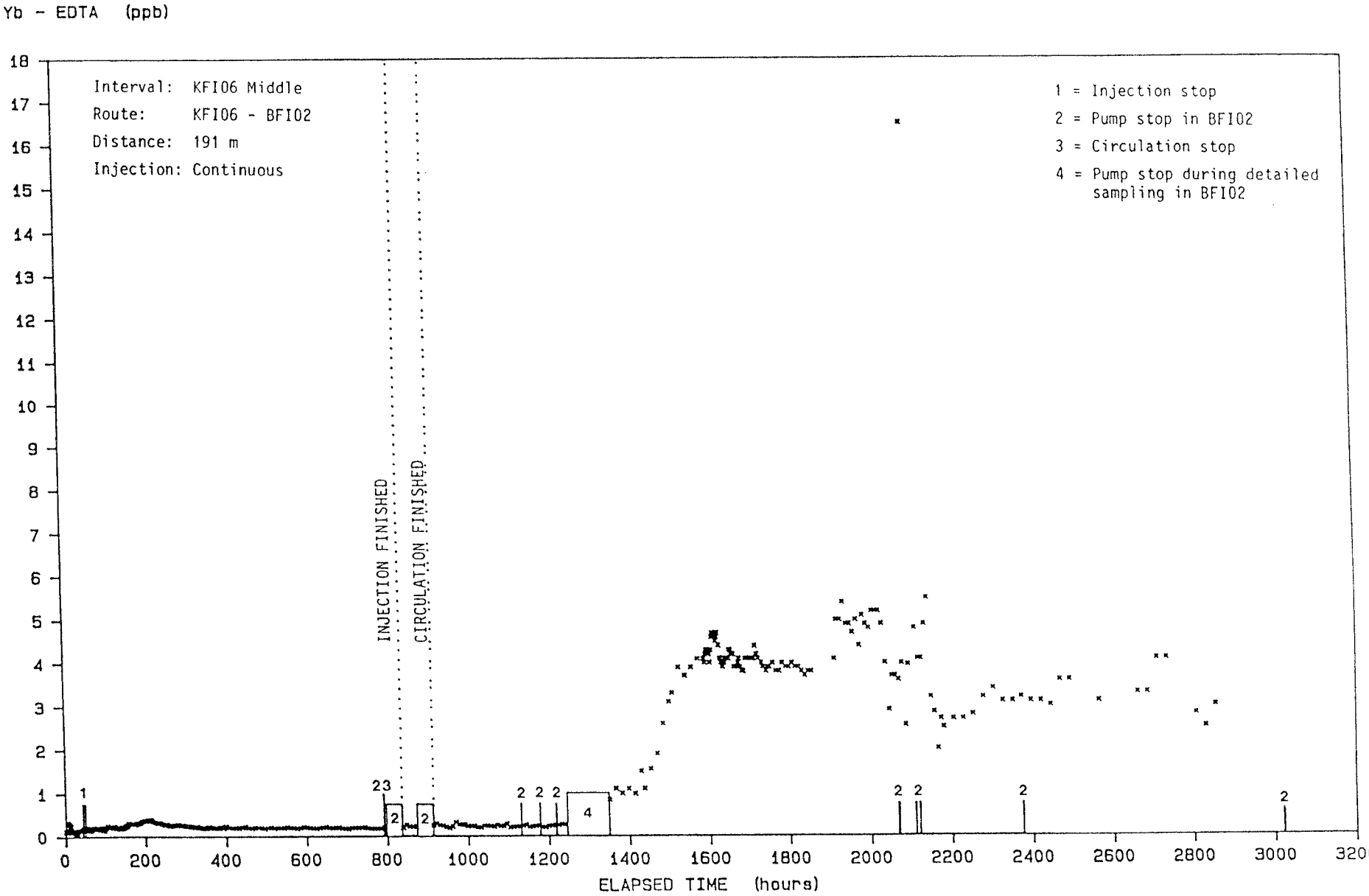


Breakthrough curve for Yb-EDTA injected in KFI06:M, 0-3200 h.

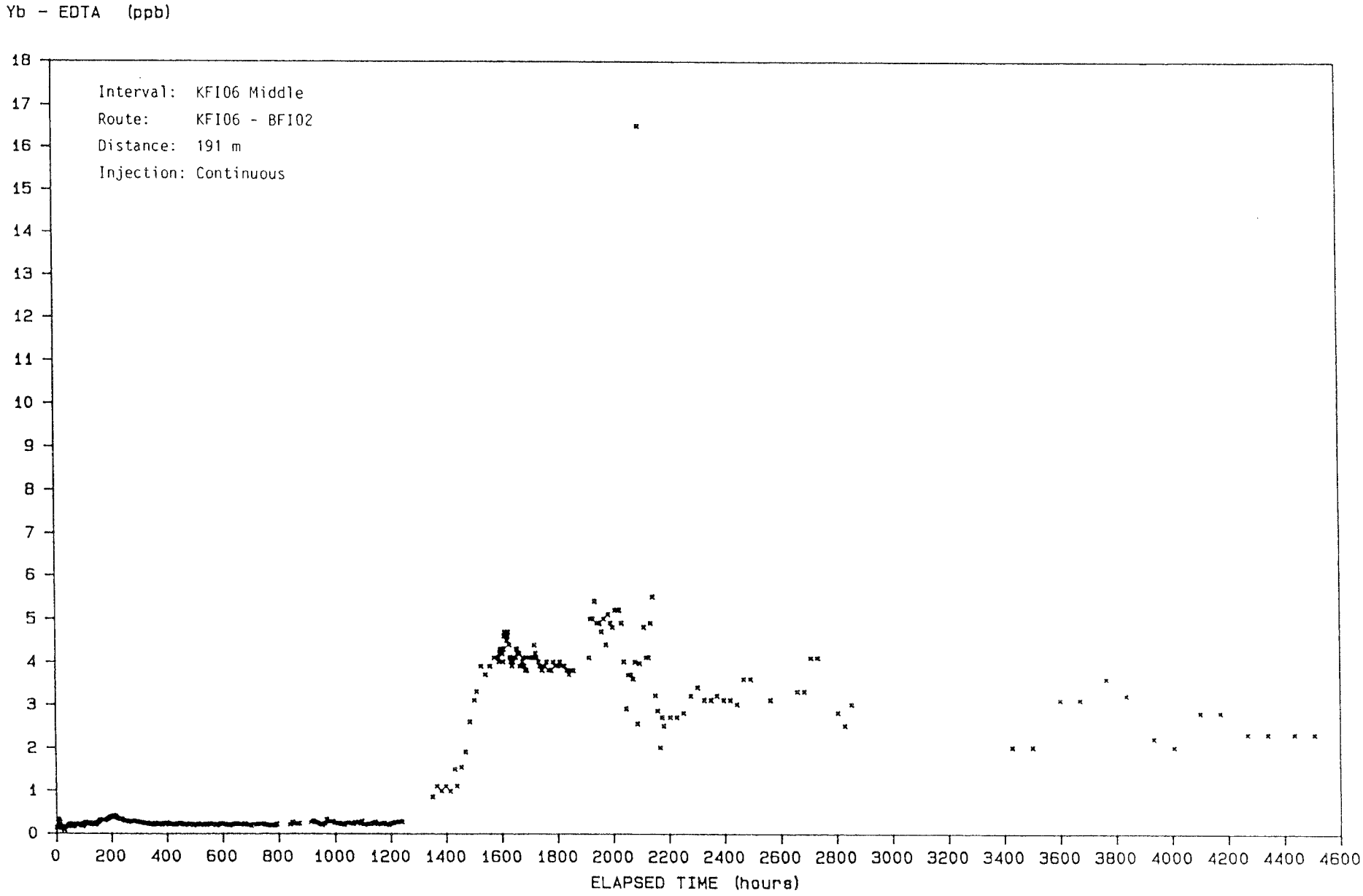


Breakthrough curve for Yb-EDTA injected in KFI06:M, 0-4600 h.

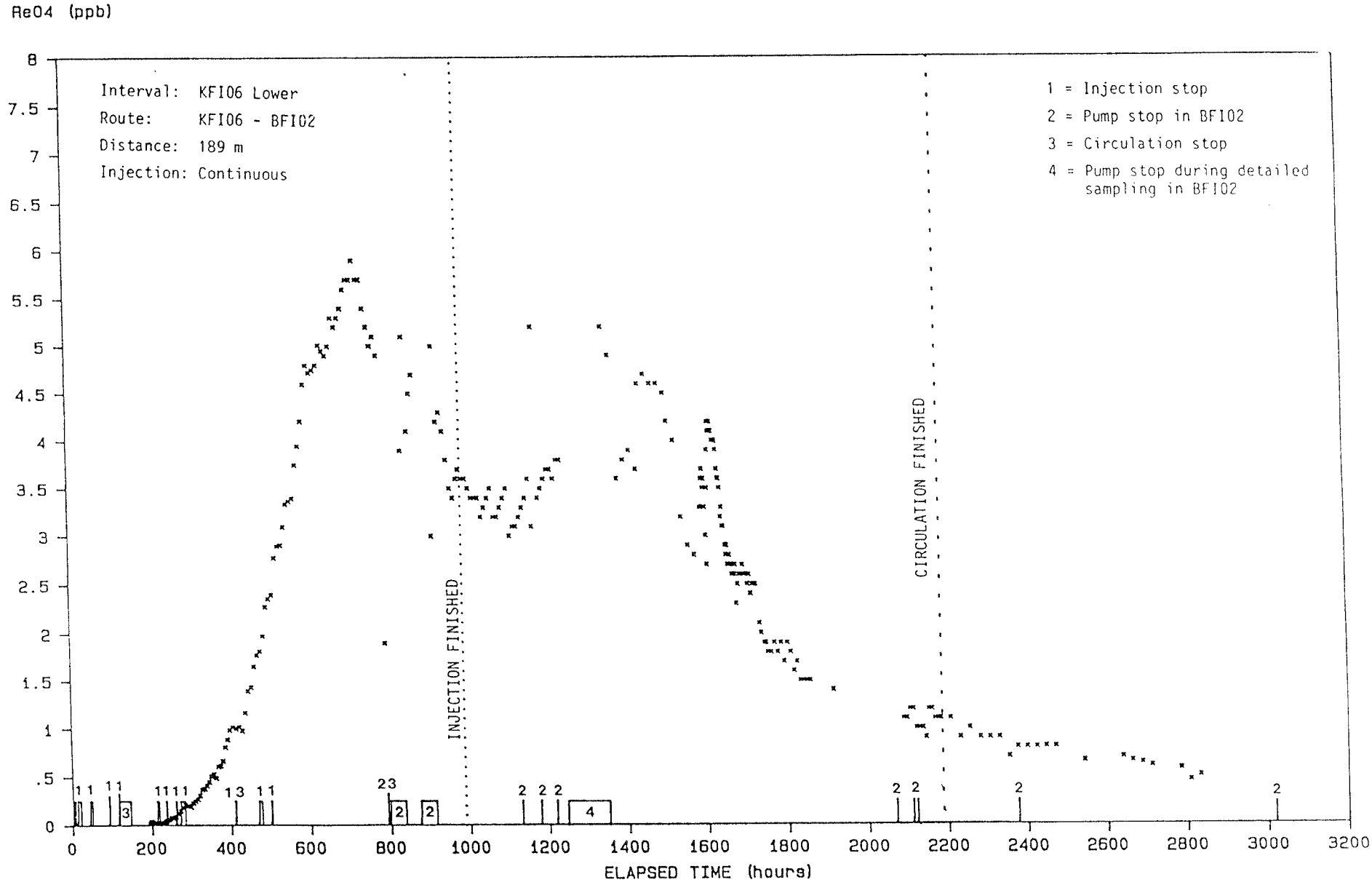


Breakthrough curve for $ReO_4^-$ injected in KFI06:L, 0-3200 h.

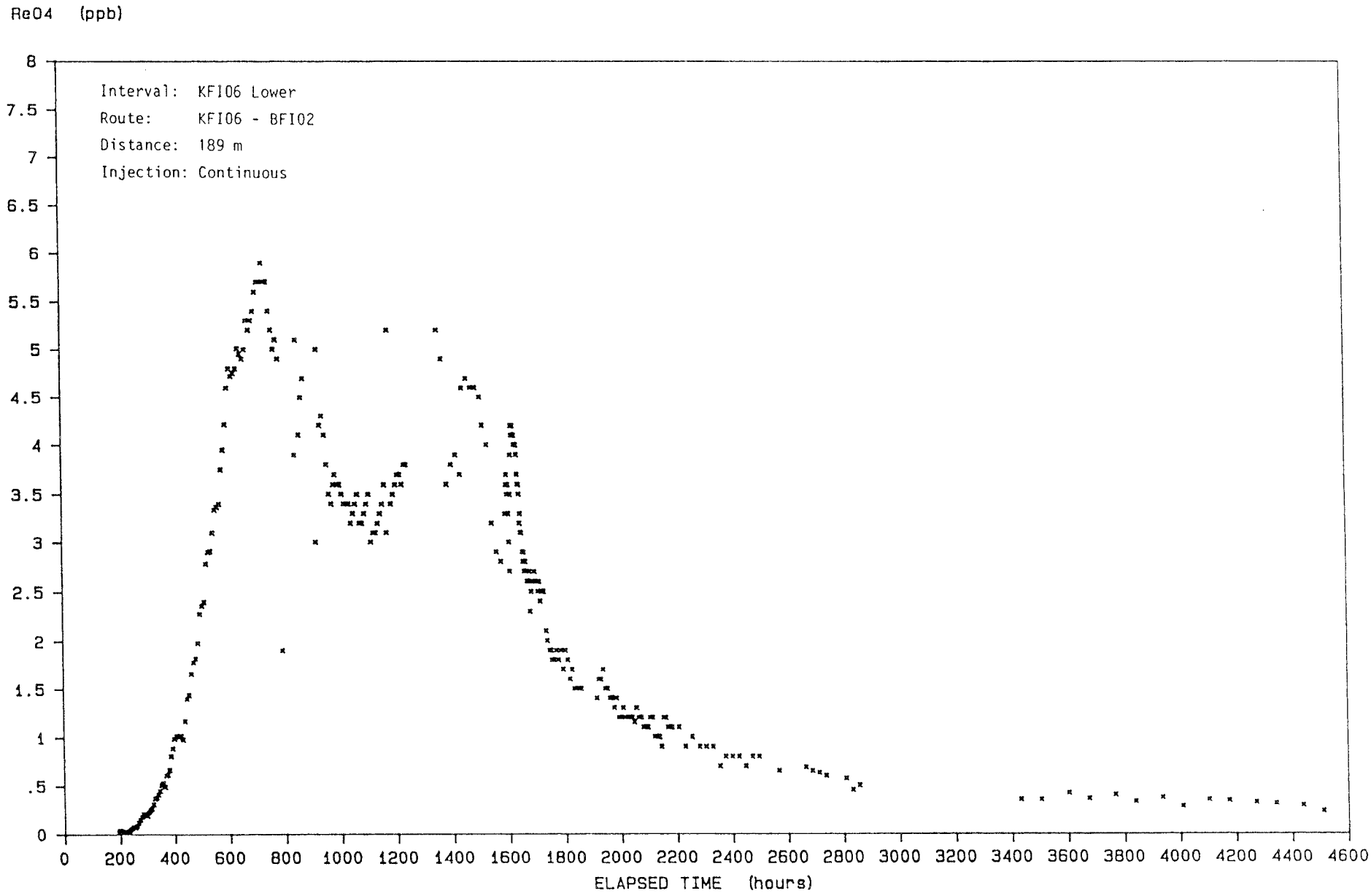


Breakthrough curve for $ReO_4^-$ injected in KFI06:L, 0-4600 h.

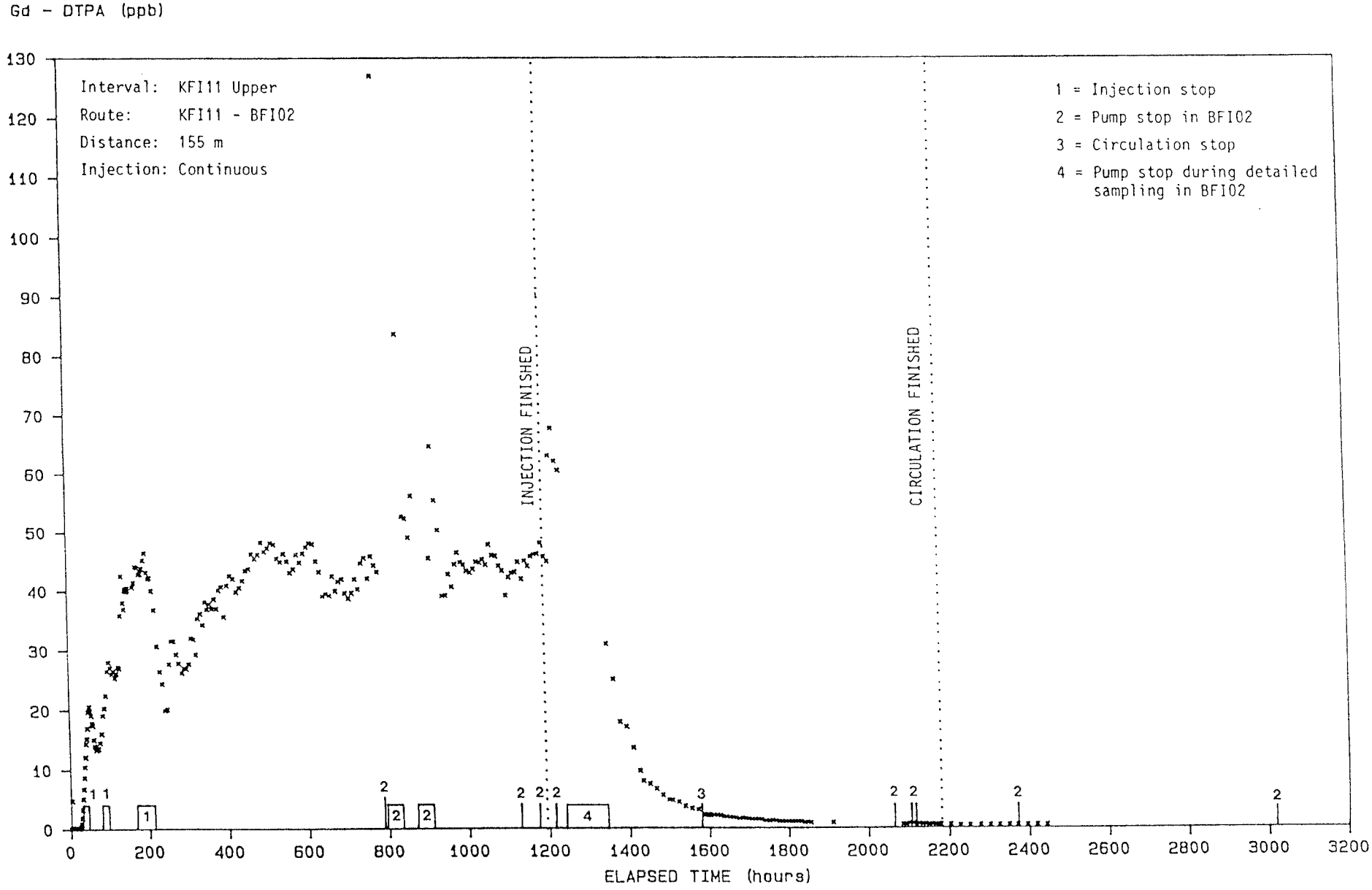


Breakthrough curve for Gd-DTPA injected in KFI11:U, 0-3200 h.

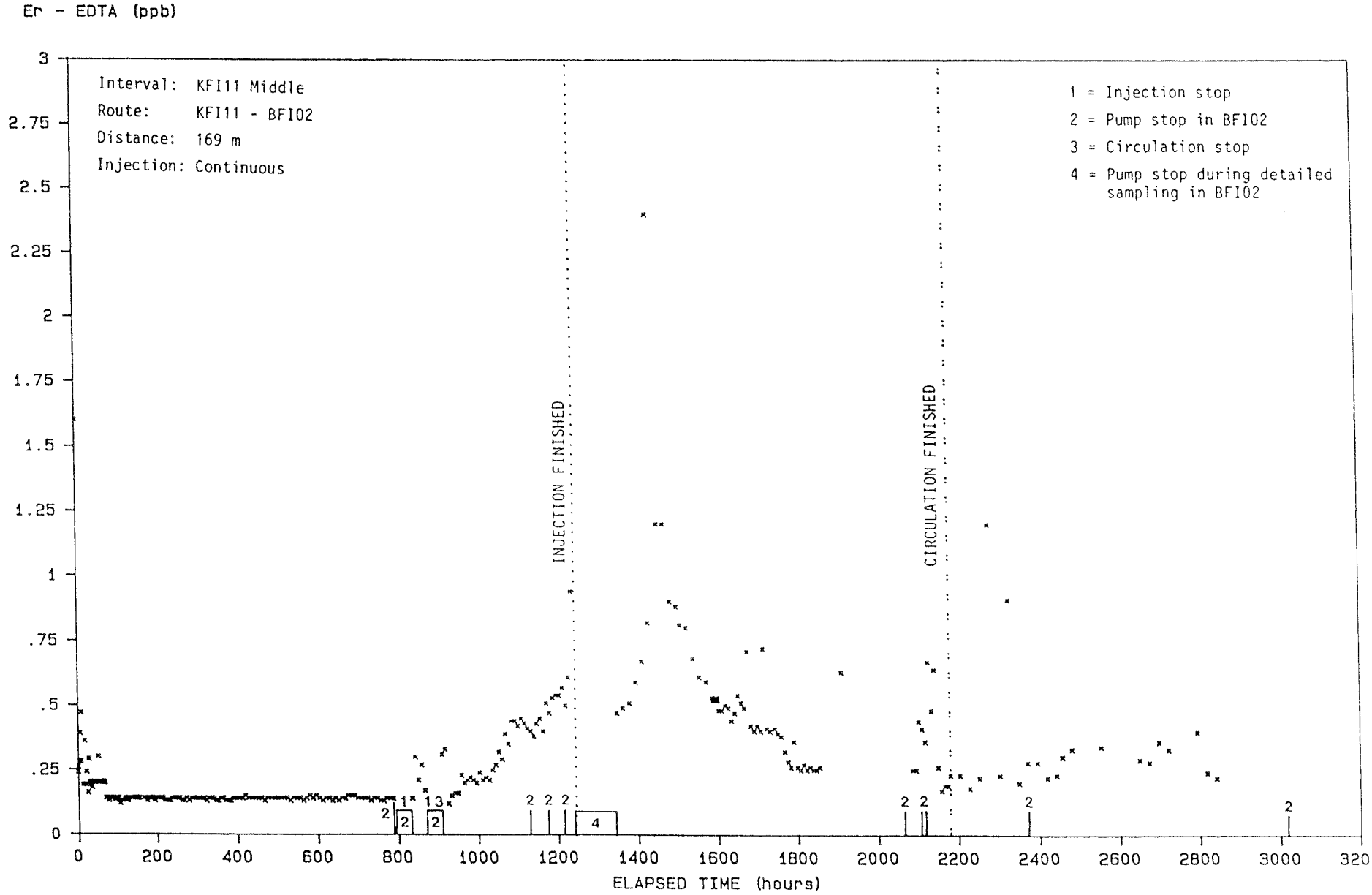


Breakthrough curve for Er-EDTA injected in KFI11:M, 0-3200 h.

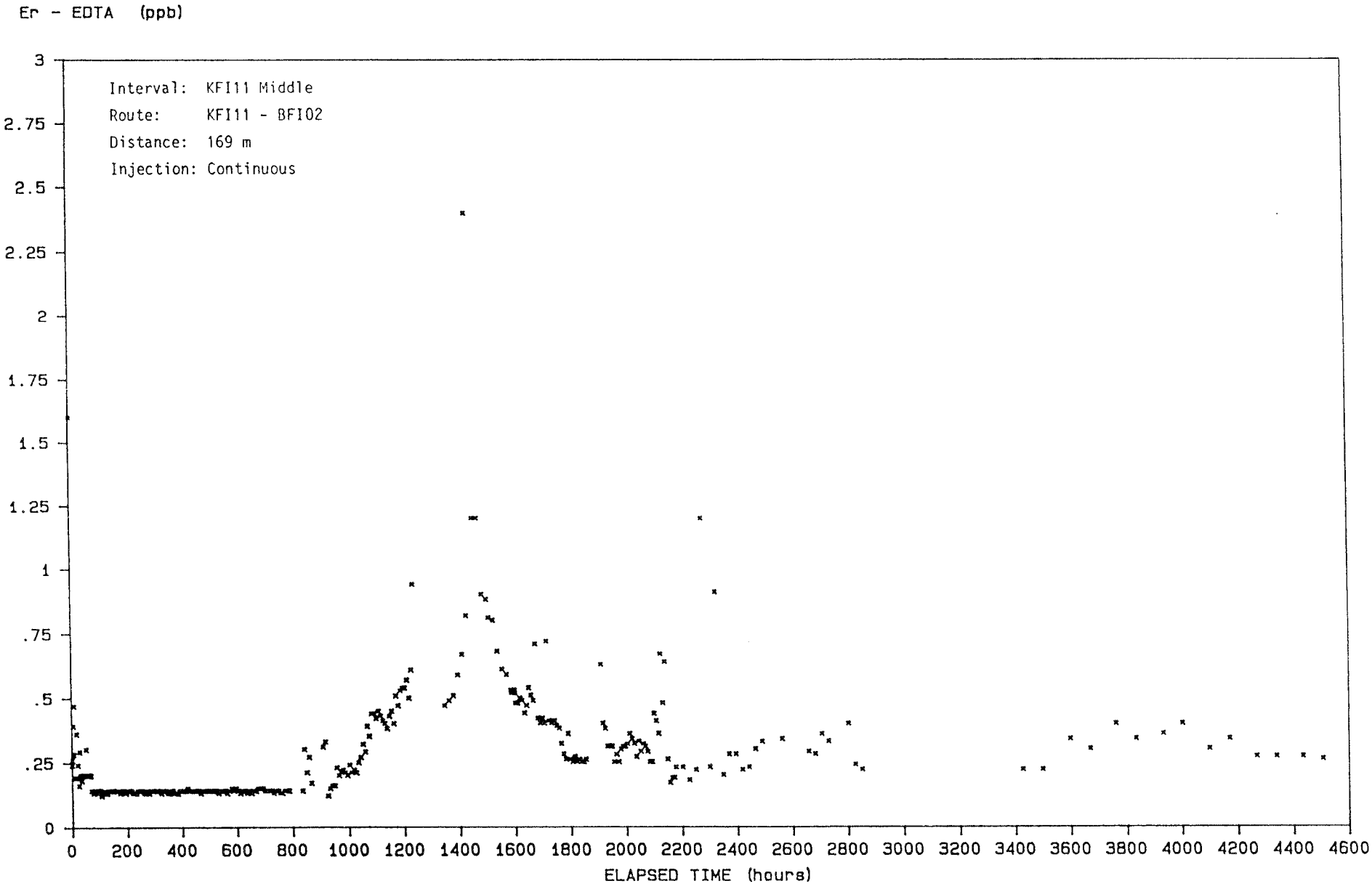


Breakthrough curve for Er-EDTA injected in KFI11:M, 0-4600 h.

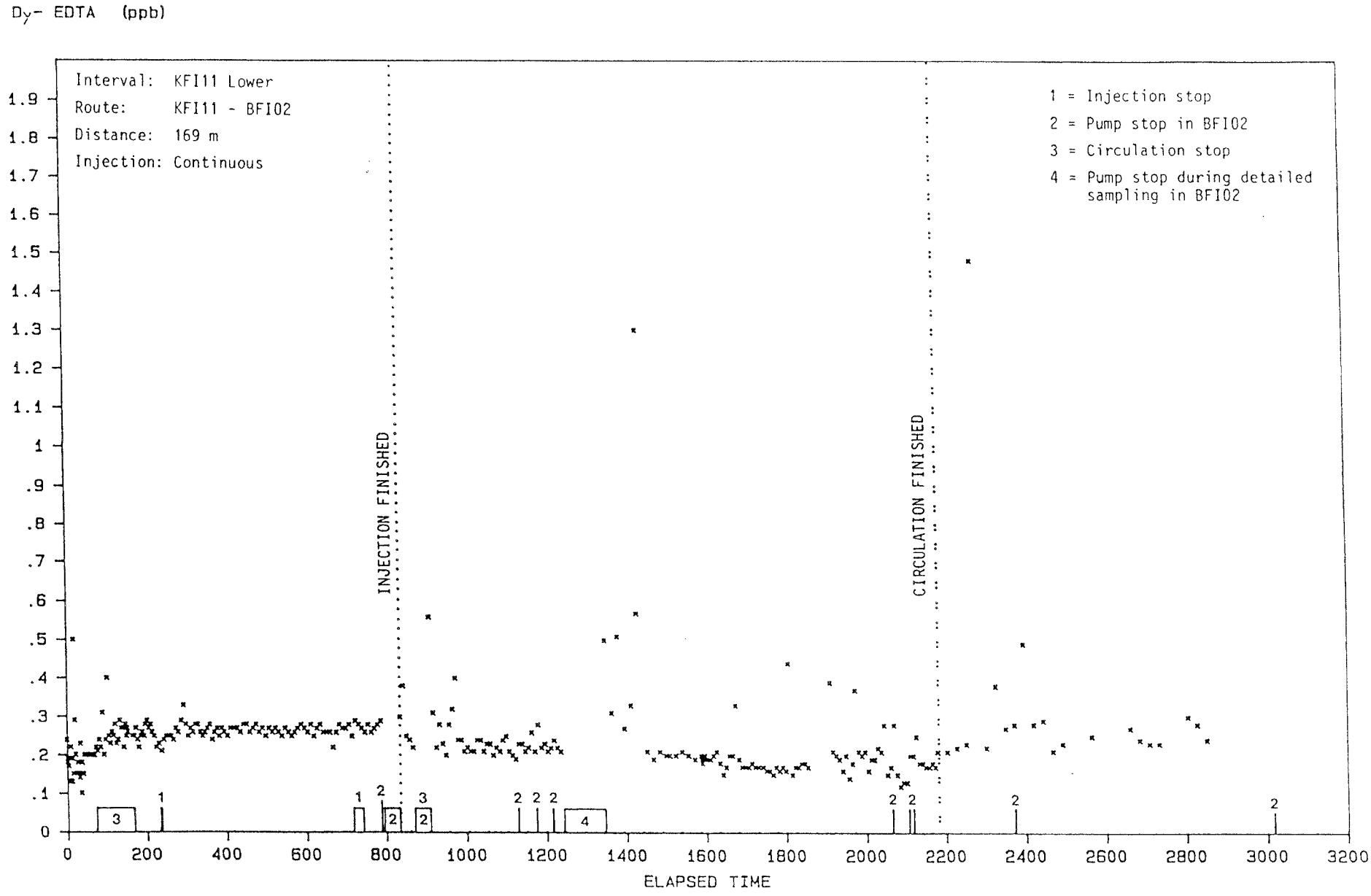


Breakthrough curve for Dy-EDTA injected in KFI11:L, 0-3200 h.

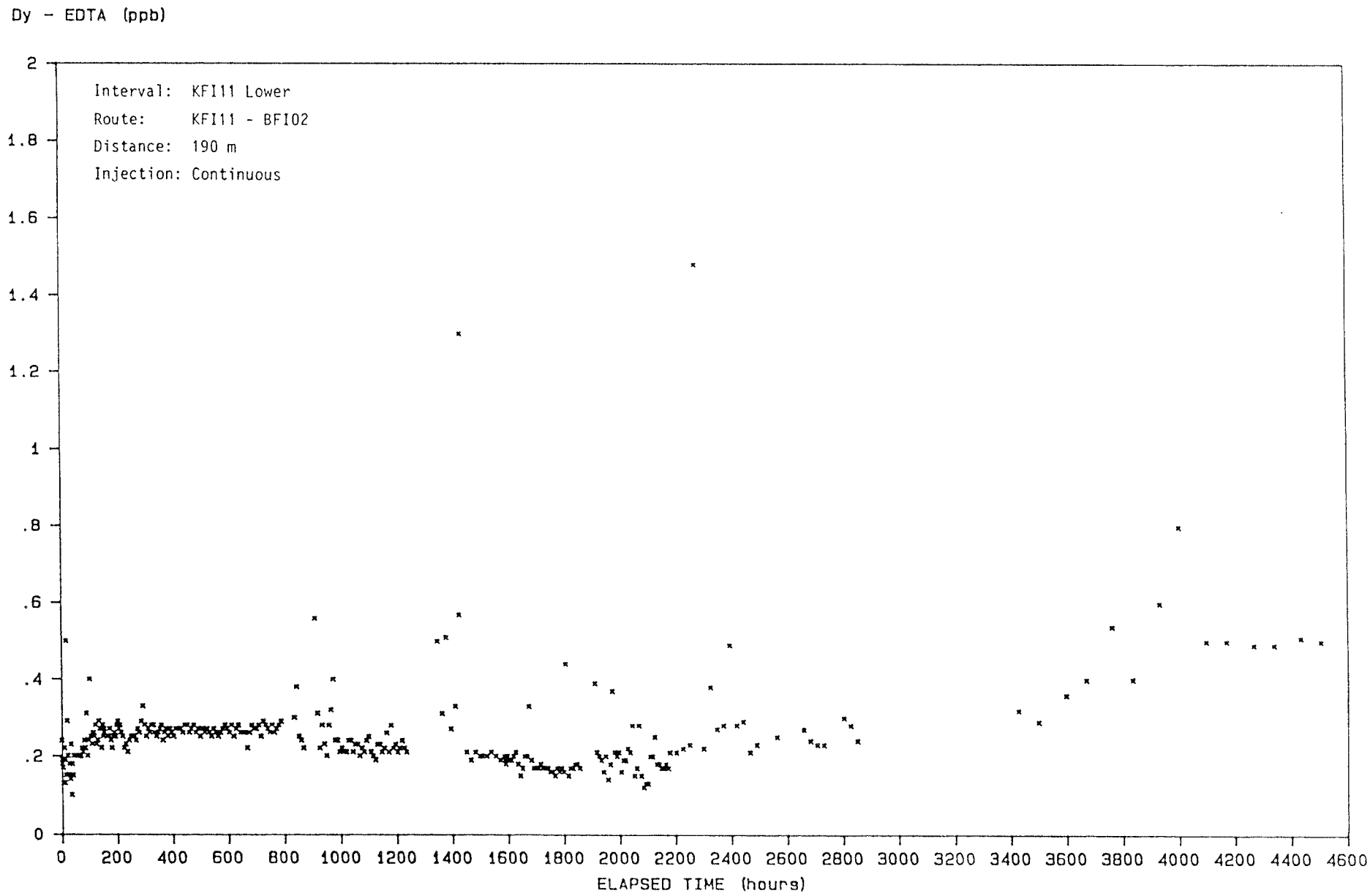


Breakthrough curve for Dy-EDTA injected in KFI11:L, 0-4600 h.

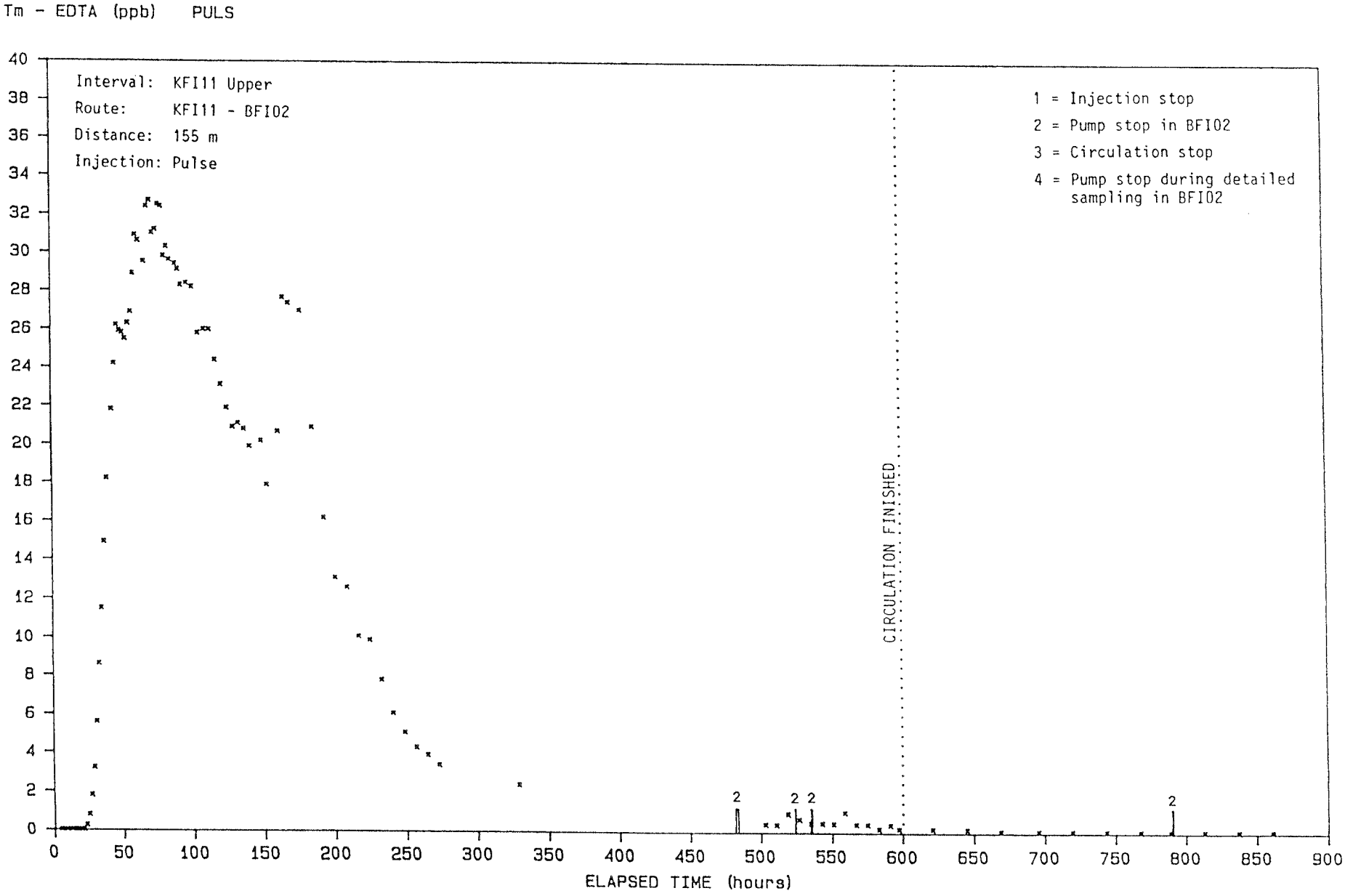


Breakthrough curve for Tm-EDTA injected in KFI11:U, 0-900 h.

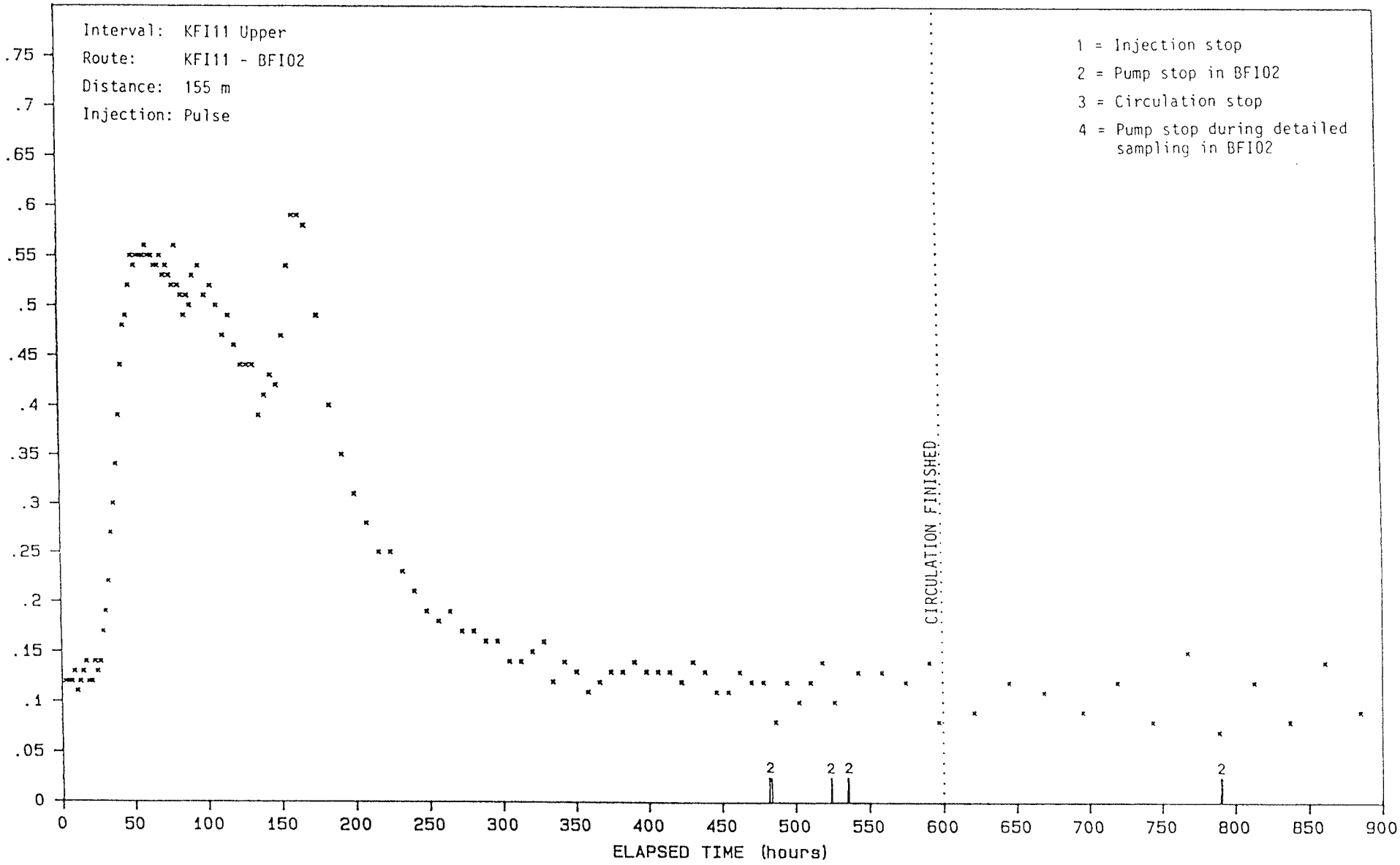


Breakthrough curve for Amino G Acid injected in KFI11:U, 0-900h

# APPENDIX D

## LOG OF EVENTS

CONTENTS Page

Log of events for continuous injection of In-EDTA in interval BFI01:U.

| ELAPSED TIME (hours) | I.S (h) | C.S (h) | W.S (h) | REMARKS |
|---|---|---|---|---|
| 22- 62 | 40+- | | | Estimation from inj. data |
| 698- 749 | | 51 | | |
| 793 | | | 0.25 | |
| 800- 839 | | | 39 | |
| 876- 915 | | | 39 | |
| 1134 | | | 0.25 | |
| 1180 | | | 0.5 | |
| 1220 | | | 0.5 | |
| 1246 | | | | INJECTION FINISHED |
| 1247-1351 | | | 104 | DETAILED SAMPLING |
| 1279 | | 0.5 | | |
| 2069-2071 | | | 2 | |
| 2069-2087 | | 18 | | |
| 2111 | | | 0.5 | |
| 2122-2123 | | | 1 | |
| 2187 | | | | CIRCULATION FINISHED |
| 2377-2378 | | | 1 | |
| 3021-3022 | | | 0.5 | |
| 3682-3698 | | | 16 | |
| 3802-3822 | | | 20 | |
| 3847-3848 | | | 1 | |
| 4007-4031 | | | 24 | |

I.S = INJECTION STOP
C.S = CIRCULATION STOP
W.S = WITHDRAWAL STOP
\+ = Estimated time, may be somewhat longer
\- = Estimated time, may be somewhat shorter

Log of events for continuous injection of Uranine in interval BF101:M.

| ELAPSED TIME (hours) | I.S (h) | C.S (h) | W.S (h) | REMARKS |
|---|---|---|---|---|
| 45- 49 | 4+ | | | |
| 93- 95 | 2+ | | | |
| 409- 434 | 25 | | | |
| 433- 434 | | 2.5 | | |
| 561- 579 | 18+ | | | |
| 792 | | | 0.25 | |
| 792- 794 | | 1.5 | | |
| 799- 837 | | | 39 | |
| 875- 914 | | | 39 | |
| 969- 981 | 12+ | | | |
| 1133 | | | 0.25 | |
| 1133 | | | | INJECTION FINISHED |
| 1133-1172 | | 39 | | |
| 1177-1246 | | 69 | | |
| 1179 | | | 0.5 | |
| 1219 | | | 0.5 | |
| 1246-1350 | | | 104 | DETAILED SAMPLING |
| 2068-2070 | | | 2 | |
| 2068-2086 | | 18 | | |
| 2110 | | | 0.5 | |
| 2121-2122 | | | 1 | |
| 2186 | | | | CIRCULATION FINISHED |
| 2376-2377 | | | 1 | |
| 3020-3021 | | | 0.5 | |
| 3681-3697 | | | 16 | |
| 3801-3821 | | | 20 | |
| 3846-3847 | | | 1 | |
| 4006-4030 | | | 24 | |

I.S = INJECTION STOP
C.S = CIRCULATION STOP
W.S = WITHDRAWAL STOP
\+ = Estimated stop, may be somewhat longer

Log of events for continuous injection of Ho-EDTA in interval BFI01:L.

| ELAPSED TIME (hours) | I.S (h) | C.S (h) | W.S (h) | REMARKS |
|---|---|---|---|---|
| 46- 50 | 4+ | | | |
| 94- 96 | 2+ | | | |
| 406- 410 | 4+ | | | |
| 430- 433 | | 3+ | | |
| 432- 433 | 1 | | | |
| 793 | | | 0.25 | |
| 793- 795 | | 1.5 | | |
| 800- 839 | | | 39 | |
| 876- 915 | | | 39 | |
| 1134 | | | 0.25 | |
| 1180 | | | 0.5 | |
| 1211 | | | | INJECTION FINISHED |
| 1211-1443 | 232 | | | |
| 1220 | | | 0.5 | |
| 1247-1351 | | 104 | | DETAILED SAMPLING |
| 2069-2071 | | | 2 | |
| 2069-2087 | 18 | | | |
| 2111 | | | 0.5 | |
| 2122-2123 | | | 1 | |
| 2187 | | | | CIRCULATION FINISHED |
| 2377-2378 | | | 1 | |
| 3021-3022 | | | 0.5 | |
| 3682-3698 | | | 16 | |
| 3802-3822 | | | 20 | |
| 3847-3848 | | | 1 | |
| 4007-4031 | | | 24 | |

I.S = INJECTION STOP
C.S = CIRCULATION STOP
W.S = WITHDRAWAL STOP
\+ = Estimated time, may be somewhat longer

Log of events for continuous and pulse injection of Iodide in interval KFI06:U.

| ELAPSED TIME (hours) | I.S (h) | C.S (h) | W.S (h) | REMARKS |
|---|---|---|---|---|
| 43- 49 | 6+ | | | Continuous injection |
| 115 | | | | CIRCULATION STOPPED |
| 125- 128 | | | | Pulse injection, 125 h = new $t_o$ |
| 3 | | | | INJECTION STOPPED |
| 665 | | | 0.25 | |
| 670- 709 | | | 39 | |
| 746- 785 | | | 39 | |
| 988 | | | 0.25 | |
| 1050 | | | 0.5 | |
| 1090 | | | 0.5 | |
| 1117-1221 | | | 104 | DETAILED SAMPLING |
| 1939-1941 | | | 2 | |
| 1982 | | | 0.5 | |
| 1992-1993 | | | 1 | |
| 2247-2248 | | | 1 | |
| 2892-2893 | | | 0.5 | |
| 3553-3569 | | | 16 | |
| 3673-3693 | | | 20 | |
| 3718-3719 | | | 1 | |
| 3878-3902 | | | 24 | |

I.S = INJECTION STOP
C.S = CIRCULATION STOP
W.S = WITHDRAWAL STOP
\+ = Estimated time, may be somewhat longer

Log of events for continuous injection of Yb-EDTA in interval KFI06:M.

| ELAPSED TIME (hours) | I.S (h) | C.S (h) | W.S (h) | REMARKS |
|---|---|---|---|---|
| 44- 50 | 6+ | | | |
| 791 | | | 0.25 | |
| 791- 793 | | 2 | | |
| 798- 837 | | | 39 | |
| 837 | | | | INJECTION FINISHED |
| 874- 913 | | | 39 | |
| 914 | | | | CIRCULATION FINISHED |
| 1131 | | | 0.25 | |
| 1178 | | | 0.5 | |
| 1218 | | | 0.5 | |
| 1245-1349 | | | 104 | DETAILED SAMPLING |
| 2067-2069 | | | 2 | |
| 2110 | | | 0.5 | |
| 2120-2121 | | | 1 | |
| 2375-2376 | | | 1 | |
| 3019-3020 | | | 0.5 | |
| 3680-3696 | | | 16 | |
| 3800-3820 | | | 20 | |
| 3845-3846 | | | 1 | |
| 4005-4029 | | | 24 | |

I.S = INJECTION STOP
C.S = CIRCULATION STOP
W.S = WITHDRAWAL STOP
\+ = Estimated time, may be somewhat longer

Log of events for continuous injection of $ReO_4^-$ in interval KFI06:L.

| ELAPSED TIME (hours) | I.S (h) | C.S (h) | W.S (h) | REMARKS |
|---|---|---|---|---|
| 1- 8 | 7- | | | |
| 14- 22 | 8- | | | |
| 45- 51 | 6+ | | | |
| 93- 94 | 1+ | | | |
| 117- 119 | 2 | | | |
| 117- 147 | | 30 | | |
| 213- 218 | 5+ | | | |
| 236- 238 | 2+ | | | |
| 260- 262 | 2+ | | | |
| 410- 412 | | 2+ | | |
| 411- 412 | 1 | | | |
| 501- 503 | 2+ | | | |
| 792 | | 0.5 | 0.25 | |
| 798- 837 | | | 39 | |
| 875- 914 | | | 39 | |
| 988 | | | | INJECTION FINISHED |
| 1132 | | | 0.25 | |
| 1179 | | | 0.5 | |
| 1219 | | | 0.5 | |
| 1246-1350 | | | | DETAILED SAMPLING |
| 2068-2070 | | | 2 | |
| 2110 | | | 0.5 | |
| 2120-2121 | | | 1 | |
| 2186 | | | | CIRCULATION FINISHED |
| 2375-2376 | | | 1 | |
| 3020-3021 | | | 0.5 | |
| 3681-3697 | | | 16 | |
| 3801-3821 | | | 20 | |
| 3846-3847 | | | 1 | |
| 4006-4030 | | | 24 | |

I.S = INJECTION STOP
C.S = CIRCULATION STOP
W.S = WITHDRAWAL STOP
\+ = Estimated time, may be somewhat longer
\- = Estimated time, may be somewhat shorter

Log of events for continuous injection of Gd-DTPA in interval KFI11:U.

| ELAPSED TIME (hours) | I.S (h) | C.S (h) | W.S (h) | REMARKS |
|---|---|---|---|---|
| 30- 46 | 16- | | | |
| 80- 96 | 16- | | | |
| 168- 213 | 45- | | | |
| 788 | | | 0.25 | |
| 795- 834 | | | 39 | |
| 871- 911 | 40 | 40 | 39 | |
| 1129 | | | 0.25 | |
| 1175 | | | 0.5 | |
| 1194 | | | | INJECTION FINISHED |
| 1215 | | | 0.5 | |
| 1242-1346 | | | 104 | DETAILED SAMPLING |
| 1581-1582 | | 1.5 | | |
| 1582 | | | | Start of pulse injection (D:7) |
| 2064-2066 | | | 2 | |
| 2106 | | | 0.5 | |
| 2117-2118 | | | 1 | |
| 2182 | | | | CIRCULATION FINISHED |
| 2372-2373 | | | 1 | |
| 3016 | | | 0.5 | |
| 3677-3693 | | | 16 | |
| 3797-3817 | | | 20 | |
| 3842-3843 | | | 1 | |
| 4002-4026 | | | 24 | |

I.S = INJECTION STOP
C.S = CIRCULATION STOP
W.S = WITHDRAWAL STOP
\- = Estimated time, may be somewhat shorter

Log of events for pulse injection of Tm-EDTA and Amino G Acid in interval KFI11:U.

| ELAPSED TIME (hours) | I.S (h) | C.S (h) | W.S (h) | REMARKS |
|---|---|---|---|---|
| 482- 484 | | | 2 | |
| 524- 525 | | | 0.5 | |
| 535- 536 | | | 1 | |
| 600 | | | | CIRCULATION FINISHED |
| 790- 791 | | | 1 | |
| 1434-1435 | | | 0.5 | |
| 2095-2111 | | | 16 | |
| 2215-2235 | | | 20 | |
| 2260-2261 | | | 1 | |
| 2420-2444 | | | 24 | |

I.S = INJECTION STOP
C.S = CIRCULATION STOP
W.S = WITHDRAWAL STOP

Log of events for continuous injection of Er-EDTA in interval KFI11:M.

| ELAPSED TIME (hours) | I.S (h) | C.S (h) | W.S (h) | REMARKS |
|---|---|---|---|---|
| 788 | | | 0.25 | |
| 795- 834 | | | 39 | |
| 871- 910 | 39 | 39 | 39 | |
| 1129 | | | 0.25 | |
| 1175 | | | 0.5 | |
| 1215 | | | 0.5 | |
| 1247 | | | | INJECTION FINISHED |
| 1242-1346 | | | | DETAILED SAMPLING |
| 2064-2066 | | | 2 | |
| 2106 | | | 0.5 | |
| 2117-2118 | | | 1 | |
| 2182 | | | | CIRCULATION FINISHED |
| 2372-2373 | | | 1 | |
| 3016 | | | 0.5 | |
| 3677-3693 | | | 16 | |
| 3797-3817 | | | 20 | |
| 3842-3843 | | | 1 | |
| 4002-4026 | | | 24 | |

I.S = INJECTION STOP
C.S = CIRCULATION STOP
W.S = WITHDRAWAL STOP

Log of events for continuous injection of Dy-EDTA in interval KFIII:L.

| ELAPSED TIME (hours) | I.S (h) | C.S (h) | W.S (h) | REMARKS |
|---|---|---|---|---|
| 73- 168 | | 95 | | |
| 213 | 1+ | | | |
| 233- 237 | 4+ | | | |
| 718- 742 | 24+ | | | |
| 788 | | | 0.25 | |
| 795- 834 | | | 39 | |
| 836 | | | | INJECTION FINISHED |
| 871- 910 | | 39 | 39 | |
| 1129 | | | 0.25 | |
| 1175 | | | 0.5 | |
| 1215 | | | 0.5 | |
| 1242-1346 | | | | DETAILED SAMPLING |
| 2064-2066 | | | 2 | |
| 2106 | | | 0.5 | |
| 2117-2118 | | | 1 | |
| 2182 | | | | CIRCULATION FINISHED |
| 2372-2373 | | | 1 | |
| 3016 | | | 0.5 | |
| 3677-3693 | | | 16 | |
| 3797-3817 | | | 20 | |
| 3842-3843 | | | 1 | |
| 4002-4026 | | | 24 | |

I.S = INJECTION STOP
C.S = CIRCULATION STOP
W.S = WITHDRAWAL STOP
\+ = Estimated time, may be somewhat longer

# APPENDIX E

## SAMPLING OF MAJOR CONDUCTORS IN BFI02

CONTENTS Page

PUMP LOGGING In - EDTA Conc in ppb

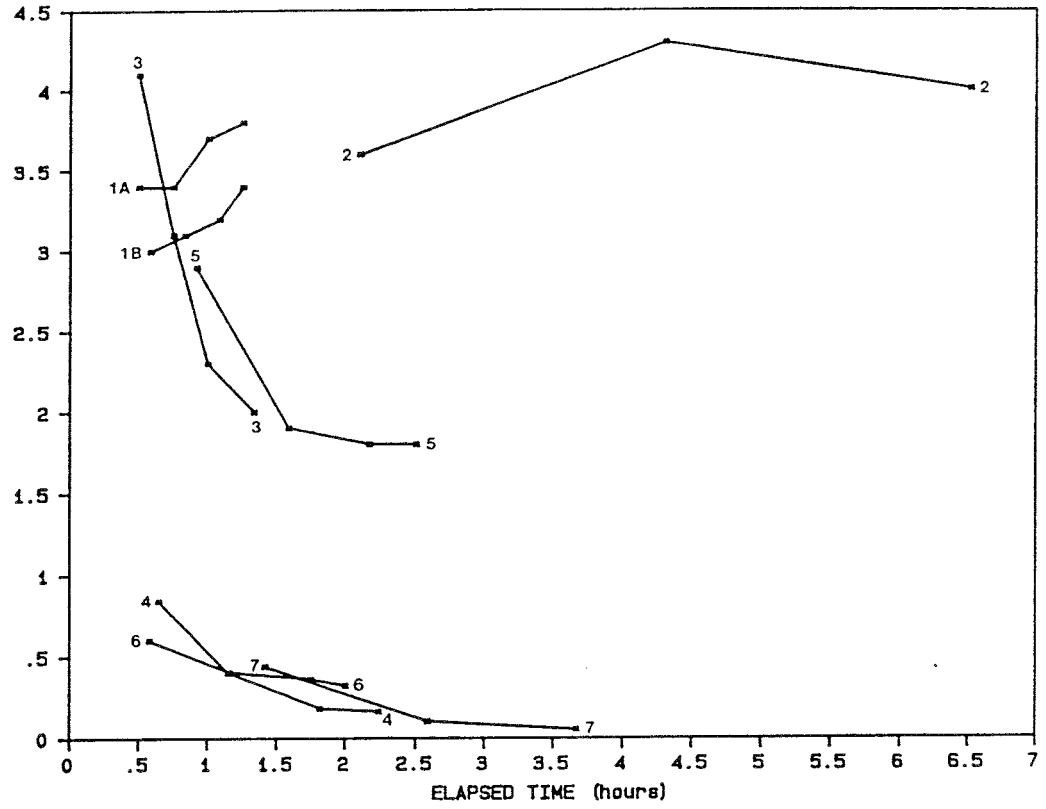


PUMP LOGGING Uranine Conc in ppb

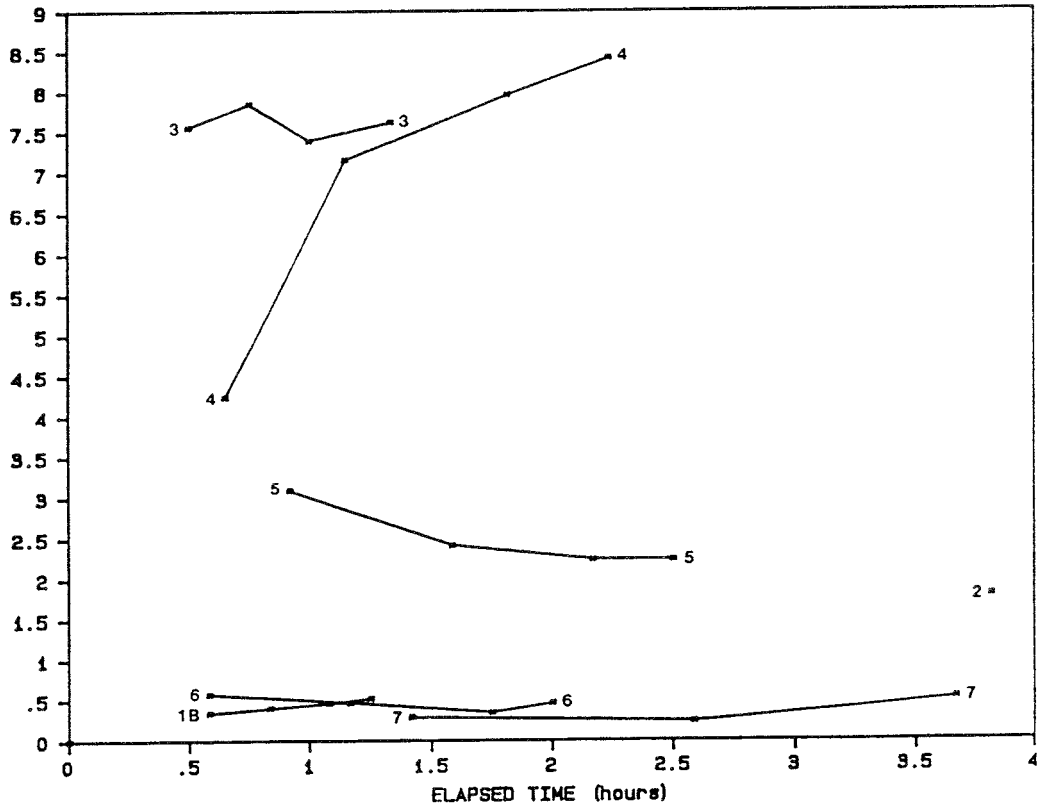


1A 203 - 205 m
1B 203 - 205 m
2 208 - 210 m
3 212 - 214 m
4 238 - 240 m
5 257.14 - 259.14 m
6 260 - 262 m
7 276 - 278 m

Detailed sampling of In-EDTA and Uranine

PUMP LOGGING Ho - EDTA Conc in ppb

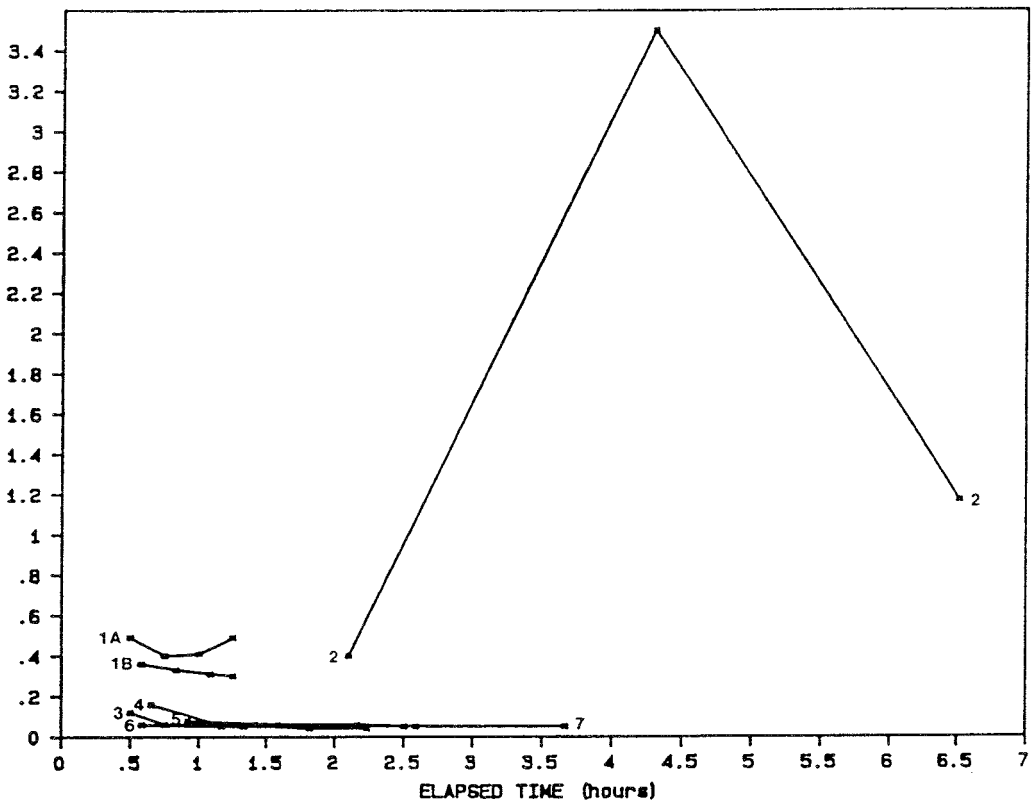


PUMP LOGGING Iodide Conc in ppm

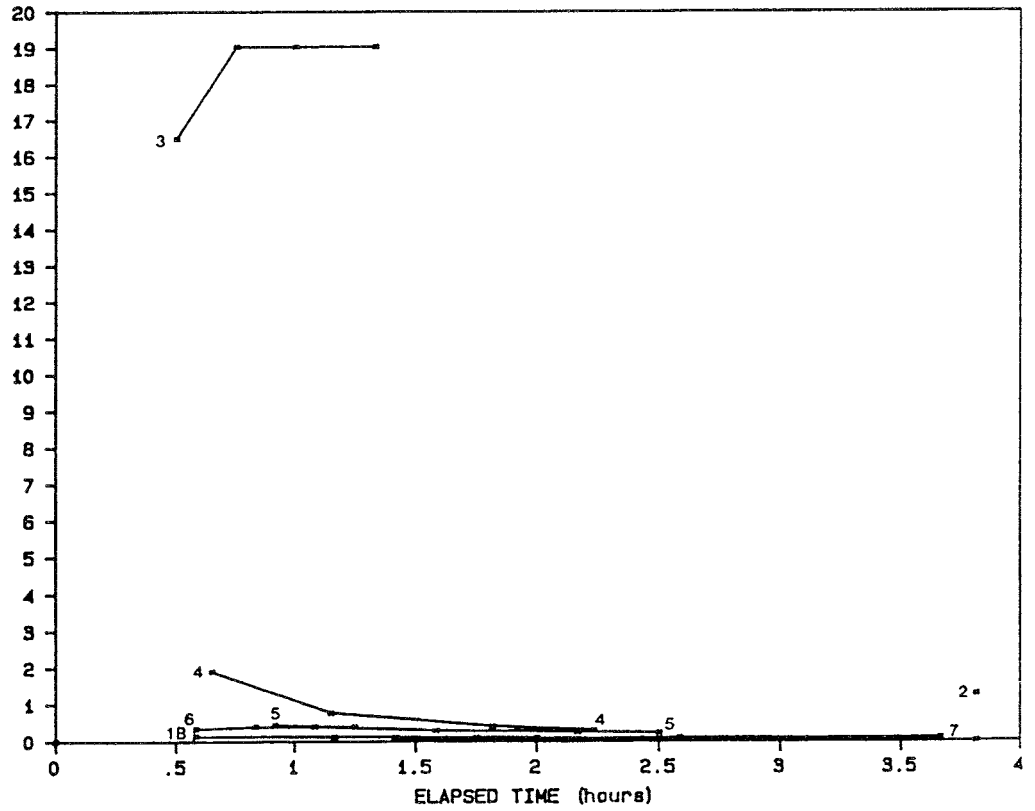


| | |
|---|---|
| 1A | 203 - 205 m |
| 1B | 203 - 205 m |
| 2 | 208 - 210 m |
| 3 | 212 - 214 m |
| 4 | 238 - 240 m |
| 5 | 257.14 - 259.14 m |
| 6 | 260 - 262 m |
| 7 | 276 - 278 m |

Detailed sampling of Ho-EDTA and Iodide

PUMP LOGGING Yb - EDTA Conc in ppb

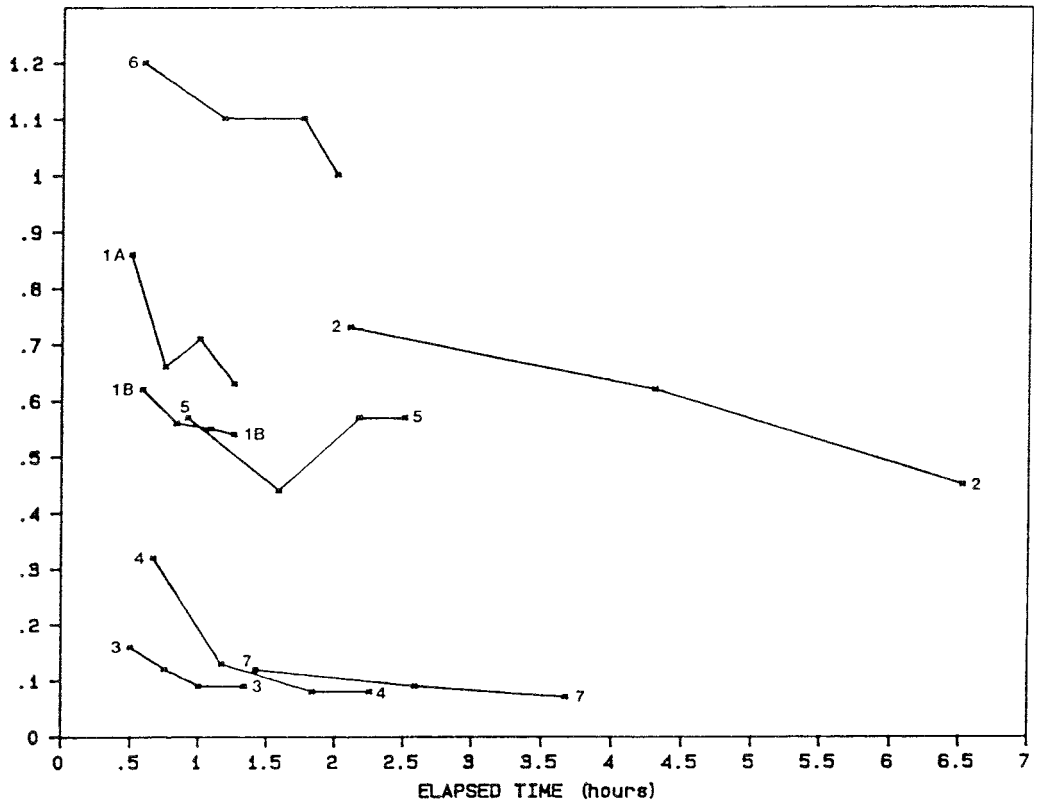


PUMP LOGGING ReO4 Conc in ppb

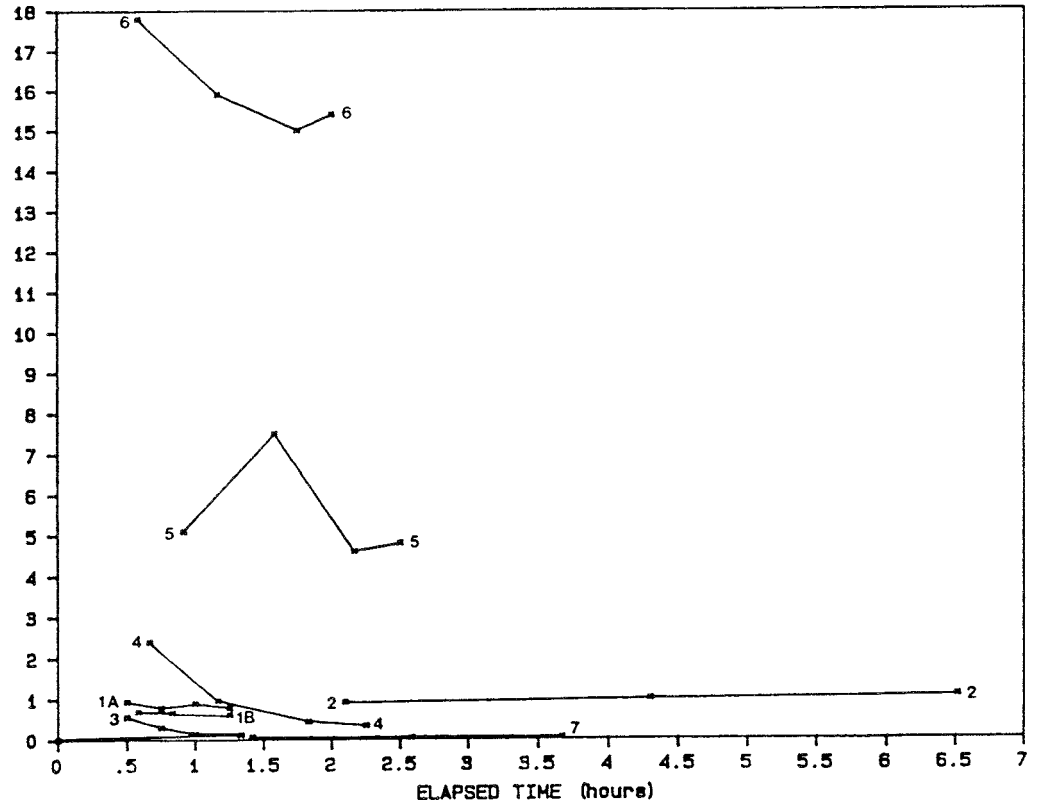


| | |
|---|---|
| 1A | 203 - 205 m |
| 1B | 203 - 205 m |
| 2 | 208 - 210 m |
| 3 | 212 - 214 m |
| 4 | 238 - 240 m |
| 5 | 257.14 - 259.14 m |
| 6 | 260 - 262 m |
| 7 | 276 - 278 m |

Detailed sampling of Yb-EDTA and $ReO_4$

PUMP LOGGING Gd - DTPA Conc in ppb

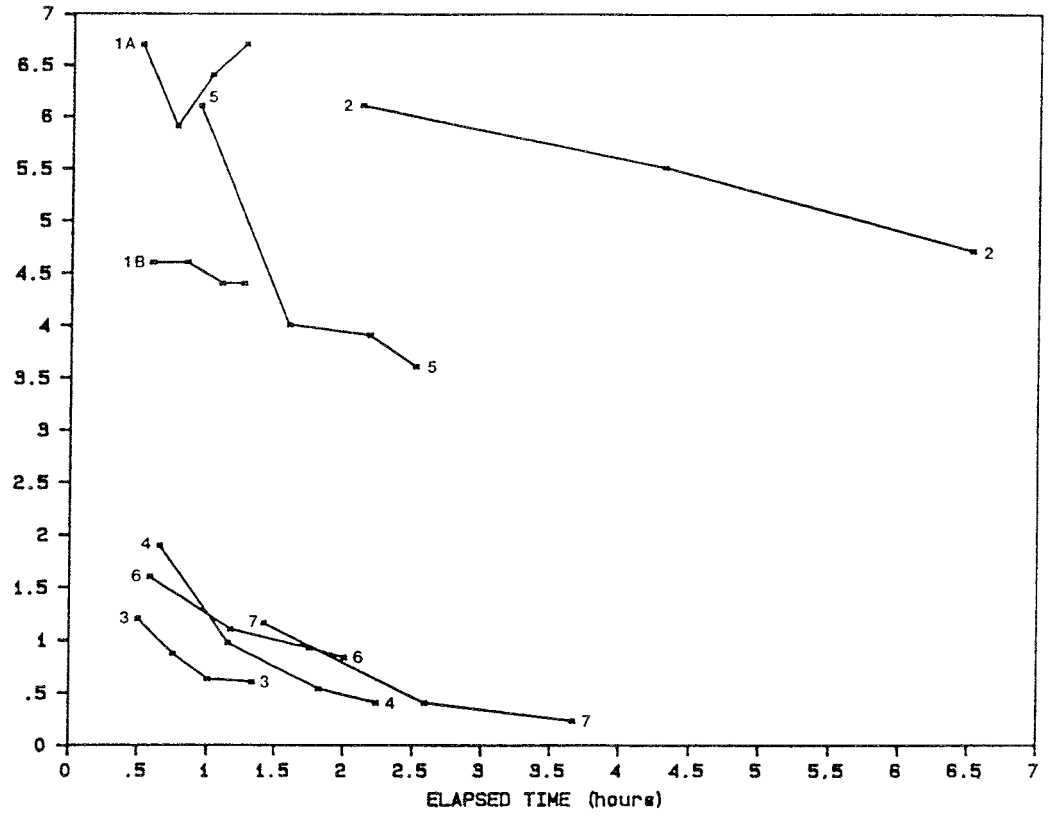


PUMP LOGGING Er - EDTA Conc in ppb

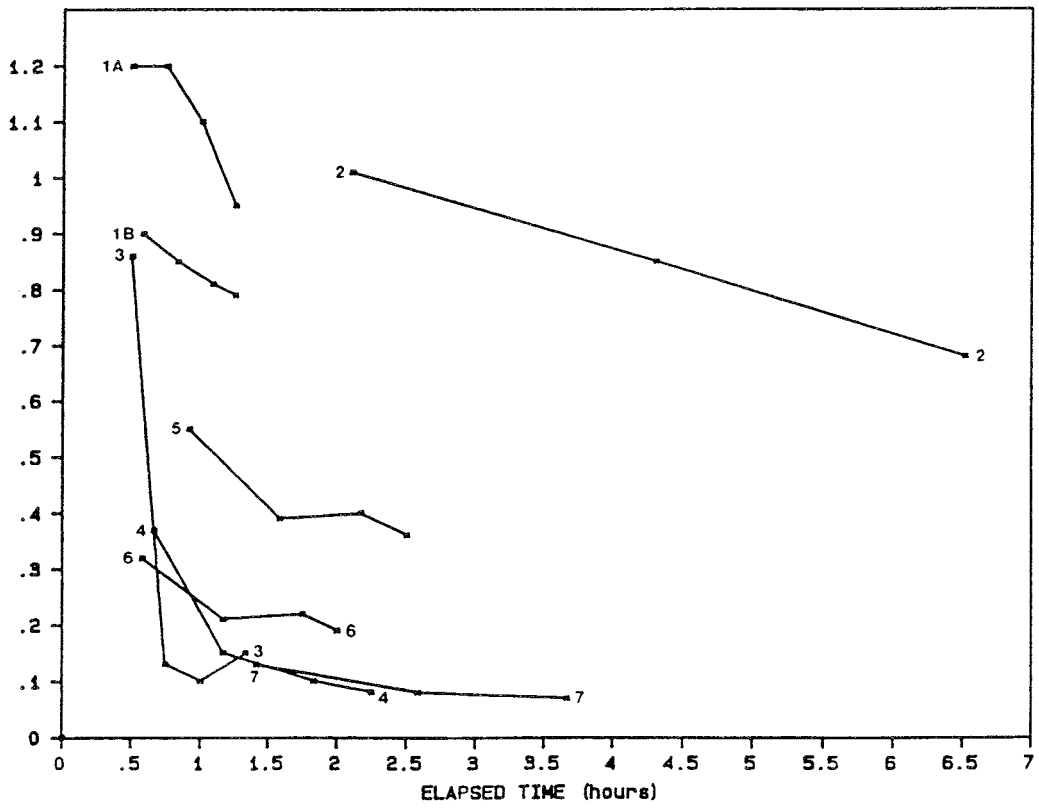


| | |
|---|---|
| 1A | 203 - 205 m |
| 1B | 203 - 205 m |
| 2 | 208 - 210 m |
| 3 | 212 - 214 m |
| 4 | 238 - 240 m |
| 5 | 257.14 - 259.14 m |
| 6 | 260 - 262 m |
| 7 | 276 - 278 m |

Detailed sampling of Gd-DTPA and Er-EDTA

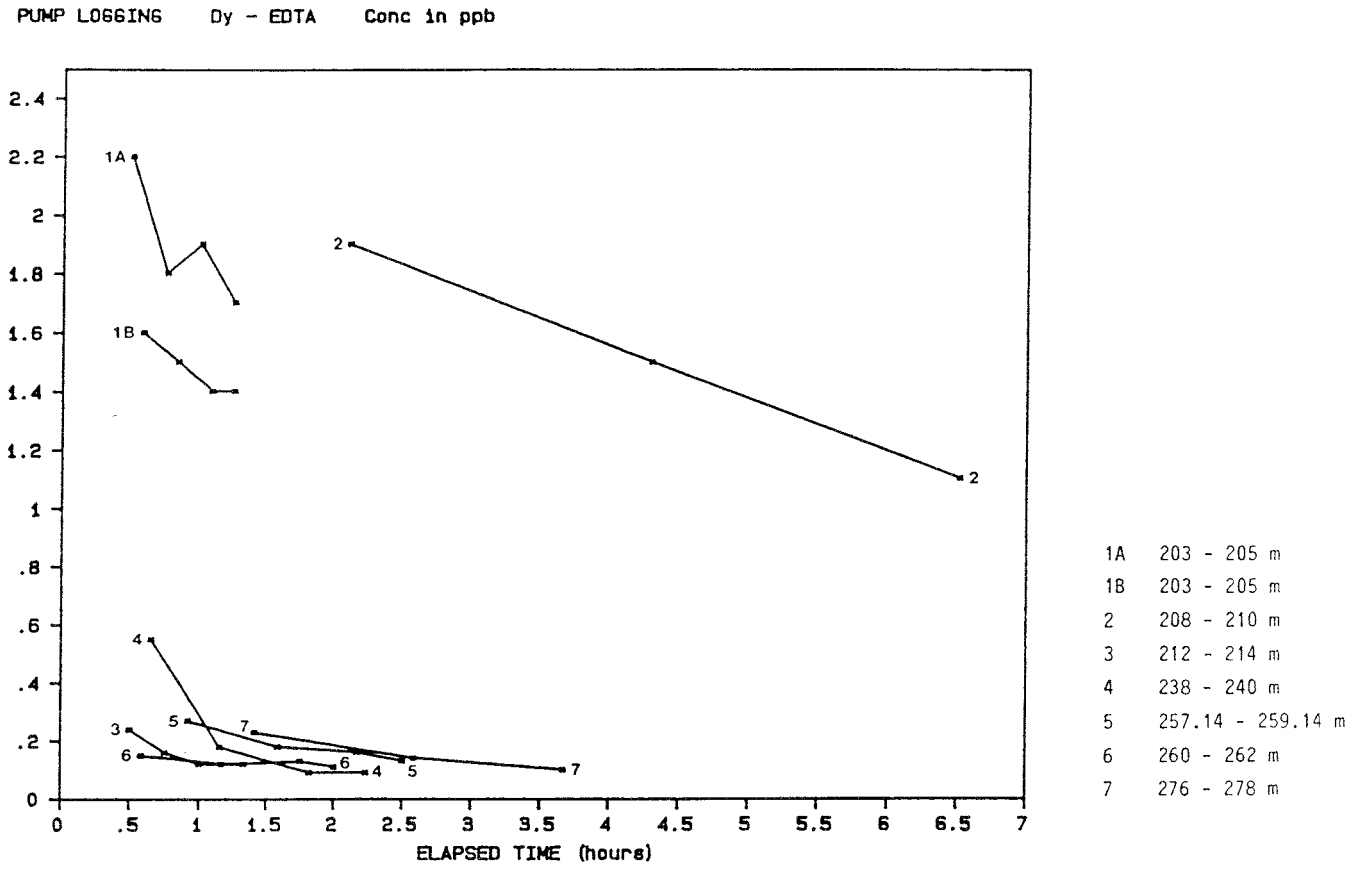


Detailed sampling of Dy-EDTA

# APPENDIX F

## REGRESSION METHODS

CONTENTS Page

# REGRESSION METHOD

## BASIC PROCEDURE

Non-linear regression is used here as a tool to accomplish two purposes. Firstly, to estimate transport parameters from tracer breakthrough curves assuming various conceptual models. Secondly, to discriminate between different models, in order to determine which models explain observed data. Estimation of parameters from field data is very common in groundwater modelling. It is often referred to as calibration, but a more general term is inverse modelling. The basic algorithm employed here is commonly used in groundwater studies and is described by for example Draper and Smith (1981), Cooley (1985), Knopmann and Voss (1987).

Inverse modelling is essentially an optimization problem in which an objective function relating differences between predictions and observed results. The first step is to select a model from which the parameters may be estimated. However, this can usually not be made with certainty for a real system, and it is necessary to incorporate uncertainty about the correct model and random error in observations.

The regression problem dealt with here has basically three components: observations, predictions and random components. It can be represented as (the dependent variable is represented as concentration):

$$\mathbf{C}^o = \mathbf{C}^m + \mathbf{M} \qquad (1)$$

where $\mathbf{C}^o$ = vector of observed concentrations
$\mathbf{C}^m$ = vector of model (predicted) concentrations
$\mathbf{M}$ = vector of random variables

The random vector $\mathbf{M}$ is considered to be a sum of two different errors: random error in observations, $\mathbf{E}_R$, and systematic errors, $\mathbf{E}_S$ due to an incorrect physical model.

The two types of errors are added to a single term, called a residual:

$$\mathbf{E} = \mathbf{E}_R + \mathbf{E}_S \qquad (2)$$

In general, an analysis of residuals can be used to help detecting systematic errors, but is not considered relevant in this report.

The objective of the regression procedure can then be stated as:

$$\text{Min } S = f(\mathbf{E}) \qquad (3)$$

where in this case :

$$f(\mathbf{E}) = \mathbf{E_R}^T \mathbf{W} \mathbf{E_R} \qquad (4)$$

where $\mathbf{W}$ = vector of reliability weights on observations

Thus, as eq. (4) implies, it is a least squares regression. The n x n (n = number of observations) weighing matrix, **W**, is related to the estimated variance in the observations. If observations are assumed to possess different degrees of uncertainty and yet be independent of one another, **W** would be a diagonal matrix. If the random errors in all observations are assumed to be independent and have a common but unknown variance, **W** would be a n x n identity matrix. It should also be noted that eq. (4) assumes that the physical model is correct, and that residuals only consists of random error in observations.

The residuals, $\mathbf{E_R}$, are here defined as the difference between observed and predicted values, and then eq. (3) becomes:

$$\text{Min } S = (\mathbf{C}^o - \mathbf{C}^m)^T \mathbf{W} (\mathbf{C}^o - \mathbf{C}^m) \qquad (5)$$

By taking the derivative of the right-hand side of eq. (5) with respect to the estimated parameters, the minimum of S can be found.

In this case, models are non-linear with respect to the parameters. The approach used here to find Min S for non-linear models is an iterative method, the Gauss-Newton method. By a Taylor series expansion eq. (1) can be written as:

$$\mathbf{C}^o = \mathbf{C}_o^m + \mathbf{X}(\mathbf{B} - \mathbf{B}_o) + \mathbf{E_R} \qquad (6)$$

where $\mathbf{B}_o$ = initial set of parameters
$\mathbf{B}$ = true set of parameters
$\mathbf{C}_o^m$ = dependent variable obtained using $\mathbf{B}_o$
$\mathbf{X}$ = matrix of parameter sensitivities

The **X** matrix is an (n x k) matrix (k = number of parameters) of sensitivity coefficients evaluated at $\mathbf{B}_o$. **X** is the most essential part of the regression procedure and is defined as:

$$\mathbf{X} = \partial C_i^m / \partial B_j \qquad (7)$$

where i refers to the ith observation point and j refers to parameter j. For example, for a two-parameter system with parameters v and D, the matrix **X** would be:

$$\mathbf{X} = \begin{bmatrix} \partial C_1/\partial v & \partial C_1/\partial D \\ \partial C_2/\partial v & \partial C_2/\partial D \\ . & . \\ . & . \\ \partial C_n/\partial v & \partial C_n/\partial D \end{bmatrix} \quad (8)$$

By combining eq. (5) and eq. (6), and take derivatives of S with respect to each parameter, a set of so called normal equations are formed:

$$\mathbf{X}^T\mathbf{W}\mathbf{X}(\mathbf{B} - \mathbf{B}_o) = \mathbf{X}^T\mathbf{W}(\mathbf{C}^o - \mathbf{C}_o^m) \quad (9)$$

Eq.(9) gives a solution for the vector **B** based on an assumed set of parameter values $\mathbf{B}_o$. The solution is only approximate for non-linear problems and must be carried out in several steps through iterations. Eq. (9) can be written in a cyclic form, where the parameter estimate at the r + 1 iteration can be found as:

$$\mathbf{B}_{r+1} = \mathbf{B}_r + (\mathbf{X}_r^T\mathbf{W}\mathbf{X}_r)^{-1}\mathbf{X}_r^T\mathbf{W}(\mathbf{C}^o - \mathbf{C}_r^m) \quad (10)$$

Thus, when solving the regression problem, eq. (10) is repeated until a local optimal solution is found. The local minimum is defined by some convergence criteria, in this case when parameter estimates are essentially identical from one iteration to the other. It should be noted that finding a local minimum does not guarantee that the global minimum is found as well. When in doubt, several sets of initial estimates can be tried. However, since it is expected that some knowledge about the parameters to be estimated and the physical system already exist, the initial estimates will likely be sufficiently good to ensure that a global minimum is found.

## Parameter Sensitivities and Scaling

The computation of **X** is performed by analytically derived derivatives. Thus, this process is entirely model-specific. Models considered in this report consists of one-dimensional models with analytical solutions, and analytical derivatives can be developed without excessive efforts. Further, in order to reduce round-off errors, scaling is performed of various variables in the regression algorithm that for computational purposes preferably would be of similar magnitudes.

Improving Convergence

Due to the high non-linearity of some models, convergence may in some cases be slow or difficult to achieve. Two features are introduced to remediate convergence problems. Firstly, the so called Marquardt correction is employed to adjust the direction of the search vector as the iterative procedure finds its way in the least-square space. Secondly, the length of the search vector is reduced so that the program does not iterate into a neighboring (and presumably incorrect) local minimum.

The principle of the Marquardt correction is to choose a maximum angle between the search vector and the direction of the steepest gradient in least square space, that never should be exceeded. The actual computation utilizes that the inner product of two vectors gives the cosine of the angle between the vectors.

The length of the search vector is restricted in such a way that the parameter estimates are allowed to change only a certain fraction from one iteration to the other. Thus, the damping parameter, p, varies from one iteration to the other.

By incorporating the convergence enhancements eq. (10) can now be written (Cooley, 1985):

$$\mathbf{B}_{r+1} = \mathbf{B}_r + p_{r+1}(\mathbf{X}_r^T\mathbf{W}\mathbf{X}_r + u_{r+1})^{-1}\mathbf{X}_r^T\mathbf{W}(\mathbf{C}^o - \mathbf{C}_r^m) \qquad (11)$$

where p = damping parameter ($\leq 1$)
u = Marquardt parameter

Convergence criterion

Convergence is defined as when the maximal change between iterations between any parameter is below a certain fraction of that parameter. The convergence criterion is defined by:

$$G = \max((b_{j,r+1} - b_{j,r})/b_{j,r}) \qquad (12)$$

## STATISTICAL ANALYSIS OF THE REGRESSION RESULTS

Below is a relatively detailed description given of the statistical analysis of the regression results. Examining some statistical measures should always be a first step in when assessing the validity of the particular model applied in the regression routines. The implemented statistics essentially follows the work by Cooley, (1979).

The available statistical measures can be divided in two main categories:

- Goodness of fit to the model data (1–3 below).

- Model conditioning as it affects reliability of the computed parameters (4–5 below).

Statistical measures

In the following listing the independent parameter is described as concentration, as the present application is focused on estimating parameters from breakthrough curves.

1. Sum of squared differences.

$$S = (\mathbf{C}^o - \mathbf{C})\mathbf{W}(\mathbf{C}^o - \mathbf{C})$$

where $\mathbf{C}^o$ = vector of observed concentrations
$\mathbf{C}$ = vector of computed concentrations
$\mathbf{W}$ = vector of reliability weights on samples

2. Error variance.

$$s^2 = \frac{(\mathbf{C}^o - \mathbf{C})^T \mathbf{W}(\mathbf{C}^o - \mathbf{C})}{J - K}$$

where J = number of observations
K = number of parameters

3. Correlation.

The correlation between observed and predicted dependent variables (concentrations) is computed as:

$$R = \frac{\left[\sum_i (C_i^o - \bar{C}^o)(C_i - \bar{C})\right]^2}{\sum_i (C_i^o - \bar{C}^o)^2 \sum_i (C_i - \bar{C})^2}$$

where $C_i^o$ = observed concentration at point i
$C_i$ = computed concentration at point i

4. Standard error of parameters

A standard error for each parameter is estimated from the diagonal elements of the variance–covariance matrix. The standard error $s_k$ for the kth parameter is given by the square root of the kth diagonal element in the matrix $(\mathbf{X}^T\mathbf{W}\mathbf{X})^{-1}s^2$, where $\mathbf{X}$ is the vector of parameter sensitivities.

The standard error $s_k$ should be seen as a measure of the range over which the respective parameter may be varied to produce a similar solution for the dependent variable as that obtained using the regression estimates of the parameters.

5. Correlation between parameters.

The correlation between two parameter estimates, $C_r$ and $C_s$, is given by:

$$r_{rs} = \frac{\mathrm{Cov}(C_r,C_s)}{(\mathrm{Var}(C_r)\ \mathrm{Var}(C_s))^{1/2}}$$

where the variance and covariance terms are components of $(\mathbf{X}^T\mathbf{W}\mathbf{X})^{-1}s^2$. This measure gives an estimate of the degree of linear dependence of one variable on another. It is useful, and important, to check these numbers in order to detect redundancy of parameters.

REFERENCES

Cooley, R., L., 1979: A Method of estimating Parameters and Assessing Reliability for Models of Steady State Groundwater Flow. 2. Application of Statistical Analysis. Water Resources Research, Vol. 15, No. 3.

Cooley, R., L., 1985: A Comparison of Several Methods of Solving Non-linear Regression Groundwater Flow Problems. Water Resources Research, Vol. 21, No. 10.

Draper, N., R and Smith, H., 1981: Applied Regression Analysis, Second Edition. John Wiley & Sons, Inc.

Knopman, D., S. and Voss, C., I., 1987: Behaviour of Sensitivities in the One-Dimensional Advection-Dispersion Equation: Implications for Parameter Estimation and Sampling Design. Water Resources Research, Vol. 23, No. 2.

# APPENDIX G

## CALCULATED INJECTION SCHEMES

CONTENTS Page

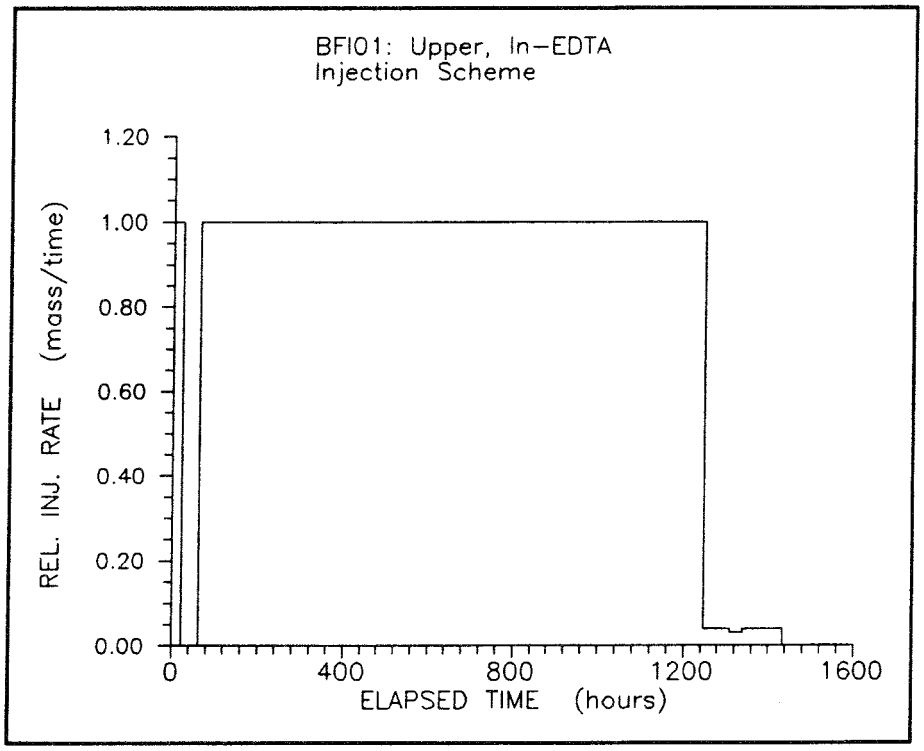


Injection scheme In-EDTA actual inj. stop

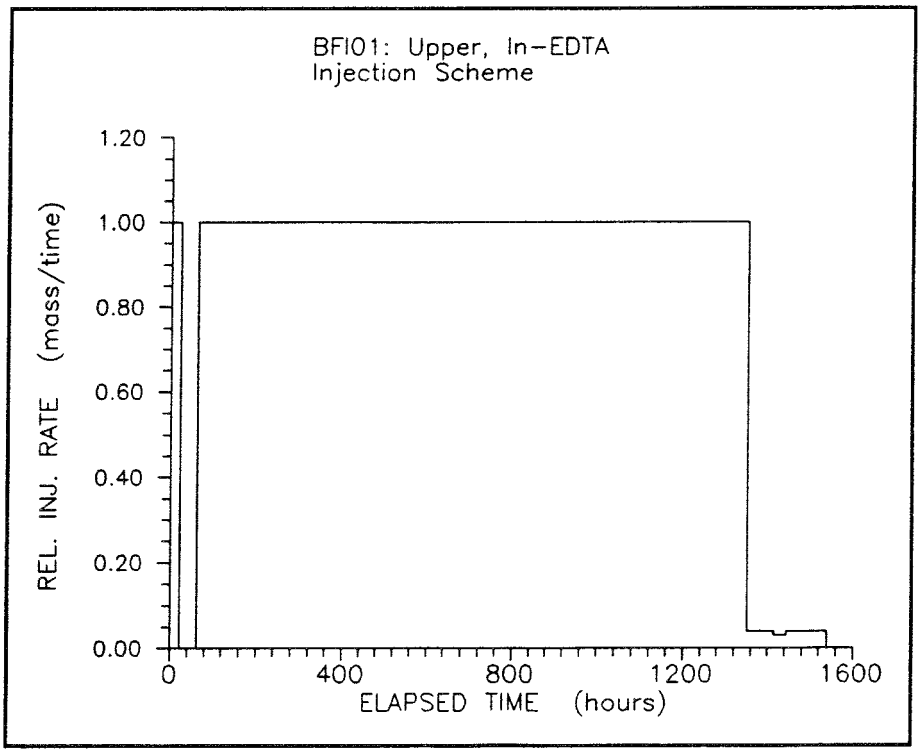


Injection scheme In-EDTA adjusted inj. stop

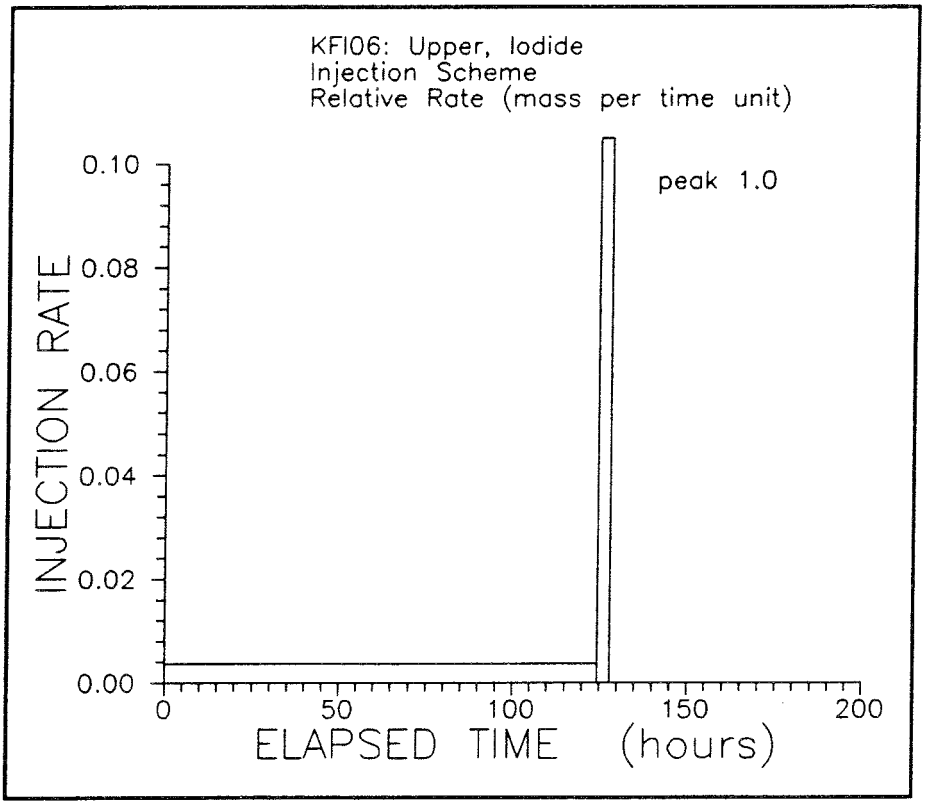


Injection scheme Iodide

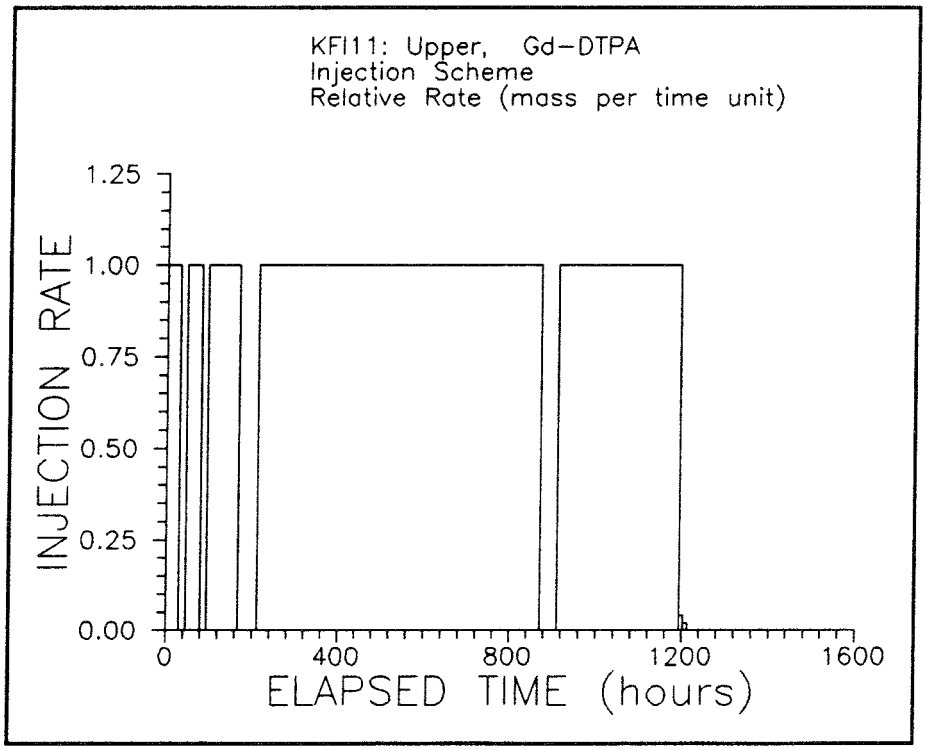


Injection scheme Gd-DTPA actual inj. stop time.

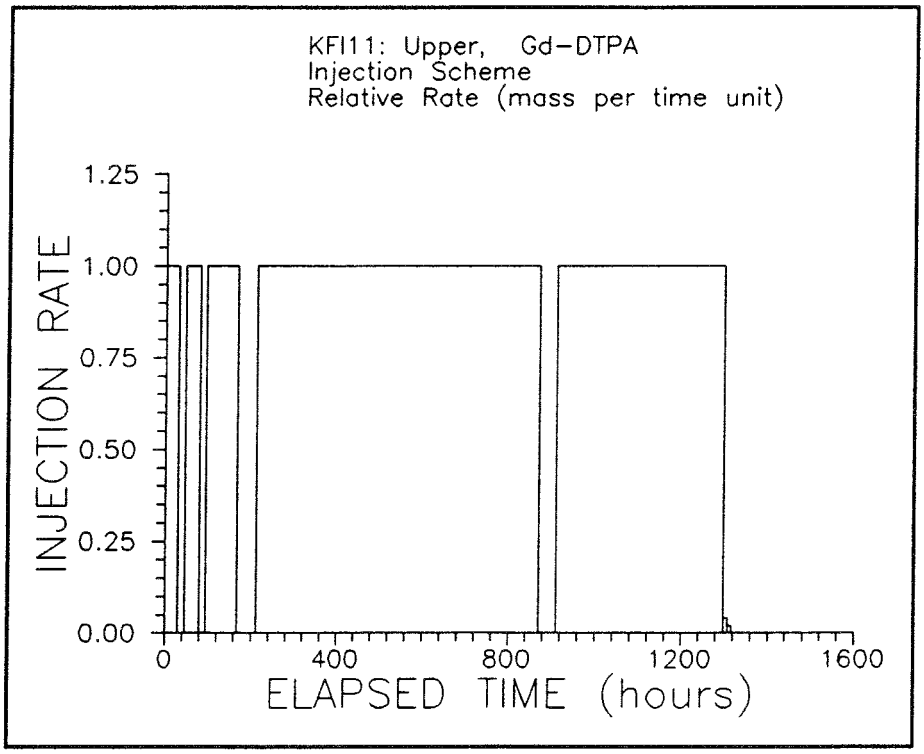


Injection scheme Gd-DTPA adjusted inj. stop time

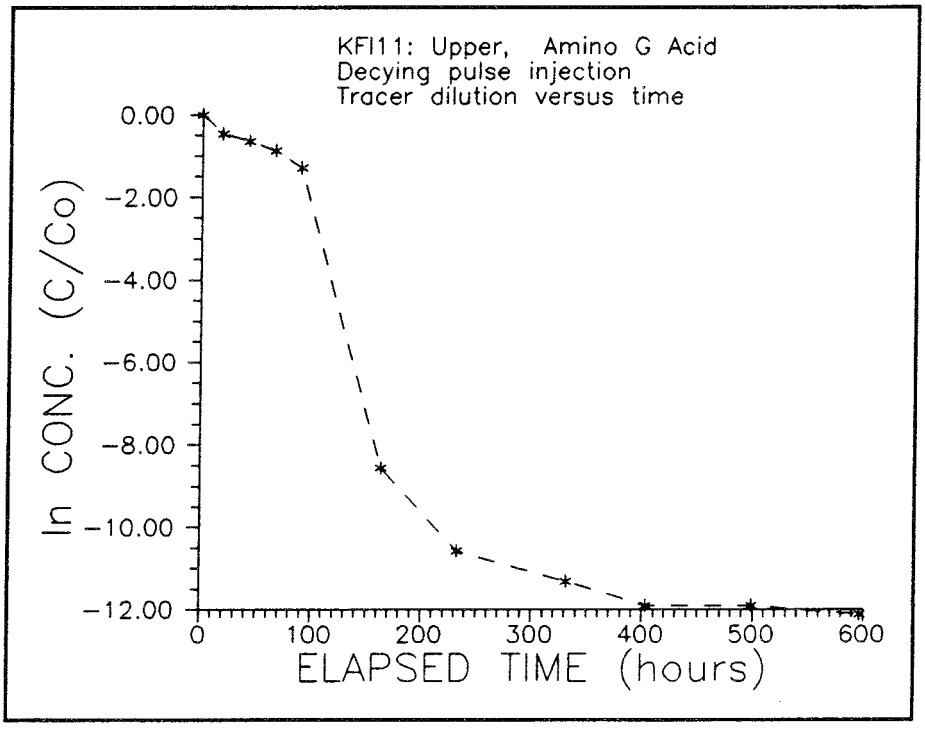


Tracer Amino G Acid dilution in injection section versus time

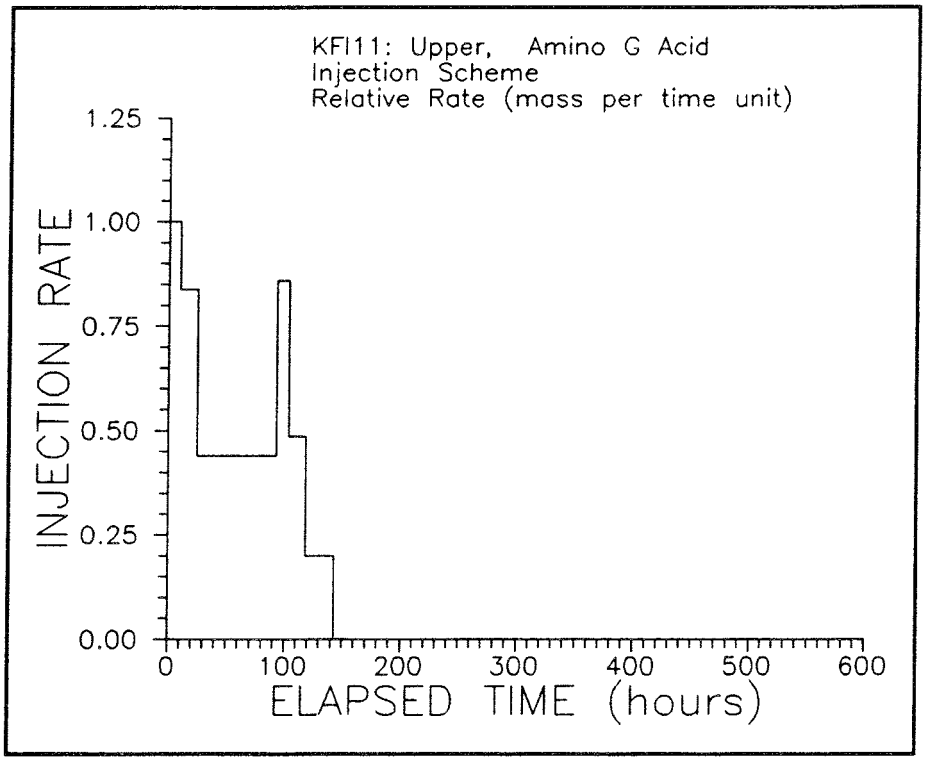


Injection scheme Amino G Acid

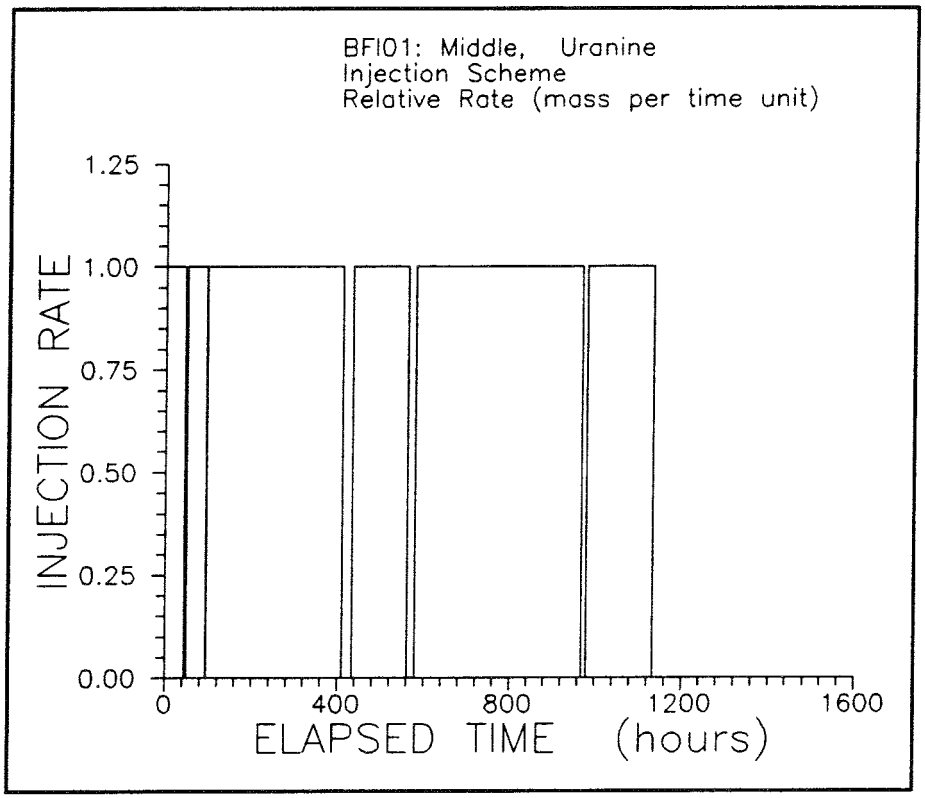


Injection scheme Uranine

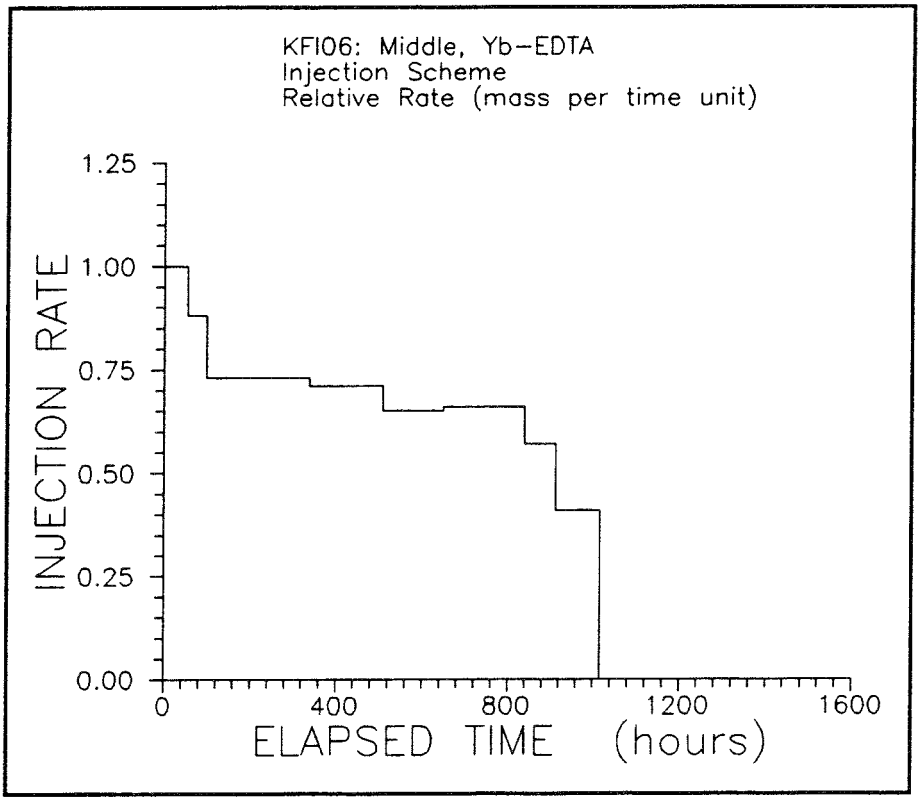


Injection scheme Yb-EDTA

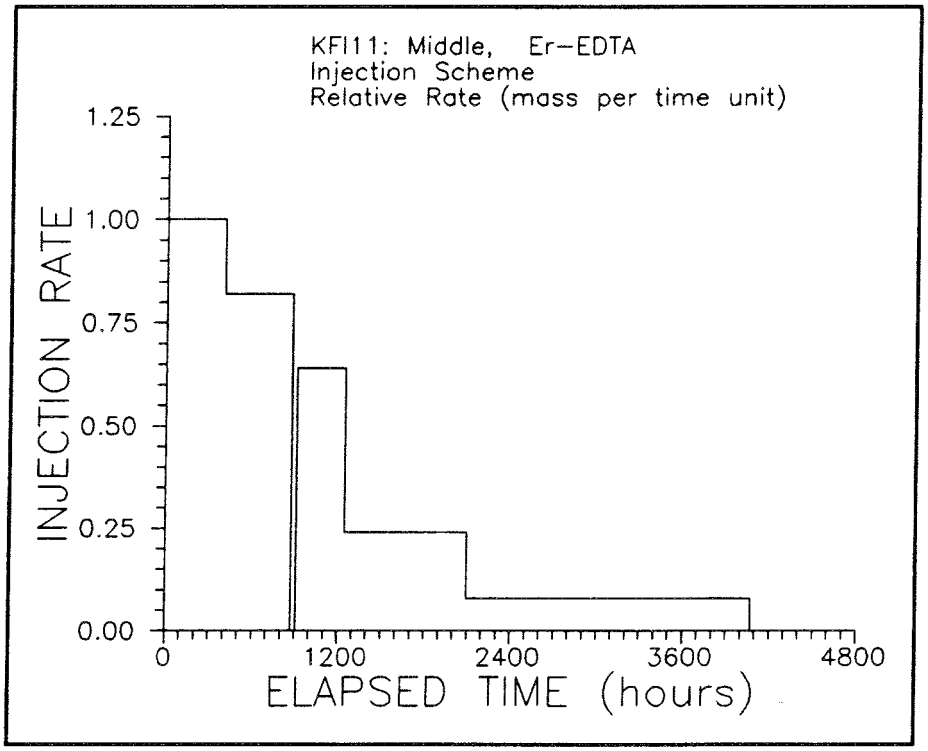


Injection scheme Er-EDTA

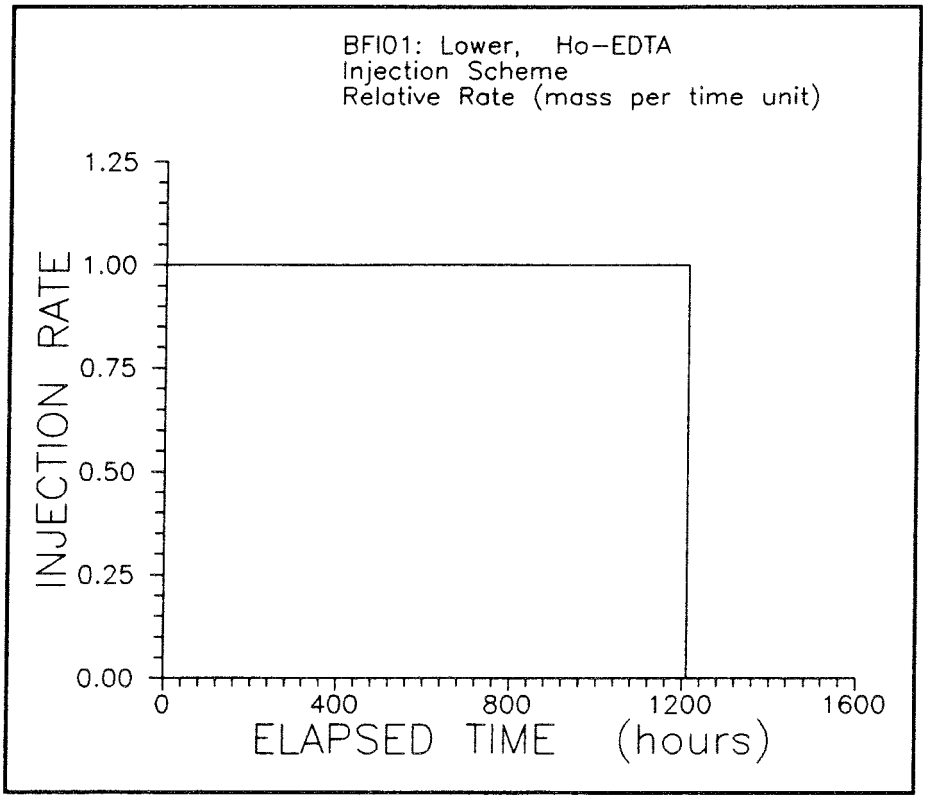


Injection scheme Ho-EDTA

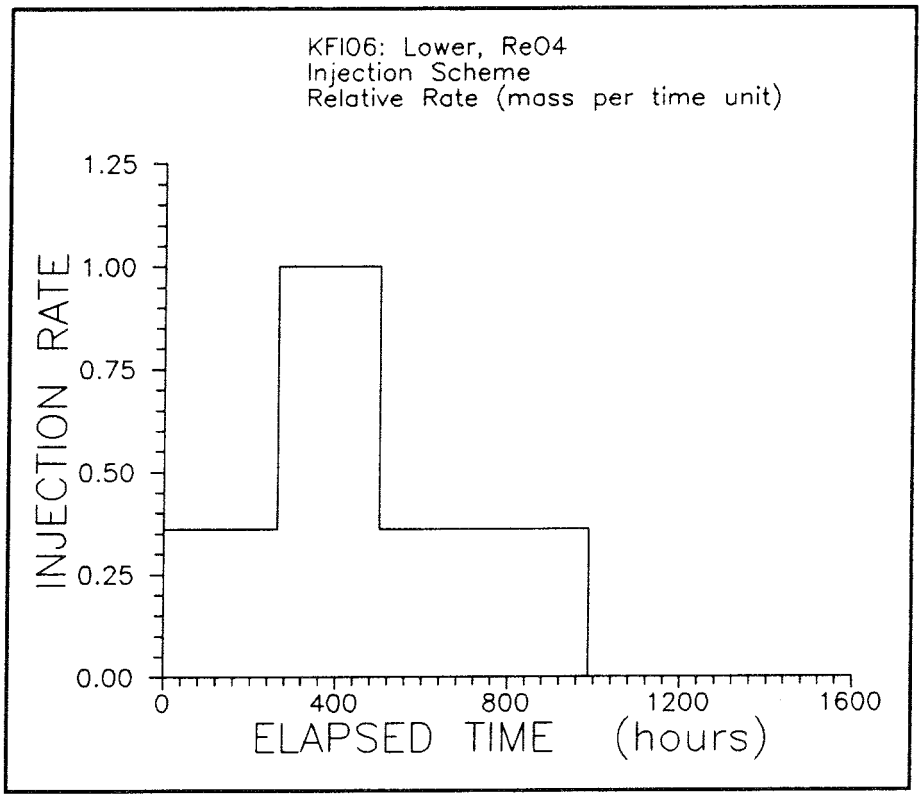


Injection scheme $ReO_4^-$

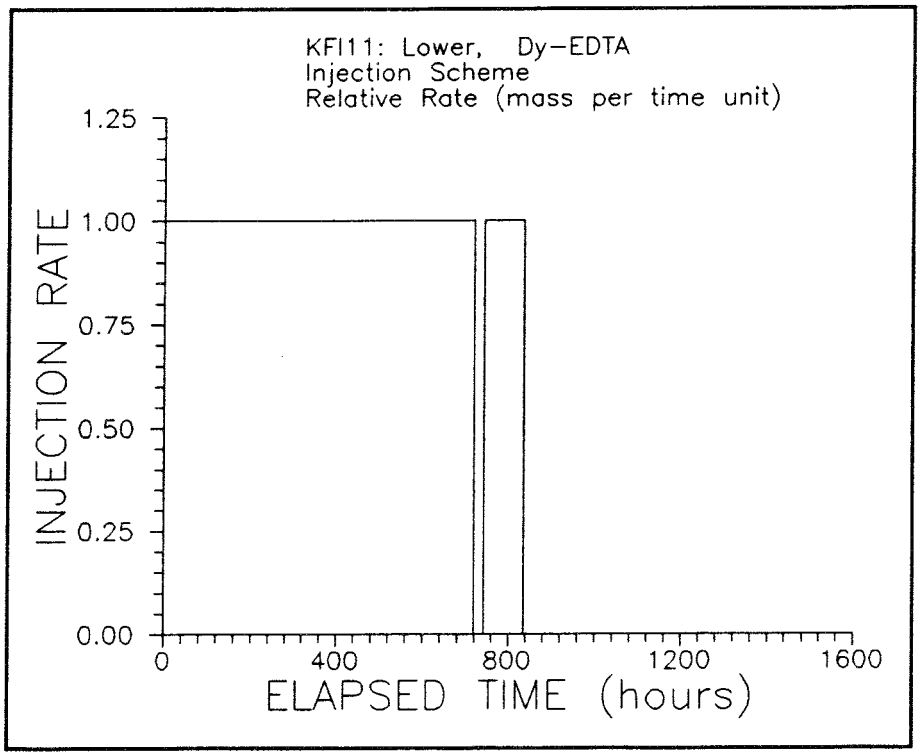


Injection scheme Dy-EDTA

# APPENDIX H

## 1-D MODEL ESTIMATES

CONTENTS Page

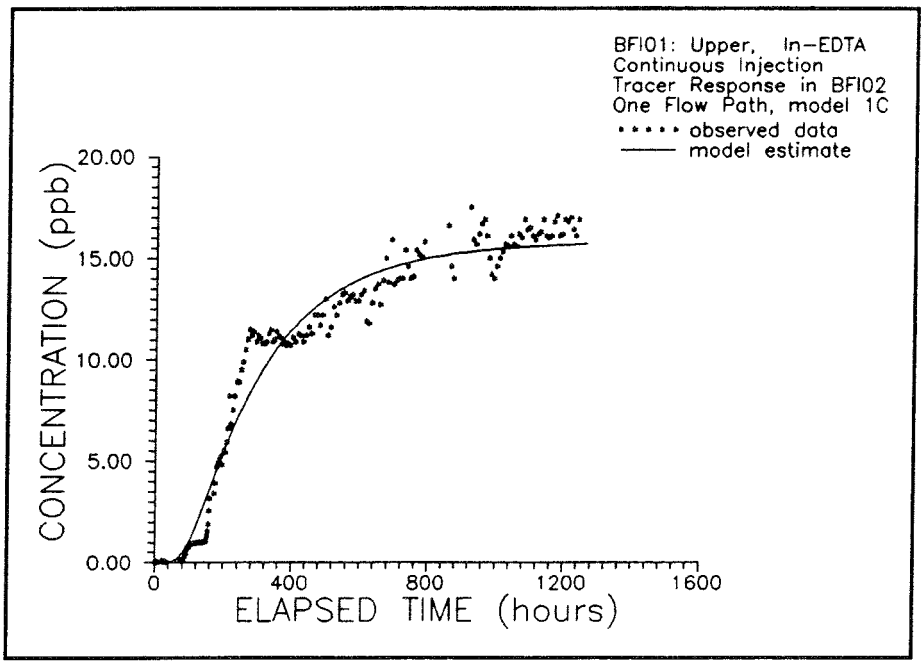


Model estimate In-EDTA, one flow path, 1C

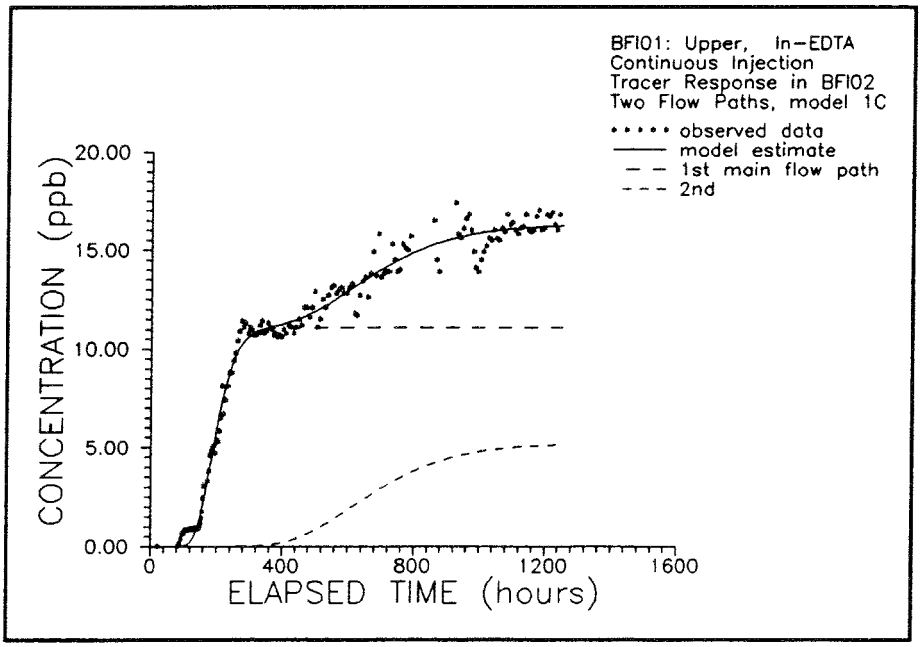


Model estimate In-EDTA, two flow paths, 1C

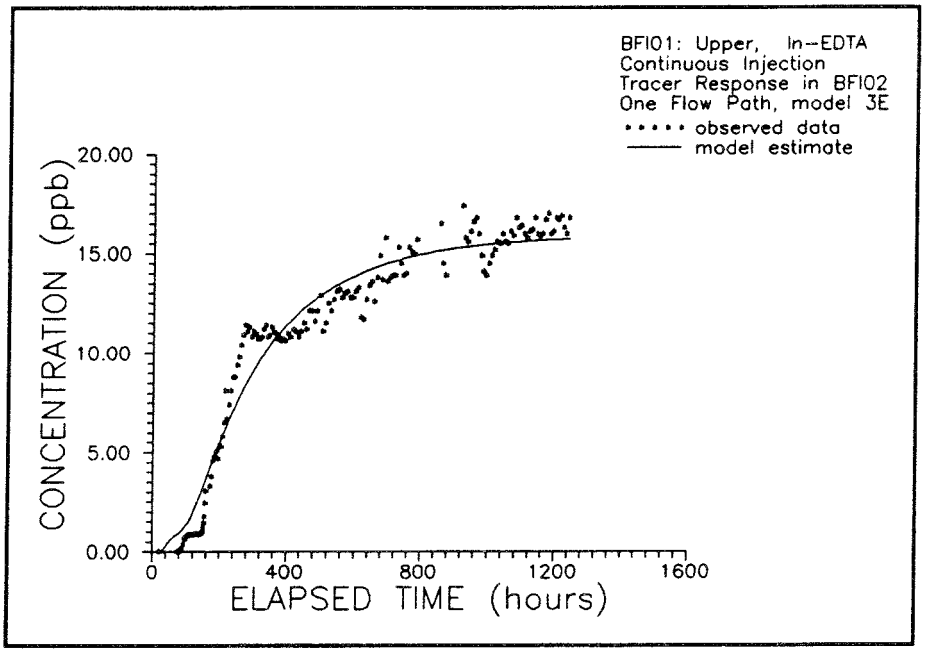


Model estimate In-EDTA, one flow path, 3E

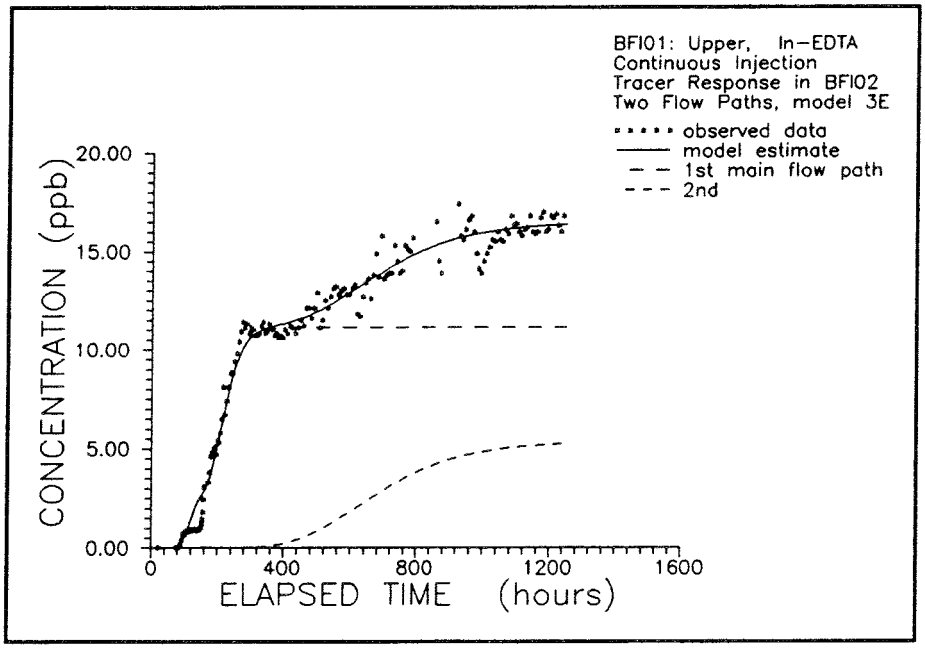


Model estimate In-EDTA, two flow paths, 3E

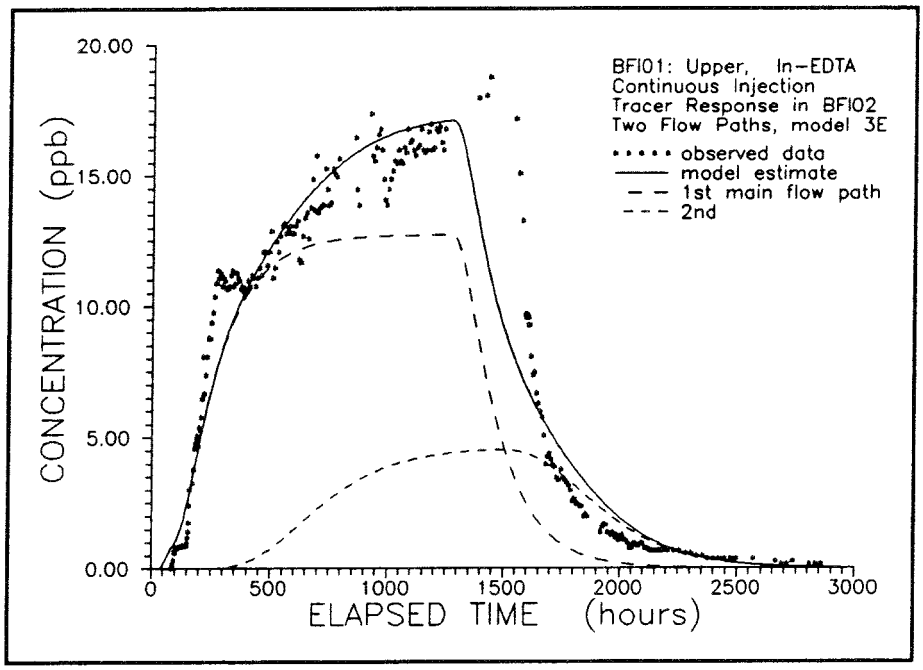


Model estimate In-EDTA, two flow paths, actual inj. stop time, 3E

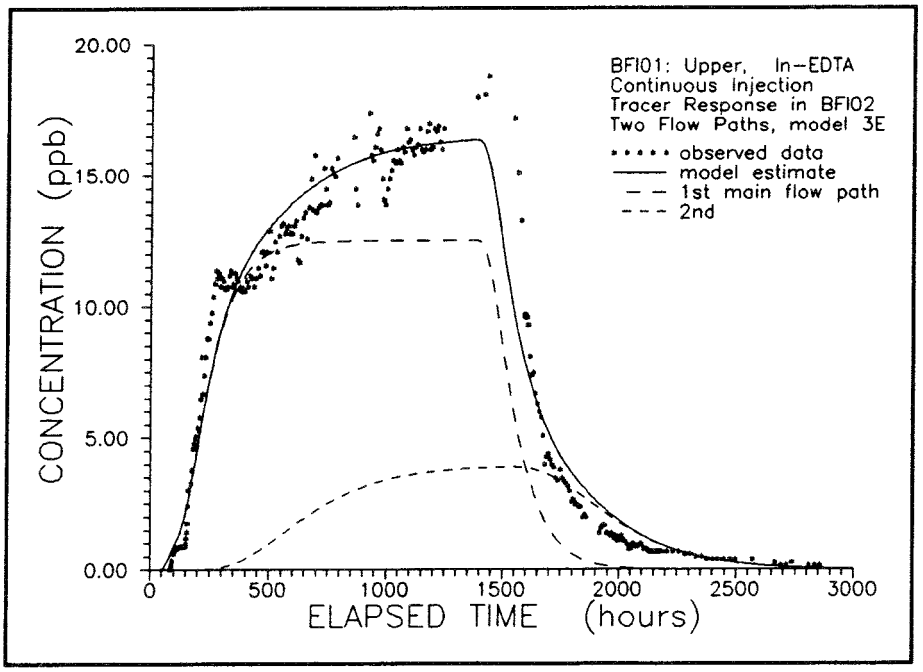


Model estimate In-EDTA, two flow paths, adjusted inj. stop time, 3E

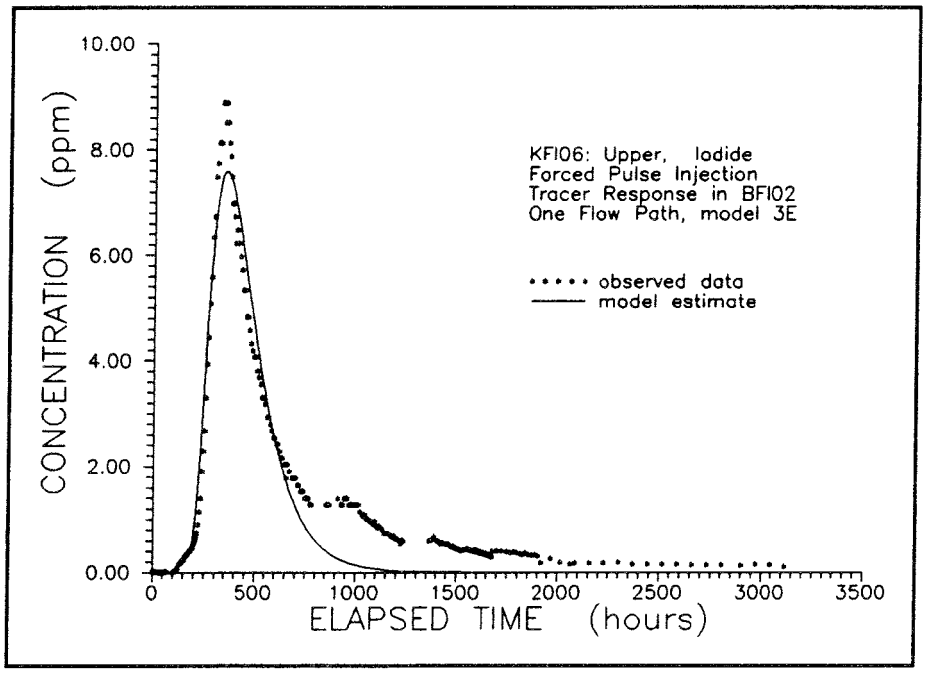


Model estimate Iodide, one flow path, 3E

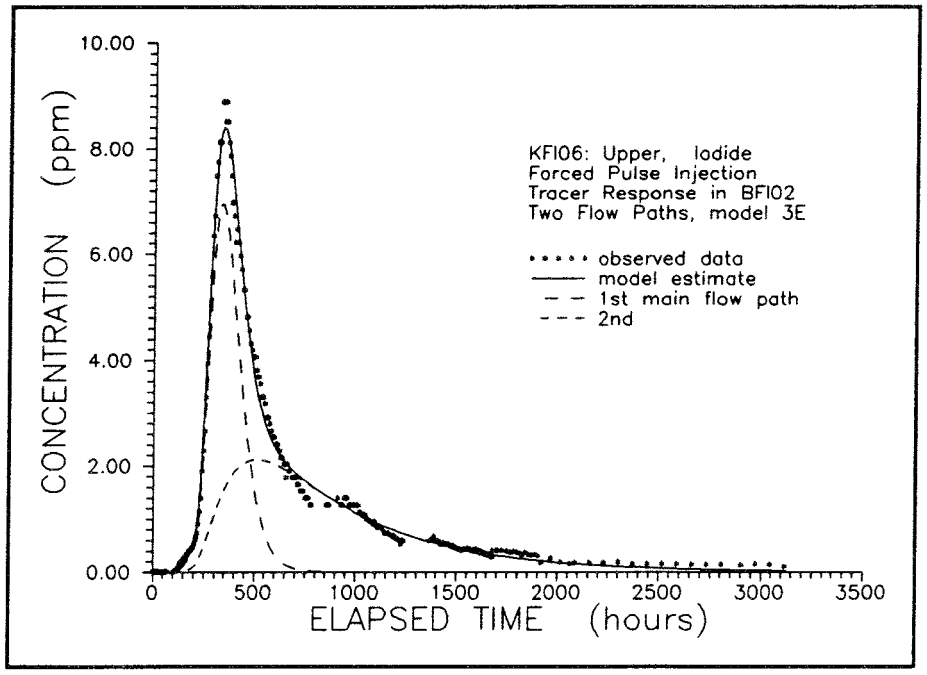


Model estimate Iodide, two flow paths, 3E

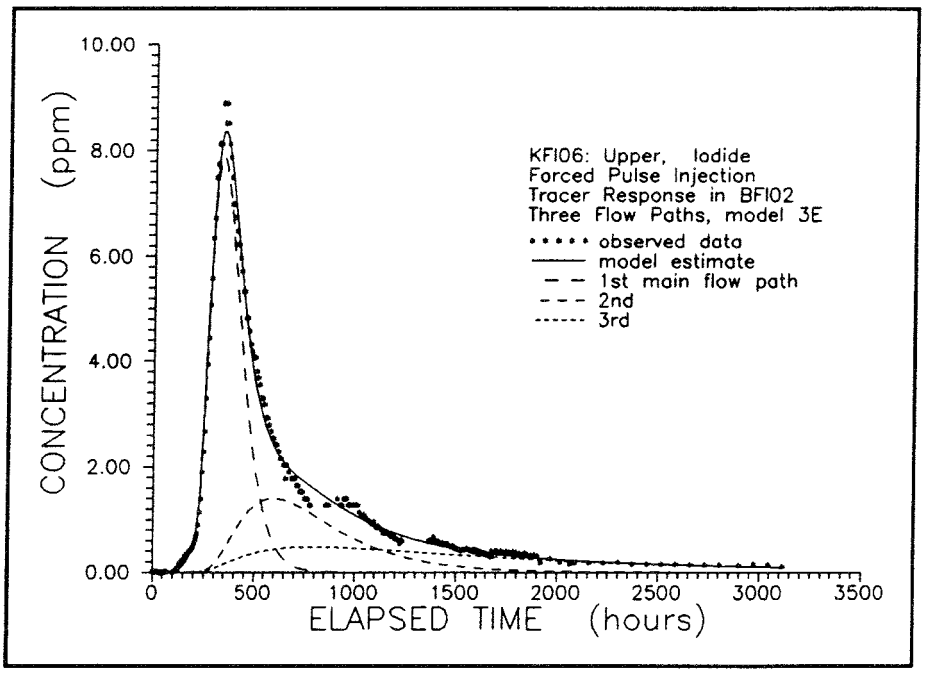


Model estimate Iodide, three flow paths, 3E

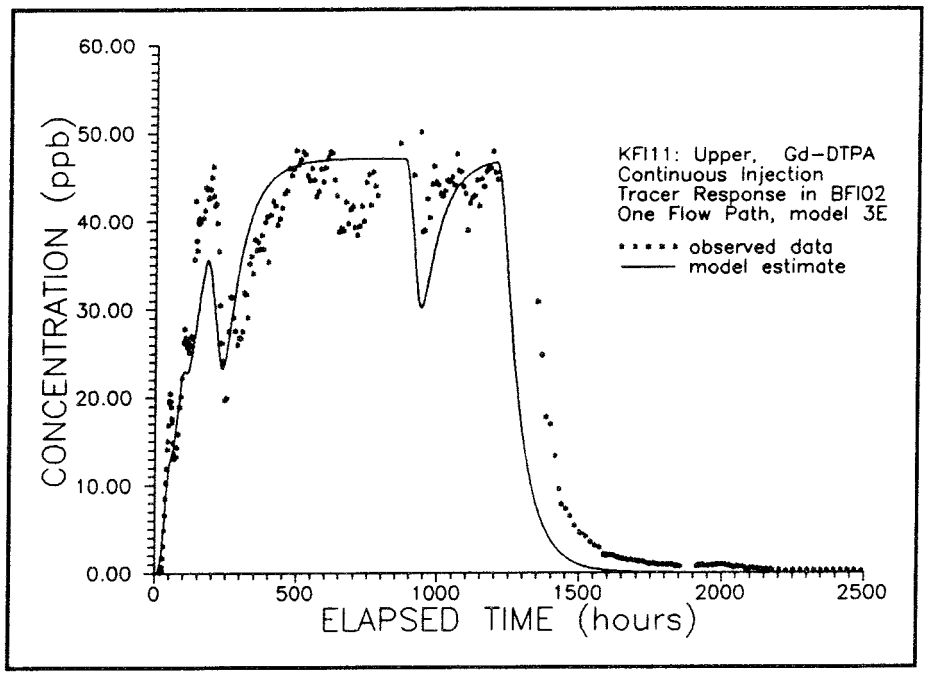


Model estimate Gd-DTPA, one flow path, actual inj. stop time, 3E

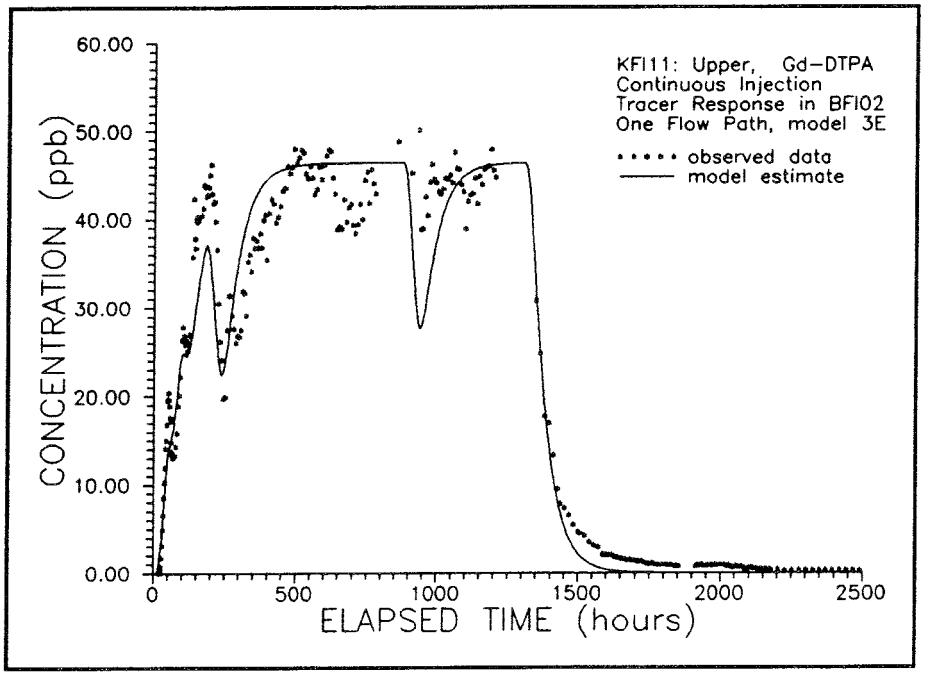


Model estimate Gd-DTPA, one flow path, adjusted inj. stop time, 3E

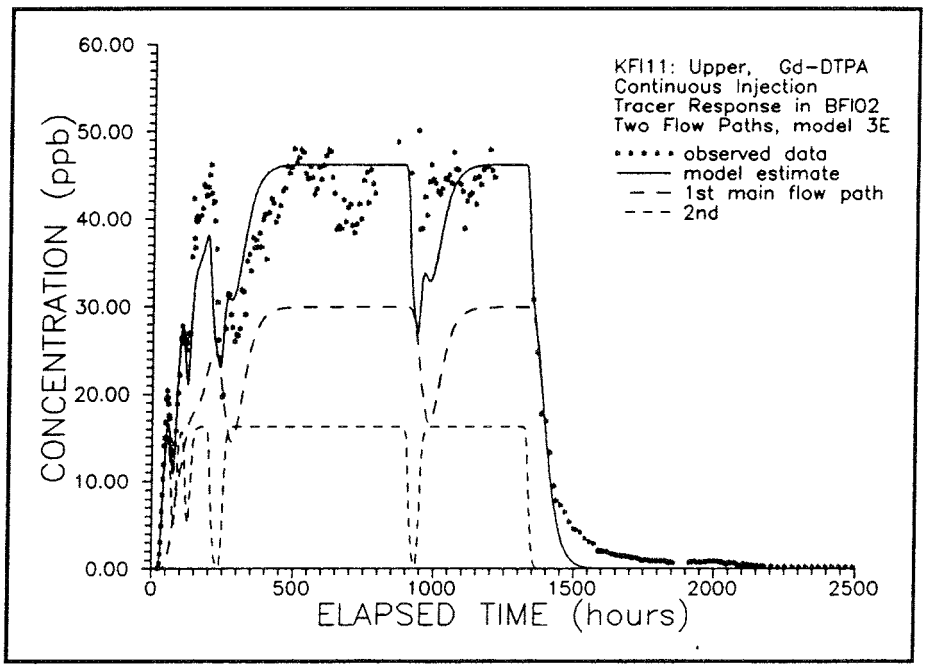


Model estimate Gd-DTPA, two flow paths, adjusted inj. stop time, 3E

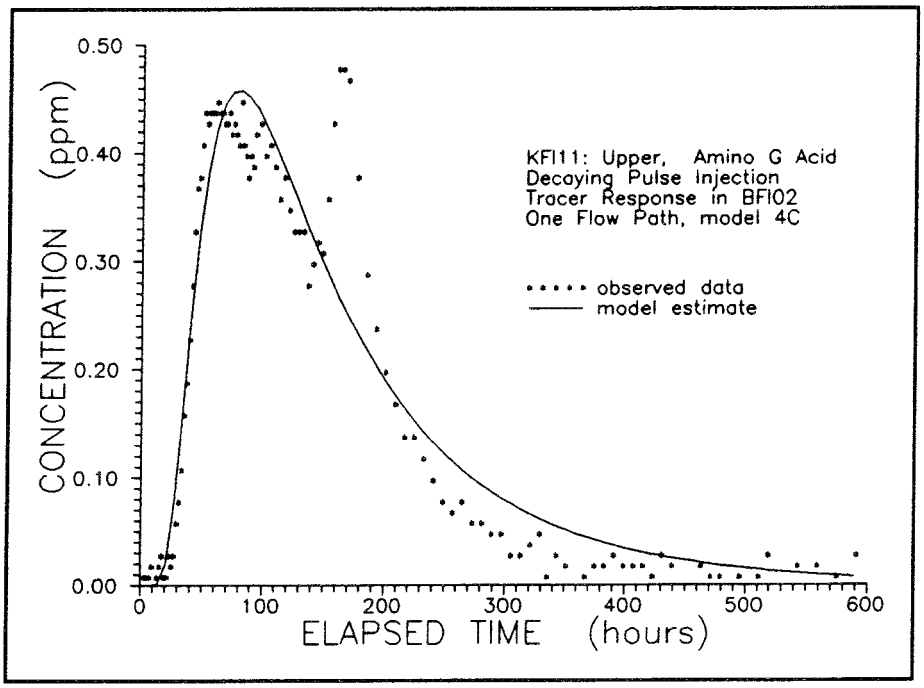


Model estimate Amino G Acid, one flow path, 4C

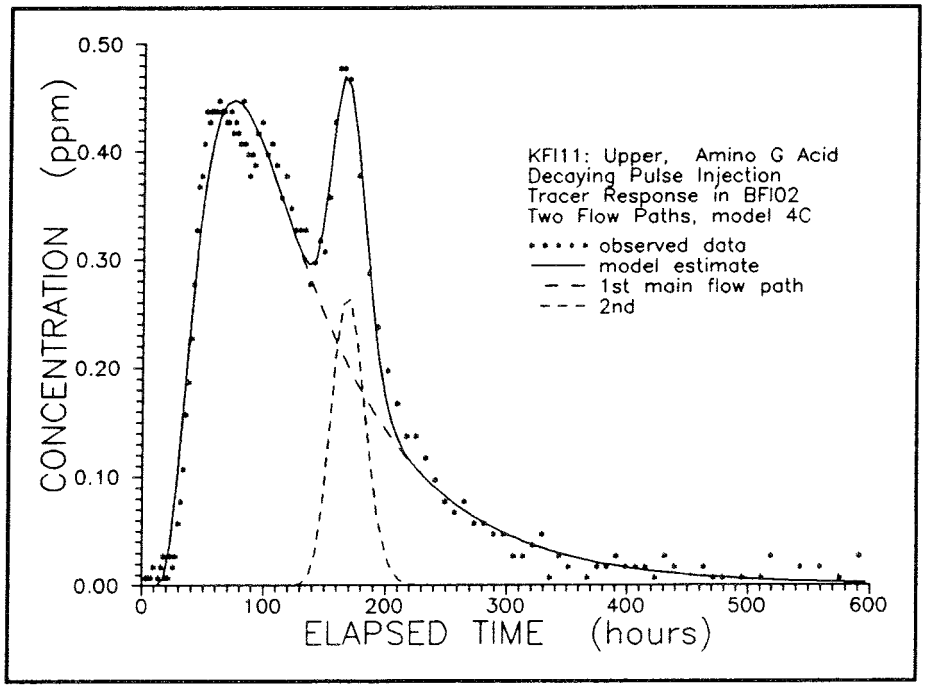


Model estimate Amino G Acid, two flow paths, 4C

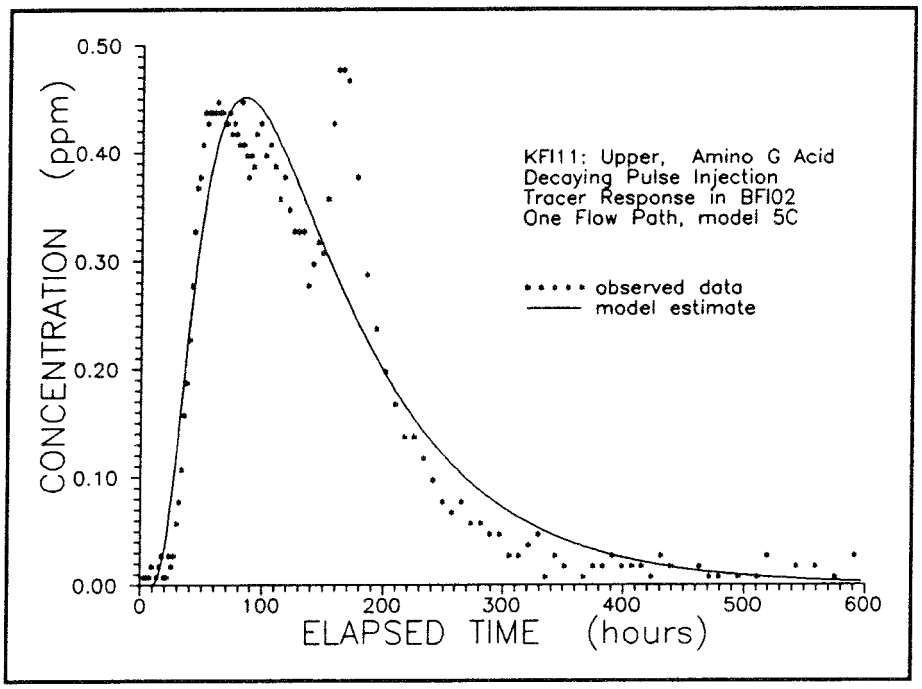


Model estimate Amino G Acid, one flow path, 5C

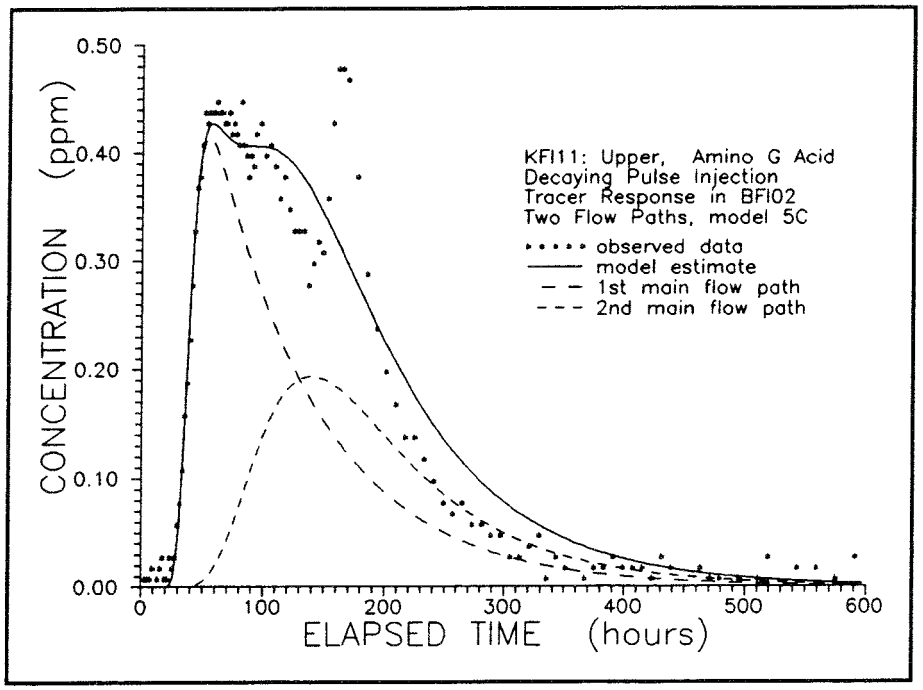


Model estimate Amino G Acid, two flow paths, 5C

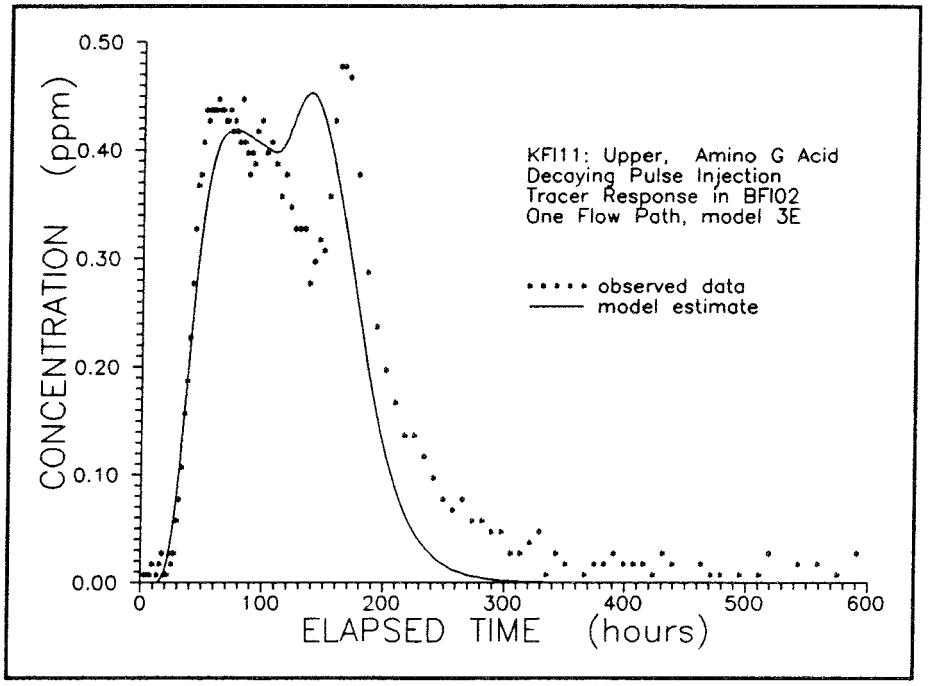


Model estimate Amino G Acid, one flow path, 3E

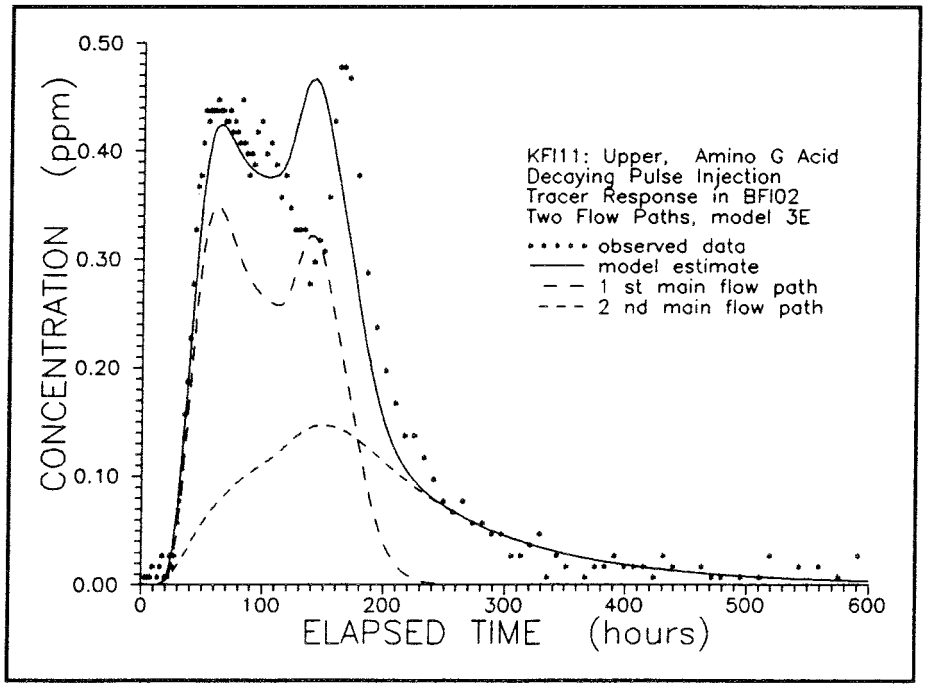


Model estimate Amino G Acid, two flow paths, 3E

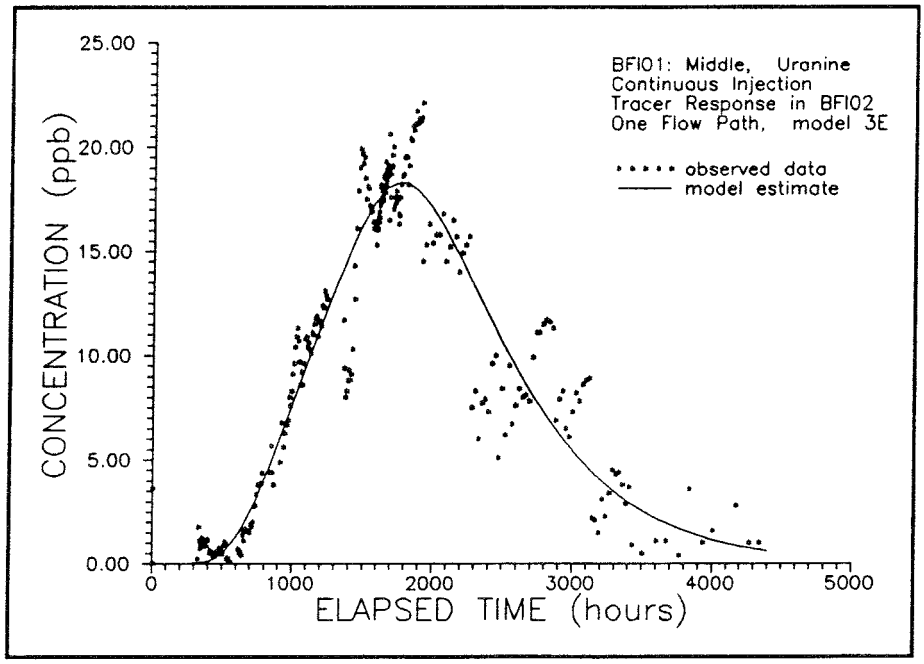


Model estimate Uranine, one flow path, 3E

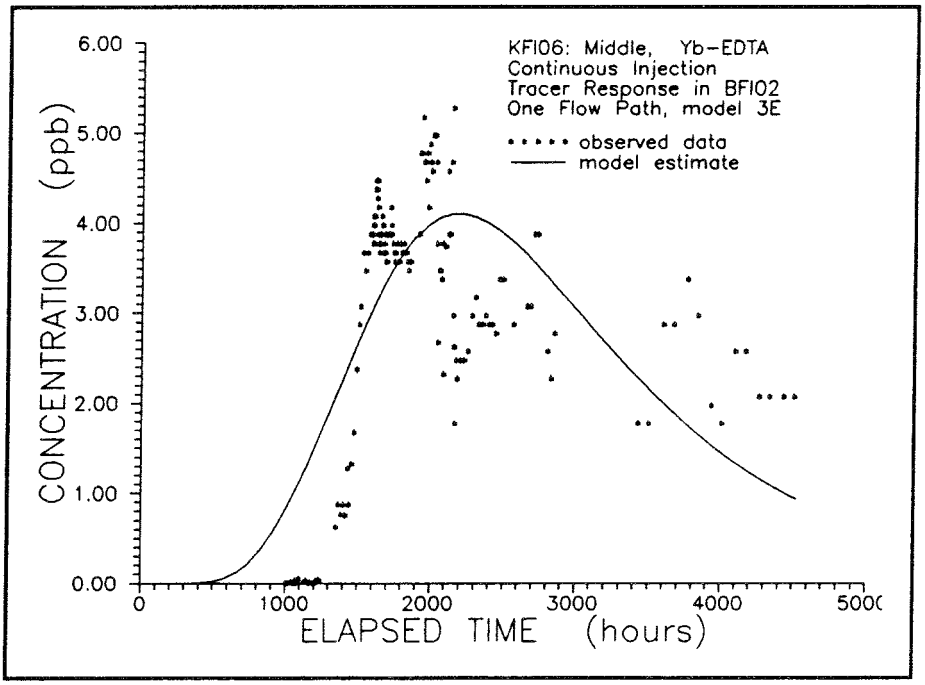


Model estimate Yb-EDTA, one flow path, 3E

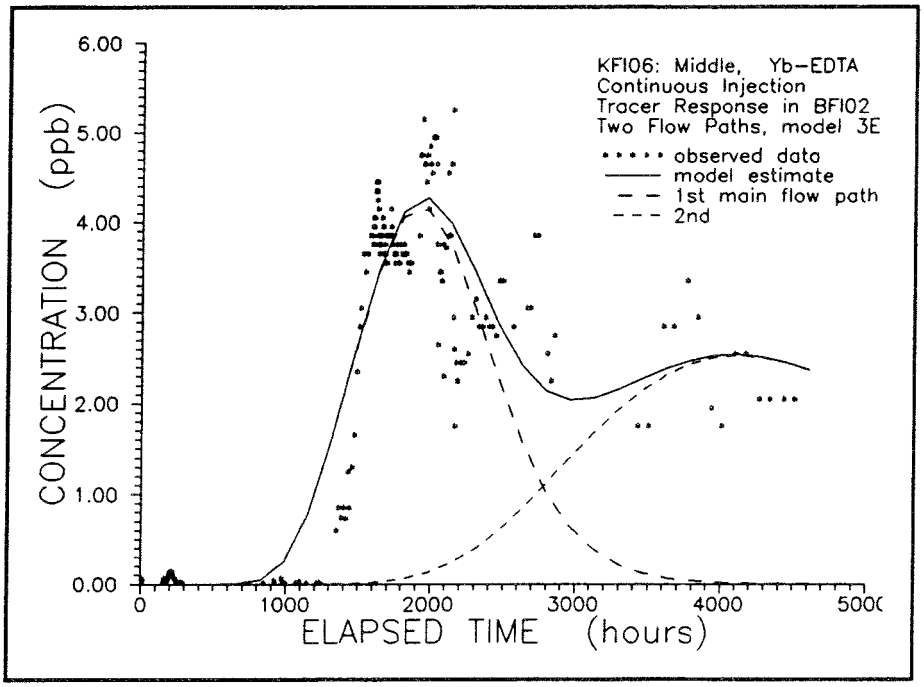


Model estimate Yb-EDTA, two flow paths, 3E

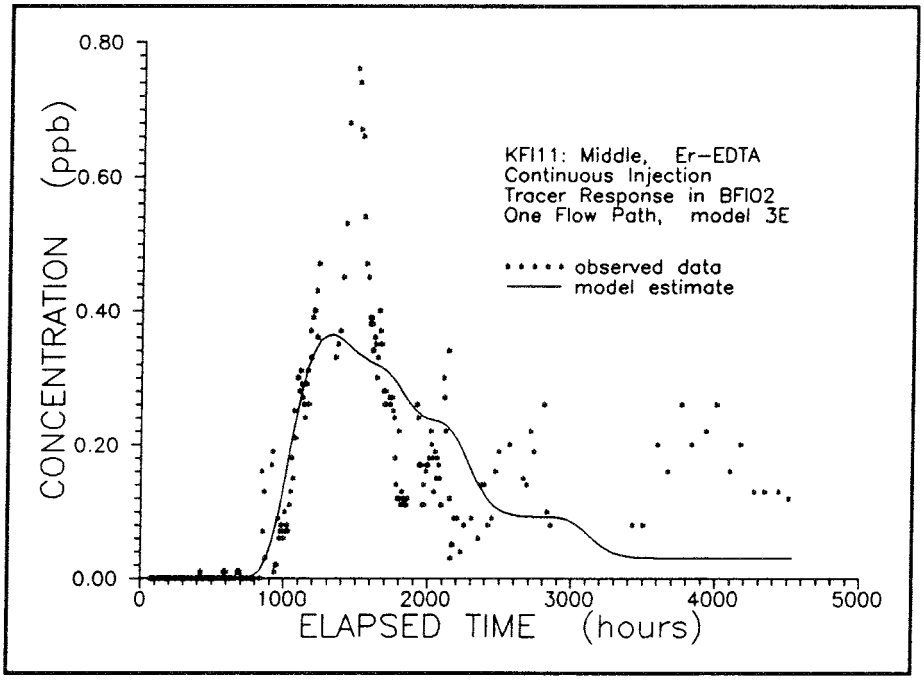


Model estimate Er-EDTA, one flow path, 3E

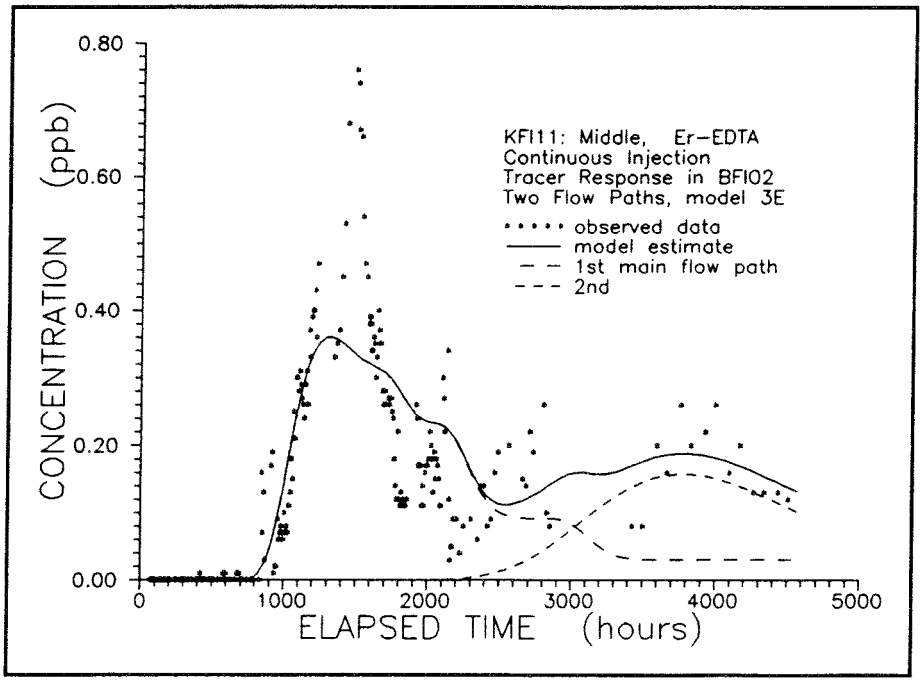


Model estimate Er-EDTA, two flow paths, 3E

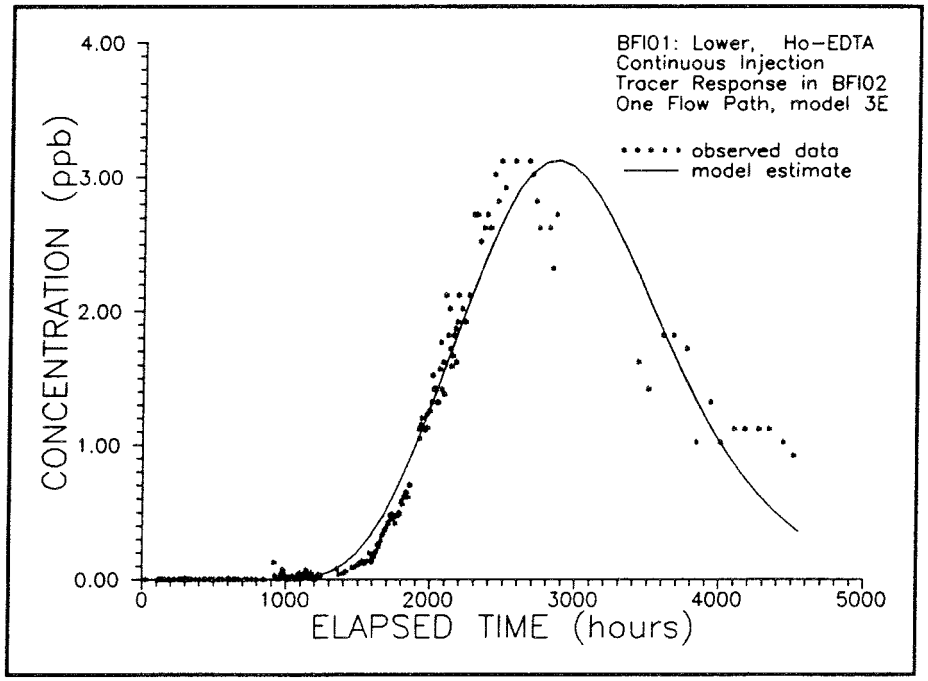


Model estimate Ho-EDTA, one flow path, 3E

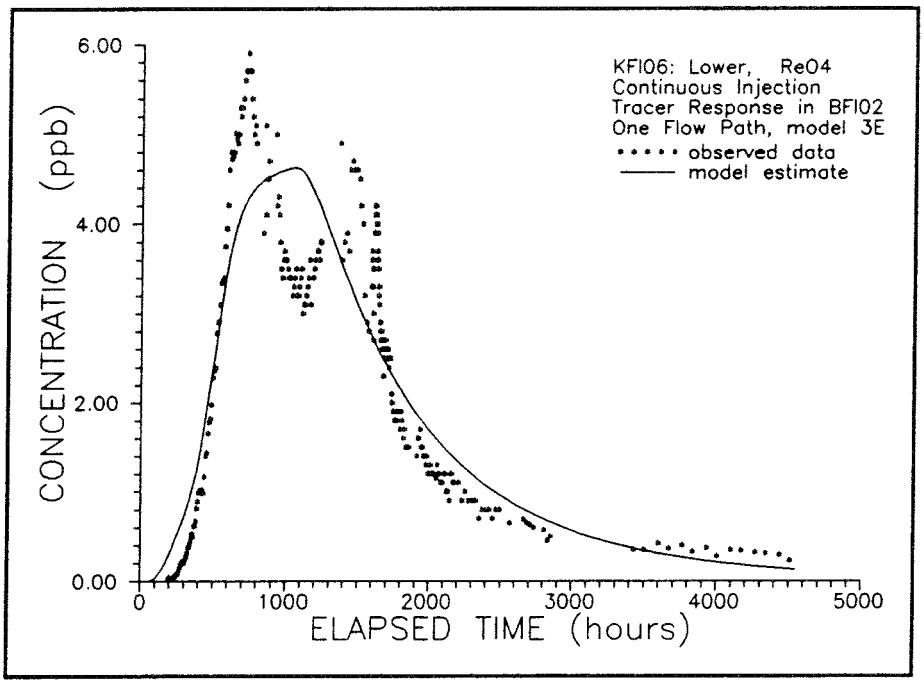


Model estimate $ReO_4^-$, one flow path, 3E

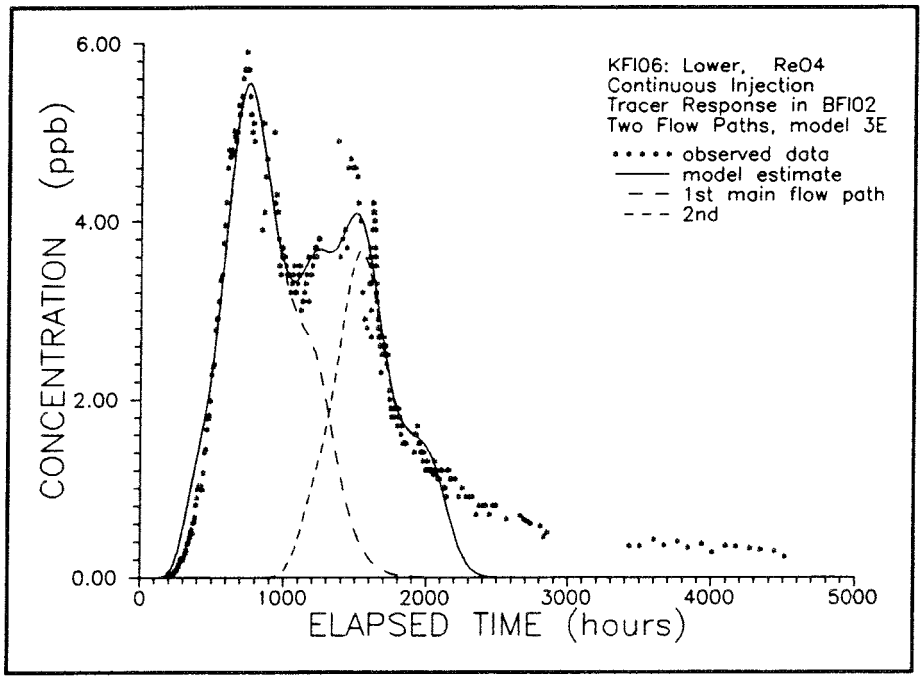


Model estimate $ReO_4^-$, two flow paths, 3E

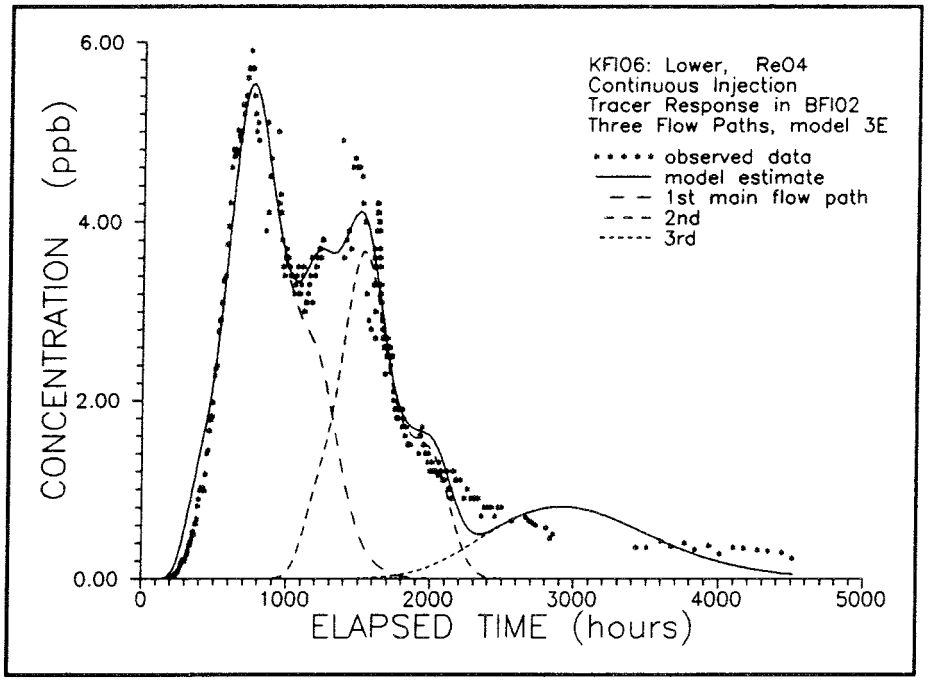


Model estimate $ReO_4^-$, three flow paths, 3E

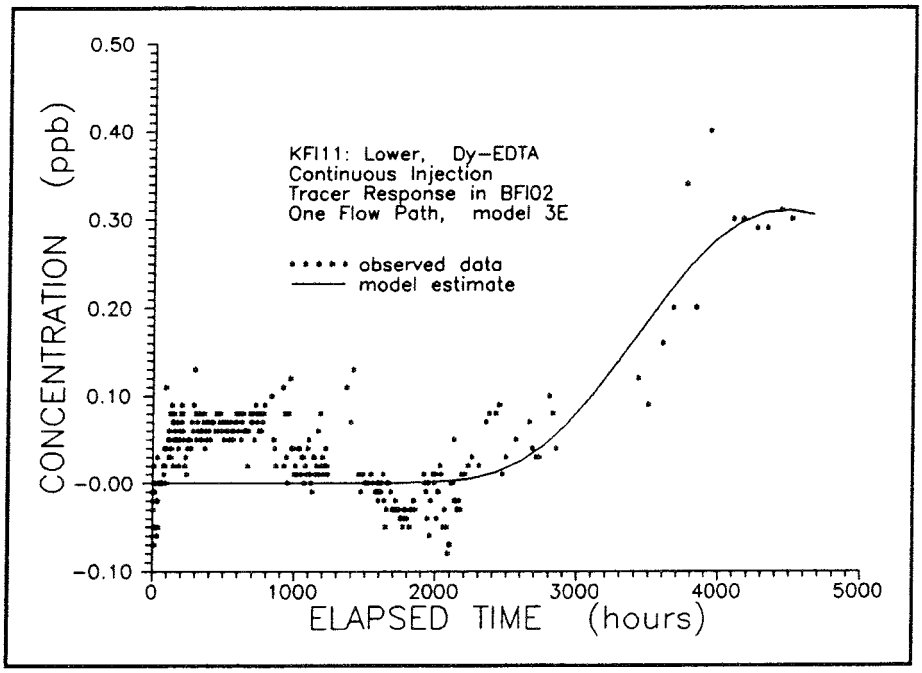


Model estimate Dy-EDTA, one flow path, 3E

# APPENDIX I

## STATISTICS OF THE 1-D MODELLING

CONTENTS Page

********** REGRESSION SUMMARY **********

In-EDTA BFI01, UPPER SECTION
DISTANCE: 168 METRES
NUMBER OF FLOW PATHS: 1

APPLIED MODEL: MODEL1C, CONSTANT INJ. RATE

NUMBER OF PARAMETERS: 3

INPUT DATA FILE NAME: 4.DAT

BACKGROUND LEVEL FOR INPUT DATA: 0.1000

FINAL ESTIMATE FOR PARAMETER 1 = 0.1401E-03
FINAL ESTIMATE FOR PARAMETER 2 = 0.6403E-02
FINAL ESTIMATE FOR PARAMETER 3 = 0.1585E+02

**********

REGRESSION STATISTICS

NO. OF OBSERVATIONS: 177

SUM OF SQUARED DIFFERENCES = 0.208E+03

ERROR VARIANCE = 0.119E+01

CORRELATION COEFFICIENT = .98330E+00

STANDARD ERROR FOR PARAMETER 1 = 0.524E-05
STANDARD ERROR FOR PARAMETER 2 = 0.505E-03
STANDARD ERROR FOR PARAMETER 3 = 0.226E+00

CORRELATION BETWEEN PARAMETERS 1 AND 2 = -.6703E+00
CORRELATION BETWEEN PARAMETERS 1 AND 3 = -.8621E+00
CORRELATION BETWEEN PARAMETERS 2 AND 3 = 0.5941E+00

********** REGRESSION SUMMARY **********

In-EDTA BFI01, UPPER SECTION
DISTANCE: 168 METRES
NUMBER OF FLOW PATHS: 2

APPLIED MODEL: MODEL1C, CONSTANT INJ. RATE

NUMBER OF PARAMETERS: 6

INPUT DATA FILE NAME: 4.DAT

BACKGROUND LEVEL FOR INPUT DATA: 0.1000

FINAL ESTIMATE FOR PARAMETER 1 = 0.2311E-03
FINAL ESTIMATE FOR PARAMETER 2 = 0.1141E-02
FINAL ESTIMATE FOR PARAMETER 3 = 0.1109E+02
FINAL ESTIMATE FOR PARAMETER 4 = 0.6701E-04
FINAL ESTIMATE FOR PARAMETER 5 = 0.4911E-03
FINAL ESTIMATE FOR PARAMETER 6 = 0.5205E+01

**********

REGRESSION STATISTICS

NO. OF OBSERVATIONS: 177

SUM OF SQUARED DIFFERENCES = 0.624E+02

ERROR VARIANCE = 0.365E+00

CORRELATION COEFFICIENT = .99501E+00

STANDARD ERROR FOR PARAMETER 1 = 0.266E-05
STANDARD ERROR FOR PARAMETER 2 = 0.124E-03
STANDARD ERROR FOR PARAMETER 3 = 0.196E+00
STANDARD ERROR FOR PARAMETER 4 = 0.192E-05
STANDARD ERROR FOR PARAMETER 5 = 0.137E-03
STANDARD ERROR FOR PARAMETER 6 = 0.328E+00

CORRELATION BETWEEN PARAMETERS 1 AND 2 = -.4728E+00
CORRELATION BETWEEN PARAMETERS 1 AND 3 = -.7432E+00
CORRELATION BETWEEN PARAMETERS 1 AND 4 = 0.1123E+00
CORRELATION BETWEEN PARAMETERS 1 AND 5 = 0.5184E+00
CORRELATION BETWEEN PARAMETERS 1 AND 6 = 0.6112E+00
CORRELATION BETWEEN PARAMETERS 2 AND 3 = 0.5609E+00
CORRELATION BETWEEN PARAMETERS 2 AND 4 = -.9911E-01
CORRELATION BETWEEN PARAMETERS 2 AND 5 = -.3723E+00
CORRELATION BETWEEN PARAMETERS 2 AND 6 = -.4519E+00
CORRELATION BETWEEN PARAMETERS 3 AND 4 = -.1381E+00
CORRELATION BETWEEN PARAMETERS 3 AND 5 = -.7144E+00
CORRELATION BETWEEN PARAMETERS 3 AND 6 = -.8310E+00
CORRELATION BETWEEN PARAMETERS 4 AND 5 = -.3800E+00
CORRELATION BETWEEN PARAMETERS 4 AND 6 = -.3578E+00
CORRELATION BETWEEN PARAMETERS 5 AND 6 = 0.8735E+00

********** REGRESSION SUMMARY **********

In-EDTA BF101, UPPER SECTION
DISTANCE: 168 METRES
NUMBER OF FLOW PATHS: 1

APPLIED MODEL: MODEL3E, VARIABLE INJ. SCHEME

NUMBER OF PARAMETERS: 3

INPUT DATA FILE NAME: 4.DAT

BACKGROUND LEVEL FOR INPUT DATA: 0.1000

FINAL ESTIMATE FOR PARAMETER 1 = 0.2326E-03
FINAL ESTIMATE FOR PARAMETER 2 = 0.1919E-01
FINAL ESTIMATE FOR PARAMETER 3 = 0.1595E+02

**********

REGRESSION STATISTICS

NO. OF OBSERVATIONS: 177

SUM OF SQUARED DIFFERENCES = 0.205E+03

ERROR VARIANCE = 0.118E+01

CORRELATION COEFFICIENT = .98380E+00

STANDARD ERROR FOR PARAMETER 1 = 0.633E-05
STANDARD ERROR FOR PARAMETER 2 = 0.270E-02
STANDARD ERROR FOR PARAMETER 3 = 0.243E+00

CORRELATION BETWEEN PARAMETERS 1 AND 2 = 0.3898E+00
CORRELATION BETWEEN PARAMETERS 1 AND 3 = -.3309E+00
CORRELATION BETWEEN PARAMETERS 2 AND 3 = 0.6231E+00

********** REGRESSION SUMMARY **********

In-EDTA BF101, UPPER SECTION
DISTANCE: 168 METRES
NUMBER OF FLOW PATHS: 2

APPLIED MODEL: MODEL3E, VARIABLE INJ. SCHEME

NUMBER OF PARAMETERS: 6

INPUT DATA FILE NAME: 4.dat

BACKGROUND LEVEL FOR INPUT DATA: 0.1000

FINAL ESTIMATE FOR PARAMETER 1 = 0.3038E-03
FINAL ESTIMATE FOR PARAMETER 2 = 0.1902E-02
FINAL ESTIMATE FOR PARAMETER 3 = 0.1119E+02
FINAL ESTIMATE FOR PARAMETER 4 = 0.7401E-04
FINAL ESTIMATE FOR PARAMETER 5 = 0.5589E-03
FINAL ESTIMATE FOR PARAMETER 6 = 0.5087E+01

**********

REGRESSION STATISTICS

NO. OF OBSERVATIONS: 177

SUM OF SQUARED DIFFERENCES = 0.777E+02

ERROR VARIANCE = 0.455E+00

CORRELATION COEFFICIENT = .99385E+00

STANDARD ERROR FOR PARAMETER 1 = 0.509E-05
STANDARD ERROR FOR PARAMETER 2 = 0.355E-03
STANDARD ERROR FOR PARAMETER 3 = 0.221E+00
STANDARD ERROR FOR PARAMETER 4 = 0.223E-05
STANDARD ERROR FOR PARAMETER 5 = 0.202E-03
STANDARD ERROR FOR PARAMETER 6 = 0.364E+00

CORRELATION BETWEEN PARAMETERS 1 AND 2 = -.1896E+00
CORRELATION BETWEEN PARAMETERS 1 AND 3 = -.6810E+00
CORRELATION BETWEEN PARAMETERS 1 AND 4 = 0.3295E+00
CORRELATION BETWEEN PARAMETERS 1 AND 5 = 0.4785E+00
CORRELATION BETWEEN PARAMETERS 1 AND 6 = 0.5661E+00
CORRELATION BETWEEN PARAMETERS 2 AND 3 = 0.5161E+00
CORRELATION BETWEEN PARAMETERS 2 AND 4 = -.2610E+00
CORRELATION BETWEEN PARAMETERS 2 AND 5 = -.3300E+00
CORRELATION BETWEEN PARAMETERS 2 AND 6 = -.4132E+00
CORRELATION BETWEEN PARAMETERS 3 AND 4 = -.4799E+00
CORRELATION BETWEEN PARAMETERS 3 AND 5 = -.7122E+00
CORRELATION BETWEEN PARAMETERS 3 AND 6 = -.8361E+00
CORRELATION BETWEEN PARAMETERS 4 AND 5 = 0.4593E-01
CORRELATION BETWEEN PARAMETERS 4 AND 6 = 0.2764E-01
CORRELATION BETWEEN PARAMETERS 5 AND 6 = 0.8714E+00

********** REGRESSION SUMMARY **********

In-EDTA BFI01, UPPER SECTION
DISTANCE: 168 METRES
NUMBER OF FLOW PATHS: 2

APPLIED MODEL: MODEL3E, ACTUAL INJ. STOP TIME

NUMBER OF PARAMETERS: 6

INPUT DATA FILE NAME: 5.dat

BACKGROUND LEVEL FOR INPUT DATA: 0.1320

FINAL ESTIMATE FOR PARAMETER 1 = 0.2487E-03
FINAL ESTIMATE FOR PARAMETER 2 = 0.1099E-01
FINAL ESTIMATE FOR PARAMETER 3 = 0.1273E+02
FINAL ESTIMATE FOR PARAMETER 4 = 0.7063E-04
FINAL ESTIMATE FOR PARAMETER 5 = 0.8662E-03
FINAL ESTIMATE FOR PARAMETER 6 = 0.4605E+01

**********

REGRESSION STATISTICS

NO. OF OBSERVATIONS: 291

SUM OF SQUARED DIFFERENCES = 0.652E+03

ERROR VARIANCE = 0.229E+01

CORRELATION COEFFICIENT = .97075E+00

STANDARD ERROR FOR PARAMETER 1 = 0.742E-04
STANDARD ERROR FOR PARAMETER 2 = 0.743E-02
STANDARD ERROR FOR PARAMETER 3 = 0.480E+01
STANDARD ERROR FOR PARAMETER 4 = 0.201E-04
STANDARD ERROR FOR PARAMETER 5 = 0.101E-02
STANDARD ERROR FOR PARAMETER 6 = 0.483E+01

CORRELATION BETWEEN PARAMETERS 1 AND 2 = -.9047E+00
CORRELATION BETWEEN PARAMETERS 1 AND 3 = -.9934E+00
CORRELATION BETWEEN PARAMETERS 1 AND 4 = 0.9758E+00
CORRELATION BETWEEN PARAMETERS 1 AND 5 = 0.9112E+00
CORRELATION BETWEEN PARAMETERS 1 AND 6 = 0.9927E+00
CORRELATION BETWEEN PARAMETERS 2 AND 3 = 0.9328E+00
CORRELATION BETWEEN PARAMETERS 2 AND 4 = -.8666E+00
CORRELATION BETWEEN PARAMETERS 2 AND 5 = -.7733E+00
CORRELATION BETWEEN PARAMETERS 2 AND 6 = -.9313E+00
CORRELATION BETWEEN PARAMETERS 3 AND 4 = -.9813E+00
CORRELATION BETWEEN PARAMETERS 3 AND 5 = -.9183E+00
CORRELATION BETWEEN PARAMETERS 3 AND 6 = -.9990E+00
CORRELATION BETWEEN PARAMETERS 4 AND 5 = 0.9506E+00
CORRELATION BETWEEN PARAMETERS 4 AND 6 = 0.9804E+00
CORRELATION BETWEEN PARAMETERS 5 AND 6 = 0.9247E+00

********** REGRESSION SUMMARY **********

In-EDTA BFI01, UPPER SECTION
DISTANCE: 168 METRES
NUMBER OF FLOW PATHS: 2

APPLIED MODEL: MODEL3E, COMPENSATED INJ. STOP TIME

NUMBER OF PARAMETERS: 6

INPUT DATA FILE NAME: 5.dat

BACKGROUND LEVEL FOR INPUT DATA: 0.1320

FINAL ESTIMATE FOR PARAMETER 1 = 0.2557E-03
FINAL ESTIMATE FOR PARAMETER 2 = 0.6382E-02
FINAL ESTIMATE FOR PARAMETER 3 = 0.1251E+02
FINAL ESTIMATE FOR PARAMETER 4 = 0.7699E-04
FINAL ESTIMATE FOR PARAMETER 5 = 0.1218E-02
FINAL ESTIMATE FOR PARAMETER 6 = 0.3942E+01

**********

REGRESSION STATISTICS

NO. OF OBSERVATIONS: 291

SUM OF SQUARED DIFFERENCES = 0.380E+03

ERROR VARIANCE = 0.133E+01

CORRELATION COEFFICIENT = .98312E+00

STANDARD ERROR FOR PARAMETER 1 = 0.469E-04
STANDARD ERROR FOR PARAMETER 2 = 0.288E-02
STANDARD ERROR FOR PARAMETER 3 = 0.351E+01
STANDARD ERROR FOR PARAMETER 4 = 0.324E-04
STANDARD ERROR FOR PARAMETER 5 = 0.191E-02
STANDARD ERROR FOR PARAMETER 6 = 0.356E+01

CORRELATION BETWEEN PARAMETERS 1 AND 2 = -.8825E+00
CORRELATION BETWEEN PARAMETERS 1 AND 3 = -.9929E+00
CORRELATION BETWEEN PARAMETERS 1 AND 4 = 0.9872E+00
CORRELATION BETWEEN PARAMETERS 1 AND 5 = 0.9571E+00
CORRELATION BETWEEN PARAMETERS 1 AND 6 = 0.9924E+00
CORRELATION BETWEEN PARAMETERS 2 AND 3 = 0.9115E+00
CORRELATION BETWEEN PARAMETERS 2 AND 4 = -.8824E+00
CORRELATION BETWEEN PARAMETERS 2 AND 5 = -.8232E+00
CORRELATION BETWEEN PARAMETERS 2 AND 6 = -.9104E+00
CORRELATION BETWEEN PARAMETERS 3 AND 4 = -.9947E+00
CORRELATION BETWEEN PARAMETERS 3 AND 5 = -.9662E+00
CORRELATION BETWEEN PARAMETERS 3 AND 6 = -.9990E+00
CORRELATION BETWEEN PARAMETERS 4 AND 5 = 0.9759E+00
CORRELATION BETWEEN PARAMETERS 4 AND 6 = 0.9935E+00
CORRELATION BETWEEN PARAMETERS 5 AND 6 = 0.9699E+00

********** REGRESSION SUMMARY **********

**Iodide** KFI06, UPPER SECTION
DISTANCE: 189 METRES
NUMBER OF FLOW PATHS: 1

APPLIED MODEL: MODEL3E, VARIABLE INJ. SCHEME

NUMBER OF PARAMETERS: 3
INPUT DATA FILE NAME: 3.dat
BACKGROUND LEVEL FOR INPUT DATA: 0.0000

FINAL ESTIMATE FOR PARAMETER 1 = 0.1821E-03
FINAL ESTIMATE FOR PARAMETER 2 = 0.4376E-02
FINAL ESTIMATE FOR PARAMETER 3 = 0.6044E+03

**********

REGRESSION STATISTICS

NO. OF OBSERVATIONS: 292
SUM OF SQUARED DIFFERENCES = 0.844E+02
ERROR VARIANCE = 0.292E+00
CORRELATION COEFFICIENT = .97657E+00

STANDARD ERROR FOR PARAMETER 1 = 0.186E-05
STANDARD ERROR FOR PARAMETER 2 = 0.165E-03
STANDARD ERROR FOR PARAMETER 3 = 0.107E+02

CORRELATION BETWEEN PARAMETERS 1 AND 2 = -.2646E+00
CORRELATION BETWEEN PARAMETERS 1 AND 3 = -.5811E+00
CORRELATION BETWEEN PARAMETERS 2 AND 3 = 0.5208E+00

********** REGRESSION SUMMARY **********

**Iodide** KFI06, UPPER SECTION
DISTANCE: 189 METRES
NUMBER OF FLOW PATHS: 2

APPLIED MODEL: MODEL3E, VARIABLE INJ. SCHEME

NUMBER OF PARAMETERS: 6
INPUT DATA FILE NAME: 3.dat
BACKGROUND LEVEL FOR INPUT DATA: 0.0000

FINAL ESTIMATE FOR PARAMETER 1 = 0.2229E-03
FINAL ESTIMATE FOR PARAMETER 2 = 0.2442E-02
FINAL ESTIMATE FOR PARAMETER 3 = 0.3364E+03
FINAL ESTIMATE FOR PARAMETER 4 = 0.8422E-04
FINAL ESTIMATE FOR PARAMETER 5 = 0.4786E-02
FINAL ESTIMATE FOR PARAMETER 6 = 0.4727E+03

**********

REGRESSION STATISTICS

NO. OF OBSERVATIONS: 292
SUM OF SQUARED DIFFERENCES = 0.690E+01
ERROR VARIANCE = 0.241E-01
CORRELATION COEFFICIENT = .99732E+00

STANDARD ERROR FOR PARAMETER 1 = 0.108E-05
STANDARD ERROR FOR PARAMETER 2 = 0.115E-03
STANDARD ERROR FOR PARAMETER 3 = 0.240E+02
STANDARD ERROR FOR PARAMETER 4 = 0.430E-05
STANDARD ERROR FOR PARAMETER 5 = 0.862E-03
STANDARD ERROR FOR PARAMETER 6 = 0.272E+02

CORRELATION BETWEEN PARAMETERS 1 AND 2 = -.6968E+00
CORRELATION BETWEEN PARAMETERS 1 AND 3 = -.6879E+00
CORRELATION BETWEEN PARAMETERS 1 AND 4 = 0.6875E+00
CORRELATION BETWEEN PARAMETERS 1 AND 5 = 0.5598E+00
CORRELATION BETWEEN PARAMETERS 1 AND 6 = 0.6311E+00
CORRELATION BETWEEN PARAMETERS 2 AND 3 = 0.9564E+00
CORRELATION BETWEEN PARAMETERS 2 AND 4 = -.9271E+00
CORRELATION BETWEEN PARAMETERS 2 AND 5 = -.9144E+00
CORRELATION BETWEEN PARAMETERS 2 AND 6 = -.9231E+00
CORRELATION BETWEEN PARAMETERS 3 AND 4 = -.9790E+00
CORRELATION BETWEEN PARAMETERS 3 AND 5 = -.9769E+00
CORRELATION BETWEEN PARAMETERS 3 AND 6 = -.9716E+00
CORRELATION BETWEEN PARAMETERS 4 AND 5 = 0.9485E+00
CORRELATION BETWEEN PARAMETERS 4 AND 6 = 0.9195E+00
CORRELATION BETWEEN PARAMETERS 5 AND 6 = 0.9712E+00

********** REGRESSION SUMMARY **********

**Iodide** KFI06, UPPER SECTION
DISTANCE: 189 METRES
NUMBER OF FLOW PATHS: 3

APPLIED MODEL: MODEL3E, VARIABLE INJ. SCHEME

NUMBER OF PARAMETERS: 9
INPUT DATA FILE NAME: 3.dat
BACKGROUND LEVEL FOR INPUT DATA: 0.0000

FINAL ESTIMATE FOR PARAMETER 1 = 0.2188E-03
FINAL ESTIMATE FOR PARAMETER 2 = 0.2626E-02
FINAL ESTIMATE FOR PARAMETER 3 = 0.4030E+03
FINAL ESTIMATE FOR PARAMETER 4 = 0.8835E-04
FINAL ESTIMATE FOR PARAMETER 5 = 0.2100E-02
FINAL ESTIMATE FOR PARAMETER 6 = 0.2269E+03
FINAL ESTIMATE FOR PARAMETER 7 = 0.4248E-04
FINAL ESTIMATE FOR PARAMETER 8 = 0.3371E-02
FINAL ESTIMATE FOR PARAMETER 9 = 0.2306E+03

**********

REGRESSION STATISTICS

NO. OF OBSERVATIONS: 292
SUM OF SQUARED DIFFERENCES = 0.699E+01
ERROR VARIANCE = 0.247E-01
CORRELATION COEFFICIENT = .99727E+00

STANDARD ERROR FOR PARAMETER 1 = 0.470E-05
STANDARD ERROR FOR PARAMETER 2 = 0.288E-03
STANDARD ERROR FOR PARAMETER 3 = 0.199E+03
STANDARD ERROR FOR PARAMETER 4 = 0.427E-04
STANDARD ERROR FOR PARAMETER 5 = 0.554E-02
STANDARD ERROR FOR PARAMETER 6 = 0.150E+04
STANDARD ERROR FOR PARAMETER 7 = 0.321E-03
STANDARD ERROR FOR PARAMETER 8 = 0.676E-01
STANDARD ERROR FOR PARAMETER 9 = 0.178E+04

CORRELATION BETWEEN PARAMETERS 1 AND 2 = -.4682E+00
CORRELATION BETWEEN PARAMETERS 1 AND 3 = -.4281E+00
CORRELATION BETWEEN PARAMETERS 1 AND 4 = -.2118E+00
CORRELATION BETWEEN PARAMETERS 1 AND 5 = -.6489E-01
CORRELATION BETWEEN PARAMETERS 1 AND 6 = -.1992E+00
CORRELATION BETWEEN PARAMETERS 1 AND 7 = 0.2328E+00
CORRELATION BETWEEN PARAMETERS 1 AND 8 = 0.2685E+00
CORRELATION BETWEEN PARAMETERS 1 AND 9 = 0.2408E+00
CORRELATION BETWEEN PARAMETERS 2 AND 3 = 0.9890E+00
CORRELATION BETWEEN PARAMETERS 2 AND 4 = 0.9408E+00
CORRELATION BETWEEN PARAMETERS 2 AND 5 = 0.9034E+00
CORRELATION BETWEEN PARAMETERS 2 AND 6 = 0.9496E+00
CORRELATION BETWEEN PARAMETERS 2 AND 7 = -.9584E+00
CORRELATION BETWEEN PARAMETERS 2 AND 8 = -.9665E+00
CORRELATION BETWEEN PARAMETERS 2 AND 9 = -.9608E+00
CORRELATION BETWEEN PARAMETERS 3 AND 4 = 0.9675E+00
CORRELATION BETWEEN PARAMETERS 3 AND 5 = 0.9264E+00
CORRELATION BETWEEN PARAMETERS 3 AND 6 = 0.9690E+00
CORRELATION BETWEEN PARAMETERS 3 AND 7 = -.9767E+00
CORRELATION BETWEEN PARAMETERS 3 AND 8 = -.9853E+00
CORRELATION BETWEEN PARAMETERS 3 AND 9 = -.9796E+00
CORRELATION BETWEEN PARAMETERS 4 AND 5 = 0.9729E+00
CORRELATION BETWEEN PARAMETERS 4 AND 6 = 0.9852E+00
CORRELATION BETWEEN PARAMETERS 4 AND 7 = -.9852E+00
CORRELATION BETWEEN PARAMETERS 4 AND 8 = -.9914E+00
CORRELATION BETWEEN PARAMETERS 4 AND 9 = -.9898E+00
CORRELATION BETWEEN PARAMETERS 5 AND 6 = 0.9903E+00
CORRELATION BETWEEN PARAMETERS 5 AND 7 = -.9846E+00
CORRELATION BETWEEN PARAMETERS 5 AND 8 = -.9764E+00
CORRELATION BETWEEN PARAMETERS 5 AND 9 = -.9830E+00
CORRELATION BETWEEN PARAMETERS 6 AND 7 = -.9993E+00
CORRELATION BETWEEN PARAMETERS 6 AND 8 = -.9960E+00
CORRELATION BETWEEN PARAMETERS 6 AND 9 = -.9985E+00
CORRELATION BETWEEN PARAMETERS 7 AND 8 = 0.9977E+00
CORRELATION BETWEEN PARAMETERS 7 AND 9 = 0.9991E+00
CORRELATION BETWEEN PARAMETERS 8 AND 9 = 0.9993E+00

********** REGRESSION SUMMARY **********

Gd-DTPA KFI11, UPPER SECTION
DISTANCE: 155 METRES
NUMBER OF FLOW PATHS: 1

APPLIED MODEL: MODEL3E, COMPENSATED INJ STOP TIME

NUMBER OF PARAMETERS: 3

INPUT DATA FILE NAME: 5.dat

BACKGROUND LEVEL FOR INPUT DATA: 0.2075

FINAL ESTIMATE FOR PARAMETER 1 = 0.6368E-03
FINAL ESTIMATE FOR PARAMETER 2 = 0.2575E-01
FINAL ESTIMATE FOR PARAMETER 3 = 0.4638E+02

**********

REGRESSION STATISTICS

NO. OF OBSERVATIONS: 314

SUM OF SQUARED DIFFERENCES = 0.579E+04

ERROR VARIANCE = 0.186E+02

CORRELATION COEFFICIENT = .97575E+00

STANDARD ERROR FOR PARAMETER 1 = 0.193E-04
STANDARD ERROR FOR PARAMETER 2 = 0.319E-02
STANDARD ERROR FOR PARAMETER 3 = 0.443E+00

CORRELATION BETWEEN PARAMETERS 1 AND 2 = 0.4491E+00
CORRELATION BETWEEN PARAMETERS 1 AND 3 = -.2785E+00
CORRELATION BETWEEN PARAMETERS 2 AND 3 = 0.1260E+00

********** REGRESSION SUMMARY **********

Gd-DTPA KFI11, UPPER SECTION
DISTANCE: 155 METRES
NUMBER OF FLOW PATHS: 1

APPLIED MODEL: MODEL3E, ACTUAL INJ STOP TIME

NUMBER OF PARAMETERS: 3

INPUT DATA FILE NAME: 5.dat

BACKGROUND LEVEL FOR INPUT DATA: 0.2075

FINAL ESTIMATE FOR PARAMETER 1 = 0.6023E-03
FINAL ESTIMATE FOR PARAMETER 2 = 0.3168E-01
FINAL ESTIMATE FOR PARAMETER 3 = 0.4712E+02

**********

REGRESSION STATISTICS

NO. OF OBSERVATIONS: 314

SUM OF SQUARED DIFFERENCES = 0.756E+04

ERROR VARIANCE = 0.243E+02

CORRELATION COEFFICIENT = .96950E+00

STANDARD ERROR FOR PARAMETER 1 = 0.251E-04
STANDARD ERROR FOR PARAMETER 2 = 0.480E-02
STANDARD ERROR FOR PARAMETER 3 = 0.548E+00

CORRELATION BETWEEN PARAMETERS 1 AND 2 = 0.5078E+00
CORRELATION BETWEEN PARAMETERS 1 AND 3 = -.3646E+00
CORRELATION BETWEEN PARAMETERS 2 AND 3 = 0.1101E+00

********** REGRESSION SUMMARY **********

Gd-DTPA KFI11, UPPER SECTION
DISTANCE: 155 METRES
NUMBER OF FLOW PATHS: 2

APPLIED MODEL: MODEL3E, COMPENSATED INJ STOP TIME

NUMBER OF PARAMETERS: 6

INPUT DATA FILE NAME: 5.dat

BACKGROUND LEVEL FOR INPUT DATA: 0.2075

FINAL ESTIMATE FOR PARAMETER 1 = 0.1136E-02
FINAL ESTIMATE FOR PARAMETER 2 = 0.4120E-02
FINAL ESTIMATE FOR PARAMETER 3 = 0.1627E+02
FINAL ESTIMATE FOR PARAMETER 4 = 0.4323E-03
FINAL ESTIMATE FOR PARAMETER 5 = 0.4628E-02
FINAL ESTIMATE FOR PARAMETER 6 = 0.2992E+02

**********

REGRESSION STATISTICS

NO. OF OBSERVATIONS: 314

SUM OF SQUARED DIFFERENCES = 0.524E+04

ERROR VARIANCE = 0.170E+02

CORRELATION COEFFICIENT = .97847E+00

STANDARD ERROR FOR PARAMETER 1 = 0.486E-04
STANDARD ERROR FOR PARAMETER 2 = 0.191E-02
STANDARD ERROR FOR PARAMETER 3 = 0.241E+01
STANDARD ERROR FOR PARAMETER 4 = 0.206E-04
STANDARD ERROR FOR PARAMETER 5 = 0.148E-02
STANDARD ERROR FOR PARAMETER 6 = 0.249E+01

CORRELATION BETWEEN PARAMETERS 1 AND 2 = -.5126E+00
CORRELATION BETWEEN PARAMETERS 1 AND 3 = -.7628E+00
CORRELATION BETWEEN PARAMETERS 1 AND 4 = 0.7190E+00
CORRELATION BETWEEN PARAMETERS 1 AND 5 = 0.7282E+00
CORRELATION BETWEEN PARAMETERS 1 AND 6 = 0.7508E+00
CORRELATION BETWEEN PARAMETERS 2 AND 3 = 0.7663E+00
CORRELATION BETWEEN PARAMETERS 2 AND 4 = -.6167E+00
CORRELATION BETWEEN PARAMETERS 2 AND 5 = -.5890E+00
CORRELATION BETWEEN PARAMETERS 2 AND 6 = -.7527E+00
CORRELATION BETWEEN PARAMETERS 3 AND 4 = -.8272E+00
CORRELATION BETWEEN PARAMETERS 3 AND 5 = -.8514E+00
CORRELATION BETWEEN PARAMETERS 3 AND 6 = -.9861E+00
CORRELATION BETWEEN PARAMETERS 4 AND 5 = 0.7668E+00
CORRELATION BETWEEN PARAMETERS 4 AND 6 = 0.7966E+00
CORRELATION BETWEEN PARAMETERS 5 AND 6 = 0.8534E+00

********** REGRESSION SUMMARY **********

Amino G Acid KF111, UPPER SECTION
DISTANCE: 155 METRES
NUMBER OF FLOW PATHS: 1

APPLIED MODEL: MODEL4C, INSTANTANEOUS PULSE

NUMBER OF PARAMETERS: 3

INPUT DATA FILE NAME: 2.dat

BACKGROUND LEVEL FOR INPUT DATA: 0.1130

FINAL ESTIMATE FOR PARAMETER 1 = 0.2543E-03
FINAL ESTIMATE FOR PARAMETER 2 = 0.1109E-01
FINAL ESTIMATE FOR PARAMETER 3 = 0.4720E+00

**********

REGRESSION STATISTICS

NO. OF OBSERVATIONS: 154

SUM OF SQUARED DIFFERENCES = 0.318E+00

ERROR VARIANCE = 0.211E-02

CORRELATION COEFFICIENT = .96710E+00

STANDARD ERROR FOR PARAMETER 1 = 0.114E-04
STANDARD ERROR FOR PARAMETER 2 = 0.410E-03
STANDARD ERROR FOR PARAMETER 3 = 0.937E-02

CORRELATION BETWEEN PARAMETERS 1 AND 2 = -.6568E+00
CORRELATION BETWEEN PARAMETERS 1 AND 3 = 0.3836E-01
CORRELATION BETWEEN PARAMETERS 2 AND 3 = 0.3805E+00

********** REGRESSION SUMMARY **********

Amino G Acid KF111, UPPER SECTION
DISTANCE: 155 METRES
NUMBER OF FLOW PATHS: 2

APPLIED MODEL: MODEL4C, INSTANTANEOUS PULSE

NUMBER OF PARAMETERS: 6

INPUT DATA FILE NAME: 2.dat

BACKGROUND LEVEL FOR INPUT DATA: 0.1130

FINAL ESTIMATE FOR PARAMETER 1 = 0.3032E-03
FINAL ESTIMATE FOR PARAMETER 2 = 0.1101E-01
FINAL ESTIMATE FOR PARAMETER 3 = 0.4625E+00
FINAL ESTIMATE FOR PARAMETER 4 = 0.2536E-03
FINAL ESTIMATE FOR PARAMETER 5 = 0.1284E-03
FINAL ESTIMATE FOR PARAMETER 6 = 0.5368E-01

**********

REGRESSION STATISTICS

NO. OF OBSERVATIONS: 154

SUM OF SQUARED DIFFERENCES = 0.811E-01

ERROR VARIANCE = 0.548E-03

CORRELATION COEFFICIENT = .99166E+00

STANDARD ERROR FOR PARAMETER 1 = 0.762E-05
STANDARD ERROR FOR PARAMETER 2 = 0.236E-03
STANDARD ERROR FOR PARAMETER 3 = 0.559E-02
STANDARD ERROR FOR PARAMETER 4 = 0.133E-05
STANDARD ERROR FOR PARAMETER 5 = 0.167E-04
STANDARD ERROR FOR PARAMETER 6 = 0.658E-02

CORRELATION BETWEEN PARAMETERS 1 AND 2 = -.6379E+00
CORRELATION BETWEEN PARAMETERS 1 AND 3 = -.2984E+00
CORRELATION BETWEEN PARAMETERS 1 AND 4 = -.1593E+00
CORRELATION BETWEEN PARAMETERS 1 AND 5 = 0.3700E+00
CORRELATION BETWEEN PARAMETERS 1 AND 6 = 0.5151E+00
CORRELATION BETWEEN PARAMETERS 2 AND 3 = 0.6113E+00
CORRELATION BETWEEN PARAMETERS 2 AND 4 = 0.1149E+00
CORRELATION BETWEEN PARAMETERS 2 AND 5 = -.1129E+00
CORRELATION BETWEEN PARAMETERS 2 AND 6 = -.1689E+00
CORRELATION BETWEEN PARAMETERS 3 AND 4 = 0.5544E-01
CORRELATION BETWEEN PARAMETERS 3 AND 5 = -.1502E+00
CORRELATION BETWEEN PARAMETERS 3 AND 6 = -.2053E+00
CORRELATION BETWEEN PARAMETERS 4 AND 5 = -.3159E+00
CORRELATION BETWEEN PARAMETERS 4 AND 6 = -.3684E+00
CORRELATION BETWEEN PARAMETERS 5 AND 6 = 0.9123E+00

********* REGRESSION SUMMARY **********

Amino G Acid KFI11, UPPER SECTION
DISTANCE: 155 METRES
NUMBER OF FLOW PATHS: 1

APPLIED MODEL: MODEL5C, DECAYING PULSE

NUMBER OF PARAMETERS: 4

INPUT DATA FILE NAME: 1.dat

BACKGROUND LEVEL FOR INPUT DATA: 0.1130

FINAL ESTIMATE FOR PARAMETER 1 = 0.8708E-03
FINAL ESTIMATE FOR PARAMETER 2 = 0.2579E-01
FINAL ESTIMATE FOR PARAMETER 3 = 0.3891E-04
FINAL ESTIMATE FOR PARAMETER 4 = 0.2881E-05

**********

REGRESSION STATISTICS

NO. OF OBSERVATIONS: 180

SUM OF SQUARED DIFFERENCES = 0.426E+00

ERROR VARIANCE = 0.242E-02

CORRELATION COEFFICIENT = .96617E+00

STANDARD ERROR FOR PARAMETER 1 = 0.550E-04
STANDARD ERROR FOR PARAMETER 2 = 0.492E-02
STANDARD ERROR FOR PARAMETER 3 = 0.408E-05
STANDARD ERROR FOR PARAMETER 4 = 0.369E-06

CORRELATION BETWEEN PARAMETERS 1 AND 2 = -.5328E+00
CORRELATION BETWEEN PARAMETERS 1 AND 3 = -.9199E+00
CORRELATION BETWEEN PARAMETERS 1 AND 4 = -.9026E+00
CORRELATION BETWEEN PARAMETERS 2 AND 3 = 0.7205E+00
CORRELATION BETWEEN PARAMETERS 2 AND 4 = 0.6432E+00
CORRELATION BETWEEN PARAMETERS 3 AND 4 = 0.9691E+00

********** REGRESSION SUMMARY **********

Amino G Acid KFI11, UPPER SECTION
DISTANCE: 155 METRES
NUMBER OF FLOW PATHS: 2

APPLIED MODEL: MODEL5C, DECAYING PULSE

NUMBER OF PARAMETERS: 7

INPUT DATA FILE NAME: 1.dat

BACKGROUND LEVEL FOR INPUT DATA: 0.1130

FINAL ESTIMATE FOR PARAMETER 1 = 0.1105E-02
FINAL ESTIMATE FOR PARAMETER 2 = 0.3622E-02
FINAL ESTIMATE FOR PARAMETER 3 = 0.2495E-04
FINAL ESTIMATE FOR PARAMETER 4 = 0.4194E-03
FINAL ESTIMATE FOR PARAMETER 5 = 0.4023E-02
FINAL ESTIMATE FOR PARAMETER 6 = 0.1814E-04
FINAL ESTIMATE FOR PARAMETER 7 = 0.3106E-05

**********

REGRESSION STATISTICS

NO. OF OBSERVATIONS: 180

SUM OF SQUARED DIFFERENCES = 0.310E+00

ERROR VARIANCE = 0.179E-02

CORRELATION COEFFICIENT = .97636E+00

STANDARD ERROR FOR PARAMETER 1 = 0.324E-04
STANDARD ERROR FOR PARAMETER 2 = 0.118E-02
STANDARD ERROR FOR PARAMETER 3 = 0.209E-05
STANDARD ERROR FOR PARAMETER 4 = 0.309E-04
STANDARD ERROR FOR PARAMETER 5 = 0.308E-02
STANDARD ERROR FOR PARAMETER 6 = 0.819E-05
STANDARD ERROR FOR PARAMETER 7 = 0.598E-06

CORRELATION BETWEEN PARAMETERS 1 AND 2 = -.4768E+00
CORRELATION BETWEEN PARAMETERS 1 AND 3 = -.7912E+00
CORRELATION BETWEEN PARAMETERS 1 AND 4 = 0.4947E+00
CORRELATION BETWEEN PARAMETERS 1 AND 5 = 0.6063E+00
CORRELATION BETWEEN PARAMETERS 1 AND 6 = 0.4303E+00
CORRELATION BETWEEN PARAMETERS 1 AND 7 = 0.2244E+00
CORRELATION BETWEEN PARAMETERS 2 AND 3 = 0.7011E+00
CORRELATION BETWEEN PARAMETERS 2 AND 4 = -.4125E+00
CORRELATION BETWEEN PARAMETERS 2 AND 5 = -.4754E+00
CORRELATION BETWEEN PARAMETERS 2 AND 6 = -.3575E+00
CORRELATION BETWEEN PARAMETERS 2 AND 7 = -.1890E+00
CORRELATION BETWEEN PARAMETERS 3 AND 4 = -.6354E+00
CORRELATION BETWEEN PARAMETERS 3 AND 5 = -.6957E+00
CORRELATION BETWEEN PARAMETERS 3 AND 6 = -.4494E+00
CORRELATION BETWEEN PARAMETERS 3 AND 7 = -.1929E+00
CORRELATION BETWEEN PARAMETERS 4 AND 5 = 0.2280E-01
CORRELATION BETWEEN PARAMETERS 4 AND 6 = -.2757E+00
CORRELATION BETWEEN PARAMETERS 4 AND 7 = -.4668E+00
CORRELATION BETWEEN PARAMETERS 5 AND 6 = 0.8976E+00
CORRELATION BETWEEN PARAMETERS 5 AND 7 = 0.7609E+00
CORRELATION BETWEEN PARAMETERS 6 AND 7 = 0.9541E+00

********** REGRESSION SUMMARY **********

**Amino G Acid** KFI11, UPPER SECTION
DISTANCE: 155 METRES
NUMBER OF FLOW PATHS: 1

APPLIED MODEL: MODEL3E, VARIABLE INJECTION SCHEME

NUMBER OF PARAMETERS: 3

INPUT DATA FILE NAME: 2.dat

BACKGROUND LEVEL FOR INPUT DATA: 0.1130

FINAL ESTIMATE FOR PARAMETER 1 = 0.8270E-03
FINAL ESTIMATE FOR PARAMETER 2 = 0.1550E-01
FINAL ESTIMATE FOR PARAMETER 3 = 0.8630E+00

**********

REGRESSION STATISTICS

NO. OF OBSERVATIONS: 154

SUM OF SQUARED DIFFERENCES = 0.360E+00

ERROR VARIANCE = 0.238E-02

CORRELATION COEFFICIENT = .96425E+00

STANDARD ERROR FOR PARAMETER 1 = 0.191E-04
STANDARD ERROR FOR PARAMETER 2 = 0.199E-02
STANDARD ERROR FOR PARAMETER 3 = 0.209E-01

CORRELATION BETWEEN PARAMETERS 1 AND 2 = -.2170E-01
CORRELATION BETWEEN PARAMETERS 1 AND 3 = -.4577E+00
CORRELATION BETWEEN PARAMETERS 2 AND 3 = 0.5095E+00

********** REGRESSION SUMMARY **********

**Amino G Acid** KFI11, UPPER SECTION
DISTANCE: 155 METRES
NUMBER OF FLOW PATHS: 2

APPLIED MODEL: MODEL3E, VARIABLE INJECTION SCHEME

NUMBER OF PARAMETERS: 6

INPUT DATA FILE NAME: 2.dat

BACKGROUND LEVEL FOR INPUT DATA: 0.1130

FINAL ESTIMATE FOR PARAMETER 1 = 0.9388E-03
FINAL ESTIMATE FOR PARAMETER 2 = 0.8577E-02
FINAL ESTIMATE FOR PARAMETER 3 = 0.5734E+00
FINAL ESTIMATE FOR PARAMETER 4 = 0.4197E-03
FINAL ESTIMATE FOR PARAMETER 5 = 0.2737E-01
FINAL ESTIMATE FOR PARAMETER 6 = 0.4273E+00

**********

REGRESSION STATISTICS

NO. OF OBSERVATIONS: 154

SUM OF SQUARED DIFFERENCES = 0.281E+00

ERROR VARIANCE = 0.190E-02

CORRELATION COEFFICIENT = .97058E+00

STANDARD ERROR FOR PARAMETER 1 = 0.355E-04
STANDARD ERROR FOR PARAMETER 2 = 0.408E-02
STANDARD ERROR FOR PARAMETER 3 = 0.219E+00
STANDARD ERROR FOR PARAMETER 4 = 0.237E-03
STANDARD ERROR FOR PARAMETER 5 = 0.365E-01
STANDARD ERROR FOR PARAMETER 6 = 0.224E+00

CORRELATION BETWEEN PARAMETERS 1 AND 2 = 0.3074E+00
CORRELATION BETWEEN PARAMETERS 1 AND 3 = 0.3021E+00
CORRELATION BETWEEN PARAMETERS 1 AND 4 = -.3589E+00
CORRELATION BETWEEN PARAMETERS 1 AND 5 = -.5526E+00
CORRELATION BETWEEN PARAMETERS 1 AND 6 = -.3394E+00
CORRELATION BETWEEN PARAMETERS 2 AND 3 = 0.9492E+00
CORRELATION BETWEEN PARAMETERS 2 AND 4 = -.9237E+00
CORRELATION BETWEEN PARAMETERS 2 AND 5 = -.8869E+00
CORRELATION BETWEEN PARAMETERS 2 AND 6 = -.9346E+00
CORRELATION BETWEEN PARAMETERS 3 AND 4 = -.9854E+00
CORRELATION BETWEEN PARAMETERS 3 AND 5 = -.9345E+00
CORRELATION BETWEEN PARAMETERS 3 AND 6 = -.9825E+00
CORRELATION BETWEEN PARAMETERS 4 AND 5 = 0.9367E+00
CORRELATION BETWEEN PARAMETERS 4 AND 6 = 0.9509E+00
CORRELATION BETWEEN PARAMETERS 5 AND 6 = 0.9488E+00

********** REGRESSION SUMMARY **********

URANINE FROM BF101, MIDDLE SECTION
DISTANCE: 168 METRES
NUMBER OF FLOW PATHS: 1

APPLIED MODEL: MODEL3E

NUMBER OF PARAMETERS: 3

INPUT DATA FILE NAME: 1.DAT

BACKGROUND LEVEL FOR INPUT DATA: 3.0000

FINAL ESTIMATE FOR PARAMETER 1 = 0.3564E-04
FINAL ESTIMATE FOR PARAMETER 2 = 0.7699E-03
FINAL ESTIMATE FOR PARAMETER 3 = 0.2907E+02

**********

REGRESSION STATISTICS

NO. OF OBSERVATIONS: 392

SUM OF SQUARED DIFFERENCES = 0.148E+04

ERROR VARIANCE = 0.381E+01

CORRELATION COEFFICIENT = .97175E+00

STANDARD ERROR FOR PARAMETER 1 = 0.427E-06
STANDARD ERROR FOR PARAMETER 2 = 0.452E-04
STANDARD ERROR FOR PARAMETER 3 = 0.570E+00

CORRELATION BETWEEN PARAMETERS 1 AND 2 = -.2828E+00
CORRELATION BETWEEN PARAMETERS 1 AND 3 = -.7379E+00
CORRELATION BETWEEN PARAMETERS 2 AND 3 = 0.6763E+00

********** REGRESSION SUMMARY **********

Yb-EDTA KFI06, MIDDLE SECTION
DISTANCE: 191 METRES
NUMBER OF FLOW PATHS: 1

APPLIED MODEL: MODEL3E

NUMBER OF PARAMETERS: 3

INPUT DATA FILE NAME: 2.dat

BACKGROUND LEVEL FOR INPUT DATA: 0.2300

FINAL ESTIMATE FOR PARAMETER 1 = 0.2580E-04
FINAL ESTIMATE FOR PARAMETER 2 = 0.7328E-03
FINAL ESTIMATE FOR PARAMETER 3 = 0.1412E+02

**********

REGRESSION STATISTICS

NO. OF OBSERVATIONS: 187

SUM OF SQUARED DIFFERENCES = 0.170E+03

ERROR VARIANCE = 0.924E+00

CORRELATION COEFFICIENT = .79799E+00

STANDARD ERROR FOR PARAMETER 1 = 0.119E-05
STANDARD ERROR FOR PARAMETER 2 = 0.904E-04
STANDARD ERROR FOR PARAMETER 3 = 0.112E+01

CORRELATION BETWEEN PARAMETERS 1 AND 2 = -.6556E+00
CORRELATION BETWEEN PARAMETERS 1 AND 3 = -.9535E+00
CORRELATION BETWEEN PARAMETERS 2 AND 3 = 0.7024E+00

********** REGRESSION SUMMARY **********

Yb-EDTA KFI06, MIDDLE SECTION
DISTANCE: 191 METRES
NUMBER OF FLOW PATHS: 2

APPLIED MODEL: MODEL3E

NUMBER OF PARAMETERS: 6

INPUT DATA FILE NAME: 1.dat

BACKGROUND LEVEL FOR INPUT DATA: 0.2500

FINAL ESTIMATE FOR PARAMETER 1 = 0.1289E-04
FINAL ESTIMATE FOR PARAMETER 2 = 0.1467E-03
FINAL ESTIMATE FOR PARAMETER 3 = 0.1011E+02
FINAL ESTIMATE FOR PARAMETER 4 = 0.3435E-04
FINAL ESTIMATE FOR PARAMETER 5 = 0.2387E-03
FINAL ESTIMATE FOR PARAMETER 6 = 0.5933E+01

**********

REGRESSION STATISTICS

NO. OF OBSERVATIONS: 360

SUM OF SQUARED DIFFERENCES = 0.967E+02

ERROR VARIANCE = 0.273E+00

CORRELATION COEFFICIENT = .96043E+00

STANDARD ERROR FOR PARAMETER 1 = 0.242E-05
STANDARD ERROR FOR PARAMETER 2 = 0.131E-03
STANDARD ERROR FOR PARAMETER 3 = 0.608E+01
STANDARD ERROR FOR PARAMETER 4 = 0.157E-05
STANDARD ERROR FOR PARAMETER 5 = 0.457E-04
STANDARD ERROR FOR PARAMETER 6 = 0.903E+00

CORRELATION BETWEEN PARAMETERS 1 AND 2 = -.8945E+00
CORRELATION BETWEEN PARAMETERS 1 AND 3 = -.9673E+00
CORRELATION BETWEEN PARAMETERS 1 AND 4 = -.7097E+00
CORRELATION BETWEEN PARAMETERS 1 AND 5 = 0.5591E+00
CORRELATION BETWEEN PARAMETERS 1 AND 6 = 0.7237E+00
CORRELATION BETWEEN PARAMETERS 2 AND 3 = 0.9699E+00
CORRELATION BETWEEN PARAMETERS 2 AND 4 = 0.9330E+00
CORRELATION BETWEEN PARAMETERS 2 AND 5 = -.8013E+00
CORRELATION BETWEEN PARAMETERS 2 AND 6 = -.9415E+00
CORRELATION BETWEEN PARAMETERS 3 AND 4 = 0.8506E+00
CORRELATION BETWEEN PARAMETERS 3 AND 5 = -.7113E+00
CORRELATION BETWEEN PARAMETERS 3 AND 6 = -.8618E+00
CORRELATION BETWEEN PARAMETERS 4 AND 5 = -.9083E+00
CORRELATION BETWEEN PARAMETERS 4 AND 6 = -.9898E+00
CORRELATION BETWEEN PARAMETERS 5 AND 6 = 0.9312E+00

********** REGRESSION SUMMARY **********

Er-EDTA KFI11, MIDDLE SECTION
DISTANCE: 169 METRES
NUMBER OF FLOW PATHS: 1

APPLIED MODEL: MODEL3E

NUMBER OF PARAMETERS: 3

INPUT DATA FILE NAME: 2.dat

BACKGROUND LEVEL FOR INPUT DATA: 0.1400

FINAL ESTIMATE FOR PARAMETER 1 = 0.4515E-04
FINAL ESTIMATE FOR PARAMETER 2 = 0.5765E-04
FINAL ESTIMATE FOR PARAMETER 3 = 0.3847E+00

**********

REGRESSION STATISTICS

NO. OF OBSERVATIONS: 279

SUM OF SQUARED DIFFERENCES = 0.206E+01

ERROR VARIANCE = 0.745E-02

CORRELATION COEFFICIENT = .83828E+00

STANDARD ERROR FOR PARAMETER 1 = 0.582E-06
STANDARD ERROR FOR PARAMETER 2 = 0.190E-04
STANDARD ERROR FOR PARAMETER 3 = 0.114E-01

CORRELATION BETWEEN PARAMETERS 1 AND 2 = 0.6849E-01
CORRELATION BETWEEN PARAMETERS 1 AND 3 = -.1605E+00
CORRELATION BETWEEN PARAMETERS 2 AND 3 = 0.2534E+00

********** REGRESSION SUMMARY **********

Er-EDTA KFI11, MIDDLE SECTION
DISTANCE: 169 METRES
NUMBER OF FLOW PATHS: 2

APPLIED MODEL: MODEL3E

NUMBER OF PARAMETERS: 6

INPUT DATA FILE NAME: 2.dat

BACKGROUND LEVEL FOR INPUT DATA: 0.1400

FINAL ESTIMATE FOR PARAMETER 1 = 0.4520E-04
FINAL ESTIMATE FOR PARAMETER 2 = 0.5619E-04
FINAL ESTIMATE FOR PARAMETER 3 = 0.3803E+00
FINAL ESTIMATE FOR PARAMETER 4 = 0.1458E-04
FINAL ESTIMATE FOR PARAMETER 5 = 0.3012E-04
FINAL ESTIMATE FOR PARAMETER 6 = 0.2432E+00

**********

REGRESSION STATISTICS

NO. OF OBSERVATIONS: 279

SUM OF SQUARED DIFFERENCES = 0.176E+01

ERROR VARIANCE = 0.646E-02

CORRELATION COEFFICIENT = .86419E+00

STANDARD ERROR FOR PARAMETER 1 = 0.549E-06
STANDARD ERROR FOR PARAMETER 2 = 0.176E-04
STANDARD ERROR FOR PARAMETER 3 = 0.108E-01
STANDARD ERROR FOR PARAMETER 4 = 0.991E-06
STANDARD ERROR FOR PARAMETER 5 = 0.254E-04
STANDARD ERROR FOR PARAMETER 6 = 0.507E-01

CORRELATION BETWEEN PARAMETERS 1 AND 2 = 0.5570E-01
CORRELATION BETWEEN PARAMETERS 1 AND 3 = -.1834E+00
CORRELATION BETWEEN PARAMETERS 1 AND 4 = 0.1202E-02
CORRELATION BETWEEN PARAMETERS 1 AND 5 = 0.1052E+00
CORRELATION BETWEEN PARAMETERS 1 AND 6 = 0.7976E-01
CORRELATION BETWEEN PARAMETERS 2 AND 3 = 0.2705E+00
CORRELATION BETWEEN PARAMETERS 2 AND 4 = -.1706E-01
CORRELATION BETWEEN PARAMETERS 2 AND 5 = -.8267E-01
CORRELATION BETWEEN PARAMETERS 2 AND 6 = -.6995E-01
CORRELATION BETWEEN PARAMETERS 3 AND 4 = -.1648E-01
CORRELATION BETWEEN PARAMETERS 3 AND 5 = -.1836E+00
CORRELATION BETWEEN PARAMETERS 3 AND 6 = -.1612E+00
CORRELATION BETWEEN PARAMETERS 4 AND 5 = -.4351E+00
CORRELATION BETWEEN PARAMETERS 4 AND 6 = -.4055E+00
CORRELATION BETWEEN PARAMETERS 5 AND 6 = 0.6911E+00

********** REGRESSION SUMMARY **********

Ho-EDTA FROM BF101, LOWER SECTION
DISTANCE: 201 METRES
NUMBER OF FLOW PATHS: 1

APPLIED MODEL: MODEL3E

NUMBER OF PARAMETERS: 3

INPUT DATA FILE NAME: 1.dat

BACKGROUND LEVEL FOR INPUT DATA: 0.0800

FINAL ESTIMATE FOR PARAMETER 1 = 0.2404E-04
FINAL ESTIMATE FOR PARAMETER 2 = 0.1736E-03
FINAL ESTIMATE FOR PARAMETER 3 = 0.4533E+01

**********

REGRESSION STATISTICS

NO. OF OBSERVATIONS: 320

SUM OF SQUARED DIFFERENCES = 0.777E+01

ERROR VARIANCE = 0.245E-01

CORRELATION COEFFICIENT = .98102E+00

STANDARD ERROR FOR PARAMETER 1 = 0.126E-06
STANDARD ERROR FOR PARAMETER 2 = 0.639E-05
STANDARD ERROR FOR PARAMETER 3 = 0.699E-01

CORRELATION BETWEEN PARAMETERS 1 AND 2 = -.4778E+00
CORRELATION BETWEEN PARAMETERS 1 AND 3 = -.7727E+00
CORRELATION BETWEEN PARAMETERS 2 AND 3 = 0.3444E+00

********** REGRESSION SUMMARY **********

Ho-EDTA FROM BF101, LOWER SECTION
DISTANCE: 201 METRES
NUMBER OF FLOW PATHS: 2

APPLIED MODEL: MODEL3E

NUMBER OF PARAMETERS: 6

INPUT DATA FILE NAME: 1.dat

BACKGROUND LEVEL FOR INPUT DATA: 0.0800

FINAL ESTIMATE FOR PARAMETER 1 = 0.2417E-04
FINAL ESTIMATE FOR PARAMETER 2 = 0.1663E-03
FINAL ESTIMATE FOR PARAMETER 3 = 0.3074E+01
FINAL ESTIMATE FOR PARAMETER 4 = 0.2383E-04
FINAL ESTIMATE FOR PARAMETER 5 = 0.1852E-03
FINAL ESTIMATE FOR PARAMETER 6 = 0.1446E+01

**********

REGRESSION STATISTICS

NO. OF OBSERVATIONS: 320

SUM OF SQUARED DIFFERENCES = 0.776E+01

ERROR VARIANCE = 0.247E-01

CORRELATION COEFFICIENT = .98102E+00

STANDARD ERROR FOR PARAMETER 1 = 0.192E-03
STANDARD ERROR FOR PARAMETER 2 = 0.110E-01
STANDARD ERROR FOR PARAMETER 3 = 0.378E+04
STANDARD ERROR FOR PARAMETER 4 = 0.482E-03
STANDARD ERROR FOR PARAMETER 5 = 0.263E-01
STANDARD ERROR FOR PARAMETER 6 = 0.378E+04

CORRELATION BETWEEN PARAMETERS 1 AND 2 = -.9995E+00
CORRELATION BETWEEN PARAMETERS 1 AND 3 = -.9998E+00
CORRELATION BETWEEN PARAMETERS 1 AND 4 = 0.9993E+00
CORRELATION BETWEEN PARAMETERS 1 AND 5 = -.9997E+00
CORRELATION BETWEEN PARAMETERS 1 AND 6 = 0.9998E+00
CORRELATION BETWEEN PARAMETERS 2 AND 3 = 0.9998E+00
CORRELATION BETWEEN PARAMETERS 2 AND 4 = -.9997E+00
CORRELATION BETWEEN PARAMETERS 2 AND 5 = 0.9991E+00
CORRELATION BETWEEN PARAMETERS 2 AND 6 = -.9998E+00
CORRELATION BETWEEN PARAMETERS 3 AND 4 = -.9998E+00
CORRELATION BETWEEN PARAMETERS 3 AND 5 = 0.9998E+00
CORRELATION BETWEEN PARAMETERS 3 AND 6 = -.1000E+01
CORRELATION BETWEEN PARAMETERS 4 AND 5 = -.9996E+00
CORRELATION BETWEEN PARAMETERS 4 AND 6 = 0.9998E+00
CORRELATION BETWEEN PARAMETERS 5 AND 6 = -.9998E+00

********** REGRESSION SUMMARY **********

ReO4 FROM KFI06, LOWER SECTION
DISTANCE: 189 METRES
NUMBER OF FLOW PATHS: 1

APPLIED MODEL: MODEL3E

NUMBER OF PARAMETERS: 3

INPUT DATA FILE NAME: 1.dat

BACKGROUND LEVEL FOR INPUT DATA: 0.0000

FINAL ESTIMATE FOR PARAMETER 1 = 0.7578E-04
FINAL ESTIMATE FOR PARAMETER 2 = 0.8105E-02
FINAL ESTIMATE FOR PARAMETER 3 = 0.5060E+01

**********

REGRESSION STATISTICS

NO. OF OBSERVATIONS: 287

SUM OF SQUARED DIFFERENCES = 0.146E+03

ERROR VARIANCE = 0.513E+00

CORRELATION COEFFICIENT = .89590E+00

STANDARD ERROR FOR PARAMETER 1 = 0.205E-05
STANDARD ERROR FOR PARAMETER 2 = 0.804E-03
STANDARD ERROR FOR PARAMETER 3 = 0.153E+00

CORRELATION BETWEEN PARAMETERS 1 AND 2 = -.2558E+00
CORRELATION BETWEEN PARAMETERS 1 AND 3 = -.6552E+00
CORRELATION BETWEEN PARAMETERS 2 AND 3 = 0.7107E+00

********** REGRESSION SUMMARY **********

ReO4 FROM KFI06, LOWER SECTION
DISTANCE: 189 METRES
NUMBER OF FLOW PATHS: 2

APPLIED MODEL: MODEL3E

NUMBER OF PARAMETERS: 6

INPUT DATA FILE NAME: 1.dat

BACKGROUND LEVEL FOR INPUT DATA: 0.0000

FINAL ESTIMATE FOR PARAMETER 1 = 0.1364E-03
FINAL ESTIMATE FOR PARAMETER 2 = 0.1486E-02
FINAL ESTIMATE FOR PARAMETER 3 = 0.2543E+01
FINAL ESTIMATE FOR PARAMETER 4 = 0.4533E-04
FINAL ESTIMATE FOR PARAMETER 5 = 0.3482E-04
FINAL ESTIMATE FOR PARAMETER 6 = 0.1563E+01

**********

REGRESSION STATISTICS

NO. OF OBSERVATIONS: 287

SUM OF SQUARED DIFFERENCES = 0.420E+02

ERROR VARIANCE = 0.150E+00

CORRELATION COEFFICIENT = .97122E+00

STANDARD ERROR FOR PARAMETER 1 = 0.153E-05
STANDARD ERROR FOR PARAMETER 2 = 0.147E-03
STANDARD ERROR FOR PARAMETER 3 = 0.363E-01
STANDARD ERROR FOR PARAMETER 4 = 0.261E-06
STANDARD ERROR FOR PARAMETER 5 = 0.508E-05
STANDARD ERROR FOR PARAMETER 6 = 0.407E-01

CORRELATION BETWEEN PARAMETERS 1 AND 2 = 0.6195E-01
CORRELATION BETWEEN PARAMETERS 1 AND 3 = -.4154E+00
CORRELATION BETWEEN PARAMETERS 1 AND 4 = 0.3819E+00
CORRELATION BETWEEN PARAMETERS 1 AND 5 = 0.2062E+00
CORRELATION BETWEEN PARAMETERS 1 AND 6 = 0.4356E+00
CORRELATION BETWEEN PARAMETERS 2 AND 3 = 0.4209E+00
CORRELATION BETWEEN PARAMETERS 2 AND 4 = -.2421E+00
CORRELATION BETWEEN PARAMETERS 2 AND 5 = -.1432E+00
CORRELATION BETWEEN PARAMETERS 2 AND 6 = -.4362E+00
CORRELATION BETWEEN PARAMETERS 3 AND 4 = -.4720E+00
CORRELATION BETWEEN PARAMETERS 3 AND 5 = -.2976E+00
CORRELATION BETWEEN PARAMETERS 3 AND 6 = -.5620E+00
CORRELATION BETWEEN PARAMETERS 4 AND 5 = 0.3095E+00
CORRELATION BETWEEN PARAMETERS 4 AND 6 = 0.6850E+00
CORRELATION BETWEEN PARAMETERS 5 AND 6 = 0.5733E+00

********** REGRESSION SUMMARY **********

Re04 FROM KF106, LOWER SECTION
DISTANCE: 189 METRES
NUMBER OF FLOW PATHS: 3

APPLIED MODEL: MODEL3E

NUMBER OF PARAMETERS: 9

INPUT DATA FILE NAME: 1.dat

BACKGROUND LEVEL FOR INPUT DATA: 0.0000

FINAL ESTIMATE FOR PARAMETER 1 = 0.1363E-03
FINAL ESTIMATE FOR PARAMETER 2 = 0.1512E-02
FINAL ESTIMATE FOR PARAMETER 3 = 0.2545E+01
FINAL ESTIMATE FOR PARAMETER 4 = 0.4550E-04
FINAL ESTIMATE FOR PARAMETER 5 = 0.3194E-04
FINAL ESTIMATE FOR PARAMETER 6 = 0.1540E+01
FINAL ESTIMATE FOR PARAMETER 7 = 0.2075E-04
FINAL ESTIMATE FOR PARAMETER 8 = 0.8421E-04
FINAL ESTIMATE FOR PARAMETER 9 = 0.8156E+00

**********

REGRESSION STATISTICS

NO. OF OBSERVATIONS: 287

SUM OF SQUARED DIFFERENCES = 0.325E+02

ERROR VARIANCE = 0.117E+00

CORRELATION COEFFICIENT = .97852E+00

STANDARD ERROR FOR PARAMETER 1 = 0.135E-05
STANDARD ERROR FOR PARAMETER 2 = 0.133E-03
STANDARD ERROR FOR PARAMETER 3 = 0.321E-01
STANDARD ERROR FOR PARAMETER 4 = 0.227E-06
STANDARD ERROR FOR PARAMETER 5 = 0.436E-05
STANDARD ERROR FOR PARAMETER 6 = 0.380E-01
STANDARD ERROR FOR PARAMETER 7 = 0.762E-06
STANDARD ERROR FOR PARAMETER 8 = 0.273E-04
STANDARD ERROR FOR PARAMETER 9 = 0.122E+00

CORRELATION BETWEEN PARAMETERS 1 AND 2 = 0.5647E-01
CORRELATION BETWEEN PARAMETERS 1 AND 3 = -.4153E+00
CORRELATION BETWEEN PARAMETERS 1 AND 4 = 0.3589E+00
CORRELATION BETWEEN PARAMETERS 1 AND 5 = 0.2070E+00
CORRELATION BETWEEN PARAMETERS 1 AND 6 = 0.4290E+00
CORRELATION BETWEEN PARAMETERS 1 AND 7 = 0.2057E-02
CORRELATION BETWEEN PARAMETERS 1 AND 8 = -.5499E-01
CORRELATION BETWEEN PARAMETERS 1 AND 9 = -.8910E-02
CORRELATION BETWEEN PARAMETERS 2 AND 3 = 0.4279E+00
CORRELATION BETWEEN PARAMETERS 2 AND 4 = -.2113E+00
CORRELATION BETWEEN PARAMETERS 2 AND 5 = -.1644E+00
CORRELATION BETWEEN PARAMETERS 2 AND 6 = -.4446E+00
CORRELATION BETWEEN PARAMETERS 2 AND 7 = 0.1067E-01
CORRELATION BETWEEN PARAMETERS 2 AND 8 = 0.8100E-01
CORRELATION BETWEEN PARAMETERS 2 AND 9 = 0.1656E-01
CORRELATION BETWEEN PARAMETERS 3 AND 4 = -.4426E+00
CORRELATION BETWEEN PARAMETERS 3 AND 5 = -.2992E+00
CORRELATION BETWEEN PARAMETERS 3 AND 6 = -.5530E+00
CORRELATION BETWEEN PARAMETERS 3 AND 7 = -.5810E-03
CORRELATION BETWEEN PARAMETERS 3 AND 8 = 0.7135E-01
CORRELATION BETWEEN PARAMETERS 3 AND 9 = 0.1243E-01
CORRELATION BETWEEN PARAMETERS 4 AND 5 = 0.2632E+00
CORRELATION BETWEEN PARAMETERS 4 AND 6 = 0.5796E+00
CORRELATION BETWEEN PARAMETERS 4 AND 7 = 0.4086E-01
CORRELATION BETWEEN PARAMETERS 4 AND 8 = 0.1390E+00
CORRELATION BETWEEN PARAMETERS 4 AND 9 = 0.3791E-01
CORRELATION BETWEEN PARAMETERS 5 AND 6 = 0.5807E+00
CORRELATION BETWEEN PARAMETERS 5 AND 7 = -.2553E-01
CORRELATION BETWEEN PARAMETERS 5 AND 8 = -.1963E+00
CORRELATION BETWEEN PARAMETERS 5 AND 9 = -.4798E-01
CORRELATION BETWEEN PARAMETERS 6 AND 7 = -.5491E-02
CORRELATION BETWEEN PARAMETERS 6 AND 8 = -.3106E+00
CORRELATION BETWEEN PARAMETERS 6 AND 9 = -.6025E-01
CORRELATION BETWEEN PARAMETERS 7 AND 8 = -.3564E+00
CORRELATION BETWEEN PARAMETERS 7 AND 9 = -.6734E+00
CORRELATION BETWEEN PARAMETERS 8 AND 9 = 0.2752E+00

********** REGRESSION SUMMARY **********

Dy-EDTA FROM KFI11, LOWER SECTION
DISTANCE: 190 METRES
NUMBER OF FLOW PATHS: 1

APPLIED MODEL: MODEL3E

NUMBER OF PARAMETERS: 3

INPUT DATA FILE NAME: 1.dat

BACKGROUND LEVEL FOR INPUT DATA: 0.2000

FINAL ESTIMATE FOR PARAMETER 1 = 0.1222E-04
FINAL ESTIMATE FOR PARAMETER 2 = 0.8149E-04
FINAL ESTIMATE FOR PARAMETER 3 = 0.1068E+01

**********

REGRESSION STATISTICS

NO. OF OBSERVATIONS: 305

SUM OF SQUARED DIFFERENCES = 0.772E+00

ERROR VARIANCE = 0.256E-02

CORRELATION COEFFICIENT = .73397E+00

STANDARD ERROR FOR PARAMETER 1 = 0.134E-05
STANDARD ERROR FOR PARAMETER 2 = 0.292E-04
STANDARD ERROR FOR PARAMETER 3 = 0.383E+00

CORRELATION BETWEEN PARAMETERS 1 AND 2 = -.9048E+00
CORRELATION BETWEEN PARAMETERS 1 AND 3 = -.9859E+00
CORRELATION BETWEEN PARAMETERS 2 AND 3 = 0.9261E+00

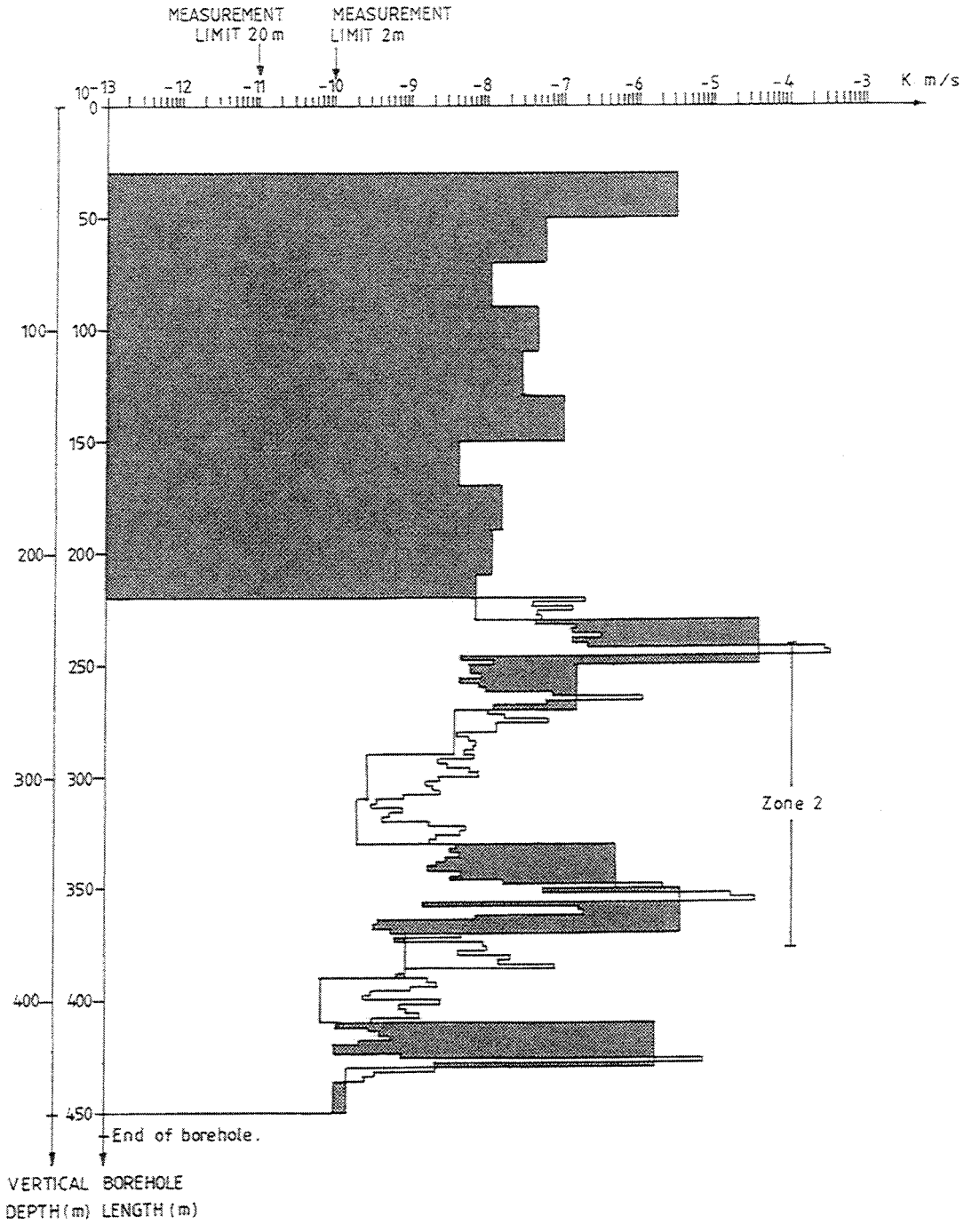


Hydraulic conductivity profile borehole BFI01

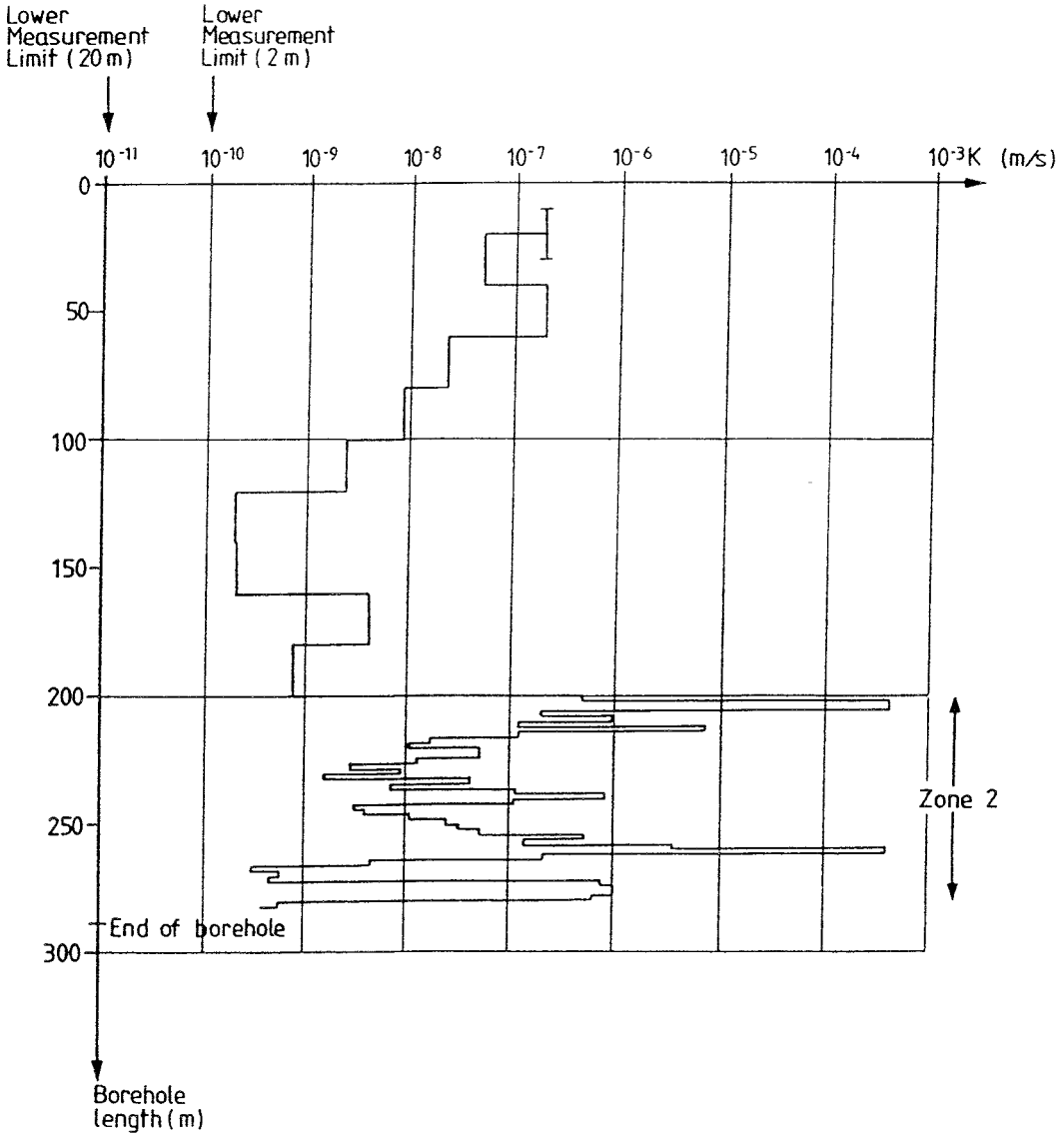


Hydraulic conductivity profile borehole BFI02

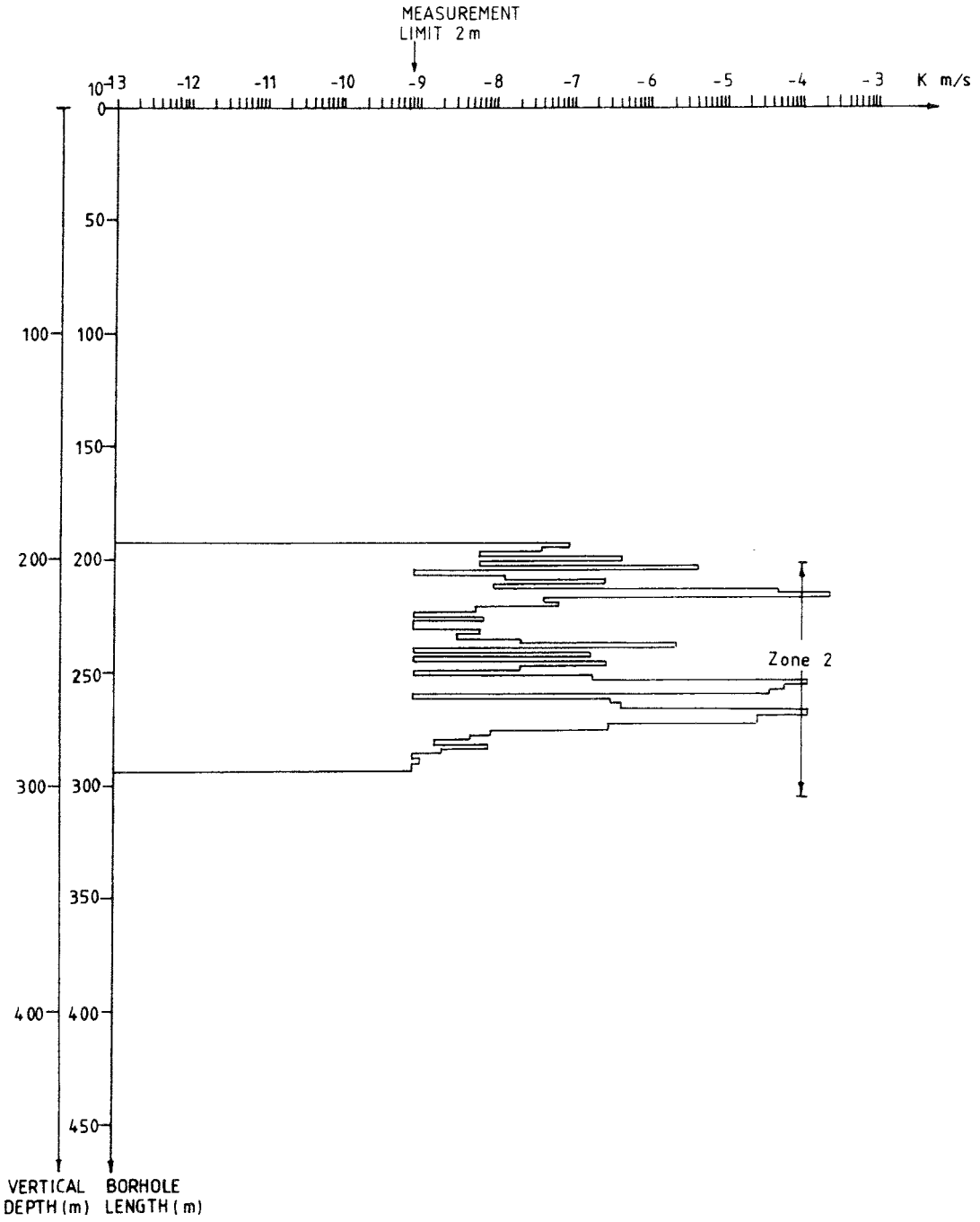


Hydraulic conductivity profile borehole KFI06

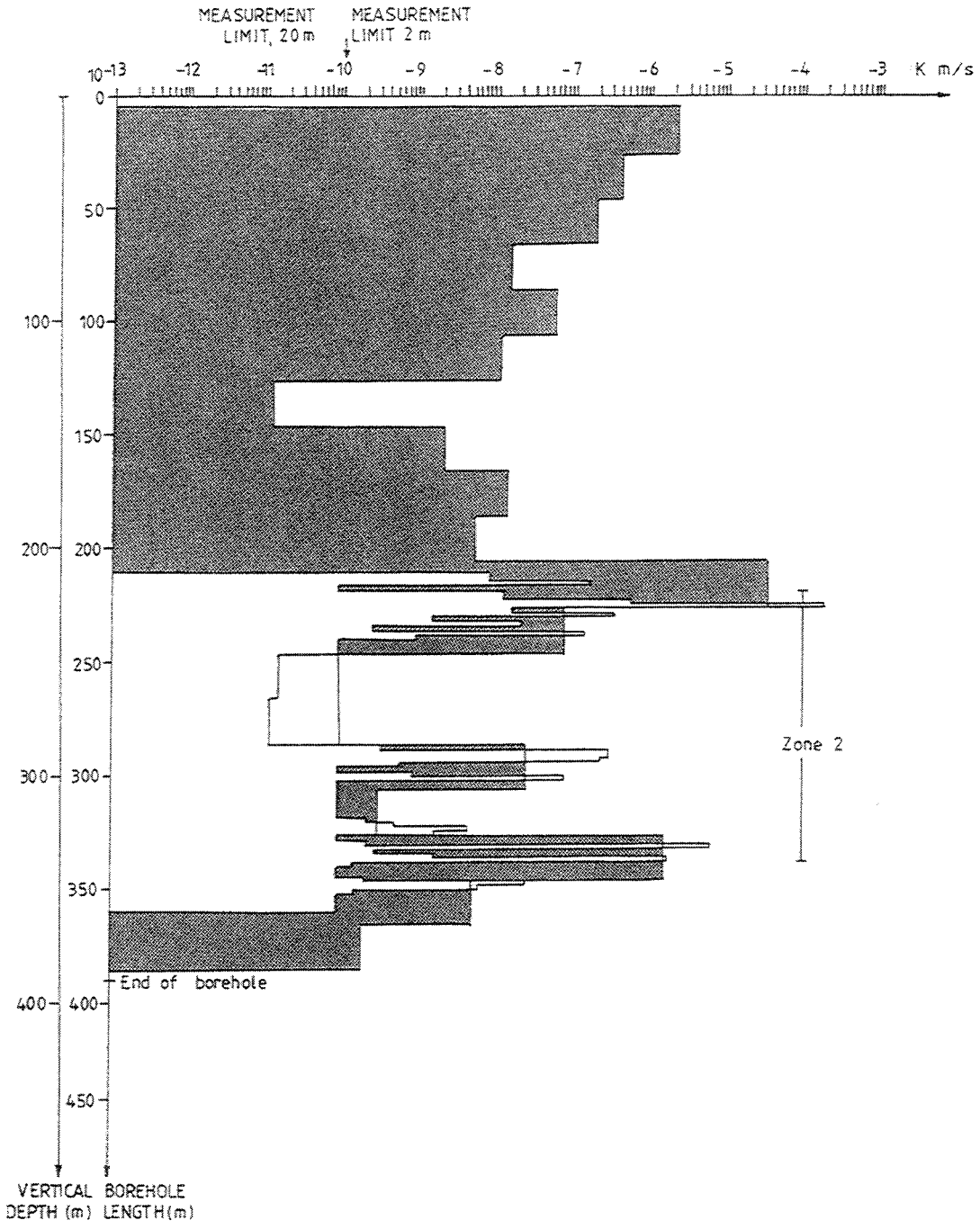


Hydraulic conductivity profile borehole KFI11

# *List of SKB reports*

## Annual Reports

*1977-78*
TR 121
**KBS Technical Reports 1 – 120**
Summaries
Stockholm, May 1979

*1979*
TR 79-28
**The KBS Annual Report 1979**
KBS Technical Reports 79-01 – 79-27
Summaries
Stockholm, March 1980

*1980*
TR 80-26
**The KBS Annual Report 1980**
KBS Technical Reports 80-01 – 80-25
Summaries
Stockholm, March 1981

*1981*
TR 81-17
**The KBS Annual Report 1981**
KBS Technical Reports 81-01 – 81-16
Summaries
Stockholm, April 1982

*1982*
TR 82-28
**The KBS Annual Report 1982**
KBS Technical Reports 82-01 – 82-27
Summaries
Stockholm, July 1983

*1983*
TR 83-77
**The KBS Annual Report 1983**
KBS Technical Reports 83-01 – 83-76
Summaries
Stockholm, June 1984

*1984*
TR 85-01
**Annual Research and Development Report 1984**
Including Summaries of Technical Reports Issued during 1984. (Technical Reports 84-01 – 84-19)
Stockholm, June 1985

*1985*
TR 85-20
**Annual Research and Development Report 1985**
Including Summaries of Technical Reports Issued during 1985. (Technical Reports 85-01 – 85-19)
Stockholm, May 1986

*1986*
TR 86-31
**SKB Annual Report 1986**
Including Summaries of Technical Reports Issued during 1986
Stockholm, May 1987

*1987*
TR 87-33
**SKB Annual Report 1987**
Including Summaries of Technical Reports Issued during 1987
Stockholm, May 1988

*1988*
TR 88-32
**SKB Annual Report 1988**
Including Summaries of Technical Reports Issued during 1988
Stockholm, May 1989

*1989*
TR 89-40
**SKB Annual Report 1989**
Including Summaries of Technical Reports Issued during 1989
Stockholm, May 1990

*1990*
TR 90-46
**SKB Annual Report 1990**
Including Summaries of Technical Reports Issued during 1990
Stockholm, May 1991

*1991*
TR 91-64
**SKB Annual Report 1991**
Including Summaries of Technical Reports Issued during 1991
Stockholm, April 1992

*1992*
TR 92-46
**SKB Annual Report 1992**
Including Summaries of Technical Reports Issued during 1992
Stockholm, May 1993

# Technical Reports
## List of SKB Technical Reports 1993

TR 93-01
**Stress redistribution and void growth in butt-welded canisters for spent nuclear fuel**
B L Josefson[1], L Karlsson[2], H-Å Häggblad[2]
[1] Division of Solid Mechanics, Chalmers University of Technology, Göteborg, Sweden
[2] Division of Computer Aided Design, Luleå University of Technology, Luleå, Sweden
February 1993

TR 93-02
**Hydrothermal field test with French candidate clay embedding steel heater in the Stripa mine**
R Pusch[1], O Karnland[1], A Lajudie[2], J Lechelle[2], A Bouchet[3]
[1] Clay Technology AB, Sweden
[2] CEA, France
[3] Etude Recherche Materiaux (ERM), France
December 1992

TR 93-03
**MX 80 clay exposed to high temperatures and gamma radiation**
R Pusch[1], O Karnland[1], A Lajudie[2], A Decarreau[3],
[1] Clay Technology AB, Sweden
[2] CEA, France
[3] Univ. de Poitiers, France
December 1992

TR 93-04
**Project on Alternative Systems Study (PASS).**
**Final report**
October 1992

TR 93-05
**Studies of natural analogues and geological systems.**
**Their importance to performance assessment.**
Fredrik Brandberg[1], Bertil Grundfelt[1], Lars Olof Höglund[1], Fred Karlsson[2],
Kristina Skagius[1], John Smellie[3]
[1] KEMAKTA Konsult AB
[2] SKB
[3] Conterra AB
April 1993

TR 93-06
**Mineralogy, geochemistry and petrophysics of red coloured granite adjacent to fractures**
Thomas Eliasson
Chalmers University of Technology and University of Göteborg, Department of Geology, Göteborg, Sweden
March 1993

TR 93-07
**Modelling the redox front movement in a KBS-3 nuclear waste repository**
L Romero, L Moreno, I Neretnieks
Department of Chemical Engineering,
Royal Institute of Technology, Stockholm, Sweden
May 1993

TR 93-08
**Äspö Hard Rock Laboratory**
**Annual Report 1992**
SKB
April 1993

TR 93-09
**Verification of the geostatistical inference code INFERENS, Version 1.1, and demonstration using data from Finnsjön**
Joel Geier
Golder Geosystem AB, Uppsala
June 1993

TR 93-10
**Mechanisms and consequences of creep in the nearfield rock of a KBS-3 repository**
Roland Pusch, Harald Hökmark
Clay Technology AB, Lund, Sweden
December 1992

TR 93-11
**Post-glacial faulting in the Lansjärv area, Northern Sweden.**
**Comments from the expert group on a field visit at the Molberget post-glacial fault area, 1991**
Roy Stanfors (ed.)[1], Lars O Ericsson (ed.)[2]
[1] R S Consulting AB
[2] SKB
May 1993

TR 93-12
**Possible strategies for geoscientific classification for high-level waste repository site selection**
Lars Rosén, Gunnar Gustafson
Department of Geology, Chalmers University of Technology and University of Göteborg
June 1993

TR 93-13
**A review of the seismotectonics of Sweden**
Robert Muir Wood
EQE International Ltd, Warrington, Cheshire, England
April 1993

TR 93-14
**Simulation of the European ice sheet trough the last glacial cycle and prediction of future glaciation**
G S Boulton, A Payne
Department of Geology and Geophysics, Edinburgh Uneversity, Grant Institute, Edinburgh, United Kingdom
December 1992

TR 93-15
**Analysis of the regional groundwater flow in the Finnsjön area**
Anders Boghammar, Bertil Grundfelt, Hans Widén
Kemakta Konsult AB
June 1993

TR 93-16
**Kinetic modelling of bentonite - canister interaction.**
**Implications for Cu, Fe, and Pb corrosion in a repository for spent nuclear fuel**
Paul Wersin, Jordi Bruno, Kastriot Spahiu
MTB Tecnologia Ambiental, Cerdanyola, Spain
June 1993

TR 93-17
**Oxidation of uraninite**
Janusz Janeczek, Rodney C Ewing
Department of Earth & Planetary Science, University of New Mexico, Albuquerque, NM, USA
June 1993

TR 93-18
**Solubility of the redox-sensitive radionuclides $^{99}$Tc and $^{237}$Np under reducing conditions in neutral to alkaline solutions. Effect of carbonate**
Trygve E Eriksen[1], Pierre Ndalamba[1], Daqing Cui[1], Jordi Bruno[2], Marco Caceci[2], Kastriot Spahiu[2]
[1] Dept. of Nuclear Chemistry, Royal Institute of Technology, Stockholm, Sweden
[2] MBT Tecnologia Ambiental, Cerdanyola, Spain
September 1993

TR 93-19
**Mechanical properties of fracture zones**
Bengt Lejon
Conterra AB
May 1993

TR 93-20
**The Fracture Zone Project - Final report**
Peter Andersson (ed.)
Geosigma AB, Uppsala, Sweden
September 1993

TR 93-21
**Development of "CHEMFRONTS", a coupled transport and geochemical program to handle reaction fronts**
Catharina Bäverman
Department of Chemical Engineering, Royal Institute of Technology, Stockholm, Sweden
October 1993

TR 93-22
**Carbon transformations in deep granitic groundwater by attached bacterial populations characterized with 16S-rRNA gene sequencing technique and scanning electron microscopy**
Susanne Ekendahl, Johanna Arlinger, Fredrik Ståhl, Karsten Pedersen
Department of General and Marine Microbiology, University of Göteborg, Göteborg, Sweden
October 1993

TR 93-23
**Accelerator trsansmutation of wastes (ATW)**
**– Prospects and safety**
Waclaw Gudowski, Kjell Pettersson, Torbjörn Thedéen
Royal Institute of Technology, Stockholm, Sweden
November 1993

TR 93-24
**Direct fault dating trials at the Äspö Hard Rock Laboratory**
R H Maddock, E A Hailwood, E J Rhodes, R Muir Wood
October 1993